THE UNIVERSITY *of* EDINBURGH

An integrated platform to assay melanoblast development *in vitro*

Olivia J. Harrison

Presented for the degree of Doctor of Philosophy

Molecular and Clinical Medicine (Molecular Medicine)

The University of Edinburgh

2018

igmm
INSTITUTE OF GENETICS & MOLECULAR MEDICINE
Medical Research Council Human Genetics Unit

National Centre for the Replacement Refinement & Reduction of Animals in Research

I declare that this thesis has been composed solely by myself and that it has not been submitted, in whole or in part, in any previous application for a degree. Except where stated otherwise by reference or acknowledgment, the work presented is entirely my own.

Abstract

Melanoblasts are the embryonic precursors of melanocytes, the pigment producing cells of the skin and hair. Melanoblasts are of key interest to developmental biologists for numerous reasons, including their ability to migrate throughout the body from a single origin in the neural crest (NC). Current methods for the study of the melanocyte lineage are limited by the heavy reliance on animal models. To challenge this, a platform of *in vitro* tools were designed to replace and complement current studies. A major obstacle is the transition from 2D cultures, which provide only limited behavioural information, to 3D models which are able to recapitulate the environmental conditions. 3D cultures are regularly created using tissue samples and synthetic matrices for attachment, but building a model from cell lines only has not been achieved. A co-culture model using immortalised keratinocyte (COCA) and melanoblast cell lines proved unsuitable for observing developmental processes, due to lack of movement at high cell densities, but may be practical in pigmentation research. Other methods were explored to examine melanoblast behaviour, including the use of cell derived matrices (CDMs) integrated with melanoblast cell lines, and aggregates formed by hanging drop (HD) culture. CDMs were successfully generated from the COCA line, as well as NIH3T3 fibroblasts which has been shown previously. These structures are denuded of cells to leave the deposited extracellular matrix (ECM) components intact, representative of the dermal (fibroblast) and epidermal (keratinocyte) layers of the skin. HDs were prepared from cultured melanoblast cell lines, and form tight aggregates which disseminate when plated, in a manner similar to the dissemination of cells from the NC in explant cultures.

The receptor tyrosine kinase KIT and its ligand (KITL), are vital for melanoblast development. Previous study of this signalling complex has often focussed on the haematopoietic lineage and spermatogenesis, where they perform essential roles. KITL is expressed in a membrane localised form found on the surface of keratinocytes thought to promote melanoblast/melanocyte survival, and a soluble isoform found sequestered in the ECM which promotes cell migration. Cell lines expressing fluorescently tagged KIT and KITL were created to visualise their

interactions using live-cell confocal imaging. Firstly, cell lines were generated to perform co-culture experiments with KIT and KITL, and we showed that these constructs are able to interact by uptake of KITL into KIT cells. Secondly, tandem fluorescent protein timers of KIT and KITL were generated which were used to observe protein kinetics. We showed that these protein timers can be manipulated using cycloheximide to block protein production, or by increasing ligand availability. These protein timers reveal that soluble KITL (sKITL) has a faster turnover than membrane bound KITL (mKITL), and that in all three proteins, there is distinct change in spatial localisation as the proteins age.

Using a novel melanoblast reporter mouse, *Pmel-CMN*, primary mouse melanoblasts between E12.5 and E14.5 were isolated for RNA sequencing. This time period is the earliest reported for melanoblast isolation for use in gene expression analysis. We show that within this time course, there are significant changes in the RNA expression profiles, including decreasing expression of other NC cell markers, and huge increasing expression of pigmentation genes.

To assess the biological relevance of using *in vitro* assays, cells of the immortalised melanoblast cell line, melb-a, were cultured under different conditions and examined via RNA sequencing. Results reveal differences in several areas between primary cells and those in culture, including loss of melanocyte specificity.

The different tools described in this thesis provide a platform on which to study various aspects of cell behaviour, including migration, morphology and cell adhesion at both the individual cell and population levels.

Lay Summary

Melanocytes in the skin produce the pigment which colours our skin and hair, and is vital to protect us from UV radiation. In the developing embryo, melanocytes are known as melanoblasts. They originate near the structure which becomes the spinal cord/brain and then migrate long distances to cover the whole body. In diseases where melanoblast development has gone wrong, it is easily visible in patches with no colour. Often diseases which have pigmentation problems will also have problems in other cells with which the melanoblasts shared a common origin e.g. peripheral neurons. Melanoblasts are therefore an important, and useful, system to study cell behaviours in. Research into melanocytes and melanoblasts relies heavily on animal models, due to the many complex interactions the cells undergo. One such complexity in development involves the dermis and epidermis which make up the main layers of the skin. They are different in structure, composition and in the proteins they produce, but melanoblasts migrate through both of these layers to reach their final destination. These conditions are extremely difficult to recreate outside the living organism. This thesis aimed to develop various experiments to address this, and reduce the reliance on mouse models for the study of melanoblasts. Using three melanoblast cell lines and one melanoma cell line, experiments were developed to study key aspects of cell behaviour *in vitro*. These behaviours include the migration patterns of cells individually and as a population and how they can break away from their neighbouring cells to move through the body.

Another focus of this project was to examine the receptor KIT and its substrate KITL (KIT ligand) which are key proteins involved in melanoblast development. Several cell lines were generated which had fluorescent versions of these proteins for use in live cell experiments. Firstly, cells were combined to view the receptor/ligand interactions, and we showed that these are indeed able to interact. Secondly, cells with protein timer constructs were generated; these proteins appear as different colours depending on how old they are. We showed that we can manipulate the age of the protein pool using drugs and increased ligand concentrations, and that these proteins are therefore very useful for studying protein kinetics.

An experiment looking at the RNA profiles of melanoblast cells early in their development from E12.5 to E14.5 was performed using a new mouse model, *Pmel-CMN*. Further RNA sequencing was performed on a commonly used melanoblast cell line (melb-a) in 3 different culture conditions, in order to examine how accurately cells in culture mimic the primary cells. Over the time course, we observed increasing expression of genes related to pigmentation, and a decreased expression of genes related to cells which share a common origin. Between the primary cells and cells in culture, the differences observed demonstrate some of the difficulties of comparing results from *in vitro* and animal experiments.

Acknowledgments

The support I've received over the years of my PhD is overwhelming. Without everyone mentioned here (and many more), I would not have completed this project. Your contributions to both my work and personal life have been incredible, and I can't express my gratitude enough.

My first thanks must go to my brilliant supervisors Dr Richard Mort and Professor Ian Jackson. Thank you for helping me navigate this project, especially when things were not going in the ideal direction, as happened so often. I sincerely hope that I have done you proud.

The IGMM has an amazing core of technical services, without whom the facility would grind to a halt. Those who helped me with specific experiments are mentioned within the text, but most definitely deserve a double mention; Lizzie, Matt, Allyson, Len – thank you. Thanks also go to the rest of the team running wash-up and technical services, and those in the mouse house. Over the years, the people working in our lab has changed so much that it'd be impossible to thank everybody. Suffice to say thank you Jackson/Mill lab for all the input at lab meetings, for supporting me at presentations and generally being a great group to work with day-to-day in the lab.

I have made a group of lifelong friends at the IGMM who made it all worthwhile. Again, so many people have come and gone over my time in Edinburgh that it's impossible to thank everybody so this list is greatly limited. Fiona, Katy, Disco, Jess, Emma, Pete and Amy, thank you all so much. Special mention to Emma who doubled as a huge scientific support throughout. And not forgetting my girls from Newcastle, who have been through the entire (very long) journey with me, putting up with my eternal student status and supporting me through all the ups and downs.

Finally, I must thank my family whose love and support is never ending. Your belief in me when I had lost all in myself has got me through the worst of times, and I can never thank you enough. So Mum, Dad, Anthony and Stephanie – this thesis is dedicated to you.

Table of Contents

Abbreviations

~	Approximately
%	Percent
^{o}C	Degrees Celsius
µM	Micromolar
µl	Microlitre
α-MSH	Alpha melanocyte stimulating hormone
2D	2-dimensional
3D	3-dimensional
4-OHT	4-hydroxytamoxifen
ALI	Air-liquid interface
ANOVA	Analysis of variance
a.u.	Arbitrary units
BMP	Bone morphogenetic protein (protein family)
bp	Base pairs
cAMP	Cyclic AMP
Cas9	CRISPR-associated protein 9 nuclease
Cdh1	E-cadherin
Cdh2	N-cadherin
Cdh3	P-cadherin
CDM	Cell derived matrix/matrices
cDNA	Complementary DNA
CFP	Cerulean fluorescent protein

CHX	Cycloheximide
cm	Centimetre
CO_2	Carbon dioxide
CreERT2	Cre recombinase (fused to a mutated) oestrogen receptor
CRISPR	Clustered Regularly Interspaced Short Palindromic Repeats
DCT	Dopachrome tautomerase
dH_2O	Deionised water
DHI	5,6- dihydroxyindol
DHICA	5,6-dihydroxyindole-2-carboxylic acid
DMSO	Dimethyl sulfoxide
dNTP	Deoxynucleotide
DNA	Deoxyribonucleic acid
DOPA	L-3,4-dihydroxyphenlyalanine
E	Embryonic day
ECM	Extracellular matrix
ECL	Enhanced chemical luminescence
E.coli	*Escherichia coli*
EdnrB	Endothelin B receptor
EDTA	Ethylene diamine tetraacetic acid
EMT	Epithelial-mesenchymal transition
ES	Embryonic stem (cells)
EtOH	Ethanol
FACIT	Fibril-associated collagen with interrupted triple helix
FACS	Fluorescence-activated cell sorting

FCS	Fetal calf serum
FFA	Free fatty acids
FGF	Fibroblast growth factor
FOXD	Forkhead box domain (protein family)
g	G-force (acceleration)
gDNA	Genomic DNA
GO	Gene ontology
GOI	Gene of interest
H&E	Haematoxylin and eosin
HCl	Hydrochloric acid
HD	Hanging drop
HDR	Homology directed repair
HEPES	4-(2-hydroxyethyl)-1-piperazineethanesulfonic acid
HRP	Horseradish peroxidase
hrs	Hours
HSE	Human skin equivalent
IF	Immunofluorescence
IGMM	Institute of Genetics and Molecular Medicine
iPSC	Induced pluripotent stem cell
K	Keratins (protein family)
Kb	Kilobase (1 thousand nucleotides)
kDa	Kilodaltons
KITL	KIT Ligand
KGF	Keratinocyte growth factor

L	Litre
LB	Luria-Bertani
LBE	Library efficiency
LE	Leading edge (culture)
LUT	Look up table
M	Molar
MAPK	Mitogen-activated protein kinase (signalling pathway)
Mb	Megabase (1 million nucleotides)
MCS	Multiple cloning site
MC1R	Melanocortin 1 receptor
mins	Minutes
MITF	Microphthalmia-associated transcription factor
mKITL	Membrane-bound KIT ligand
ml	Millilitre
MMP	Matrix metalloproteinases (protein family)
MLs	Melanoblast/melanoma cells
ms	Millisecond
MSA	Migration staging area
MSC	Melanocyte stem cell
NaOAc	Sodium acetate
NC	Neural crest
NC3Rs	National Centre for the Replacement, Refinement and Reduction of Animals in Research
ng	Nanogram
NHEJ	Non-homologous end joining

ng/ml	Nanogram per millilitre
NH_4OH	Ammonium hydroxide
nm	Nanometres
P	Post-natal day
p53-RE	P53 response element
Padj	Adjusted P-value
PAX	Paired box (protein family)
PBS	Phosphate buffered saline
PCA	Principal component analysis
PCR	Polymerase chain reaction
PDTX	Patient derived tumour xenograft
PFA	Paraformaldehyde
PI3K	Phosphoinositide 3-kinase (signalling pathway)
PKB	Protein kinase B (or Akt)
PKC	Protein kinase C
PMSF	Phenylmethanesulfonylfluoride
PNS	Peripheral nervous system
PRC2	Polycomb repressive complex 2
P/S	Penicillin/streptomycin
PTB	Phosphotyrosine binding domain
PTP	Protein tyrosine phosphatase
RNA	Ribonucleic acid
rpm	Revolutions per minute
rRNA	Ribosomal RNA

rtPCR	Reverse-transcription PCR
SAP	Shrimp alkaline phosphatase
SDS-PAGE	Sodium dodecyl sulphate - polyacrylamide gel electrophoresis
secs	Seconds
sfGFP	Super-folder green fluorescent protein
SC	Sub-cloning (efficiency)
SCF	Stem cell factor
SCP	Schwann cell precursor
SFK	Serine family kinases (protein family)
SH2	Src Homology 2
sKITL	Soluble KIT ligand
Sl	Steel (phenotype/locus)
SNP	Single nucleotide polymorphism
SOC	Super Optimal broth with catabolite repression
SOX	Sry-related HMG box (protein family)
TBE	Tris borate EDTA
TBS	Tris buffered saline
TBSt	TBS-Tween
TE	Tris EDTA (buffer)
TGFα	Transforming growth factor-α
TGFβ	Transforming growth factor-β
Tm	Melting temperature
TPB	Tyrptose phosphate broth
tRNA	Transfer RNA

TRP1	Tyrosinase related protein 1
Tyr	Tyrosinase
U	Units
UV	Ultraviolet
V	Volts
W	(dominant) White spotting (phenotype/locus)
w/v	Weight to volume
WB	Western blot
WF	Whole field (culture)
Wnt	Wingless-related integration site (signalling pathway)
X	Concentration
X-gal	5-bromo-4-chloro-3-indolyl-D-galactoside
YFP	Yellow fluorescent protein
ZEB	Zinc-finger E-box binding (protein family)

List of Figures

List of Tables

List of Videos

All video files can be found on the accompanying CD.

Video 3.2. Assembly of the CDM imaging chamber

Video 4.1. Melb-a cells stained with vital dyes

Video 4.2. B16 cells migrating into space with tracks

Video 4.3. B16 cells migrate from a HD

Video 4.4. Melb-a cells migrate from a HD

Video 4.5. Melb-s1 cells migrate from a HD

Video 4.6. Melb-m5 cell migrate from a HD

Video 4.7. Cells do not migrate in the absence of matrigel or CDM

Video 5.1. sKITL_NG marks retraction fibres during mitosis

Video 5.2 mKITL_TD is dynamic in filopodia and attachment fibres

Chapter 1
Introduction

Melanocytes are pigment producing cells found in the skin, hair follicle, eye and inner ear. In the skin they are responsible for protecting the keratinocytes from harmful UV (ultraviolet) radiation. Their developmental precursors are melanoblasts. Melanoblasts provide an excellent model system in which to study developmental processes. A major advantage of the lineage is the ability to visualise defects or changes by examining pigmentation patterns *in vivo*. Melanoblasts and melanocyte study has provided insight into other cell lineage behaviours in several areas including migration and neural crest (NC) development. However, they are particularly useful due to their isolated nature, and relatively straight-forward developmental progression. They are defined from a single, multipotent cell type during mid-developmen; they migrate from a single, well-defined location to cover the entire body; they localise to specific structures and then they finally establish their own stem cell reservoir to maintain their function throughout adult life. All the topics and experiments within this thesis are related to the laboratory mouse unless specifically stated otherwise.

1.1. Melanoblast development

1.1.1. Neural crest development

The NC is a transient structure found during early vertebrate development. It is situated above the developing neural tube, at the outermost surface of the embryo near the developing epidermis. Anatomical study, and identification of the NC dates back to the 19th century, and it has been known as the origin of the pigment cells since this early time. It arises from ectoderm tissue, and goes on to become a wide variety of cell lineages, including melanocytes, and cells of the peripheral and enteric

nervous system (Hall, 2008; Mayor and Theveneau, 2013). Figure 1.1. demonstrates the progression of NC formation; induction occurs at the border of the neural plates which invaginate and fold to create the neural tube (Bronner-Fraser, 1994). By this action, the NC cells are brought together at the dorsal aspect (shown in light blue). Cells delaminate from the NC in a continuous wave, with distinct timings which relate to the cells fate. Cells exit the NC at carefully controlled time points, depending on their future cell lineage, which is roughly determined by the position of cells along the crest (Serbedzija, Fraser and Bronner-Fraser, 1990). The time until delamination post neural tube closure is also related to position along the anterior-posterior axis (Theveneau and Mayor, 2012). Cells begin delaminating from the NC at around E9 (embryonic day) (Serbedzija, Fraser and Bronner-Fraser, 1990). Specifically in the trunk, the first cells to emerge follow a ventral migratory pathway, whilst melanoblast fated cells are later to emerge and follow the dorsolateral pathway (Thomas and Erickson, 2008) (Figure 1.1.C.). As well as being interesting to developmental scientists, the NC is of key focus to evolutionary biologists, as it is a common feature shared exclusively among vertebrates. Development of the NC is one of the major diverging points in the evolution of vertebrates as it has such a large contribution to several parts of cranial development (Le Douarin, 2004).

The formation of the NC is induced by a network of signals from wingless-related integration site (Wnt), Notch, retinoic acid, bone morphogenetic protein (BMP), and fibroblast growth factor (FGF) pathways (Mayor and Theveneau, 2013). These signals are produced by the surrounding ectoderm and mesoderm within the neural plate border region, to activate a combination of transcription factors which ultimately control NC development (Milet and Monsoro-Burq, 2012; Prasad, Sauka-Spengler and LaBonne, 2012). These include transcription factors SNAI1 (or SNAIL) and SNAI2 (or SLUG) which are also key factors in the delamination of cells from the NC (Cheung et al., 2005). Other notable factors are FOXD3, a member of the Fox (forkhead box domain) family, which is believed to be important to ‘prime’ multipotent cells during embryogenesis (Cheung et al., 2005; Plank-Bazinet and Mundell, 2016). SOX9 (Sry-related HMG box) is another key

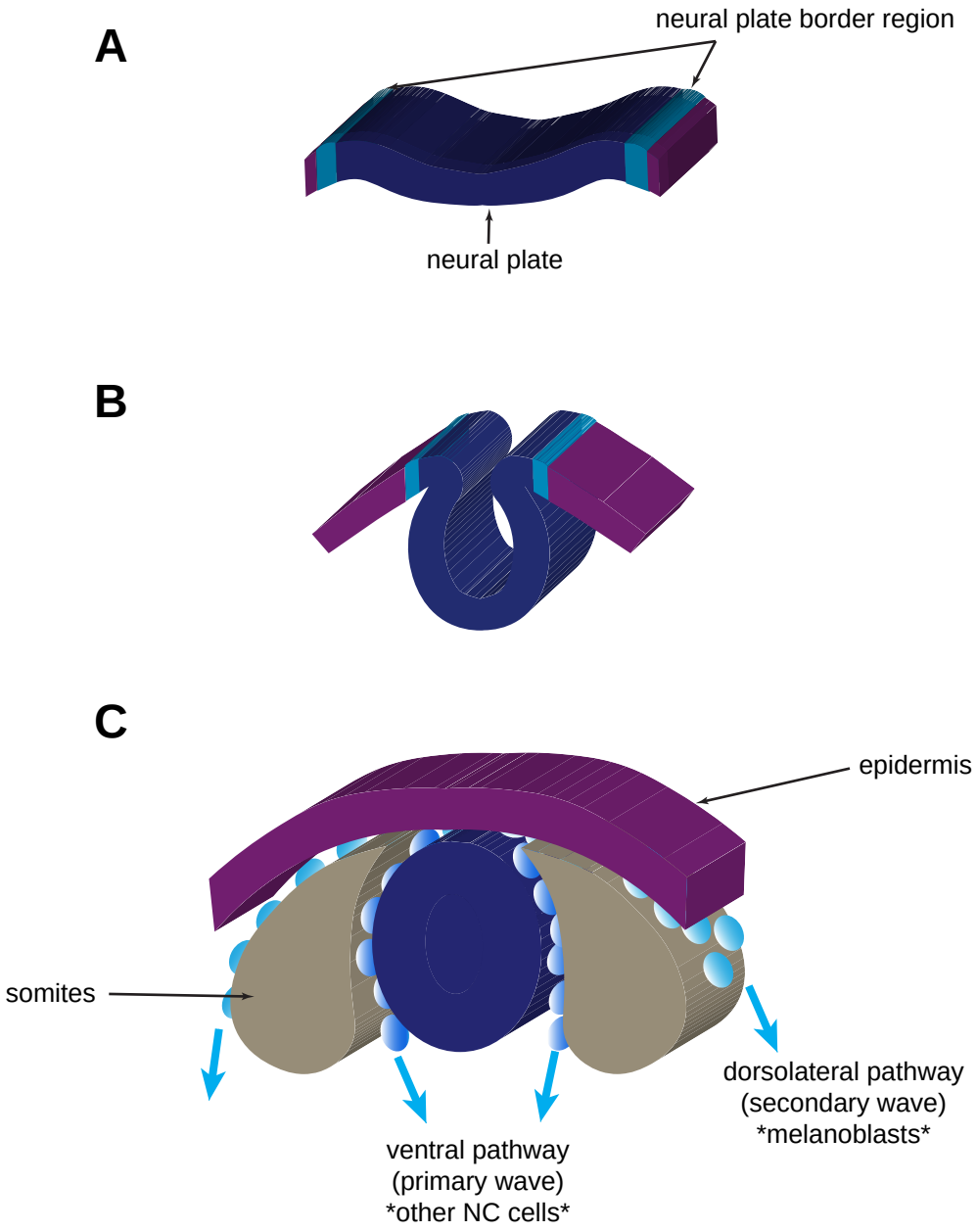

Figure 1.1. Neural crest formation and delamination in the trunk. A. Thickening of the neural plate occurs between the neural borders. The neural crest originates in the area near the neural plate borders. **B.** The neural plate folds inwards to create the neural tube, which will eventually form the brain and spinal cord. The neural plate borders from either side and neural crest precursor cells are pulled close together. **C.** Closure of the neural tube occurs, and the sides fuse together. Trunk neural crest cells exit the crest via the ventral pathway (primary wave) or the dorsolateral pathway (secondary wave). Neurons and glia of the peripheral nervous system follow the ventral pathway, while melanoblasts follow the dorsolateral pathway between the developing epidermis and the somites.

participant, without which the NC cells quickly apoptose (Cheung et al., 2005). The complex interplay between these factors are necessary for proper NC development.

There are further networks involved in the specification of the melanocyte lineage from the NC population. MITF (micropthalmia-associated transcription factor) is known as the master regulator of melanoblast development, with numerous upstream regulatory elements, including PAX3 (paired-box) and SOX10 (Thomas and Erickson, 2008), and downstream target pathways (Levy, Khaled and Fisher, 2006). The expression of MITF is crucial in the specification of melanoblasts at this early stage, and continues to regulate development and survival throughout the melanocyte lifespan (Kawakami and Fisher, 2017). In order to split from other NC cells and glial/neuronal precursors, melanoblast fated NC cells downregulate FOXD3 (Thomas and Erickson, 2009) and SOX2 (Adameyko et al., 2012), which are both repressors of MITF. Melanoblasts are identifiable by specific markers, including *Mitf*, *Kit*, *Pmel* and *Dct* (dopachrome tautomerase) at around E10.5 (Mort, Jackson and Patton, 2015; Thomas and Erickson, 2008).

1.1.2. Exiting the NC – the epithelial-mesenchymal transition

The epithelial-to-mesenchymal transition (EMT) is a process by which cells lose classical epithelial cell-cell adhesions to gain migratory behaviours characteristic of mesenchymal cells (Theveneau and Mayor, 2012). To exit the NC, cells must undergo either partial or complete EMT, causing the phenotypic changes which release the connections between adjacent cells (Theveneau and Mayor, 2012). Indeed, the NC is often used as a prototypical model for EMT. EMT can occur in reverse, i.e. mesenchymal-epithelial transition (MET). MET is especially important in cancer biology, as it enables metastasised cells to establish a tumour in the new location by integrating with other tissues (Yang and Weinberg, 2008).

Epithelial cells are closely associated by specialised adhesion structures, which are not found in mesenchymal cells. These include tight junctions which attach the cytoskeleton of adjacent cells through claudins and occludins (Shin, Fogg and Margolis, 2006), adherens junctions which are formed mainly by cadherins (Ferreri and Vincent, 2008) and gap junctions which directly link the cytoplasm of adjacent

cells with connexins that form gated channels between two cells (Hervé and Derangeon, 2013). These attachment properties are key for the function of various epithelial tissues, including in the skin epidermis. However, melanoblasts along with other migratory cells must travel through other developing tissues to reach their final destination, and so they must be free to move. To achieve this, there is considerable reprogramming of gene expression in the epithelial cells to reorganise their cytoskeletons, change their cell shape, lose their cell junctions and lose their ingrained apical-basal polarity (Thiery and Sleeman, 2006).In the literature, the onset of EMT and of cells exiting the NC is discussed as a whole rather than specifically by cell line, so it is presumed that the EMT mechanism is the same for all NC lineages. The melanoblast population that leaves the NC is very small (~98 cells (Luciani et al., 2011)). Studying them at this early stage is therefore experimentally challenging, and have primarily been examined by whole mount staining. EMT is more easily, and therefore more often studied in relation to cancers, where it is of key therapeutic interest – understanding and developing methods of stopping cells undergoing EMT, which confers the ability of the tumour cells to metastasise, has a huge potential to impact on the disease progression. However, the process may not be identical, as is discussed in relation to the cadherin switch later in this section.

The major transcription factors controlling EMT are Snail factors (*Snai1*, SNAIL and *Snai2*, SLUG), basic helix-loop-helix factors (bHLH) such as *Twist*, and ZEB factors (zinc-finger E-box-binding) *Zeb1* and *Zeb2*. These master regulators function in two ways; either they have direct action upon the expression of key proteins, or they regulate the expression of other transcription factors which will then promote a further effect. Snail transcription factors direct mechanism of action is well defined, through experiments of various researchers on E-cadherin. SNAIL recruits Polycomb repressive complex 2 (PRC2) which leads to histone modification, and silencing of the E-cadherin promoter (Herranz et al., 2008). SLUG equally acts as a repressor of E-cadherin, and was shown in 2011 to be a regulator of ZEB1 in melanoma (Wels et al., 2011). ZEB1 and ZEB2 are also transcriptional repressors which promote EMT, again with significant repression of E-cadherin (Van de Putte et al., 2003). Studies by Van de Putte and Miyoshi show that the NC is particularly affected by *Zeb1/Zeb2* changes in knockout models, adding support to the ZEB proteins as major EMT

factors (Miyoshi et al., 2006; Van de Putte et al., 2003). TWIST has been shown to function as both a positive regulator of mesodermal genes from studies in *Drosophila* (Leptin, 1991) and breast cancer (Wang et al., 2016), in addition to being a repressor of E-cadherin (Hajra, Chen and Fearon, 2002; Yang et al., 2004). It also exerts its effects by histone modification, through SET8, which is a histone methyltransferase (Yang et al., 2012) or PRC2 (Yang et al., 2010). There have also been a number of extracellular regulators of EMT identified, including Notch ligands, FGF, and transforming growth factor-β (TGF-β), and even some microRNAs (ribonucleic acid) (Jung, Fattet and Yang, 2015; Lamouille, Xu and Derynck, 2014; Zhang and Ma, 2012).

One of the core changes in EMT is the 'cadherin switch', where cells downregulate expression of E-cadherin which is a key contributor to the adherens junctions, and upregulate expression of N-cadherin which is a mesenchymal cadherin. This cadherin switch is a hallmark of EMT, and is one of the principal characteristics used to identify cells which have undergone the transformation in cancers. In the NC however, there is some conflicting evidence as to the expression of cadherins which suggest a divergence from the classic EMT model. There is evidence of a downregulation of N-cadherin in the pre-migratory cells, and a non-essential role for SLUG in mice (Jiang et al., 1998). However, the classic cadherin switch has also been demonstrated; *Xenopus* models have been used to demonstrate the E-to-N cadherin switch during NC EMT, and show it to be a key event in a cellular programme promoting a form of directional migration called contact inhibition of locomotion (CIL) (Scarpa et al., 2015). The differences observed between developmental process and between species reinforce a requirement for more specific models of EMT to characterise specifically NC EMT in the mouse.

1.1.3. Melanoblasts migrating throughout the trunk

Migration patterns of cells of the NC have been studied extensively since the 1960s, most notably by James Weston, whose earliest work in chicks focussed on the cells migrating from the NC to populate the trunk (in contrast to NC cells destined for the head, whose migratory patterns are different, and possibly of different origin)

(Weston et al., 2004). Weston was the first to identify the migratory pathways cells of the NC, by using radioactive [^{3}H]thymidine as a cell tracer (Weston, 1963). As mentioned in the previous section, cells delaminate from the NC beginning at around E9 (Serbedzija, Fraser and Bronner-Fraser, 1990). Cells destined to be melanoblasts downregulate the expression of *Foxd3* and *Sox2*, and upregulate *MITF* (Kos et al., 2001; Levy, Khaled and Fisher, 2006; Nitzan et al., 2013). The cells are held briefly in the migratory staging area (MSA) (Wehrle-Haller and Weston, 1995). They then migrate along a concentration gradient of KIT ligand (KITL) towards the dorsolateral migratory pathway (Wehrle-Haller and Weston, 1995), and emerge from the MSA at around E10.5. The KIT receptor and its ligand, form a vital signalling pathway in numerous stages of the melanocyte lineage. The cells that leave the MSA upregulate expression melanoblast specific markers, including *Pmel* and *Dct* as mentioned previously (Baxter and Pavan, 2003; Mackenzie et al., 1997). They then migrate and proliferate through the dermis during their early migration, and the majority cross to the epidermis at E12.5 in response to KIT/KITL signalling (Nishikawa et al., 1991). A small, constant dermal population remains, and this population does not undergo mass proliferation as seen in the epidermis (Luciani et al., 2011). Full colonisation of the trunk is accomplished by E15.5, at which time melanocytes begin to localise to the developing hair follicle. It is known that the density of the population plays a central role in the migratory behaviour of melanoblasts (Mort et al., 2016).

1.1.4. Alternative source of melanocytes

In 2009, Adameyko *et al.* published a study demonstrating that a large number of adult melanocytes were not derived in the traditional route that has been discussed thus far, but rather from Schwann cell precursors (SCPs) which delaminate in the first wave from the NC and follow the ventral pathway (Adameyko et al., 2009). They began investigating the possibility of an alternative source to resolve some questions surrounding melanoblast patterning and migration, particularly in the limb buds. Adameyko *et al*. used a combination of chick and mouse models to explore this contribution to the final melanocyte numbers. Their experiments show that developing melanoblasts are lost from the dorsolaterally migrating population between E10.5 and E11.5, but that they are replaced by E12 by cells migrating

outwards from near the spinal ganglion. They describe a population of *Mitf*+ cells which associate with the developing spinal nerves, and that these cells progress along the nerve fibres extending towards the skin. Data from experiments in the chick limb bud showed that after physical ablation of the dorsolaterally migrating population of cells, melanocytes were still present in the limb. Their mouse experiments focussed on lineage tracing using a *Plp*-CreERT2 line (Cre recombinase (fused to a mutated) oestrogen receptor) (Leone et al., 2003) crossed to a Rosa26-YFP (yellow fluorescent protein) reporter mouse as a SCP specific marker, and *Mitf* expression as an indicator of melanocytes. *Plp*-CreERT2 was described in 2003, where expression in epidermal melanoblasts were identified by LacZ assay after tamoxifen induction at E12.5 (Leone et al., 2003). Adameyko *et al.* injected mice at E11 and collected pups at P11 (post-natal day), and showed that up to 65% of *Mitf*+ cells in the hair follicle, and 58% of *Mitf*+ cells in the dermis were descended from the *Plp* expressing cells. There is some discussion as to the suitability of the *Plp*-CreERT2 line to distinguish between SCPs and melanoblasts from various studies. Colombo *et al.* undertook transcriptomic analysis of primary melanoblasts isolated between the ages of E14.5-E16.5, and identified *Plp* as a highly expressed gene. Melanoblasts were isolated using a classic *Tyr*-CreERT line, and cells were dissected specifically from the epidermis. Additionally, Hari *et al.* showed that *Plp*-CreERT2 specificity may be influenced by the timing of induction; if induced at E9.5, they show expression of *Plp* in the majority of NC cells indicating that unspecified NC cells are marked using this reporter. They further show that *Plp*-CreERT2 marked nerves and melanoblasts when activated at other stages (E11.5, E12.5 and E14.5) (Hari et al., 2012). Lastly, they show that an alternative SCP marker, *Dhh* fails to repeat the identification of SCP derived melanocytes. RNA-sequencing data presented in Chapter 6 also shows *Plp* expression in melanoblasts at E12.5-E14.5.

There is no doubt that many cells that follow the ventral pathway retain the ability to become melanocytes, and that some NC populations retain multipotency even after they have begun their migratory pathways (Motohashi et al., 2009). Morrison *et al.* identified a multipotent, self-renewing and persistent population of NC cells that can be isolated from the peripheral nerve, where the SCP and glial cells are located (Morrison et al., 1999). The reversibility of melanocytes to a multipotent state, able

to form neurons and glia can even be induced *in vitro* by the cytokine endothelin 3 (Dupin et al., 2000).

Biological reasons for why the suggested events would occur remain unclear; it remains to be answered why the dorsolateral population of cells would be specified, if a large portion die within a day, to be replaced by identical cells of slightly different origin. Nevertheless, it is an interesting finding, particularly in terms of the plasticity of the NC post delamination, and merits further research, perhaps using other SCP and melanoblast markers to improve confidence in the methodology. This work highlights the requirement of rigorous testing of lineage tracers, and robust CreERT2 animal models.

1.1.5. Localising to the hair follicle

In mice, a large population of melanoblasts localise to the hair follicle in the last stages of their development (Mayer, 1973). There they separate into two further lineages of different populations; the first, which enter the hair follicle proper, and pigment the developing hair matrix, the second establish a melanocyte stem cell (MSC) pool in the hair bulge (Nishimura et al., 2002). These MSCs are responsible for hair pigmentation following the first cycle, as the entire population of active melanoblasts which have pigmented the hair from the hair bulb is lost when a hair is shed (Nishimura, 2011). To localise to the hair follicle, melanoblasts respond to signalling from the outer root sheath cells (ORS), and migrate along this structure to the hair bulb in response to signalling from stromal cell derived factor 1 (SDF-1) (Belmadani et al., 2009; Yamauchi et al., 2013). KIT/KITL signalling is also important for this localisation as shown by experiments using KITL in explant cultures (Jordan and Jackson, 2000a). The position of melanocytes in the bulge and hair follicle can be seen in Figure 1.2.A.

Melanocytes are lost from the interfollicular space of the trunk epidermis postnatally, in response to a decreasing expression of *Kitl* by the keratinocytes (Hirobe, 1984; Yoshida et al., 1996). Melanocytes remain in the epidermis in hairless parts of the mice and the tail, and there are also amelanotic melanocytes present which have been suggested to represent the stem cell pool in this environment (Glover et al., 2015;

Zaidi, Day and Merlino, 2008). In humans, melanocytes do remain in the interfollicular space, and directly pigment the keratinocytes in the epidermis (Mort, Jackson and Patton, 2015). Epidermal and follicular melanocytes differ in several ways. Follicular melanocytes are larger, have a more developed Golgi and rough endoplasmic reticulum, and produce melanosomes which are 2-4 times bigger (Orfanos and Ruska, 1968). A single interfollicular melanocyte interacts with ~36 keratinocytes, whilst in the hair follicle the ratio is reduced to 1:5 (melanocyte: keratinocytes) (Figure 1.2.B.) (Fitzpatrick and Breathnach, 1963; Tobin and Paus, 2001). Interactions between melanocytes and the keratinocytes closest to the dermal papilla, located at the base of the hair structure, as an important regulator of the hair cycle (Morgan, 2014), reduces even further to an almost 1:1 ratio (Tobin and Paus, 2001).

1.1.6. Melanocytes

1.1.6.1. Pigment production

Melanogenesis is the process of producing the pigment melanin, for which the melanocytes are specialised. Melanin exists in two main forms in mammals – eumelanin which is a brownish black, and pheomelanin which is reddish yellow (Cichorek et al., 2013). The quantity, ratio and quality of these two forms affects the colour produced. Melanin is produced from the amino acid precursor L-tyrosine, via a carefully controlled chain of enzyme catalysed reactions. The main enzymes involved are tyrosinase (TYR), tyrosinase-related protein 1 (TRP1) and DCT. A representation of the pathways involved in melanogenesis is shown in Figure 1.2.C. Briefly – tyrosinase hydroxylates tyrosine to L-3,4-dihydroxyphenlalanine (DOPA) which is then oxidised to DOPAquinone (Lerner and Fitzpatick, 1953). To produce eumelanin, DOPAquinone is spontaneously cyclised to DOPAchrome (Körner and Pawelek, 1980). DOPAchrome loses carboxylic acid, forming 5,6-dihydroxyindole (DHI). Or, DCT will catalyse DOPAchrome formation to DHI-2-carboxylic acid (DHICA) (Duchoň and Matouš, 1967). These are then further catalysed to eumelanin (Olivares et al., 2001).

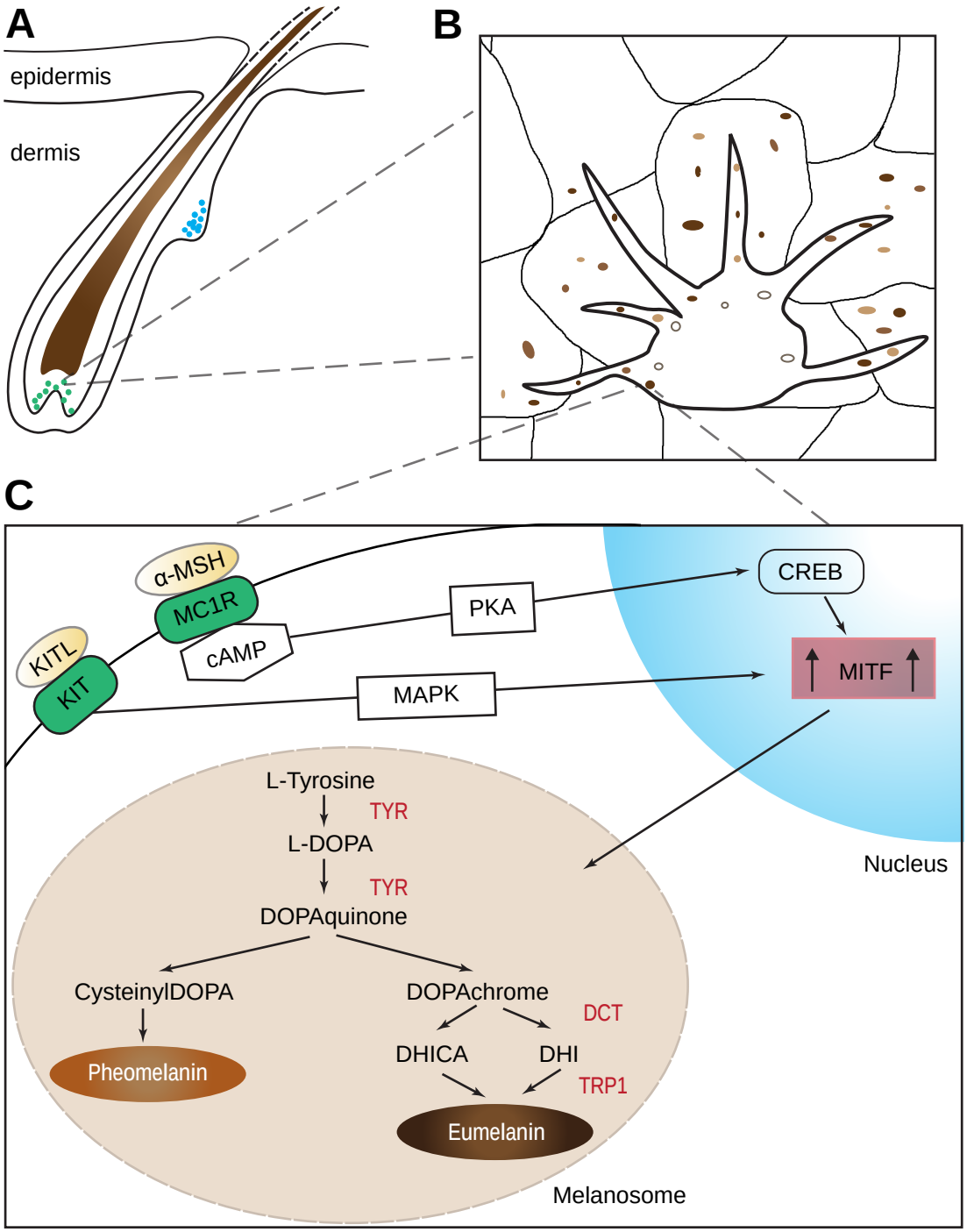

Figure 1.2. The hair follicle and pigmentation. A. The mature hair follicle extends deep in to the dermis. A stem cell resevoir of melanocytes resides in the bulge region (blue). Mature melanocytes are found in the hair bulb, and interact with the keratinocytes of the developing follicle (green). **B.** In the hair follicle, one melanocyte interacts with ~ 5 keratinocytes. Pigment is transferred via membrane bound melanosomes through dendritic processes. **C.** Stimuli from the surrounding environment induce melanogensis through several pathways. Two important pathways include signalling via KIT/KITL and the MC1R receptor. KIT/KITL signalling involves the MAPK pathway, while stimulation of MC1R receptors leads to cAMP activity and PKA activation. MITF is the master regulator of pigmentation and regulates expression of the melanocytic enzymes tyrosinase, TRP1 and DCT. Melanogenesis occurs within the melanosome, starting with L-tyrosine. The production of pheomelanin depends on the availabilty of cysteine.

To produce pheomelanin, the presence of cysteine leads to a reaction with DOPAquinone, causing oxidisation and polymerisation (Cichorek et al., 2013; Olivares et al., 2001).

Melanocytes produce and package melanin within lysosome-related organelles termed melanosomes. The whole melanosome unit is transferred to the keratinocyte/hair follicle. This act of transfer is a keen area of research in melanocyte biology, as the exact mechanism is still unknown (Ishida, Marubashi and Fukuda, 2017). Melanosomes travel down the melanocyte dendrites, and evidence suggests they pass to the keratinocyte via a filopodia mediated mechanism (Ma et al., 2014). Once in the keratinocyte, melanin can be observed covering the apical surface of the nucleus as a protective cap (Kobayashi et al., 1998). The melanosome unit itself goes through several stages of development – from a newly designated stage I melanosome situated near the Golgi, to mature stage IV melanosomes full of melanin in the melanocyte dendrites.

Melanogenesis can be induced via several pathways, including UV DNA (deoxyribonucleic acid) damage. The main regulator of melanogenesis is the Melanocortin 1 Receptor (MC1R), which is activated by α-melanocyte stimulating hormone (αMSH), and acts through cyclic AMP (cAMP). KIT/KITL signalling is another important interaction leading to activation of MITF. Regulation of MITF is achieved via pathways including the mitogen-activated protein kinase (MAPK) pathway and the phosphoinositide 3-kinase (PI3K) pathway (Hsiao and Fisher, 2014). MITF regulates the expression of the melanogenic enzymes discussed (Videira, Moura and Magina, 2013).

1.1.7. Melanoblasts and disease

Diseases involving one or more cell lineages derived from the NC are classified as neurochristopathies (Bolande, 1974). Due to the highly interlinked regulatory networks, neurochristopathies often involve more than one NC cell type, and as such there are many neurochristopathies where pigmentation defects are observed.

1.1.7.1. Developmental diseases

Genetic pigmentation defects can be broadly split into diseases that affect melanoblast development or those that affect pigment production. In a pigmentation disease such as albinism, there is a defect in the production of the tyrosinase enzyme, however the melanocytes themselves are not reported to have any phenotypic differences, and are present in the normal numbers (Boissy, Trinkle and Nordlund, 1989; Halaban et al., 1988). Other diseases however, are more directly related to the developmental pathways.

Piebaldism is a genetic disorder, typically presenting with unpigmented patches of skin in which no melanocytes are found. It is found across many species, including humans, horses, cats, dogs and cows to name a few.

There are a number of genes identified as having mutations causative of piebaldism, the primary associated gene being *Kit*. *Kit* related piebaldism is discussed further in section 1.3.3. However, *Kit* mutations do not account for all cases of human piebaldism. Some of the other genes that have been implicated have already been discussed, and are not surprising contributors given their role in melanoblast development. For example, a study in 2003 used Southern blotting to identify mutations in the *Snai2* gene in patients with non-*Kit* related piebaldism, and in fact the mouse knockout of *Snai2* also exhibits a white spotting phenotype similar to the *Kit* knockout mouse (Sánchez-Martín et al., 2003).

Other neurochristopathies where the melanocyte lineage is affected include Waardenburg syndrome, Neurofibromatosis type I, Hirschsprung's disease and congenital melanocytic nevi. Hirschsprung's disease is an excellent example of the parallels in regulatory pathways between the NC lines; mutations have been identified in genes such as *Ednrb* (endothelin receptor B), its ligand *Edn3*, *Sox10* and *Zeb2*, all of which play vital roles in melanoblast development (Bidaud et al., 1997; Puffenberger et al., 1994; Southard-Smith, Kos and Pavan, 1998; Wakamatsu et al., 2001). In Hirschsprung's disease, the enteric nerves do not migrate fully, so sections of the intestine and colon are left without nervous innervation, leading to clinical problems. Using the melanocyte lineage to study migration of NC cells is therefore

very useful. Changing gene expression in these candidates specifically in melanocytes leads to pigmentation defects, but these are not harmful to overall health. Observed behaviours can be linked back to the relevant cell line; this highlights the usefulness of the melanocyte line in research, and in applying results broadly to cells of NC origin.

1.1.7.2. Melanoma

Melanoma is a cancer arising from melanocytes. It is one of the biggest cancer groups in the Caucasian population, and although melanoma accounts for only 3 per cent of skin cancers, it causes more than 75% of skin cancer deaths (Ciarletta, Foret and Ben Amar, 2011). Prognosis is generally good, although as with many other cancers, this relies heavily on early diagnosis. Prognosis deteriorates significantly once malignancy is established; the majority of patients who do not have the tumour surgically resected before metastasis occurs will die in 6-10 months (Balch et al., 2001). Most melanomas will develop laterally to the basement membrane initially – so called ‘thin’ melanomas. Poorest prognoses are correlated with ‘vertical’ tumours, which have breached the basement membrane by degrading important proteins, and are more likely to metastasise (Schmoeckel et al., 1989).

1.1.7.2.1. Risk factors

The risk factors for developing melanoma are a complex mix, made up of interacting phenotypic, genotypic and sun exposure factors. Ethnicity and skin colour are a significant risk factor for developing melanoma, with the incidence of melanoma in non-Caucasians being significantly lower (Ribero, Glass and Bataille, 2016). If non-Caucasians do develop melanomas, it’s mainly found on the plantar surfaces (soles of feet and palms of hands), where the skin is the least pigmented. Another large risk factor is age, with occurrence in children being very rare (Stevens, Liff and Weiss, 1990). There is however, a correlation between sunburn in children and melanoma risk, suggesting that there is a long time period required for the disease to manifest post-damage (Dennis et al., 2008). Similarly, there is a link in the mouse melanoma model HGF/SF, where postnatal UV is administered to cause melanoma development in adult mice (Noonan et al., 2001; Takayama et al., 1996).

Further melanoma risk factors are difficult to quantify, as such a large proportion of risk is attributed to human behaviour. For example, individuals with the highest phenotypical risk factors of pale skin and red hair burn easily, and may therefore consciously spend less time sunbathing. Calculating their relative risk of melanoma may be compromised, because they are less likely to engage in the sun exposure that is dangerous, and thereby present less frequently. Another example may be in people who use sunbeds to promote skin tanning which have high UV radiation levels. Variances in correcting for factors like this in large cohort studies, has led to a wide array of data published over many years that rarely agrees on the risk contributions. An epidemiological study in 2005 was designed to accurately define risk factors for developing melanoma by meta-analysis (Gandini et al., 2005a, 2005b), and adjusting for human factors. After correction for the 'baseline' factors such as race and age, they showed that the number of naevi, and the type of sun exposure (chronic or intermittent) were the biggest risk factors.

1.1.7.2.2. Developmental mechanisms

Melanomas employ many of the migratory and proliferative pathways seen during NC development, and many of the genes discussed previously are found mutated in melanomas. Melanomas seem to be particularly effective at metastasising, perhaps due to the highly migratory and invasive nature of the melanoblast cells during development. These parallels observed in melanomas have supported the hypothesis that many cancers use 'hijacked' developmental programmes to grow and metastasise (Vandamme and Berx, 2014).

MITF again lies at the heart of the melanoma network. It is frequently overexpressed in human melanomas (Garraway et al., 2005). It is believed to act as a 'rheostat' – helping melanoma cells switch between invasive states dependent on expression levels (Hoek and Goding, 2010; Hsiao and Fisher, 2014). Low MITF expression leads to increased differentiation, reduced proliferation and increased invasiveness which aids tumour progression, while high MITF expression leads to more proliferation and differentiation (Carreira et al., 2006). The transcription factor BRN2 is also known to play a vital role in this model through repression of MITF

(Goodall et al., 2008), and intravital imaging shows that disseminating cells have high BRN2 expression (Pinner et al., 2009).

In support of the theory that cancers reactivate important developmental genes, are many melanoma studies identifying expression level changes in EMT genes. As in developmental EMT, interactions between the different factors in melanoma are complex, and not fully understood. For example, high SLUG expression is shown to be correlated with good prognosis (Caramel et al., 2013), but is also shown to function specifically in melanocytes promoting a strong metastatic ability (Gupta et al., 2005). Activating mutations in BRAF are believed to be a main cause of this reprogramming of EMT genes, by increasing signalling in the MAPK pathway (Caramel et al., 2013). Mutations in *BRAF* occur in ~50% of melanomas (Hodis et al., 2012). Other mutations occur in pathways linked to the MAPK pathway, including in *Kit* (discussed later) and NRAS (Hodis et al., 2012).

Although these pathways employ many of the same genes as in development and exhibit parallels in behaviour, there are also important differences as may be expected. For example, when comparing the biological process of breaching a basement membrane, melanoma cells rely on matrix metalloproteinases (MMPs) (Li et al., 2010), whereas melanoblasts do not (Li et al., 2011). This is an important biological event; melanoma cells invade the basement membrane during metastasis, and melanoblasts invade the basement membrane in early development to progress from the dermis to the epidermis.

1.2. The skin

The skin is a complex organ with many component parts. It is the primary environment for the developing melanoblast and differentiated melanocytes, and as such is vital in studying the development of the lineage. Increasingly, biologists are looking to integrate study of cell with their environment, as there is so much interaction; cells do not act alone, and are constantly receiving stimuli and instruction from the surrounding environment, in particular through the extracellular matrix (ECM) (Hansen et al., 2015; Pillet et al., 2017). Melanoblasts/melanocytes are part of

the skin as a whole organ, and research must try to reflect this fact, or risk being biologically irrelevant. The skin is broadly composed of two layers – the epidermis apically and the dermis basally. These two structures are intrinsically linked via a basement membrane, but are composed of entirely different cells and originate from different germ layers (Fuchs, 2007). Skin in adult mammals has been studied extensively, from research into wound-healing and genetic diseases such as eczema, and often concentrate on the involvement of the inflammatory response. However, developmental study of how the structures come to exist, particularly in early-development, is not as highly researched.

1.2.1. The epidermis

The epidermis is a specialised structure, composed of many layers of keratinocytes at various points of differentiation, which gives rise to the classic stratified structure. It is ectodermal in origin (Van Exan and Hardy, 1984), and covers the embryo after neurulation. The initial, single layer of cells is characterised by early expression of cytokeratins K8/K18 (Byrne, Tainsky and Fuchs, 1994). At around E9.5, expression of the major keratins K5/K14 become detectable, which marks the event of epidermal commitment, and these keratins continue to be the major marker of the epidermal/dermal basement membrane from this point (Byrne, Tainsky and Fuchs, 1994). The basal membrane which separates the epidermis from the dermis, is composed of a proliferative layer of keratinocytes and keratinocyte stem cells. At around E14, a layer of cells forms above the basement membrane, known as the suprabasal layer. The commitment of cells to leave the basal layer and begin the stratification process, and also for new cells to ascend the stratified layers is controlled by canonical Notch signalling (Blanpain et al., 2006). The suprabasal layer then becomes the spinous layer post initial development, and is characterised by the expression of K1/K10 (Smart, 1970). Keratinocytes in the layer above this, the granular layer, loose their nuclei and begin to excrete lipids, to form an impermeable barrier, aided by involucrin and transglutaminase (Koster and Roop, 2007). The final layers of keratinocytes are those in which the cells have terminally differentiated into specialised cells known as corneocytes. The upper layers are the stratum lucidum and stratum corneum, where expression of filaggrin and loricrin is seen (Koster and

Roop, 2007). The cells in these layers are flat and surrounded by proteins and lipids which maintain the barrier function of the epidermis, but the cells themselves are considered ‘dead’ as they have no organelles at this point. Cells at the surface are constantly shed, and replaced by cells below; the process of cells moving up the layers is called desquamation. By birth, the epidermis is fully formed, and able to function in its capacity as a barrier to the external environment. In synchrony with the development of the skin layers vertically, there are several appendages which form from the basal layer including sweat glands and hair follicles, which will be discussed further.

The epidermis develops due to stimulation from various factors in addition to Notch. The first is transforming growth factor-α (TGF-α) which acts in an autocrine manner to stimulate cell division in the basal layer (Gilbert, 2000). Conditions such as psoriasis are linked to over-expression of TGF-α, where there is vast overproduction of epidermal cells (Elder et al., 1989; Vassar and Fuchs, 1991). Another important growth signal is a paracrine factor produced by the dermis below, known as keratinocyte growth factor (KGF) (Gilbert, 2000).

1.2.2. The dermis

The dermis is the lower part of the skin, formed of mesoderm tissue (Van Exan and Hardy, 1984). It is much thicker than the epidermis, and is made of connective tissue, whose major cell type is the fibroblast. Fibroblasts are mesenchymal, but for a cell type that is a major contributor to tissues throughout the body, surprisingly little is known about their development, although they are now known to develop from two distinct lineages (Driskell et al., 2013). They are generally believed to be undifferentiated, due to the lack of any specific markers. In a tissue there is functional heterogeneity of the fibroblast cells, which makes isolating their precursors to characterise difficult (Shamis et al., 2011). The dermis is subdivided into the upper dermis, where the hair follicle is located, and the lower dermis, with these layers developing from the separate lineages. The lower dermis is responsible for initiating wound healing, and the upper dermis is only involved when the epidermis is being re-formed (Driskell et al., 2013).

1.2.3. Hair development and cycle

Hair follicles form from the epidermis, although the structure is physically located deep within the dermis (see Figure 1.2.A.). At around E16, keratinocytes of the basal layer aggregate to form hair placodes, in response to Wnt signalling from the dermal cells below (structures known as the dermal condensates) (van der Veen et al., 1999). These aggregates then proliferate downwards, into the dermis - all the time maintaining the basement membrane between the two layers. The structure develops into various components including the inner and outer root sheath, the matrix and the hair shaft until the hair follicle is fully formed by P6 (van der Veen et al., 1999). Melanocytes are found at the base of the follicle, to provide melanin to the growing hair, and also in the bulge. When a hair is shed, the entire hair shaft is lost, including the melanocytes. They are replenished for a new hair cycle by the bulge, in which resides a stem cell pool of melanoblasts (Nishimura et al., 2002). These migrate down to the developing hair, and hair shaft precursors when required. Melanin produced in the hair shaft is minimally digested, so the whole hair can be pigmented (Bell, 1967).

The adult hair cycle is a complex process, governed by interaction between signalling pathways including Wnt, Hedgehog, Notch and BMP (Rishikaysh et al., 2014). Hair growth is a cycle which goes through active and quiescent periods. There are 3 main phases in the cycle: anagen is the growth phase where there is rapid proliferation of cells in the hair bulb. Catagen is the regression phase, where differentiation of hair shaft cells ceases, and apoptosis of the hair structures occurs. Telogen is the final stage, where the hair follicle is in its quiescent resting phase (Lang, Mascarenhas and Shea, 2013). In mice, the first hair cycle is synchronous between follicles, but becomes progressively more asynchronous in successive cycles. In an adult, the majority of hair follicles will be in anagen at any given time. The dense packing of hair follicles in mice binds the epidermis and dermis very tightly during the growth stages making it difficult to separate the layers (Pasparakis, Haase and Nestle, 2014).

1.2.4. The ECM

The ECM of the skin is discussed most frequently with regards to the basement membrane between the epithelial and mesenchymal layer, although both the epidermis and dermis also produce separate and vital ECMs. The ECM of the skin establishes some key characteristics of the skin as an organ; namely that it is impenetrable (minus wounding) and strong, but also flexible and pliable. Collagen fibres provide a large portion of these properties, and their deposition has been well studied. There are over 40 different collagen related genes, and 28 types of collagen (Gordon and Hahn, 2010; Krieg and Aumailley, 2011). Collagens are grouped based on the number and length of the triple helix domains that they possess, which is core to their secondary structure. The five sub-groups are fibril-forming, micro-fibrillar, network-forming, transmembrane collagens, and fibril-associated collagen with interrupted triple helix (FACIT) (MacFie, Light and Bailey, 1988). These groups of collagen provide the main structural architectures which can be seen when observing ECM deposition. Other important 'core' components of the ECM include the proteoglycans hyaluronic acid, keratan sulphate, chondroitin/dermatan sulphate, and heparan sulphate, the laminin family of proteins, elastin and fibronectin (Yue, 2014).

1.2.4.1. Dermal ECM

In the dermis ECM, the primary collagens are collagens I and III (Watt and Fujiwara, 2011), which are classed in the fibril-forming collagen group. As mentioned, the dermis is further divided into sublayers, which also differ in their ECM composition. The upper layer is also known as the papillary layer, and has thin collagen fibres, whilst the lower layer, or reticular layer, has dense collagen fibres. The collagen fibres provide an important scaffold for securing other ECM proteins. The links between the collagens and other ECM molecules are believed to regulate the formation of new fibrils, and determine their size, diameter and spacing (Gordon and Hahn, 2010).

1.2.4.2. Epidermal ECM

It was long believed that the outermost layer of the epidermis, composed of 'dead' keratinocytes, merely provided an inert physical barrier, and that all important processes were undertaken at deeper skin levels. It is now recognised that the stratum corneum contributes significantly to the overall protection role of the skin, even though the cells are lacking in organelles. In particular, the ECM surrounding cells in the outermost layer of the epidermis is designed to fulfil protective roles. The ECM is rich in free fatty acids (FFA) and sphingosine which exhibits potent antibacterial, antiviral and antifungal activity (Bibel, Aly and Shinefield, 1992; Miller et al., 1988; Wille and Kydonieus, 2003). The ECM helps maintain the structural integrity of the skin; the junctions between cells in the upper layers that provide integrity are known as corneodesmosomes. These are composed mainly of desmosomal cadherins, and are immobilised in the ECM at the cell junctions by enzymatic cross-linking (Haftek et al., 1991; Hitomi, 2005). Additionally, cells in the granular layer produce corneodesmosin, a glycoprotein which embeds within the desmosomes to reinforce the junction (Haftek et al., 1997; Serre et al., 1991). For cells to be shed by desquamation, these ECM components must be degraded. Corneocytes are surrounded by an insoluble envelope, comprised primarily of loricrin and involucrin (Steven and Steinert, 1994). Attached to this envelope, are ceramide lipids which maintain the skins impermeability (Marekov and Steinert, 1998).

1.2.4.3. The basement membrane

A major structure in the skin is the basement membrane which forms between the dermis and epidermis. Historically, it was thought that it was primarily produced by the keratinocytes of the epidermis, but it is now known to be produced by a combination of the keratinocyte and fibroblast cells (Marinkovich et al., 1993). This is supported by evidence from wound healing experiments, showing that both layers from either side of the wound must function to ensure the new basement membrane is formed. Keratinocytes and fibroblasts communicate with each other in paracrine signalling loops to co-ordinate their actions in response to inflammatory signals (Schultz et al., 2011).

Basement membrane structures throughout the body contain a few proteins ubiquitously, for example collagen IV. Collagen IV is a network-forming collagen, and is also known as basement membrane collagen. The 3D (3-dimensional) supramolecular structure is described as resembling chicken wire due to its diamond pattern, formed from laterally connecting 2D (2-dimensional) molecules (Barge, Ruggiero and Garrone, 1991; Yurchenco and Ruben, 1988). The largest non-collagenous component of the basement membrane are laminin proteins. Laminin is required for the assembly of the basement membrane, and like collagens, form structural networks. Laminins are also known to have properties for controlling cell adhesion, migration and polarity (Aumailley and Smyth, 1998; Terranova, Rohrbach and Martin, 1980).

1.3. KIT and KITL

KIT and KITL play an integral role in the development of the melanoblast, erythrocyte and gamete lineages. KITL is also known as stem cell factor (SCF), mast cell growth factor and steel factor. KITL is expressed by keratinocytes in the microenvironment, whilst KIT is expressed by melanoblasts.

KIT is a member of the large type II receptor tyrosine kinase family. KIT has two major isoforms, formed by alternative splicing, that differ in the absence or presence of a GNNK tetrapeptide sequence in the extracellular juxtamembrane region (Hayashi et al., 1991). Both isoforms are co-expressed in most tissues, with the -GNNK version usually found in higher quantities although ratios between the isoforms varies by tissue (Crosier et al., 1993). A study conducted in NIH3T3 cells demonstrated that upon KITL stimulation, the predominant -GNNK isoform underwent higher tyrosine phosphorylation and faster internalisation post-activation, than the +GNNK isoform (Caruana, Cambareri and Ashman, 1999).

KITL also has two major isoforms with different functions, although both stimulate the same receptor. One isoform is cleaved readily from the cell membrane, and is termed soluble KIT ligand (sKITL). The other isoform is initially bound to the cell membrane, and is termed membrane-bound KIT ligand (mKITL). It is cleaved more

slowly from the membrane via a less efficient cleavage site (Majumdarsb et al., 1994). sKITL is reported to produce rapid and transient activation of the KIT receptor, whilst mKITL activation is sustained for longer (Miyazawa et al., 1995). It is hypothesised that this is due to mKITL being anchored to the cell membrane, thereby inhibiting internalisation of the KIT/mKITL complex which occurs once activation has completed (Rönnstrand, 2004). There does not appear to be any discernible difference between the affinity of either isoform of KITL binding of the receptors (Caruana, Cambareri and Ashman, 1999).

1.3.1. Mouse mutations

1.3.1.1. The *W* locus

Mice presenting with the dominant white spotting phenotype (*W*) were first described in 1908 (Durham, 1908), and were of genetic interest for 80 years before the gene product was identified as the KIT receptor (Geissler, Ryan and Housman, 1988). Two alleles are most often described, both arising from spontaneous mutations. First, Kit^{W} is a guanosine to adenosine substitution that produces different mutant transcripts with significant deletions due to exon skipping (Hayashi et al., 1991). Kit^{W} mice are sterile with no pigmentation, and die perinatally due to anaemia (de Aberle, 1927), which is detectable by E12.5 (Russel, Thompson and McFarland, 1968). $Kit^{W/+}$ mice show only pigmentation defects, with white spotting and irregular dispersal of unpigmented hairs (Dunn, 1937), and do not show deficiencies in the gametes or erythrocytes (Grüneberg, 1942). The Kit^{W-v} (viable dominant spotting) allele was described in 1937 (Little and Cloudman, 1937), and is a threonine to methionine substitution (Cable, Jackson and Steel, 1995). Kit^{W-v} are viable for weeks after birth, with some animals surviving to adulthood (de Aberle, 1927). These mice have unpigmented coats, although some pigment may be present on the ears (Little and Cloudman, 1937). In addition, some strains are anaemic, males are sterile and females have a greatly reduced number of oocytes (Kissel et al., 2000; Mintz and Russell, 1957; Russell, 1949). $Kit^{W-v/+}$ mice have a diluted coat colour which is not seen in $Kit^{W/+}$ mice. A common presentation in mice with heterozygous *Kit* mutations is of unpigmented patches of skin on the belly – the most ventral location

from the origin of the NC melanoblasts. Unpigmented patches in these mutants have no melanocyte population (Jordan and Jackson, 2000b).

1.3.1.2. The *Steel* locus

The Steel phenotype (*Sl*) arose from inbreeding of the C3H strain (Sarvella and Russell, 1956). KITL was identified as the protein coded for at the *Sl* locus in 1990 (Zsebo et al., 1990). The $Kitl^{Sl}$ allele has a deletion encompassing the majority of the coding region (Zsebo et al., 1990). $Kitl^{Sl}$ mice are embryonic lethal, also due to anaemia (Sarvella and Russell, 1956). Conversely, $Kitl^{Sl/+}$ mice have normal lifespans and a relatively mild phenotype; they have a diluted coat colour, an unpigmented belly spot and lack of pigment at the extremities of the feet and tail (Bennett, 1956). The two models were always linked due to their similar phenotypes, and hypothesised to be a receptor/ligand pair long before it was proven by Zsebo *et al*. (1990).

1.3.2. Biological function in development

Many mutations at the *W* and *Sl* loci have been described in addition to those detailed above. The three main lineages affected in the *W* and *Sl* mouse series are erythrocytes, gametes and melanoblasts, although KIT and KITL are not expressed exclusively in these cells (Bernex et al., 1996; Yue et al., 2014). Early in the studies of KIT and KITL mutants, it was noted that the affected lineages all undergo extensive migration paths during development, and so early hypotheses believed KIT/KITL interactions functioned specifically to direct and guide migration. The developmental roles of KIT/KITL signalling are more diverse than this however, and have been best studied in haemopoiesis – it is vital for the maturation, proliferation and survival of some blood cells (Kapur and Zhang, 2001), and in some subtypes it has to be shown to have chemoattractant properties (Meininger et al., 1992). There is also a wealth of evidence for similar roles during gametogenesis, where a local KITL expression has been shown to direct migration of the cells both during development and in subsequent meiotic events (Bialas et al., 2010; Hutt, McLaughlin and Holland, 2006). In embryonic stem cells (ES), KIT/KITL pathways are involved in

suppressing apoptosis in the differentiating cells, thereby promoting survival (Bashamboo et al., 2006).

As discussed previously, KIT/KITL signalling is known to be vital in early melanoblast development and in final localisation steps to the hair follicle. However, further to this, KIT/KITL is required for the survival, migration and proliferation of cells in mid-development. The mechanisms of action, and the biological function in between the MSA and the hair follicle stages is not fully understood. Whilst KITL is known to have chemoattractant properties in other lineages, data shows that KITL promotes migration to the hair follicle, it is not in a chemoattractant manner (Jordan and Jackson, 2000a). This was demonstrated using slow-release Affi-Gel beads coated in sKITL, and sKITL added directly to culture medium; in both experiments there was ~ a two-fold increase in the number of melanoblasts localised to the hair follicles, but no melanoblasts localised to the beads in the first (Jordan and Jackson, 2000a). KITL has been shown to alter the interactions of human melanocytes with some ECM proteins, and thereby alter properties of adhesion and migration, by regulating levels of integrin (Scott et al., 1994). In haematopoiesis, KITL is reported to induce adhesion of cells with fibronectin, again through integrin (Broudy, 1997). It is also hypothesised that the interaction of KIT with mKITL may help anchor cells to the surrounding fibroblast environment (Kurzrock, 2003).

In adults, KIT/KITL signalling is involved in the maintenance of melanogenesis in successive cycles of anagen (Hachiya et al., 2009). KITL is not expressed in the adult mouse epidermis of the trunk, whilst it is in humans, possibly indicating a role in maintaining the interfollicular melanocytes there (Longley and Carter, 1999).

1.3.3. Mechanism and signalling pathways

KIT receptor activation is achieved by the simultaneous binding of two KITL molecules to two KIT receptor molecules (Lev, Yarden and Givol, 1992). This dimerisation activates the autophosphorylation of specific tyrosine residues on KIT (Blume-Jensen et al., 1991; Lev, Yarden and Givol, 1992). The phosphorylated residues allow docking of signalling molecules. Signalling molecules which bind to

the tyrosine residues dock due to the presence of either a phosphotyrosine binding domain (PTB) or Src Homology 2 (SH2) (Masson et al., 2006; Wagner et al., 2013).

1.3.3.1. Downstream of KIT/KITL

There are 3 main signalling pathways that are triggered by activation of KIT. These are the PI3-K, MAPK and Src family kinases (SFKs) pathways. The PI3-K pathway is well studied, and in melanocyte biology is believed to be involved in promoting survival of the lineage (Blume-Jensen, Janknecht and Hunter, 1998). The major target of PI3-K is the serine/threonine-specific protein kinase Akt (also known as protein kinase B (PKB)). Akt is believed to be a key determinant in apoptosis, where it promotes cell survival (Oka et al., 2004). In mast cells, the PI3-K pathway is also known to regulate cell migration and proliferation through KIT signalling (Vosseller et al., 1997). The MAPK pathway is also well studied, and known to be vital for melanoblast proliferation, differentiation and survival. The main MAP-kinases involved are Erk1/2, which are activated after KIT phosphorylation, through a protein kinase cascade (Liang et al., 2013). Ultimately, the activated Erk1/2 targets multiple transcription factors to exert control over cellular functions (Whitmarsh, 2007). Finally, signalling to SFKs are again thought to be important in survival, proliferation and migration, as well as a role internalising KIT after signalling (Broudy et al., 1999). Interactions with phosphorylated residues on KIT cause a conformational change in SFKs which increases catalytic activity (Lennartsson and Ronnstrand, 2012). The response of the isoforms of KIT to KITL stimulation have been shown to be a result of their ability to activate SFKs (Voytyuk et al., 2003).

1.3.3.2. Downregulating KIT signalling

KIT activity can be modulated in a number of ways. The receptor can be internalised and degraded, the kinase domain can be dephosphorylated and the specific tyrosine residues can also be dephosphorylated (Lennartsson and Ronnstrand, 2012). Degradation of the receptor (after binding of KITL) is suggested to occur by targeting to the lysosomes via E3 ligase mediated ubiquitination, once it has been internalised (Haglund et al., 2003). KIT is also under negative feedback regulation, through the protein kinase C (PKC) family. KITL stimulation leads to activation of

phospholipase D, which further leads to the release of phosphatidic acid, a precursor of DAG (diacylglycerol) which activates PKCs. PKCs phosphorylate residues in the kinase insert region of KIT, which prevents further kinase activity (Blume-Jensen et al., 1994). Mutating these residues (S741 and S746) results in increased KIT activation (Blume-Jensen, Janknecht and Hunter, 1998). The protein tyrosine phosphatase (PTP) SHP1 has been shown to bind and supress KIT signalling in haematopoietic cells, and other PTPs likely function in melanocytes (Lennartsson and Ronnstrand, 2012; Lorenz, 2009).

1.3.4. KIT/KITL signalling and disease

1.3.4.1. Developmental diseases

The effect of mutations in *Kit* or *Kitl* mutations in mouse mutants is predictable and consistent in either the dominant white spotting (*W*) or steel (*Sl*) mouse phenotypes respectively. Mice present with a white belly spot, which has not been colonised by melanoblasts during development. The centre of the belly is the furthest area that melanoblasts must reach, having begun their journey on the dorsal midline. In $Kit^{W/+}$ mice, the rest of the coat shows normal pigmentation, while $Kitl^{Sl/+}$ have a diluted coat colour (Bennett, 1956; Dunn, 1937). As there is no sign of melanoblast apoptosis, it is hypothesised that for an unknown reason, the melanoblasts do not migrate far enough during development (Mort, Jackson and Patton, 2015).

In humans, the pigmentation disease piebaldism has been shown to be caused by heterozygous mutations in *Kit*, presenting in an autosomal dominant manner (Giebel and Spritz, 1991). Patients present clinically with white patches of skin, commonly including a patch on the forehead – the congenital white forelock. Patches are present from birth, and generally remain stable throughout life (Oiso et al., 2013). The first mutation was identified by Giebel in 1991, and over 60 other mutations have since been described (Giebel and Spritz, 1991; Oiso et al., 2013). The severity of the phenotype correlates to the mutation severity. The mildest mutations/phenotypes occur in the N-terminal domain, and the most severe in the tyrosine-kinase domain (Richards et al., 2001). Mutations severity, and therefore phenotype, correlate with haploinsufficiency, with mild mutations exhibiting 50% of normal KIT function,

while the severest mutations preserve only 25% of KIT function, due to dominant-negative inhibition (Oiso et al., 2013). Conversely, gain of function mutations in *Kitl* have been implicated in a rare hyperpigmentation disorder (Wang et al., 2009).

1.3.4.2. Cancers

Kit and *Kitl* expression changes in adults have been reported in various cancers, including but not limited to, lineages of NC origin. Loss of *Kit* expression has been associated with melanoma, breast cancer and thyroid cancer (Franceschi et al., 2017; Montone et al., 1997; Talaiezadeh, Jazayeri and Nateghi, 2012). Overexpression of KIT and KITL have been reported in melanoma, colorectal cancer, breast cancer, small cell lung carcinoma, gastrointestinal tumours and neuroblastomas (Bellone et al., 1997; Hines et al., 1995; Hirota et al., 2001; Inoue et al., 1994; Krystal, Hines and Organ, 1996). Interestingly, these have often been found to have developed positive feedback loops leading to constant and autonomous stimulation between the receptor and ligand. In a small cell lung carcinoma study, the number of tumours that this KIT/KITL loop was reported in was as high as 70%. The study demonstrated that inhibiting this mechanism reduced the capacity of the cancer cells to grow, indicating a substantial role of this interaction in disease progression (Krystal, Hines and Organ, 1996). Other studies have also reported that blocking KIT/KITL activity inhibits tumour growth (Kuonen et al., 2012; Olgasi et al., 2014).

Kit mutations are driver mutations in melanomas (Hodis et al., 2012), but only account for a small patient group (2-8%) (Beadling et al., 2008; Curtin et al., 2006; Willmore-Payne et al., 2005). Clinically, melanomas are further subdivided by area of presentation, and are increasingly viewed as distinct cancers. *Kit* mutations are found in much higher frequency in some of these subcategories. For example, one study found activating mutations in *Ki*t in 39% of mucosal melanomas, 36% of acral melanomas, and in 28% of melanoma in chronically sun damaged skin (Curtin et al., 2006). Others have also reported elevated rates of mutations in these subtypes (Beadling et al., 2008).

Specific mutations of *Kitl* in melanoma have not been reported, despite the often elevated levels of expression. A pivotal study in oncology, however, associated *Kitl*

with cancers through p53. Zeron-Madina *et al.* reported a polymorphic SNP (single nucleotide polymorphism) in the p53-RE (p53-response element) of *Kitl*, identified through a genome-wide association study (GWAS) (Zeron-Medina et al., 2013). P53 is described as the "guardian of the genome", acting on a range of targets to control many cellular processes related to cancer, including DNA repair, cell cycle, apoptosis and senescence (Lane, 1992). P53 binds to targets through a consensus sequence that is well defined – the response element (Wang et al., 2010). The SNP discovered in the *Kitl* p53-RE alters the functional ability of p53 to bind to and regulate transcription of *Kitl*. The group report that the SNP "associates with one of the largest risks identified among cancer genome-wide studies", and that there is evidence of evolutionary selection to maintain the change, despite evidence that other SNPs in p53-REs are rare and considered unfavourable (Zeron-Medina et al., 2013).

1.4. Current methods of studying melanoblast behaviour

1.4.1. In vivo studies

Mouse models of pigmentation diseases exist either through spontaneous mutations (e.g. the Kit^{W} or $Kitl^{Sl}$ mice) or through genetic engineering. Genetic engineering can be used to great effect, whether it be in developing a specific reporter line, or modelling specific disease mutations. Mouse models designed to recapitulate human disease mutations directed at the melanocytes are predominant, for reasons discussed previously. With the emergence of new tools for introducing mutations, for example the CRISPR/Cas9 system (Clustered Regularly Interspaced Short Palindromic Repeats/CRISPR-associated protein-9 nuclease), creating models with specific mutations is becoming increasingly practical. The use of inducible models combined with the Cre/Lox system, allow temporal and spatial control of gene expression and visualisation *in vivo*. The classical melanocyte models use components of the melanogenesis pathways as cell specific markers. These are usually *Dct* or *Tyr* based and have been described many times in line with the continual development of Cre

recombination, to the current models which use the CreERT2 recombinase to control gene expression via tamoxifen (Bosenberg et al., 2006; Delmas et al., 2003; Feil et al., 1997; Guyonneau et al., 2002). In this thesis, we use a novel mouse with the melanoblast specific marker, *Pmel*, to isolate melanoblasts in the skin (Mort et al., 2016).

One of the most effective, and widely used techniques to study early melanoblast development uses the LacZ reporter assay. Again, the LacZ gene is commonly combined with *Dct* or *Tyr* in transgenic lines (Mackenzie et al., 1997). LacZ expression is then examined histopathologically by staining for the product of LacZ, β-galactosidase, using X-gal (5-bromo-4-chloro-3-indolyl--D-galactoside) (Burn, 2012). It is useful for studying melanoblasts *in situ*. For example, this technique has been used to count the number of melanoblasts at various stages (Luciani et al., 2011). The main disadvantage of this technique is the inability to study cells in real time.

In melanoma research, *in vivo* studies range from studying the development of the disease, to testing therapeutic agents. Xenograft models, where human cells are transplanted into a mouse are commonly used to study the original metastatic events (McKinney and Holmen, 2011). Studying human cells, and human mutations is obviously clinically relevant, however the mix of human cells in mouse tissues is not ideal. Xenografts in immunocompromised mice, are implants with either cloned cancer lines, or more recently patient derived tumour xenografts (PDTX) (Kuzu et al., 2015). Although useful in studying metastatic events, a major drawback is the lack of immune system interaction which is vital in a comprehensive model, and can be particularly important if using models for drug discovery or testing (Pickup, Mouw and Weaver, 2014). Syngeneic mouse models also exist with either the introduction of whole tumours or a cancerous cells. Tumours found in immune-compromised mice are transplanted onto mice with functional immune systems, to address the need for an appropriate immune response (Kuzu et al., 2015). The main disadvantages to this technique is that the tumour has already formed, so are not good models for studying initiation events. The most prevalent syngeneic cell models use B16 murine melanoma cells. These cells form tumours spontaneously and

metastasise in vivo (Kuzu et al., 2015). One common subclone is B16F10, which is highly metastatic and causes death in the mice by ~4 weeks post-transplantation (Fidler and Nicolson, 1976; Gehlsen and Hendrix, 1986; Kuzu et al., 2015).

1.4.2. Ex vivo studies

Explant cultures of mouse skin are a popular method which are used to separate the organ or structure of interest; they are generally easy to isolate, and can be maintained in culture for a number of days. The caveat, however, is that isolating the skin is limited to later development – removing the skin from an embryo at E13.5 is technically challenging, and is it difficult to keep the tissue intact. Removing the skin whole before E13.5 is impossible. This is a limitation to *ex vivo* techniques in melanoblast development, as a large portion of the dermal migration has finished by this point. An *ex vivo* technique developed by Mort *et al.* has allowed study of the developing melanoblast population using live-imaging (Mort et al., 2014). The technique expands on previous methods of explant cultures, by developing an inverted confocal microscope-compatible culture chamber with an air-liquid interface (ALI). Crucially, it allows tracking of the cells in real time, and has been used to measure cell behaviours including migration and proliferation. The disadvantages of this technique are the limited time window in which it can be performed. The ideal age is E14.5, when the skin is easily dissectible, but the skin remains thin enough to be transparent. After E15.5, the skin becomes difficult to penetrate by microscopy.

Traditionally, NC migration events have also been studied via neural tube explant cultures. The developing neural tube can be microdissected from the embryo, and maintained for days in culture (Girdlestone and Weston, 1985; Loring, Barker and Erickson, 1988). Using this technique, various cell behaviours can be examined, including but not limited to, migration, proliferation and differentiation status. Loring *et al.* describe a clustered population of cells on neural tube explants, which when cultured further differentiate into melanocytes (Loring et al., 1981). Building on the original neural tube methodology, researchers have refined and developed the protocols to isolate as pure a population of the NC as possible, while maintaining the

structure (Pfaltzgraff, Mundell and Labosky, 2012). The obvious disadvantages to NC explants is the lack of a microenvironment to migrate within, which is undoubtedly essential.

An overall disadvantage of any *ex vivo* study is that it is difficult to predict whether the organ/cells would function in the same way, had they been part of the whole organism. For example, there are many examples of long range cues in development, including signalling from the dermis to induce melanoblast migration *in vivo* (Tosney, 2004). The burden of this disadvantage probably varies by system, as indeed in the two *ex vivo* cultures described here. In the skin explant, local melanoblast behaviour is likely to reflect the *in vivo* behaviour accurately because the microenvironment is intact, although there remains the possibility that there are influences upon the skin that are lost. In the NC explant cultures, there is complete loss of the environment, which could have a major impact on the cells behaviours. It is therefore vital for researchers to determine what questions their chosen method can explore.

1.4.3. In vitro studies

In vitro models provide a great deal of flexibility that is not achievable when working with animals. The diversity in the assays that have been developed reflect this. As in animal models, *in vitro* models can be genetically engineered with increasing ease, with *in vitro* tools being particularly valuable for looking at mutations which have harmful effects, for example homozygote Kit^{W} or Kit^{Sl} which are lethal (de Aberle, 1927; Sarvella and Russell, 1956). Complex biological hypotheses can be broken down into component questions, using separate experiments to identify single outcomes. Migration for example, can be studied in multiple ways, in assays that can be modified to a specific need. Experiments could be performed using a chemotaxis chamber to look at migration events in response to a chemoattractant gradient. Then, using a scratch-assay, migration could be looked at in response to signalling in an immune response. Using multiple assays then allows researchers to combine different results to reach conclusions.

As mentioned, the number of melanoblasts present during early development is very small, and remains under 10,000 cells by E14.5 (Luciani et al., 2011). This presents challenges for a number of experiments, including when trying to isolate genetic material or proteins from this population. Selective cultures of melanocytes/melanoblasts following epidermis dissection can be a useful tool as a pure population can be isolated, then immortalised for further study (Sviderskaya, Wakeling and Bennett, 1995). Expansion of these cells can then provide the material needed and the ability to repeat experiments without introducing variation between individual mice. Numerous cell lines for the study of melanocytes have been established. Both melanoblast and melanocyte lines have been isolated from wildtype mice, and mice with mutations leading to various pigmentation diseases. A principal cell bank dedicated to pigment cell biology is maintained and run in association with the Wellcome Trust, and is the source of the three melanoblast cell lines in this thesis which will be introduced in Chapter 3.

1.5. Project aims

The National Centre for the Replacement, Refinement and Reduction of Animals in Research (NC3Rs) provided the funding for this PhD project. This organisation supports and promotes research which focuses on reducing the use of animal models, or which aims to improve animal welfare. The mouse has been at the core of pigment cell research for generations due to the ability to observe pigmentation patterns in the fur as a direct outcome of genetics, and the fact that mutations targeted specifically to the melanoblast/melanocyte cells do not cause adverse health effects. This project addresses two of the principals of the NC3Rs; replacement and reduction. *In vitro* tools can be used to directly replace *in vivo* experiments, if they are deemed effective. *In vitro* tools further allow biological data to be collected on a subject before explorations begin in animals – this both reduces the amount of animals used by refining the hypothesis, and also provides more background evidence that the animal study could lead to useful data; this can be an important factor in gaining ethical approval for animal research. At all points in animal research, their use must be fully justified.

In accordance with the principles of the NC3Rs, the objectives and biological questions explored in this thesis are as follows;

1. To develop novel *in vitro* tools to explore melanoblast development in a relevant environment.

2. To investigate the interactions of KIT and KITL, as key factors necessary for melanoblast development.

3. To investigate the changes in melanoblast gene expression during their early development using a novel mouse reporter line.

4. To investigate whether transformed melanoblast cell lines are reliable *in vitro* models.

Chapter 2

Materials and Methods

2.1. Microbiology methods

2.1.1. Bacterial transformation

Transformations were performed in DH5α *E.coli* cells; either subcloning (SC) efficiency cells for routine applications or library efficiency (LBE) cells for more difficult cloning steps (both Invitrogen). For SC cells, 50µl (microlitres) DH5α cells were incubated with ~1ng (nanogram) plasmid for 30 minutes (mins), before heat shock at 42^{o}C (degrees Celsius) for 20 seconds (secs). For LBE cells, 100µl DH5α*E.coli* cells were incubated with ~1ng plasmid for 30 mins, before heat shock at 42^{o}C for 45 secs. Cells were incubated on ice for 2 mins to recover. Cells were then supplied with pre-warmed LB (Luria-Bertani medium) or SOC (Super Optimal broth with Catabolite repression) (SC-950µl LB, LBE-900µl SOC), and placed in a shaking incubator for 1hour (hr) at 37^{o}C. Cultures were spread on pre-warmed L-agar plates, containing the appropriate antibiotic selection, in various amounts (50µl, 200µl and the remaining culture). Plates were incubated inverted, overnight at 37^{o}C, and checked the following morning for bacterial colonies.

LB and L-agar plates were pre-made by the Institute of Genetics and Molecular Medicine (IGMM) core technical services team to the following recipes; LB medium – 10g/L (grams per litre) NaCl, 10g/L Tryptone, 5g/L Yeast extract. L-agar plates - 10g/L NaCl, 10g/L, Tryptone, 5g/L, Yeast extract, 15g/L Difco Agar, ampicillin or kanamycin 50µg/L.

2.1.2. Growth and purification of DNA from bacterial transformations

2.1.2.1. For Miniprep

Following transformation, single cell colonies were picked using a pipette tip, and used to inoculate 3mls (millilitres) of warm LB with appropriate antibiotic. This was incubated at 37^{o}C for 16hrs. Cells were harvested by centrifuging ~1.5mls of culture for 3 mins. The remaining culture was kept at 4^{o}C for use in making glycerol stocks. DNA isolation was performed using PureLink Quick Plasmid Miniprep kit (Invitrogen) according to the manufacturer's instructions. Plasmid sequences were confirmed by restriction digest.

2.1.2.2. For Maxiprep

Using a disposable inoculating loop, bacteria (from culture remaining in 2.1.2.1. or glycerol stock in 2.1.3.) were streaked on an agar plate with appropriate antibiotic and incubated at 37^{o}C for 16 hrs. A new loop was used with every streak to ensure single colonies would be achieved. Single colonies were picked (depending on the number of maxipreps desired) and grown in 5mls LB at 37^{o}C for 8hrs. This culture was then used to inoculate 250mls of LB with antibiotic, and left to grow overnight in a shaking incubator at 37^{o}C. DNA was isolated using the PureLink HiPure Plasmid Filter Maxiprep Kit (Invitrogen) according to the manufacturer's instructions. Plasmids were confirmed by restriction digest.

2.1.3. Glycerol stocks

Plasmids were stored long-term by mixing 800µl of bacterial culture with 500µl 80% glycerol in 2ml cryo-screw capped tubes (Greiner), then freezing at -80^{o}C. To recover bacteria from a glycerol stock, the culture was thawed very slightly, until a sterile disposable loop could collect some frozen culture. This was streaked out on an agar plate, and then miniprep or maxiprep procedures followed as appropriate.

2.2. DNA methods

2.2.1. Restriction digestion

Restriction digests were performed with enzymes from New England BioLabs (NEB) Depending on the volume required, reactions were mixed as follows;

Digest to check plasmid structure;		Digest to cut plasmids for cloning;	
DNA	1ng	DNA	2ng
Enzyme 1	1µl	Enzyme 1	1µl
NEB buffer	2µl	NEB buffer	7.5µl
dH_20 up to	20µl	dH20 up to	75µl

Multiple enzymes were used in a single reaction as required, and the volume of the reaction adjusted with dH_2O (distilled water). Digestion mixture was incubated at 37^oC for 1hr.

2.2.2. SAP treatment

For cloning protocols, SAP treatment (shrimp alkaline phosphatase) was performed to prevent the linearised template DNA ends from re-ligating; this greatly increases cloning efficiency. 2µl of SAP was added to the digestion mix (after 1hr incubation), and incubated for a further 30 mins at 37^oC.

2.2.3. Gel electrophoresis

DNA samples were analysed for size by agarose gel electrophoresis, using gels ranging from 0.8-2% agarose/TBE (w/v) (Tris borate EDTA (ethylene diamine tetraacetic acid)) depending on application; where bands were to be excised and DNA extracted, a 0.8% gel was used, for analysing small fragments, a 2% gel was used, and for routine applications, a 1% gel was used. Gels were cast by dissolving agarose (Hi-Pure Low EEO Agarose, Biogene) in TBE buffer (89mM Tris base, 89mM boric acid and 20mM EDTA), and heating in a microwave oven. Ethidium bromide was added at 0.5µg/ml to cooled gel, before pouring into gel trays with combs. Markers containing DNA fragments of known sizes were added as a ladder

for reference. Ladders were chosen depending on predicted band size; 1kb (kilobase) DNA ladder (Invitrogen) or 100bp (base pairs) DNA ladder (Promega).

For checking DNA structure/sequence, the entire volume (20µl + 5µl loading buffer) was run by gel electrophoresis. To check the complete digest of plasmids for cloning, 5µl of reaction was mixed with 5µl loading buffer and 15µl H_2O, then this entire mix run by gel electrophoresis.

80-120V was applied, and the gels were visualised with a UV transilluminator (BioDoc-It System, UVP).

2.2.4. Gel purification

Where separated DNA was to be excised for further use, the entire 75µl reaction was run in a single wide well to minimise gel content. DNA was run by gel electrophoresis until the required band was separated enough from its neighbouring bands to cut out. The correct bands were identified by fragment size, then excised using a clean scalpel blade under a UV light. DNA was extracted using a QIAquick Gel Extraction Kit (Qiagen) according to the manufacturer's instructions.

2.2.5. Purification of DNA

2.2.5.1. Phenol/Chloroform extraction

The DNA preparation (from 2.2.1.-2.2.3.) was adjusted to 100µl with dH_2O. An equal volume of phenol:chloroform:isoamyl alcohol solution (25:24:1) (ThermoFisher Scientific) was added and mixed by pipetting. Mix was centrifuged at full speed for 5 mins. The aqueous top layer was removed into a fresh tube, being careful not to disturb the interface. DNA was precipitated as detailed below.

2.2.5.2. Ethanol precipitation

10µl 3M NaOAc (sodium acetate) and 3µl glycogen (GlycoBlue ThermoFisher Scientific) were added to the DNA and mixed. 2.5 volumes (250µl) 100% EtOH (ethanol) was added and mixed. The mixture was incubated on dry ice for 15 mins, ensuring that it was not allowed to freeze. The mixture was then centrifuged at

14000rpm (revolutions per minute) at 4ºC for 30 mins. The supernatant was removed, and the DNA pellet washed twice, by adding 250µl 70% EtOH and spinning for 2 mins. All traces of EtOH were removed and the pellet left to air-dry until translucent. DNA was dissolved in dH_2O; 10µl for insert sequences and 40µl for recipient sequences.

2.2.6. Ligation

2.2.6.1. Annealing primers

To create polylinkers, two complimentary oligonucleotide sequences were ligated together. Polylinkers were designed to insert new multiple cloning sites containing restriction sites needed for cloning. To join oligonucleotides, 5µl of each primer was mixed with 5µl ligation buffer (Invitrogen), and 35µl dH_2O. This reaction was incubated at 95ºC for 10 mins, then allowed to cool to room temperature. Once cooled, the annealed polylinker was used as the 'insert DNA' in the next stage (see 2.2.6.2.).

2.2.6.2. Ligating DNA fragments

Ligations were performed in triplicate with increasing amounts of insert sequence to maximise chances of success i.e. increasing molar ratios;

	Mix 1	Mix 2	Mix 3
Backbone DNA	1	1	1
Insert DNA	1	2	3
T4 ligase (Invitrogen)	1	1	1
Ligation buffer	1	1	1
H_2O	6	5	4

Reactions were mixed at room temperature, and left to incubate overnight at 16ºC. Ligations were then transformed as described in 2.1.1. and analysed by restriction digest.

2.2.7. Polymerase chain reaction

DNA amplification was achieved using polymerase chain reaction (PCR). Primers were designed either manually based on the sequence of interest, or by using Primer3 software (freely available at http://primer3.ut.ee/). Primer pairs were typically designed to span the entire coding region of the gene of interest. A list of primer pairs used in this thesis can be found in Table 2.2.

The reaction mix was set-up in line with manufacturer's instructions to the following final concentrations in dH_2O – template DNA <250ng, Phusion DNA polymerase 1.0 U/50µl, 0.5µM (micromolar) forward primer, 0.5µM reverse primer, 200µM DNTPs (deoxynucleotides), 1X Phusion HF Buffer.

PCRs were carried out using standard temperature and time cycles, in a thermal cycler.

Initial Denaturation	95°C	5 mins	
Denaturation	94°C	30 sec	35 cycles
Annealing	58°C	30 sec	
Extension	72°C	45 sec	
Final Extension	72°C	5 mins	

2.3. Cell culture methods

All cell culture methods were performed in a laminar flow hood. Cells were maintained under standard cell culture conditions of 37°C with 5% CO_2 (carbon dioxide).

2.3.1. Routine cell maintenance

Cells were passaged at ~80% confluency, in a ratio determined by cell growth. To detach cells, culture media was removed using a glass pipette in an aspirator, and the flask was washed in PBS (phosphate buffered saline) to remove any residual media. Cells were detached from the surface using trypsin-EDTA (Sigma-Aldrich) diluted in

PBS. Cells were incubated with 1X trypsin-EDTA for ~ 3 mins, apart from COCA cells which require ~12 mins to detach. Trypsin was neutralised using an equal amount of cell media containing FCS (fetal calf serum). For COCA cells, trypsin was neutralised with an equal amount of soybean serine protease inhibitor (from *Glycine max*, Sigma-Aldrich). The cell suspension was centrifuged at 13,000rpm for 3 mins. All liquid was removed, and cells were reseeded at desired density. A list of the cell media for each cell line used can be found in Table 2.1.

2.3.2 Thawing and freezing cell lines

Cell vials were recovered from liquid nitrogen storage, and plunged directly into water at 37^{o}C. Pre-warmed media was immediately added, dropwise, to the vial and the cells resuspended. This was then centrifuged and the freezing media, containing DMSO (dimethyl sulfoxide), removed. Cells were resuspended in media and plated into the appropriate sized flask.

2.3.3. Cell counting

Cell counts were performed either using a standard haemocytometer, or with a Scepter 2.0 Handheld Automated Cell Counter. For use in the Scepter, 10µl of cell suspension was diluted in 290µl cell media before counting.

2.3.4. DNA transfections

DNA transfections were performed either by electroporation or lipofection. Electroporation was achieved using the Invitrogen Neon transfection system (100µl), according to the manufacturer's instructions. 1x10^{6} cells were suspended in 100µl buffer R and 5µg total of high quality DNA (to equal no more than 20µl). 5ml of buffer E was added to the Neon chamber tube. Cells were drawn into 100µl pipette, carefully ensuring no bubbles entered the tip. B16F10 cells were electroporated at 1200V, 2 times for 20 ms (milliseconds). COCA cells were electroporated at 1300V, 2 times for 20ms. 3T3 cells were electroporated at 1350V, 2 times for 20ms. Cells were immediately plated in 6-well plates, containing ~2mls of antibiotic free media.

Table 2.1. Cell lines and culture conditions.

All cell media (barring COCA) was from Gibco. COCA cell media, and complete supplements were from CELLnTEC. Media was supplemented with 10% FCS (barring COCA) and 1:100 P/S (penicillin/streptomycin).

Cell name	Media	Source
COCA	Cnt-07 or CnT-02-3D	ECCACC General cell collection
NIH3T3	DMEM	Peter Budd/ Dr Emma Hall
B16F10	RPMI	Professor C Goding
Melb-a	RPMI + KITL + bFGF	Wellcome Trust Functional Genomics Cell Bank
Melb-s1	RPMI + KITL + bFGF	Wellcome Trust Functional Genomics Cell Bank
Melb-m5	RPMI + KITL + bFGF	Wellcome Trust Functional Genomics Cell Bank
NIH3T3-mKITL_NeonGreen	DMEM	Generated within thesis
NIH3T3-mKITL_sfGFP/Cherry	DMEM	Generated within thesis
NIH3T3-sKITL_NeonGreen	DMEM	Generated within thesis
NIH3T3-sKITL_sfGFP/Cherry	DMEM	Generated within thesis
NIH3T3-KIT_Cherry	DMEM	Generated within thesis
NIH3T3-KIT_sfGFP/Cherry	DMEM	Generated within thesis

To freeze cells, a confluent flask of cells was detached as described in 2.5.1. The cell pellet was resuspended in 1ml freezing mix (48% Ham's F10 media, 40% TPB (tyrptose phosphate broth), 12% DMSO) in a 2ml cryotube (Greiner). Vials were frozen slowly in polystyrene at -80^{o}C before being transferred to liquid nitrogen storage.

For lipofection, transfection was performed with Lipofectamine2000 (Invitrogen), according to the manufacturer's instructions. 1 x 10^6 cells were plated in a T25 flask. 24 hrs (hours) later, 625µl of Optimem media (Invitrogen) was mixed with 25µl of Lipofectamine2000 transfection reagent, and left to incubate for 5 mins. This was then mixed with a further 625µl of Optimem plus 5µg of high quality DNA, and incubated at room temperature for 20 mins. This mix was then added to the cells (in antibiotic free medium).

After 24hrs, cell media was replaced with media containing selection antibiotics. For DNA transfections with fluorescent constructs, cells were checked by light microscopy after ~48 hrs.

2.3.5. Stratified COCA cultures

For diagrammatic representation of the following, refer to Figure 3.3.

2.3.5.1. Original orientation

To create the 3D COCA culture, the protocol detailed in Segrelles *et al*. was followed (Segrelles et al., 2011). Cells were first detached as described in 2.5.1. COCA cells were counted, and 200,000 seeded onto Millicell PCF 0.4µm inserts (Millipore), placed in a petri dish. Both the inserts, and the petri dish were filled with CnT-07 media. Cells were grown until they reach confluency across the whole membrane. Cells media was switched to Cnt-02-3D both inside the insert and in the petri dish. After ~16hrs, cell media was removed from inside the insert to begin the stratification process. Media outside the inserts was changed every 2 days.

2.3.5.2. Inverted orientation

In order to grow cells on the reverse side of the Millicell insert, a new temporary chamber was created. The plastic feet of the Millicell insert were removed using a scalpel blade. A sterile pastette bulb was cut to ~1cm (centimetre) long, and the end removed to leave a tube. This was carefully pulled over the bottom end of the Millicell insert, and further secured by wrapping the joint with Parafilm. To ensure media in the petri dish would reach the membrane, a low density agarose gel was

used to fill the chamber, and lift it from the bottom of the dish. A 1% agarose gel was made as described in 2.2.3., with PBS, and diluted to 0.5% with Cnt-07 media. This was pipetted into the insert, in excess so that a large dome of agarose formed. Once cooled, the protruding agarose was levelled flat using a scalpel, and the insert inverted, directly into media. COCA cells were plated as described for the original orientation.

2.3.6. CDMs

2.3.6.1. Growth and preparation of CDM

Cell derived matrices (CDMs) were prepared following the protocol published in 2017 by Kaukonen *et al*.

2.3.6.1.1. Preparing coverslips

CDMS were prepared on sterile 13mm glass coverslips, for use in the magnetised imaging chamber. The coverslips were prepared by incubating in 0.2% gelatin (Sigma-Aldrich) for 60 mins at 37^{o}C, followed by crosslinking with 1% glutaraldehyde (Sigma-Aldrich) for 30 mins at room temperature. Crosslinking was quenched with 1M sterile glycine in PBS for 20 mins at room temperature. Finally, coverslips were incubated in relevant cell media for 30 mins before seeding cells atop.

2.3.6.1.2. Growing cells

NIH3T3, Sl/Sl and COCA cells were detached as described in 2.5.1. and plated at a density of 5x10^{4} cells/ml on individual coverslips in a 24-well plate. Cells were left to reach confluency. Once confluent, cell media was changed to media supplemented with 50µg/ml ascorbic acid (Sigma-Aldrich). Media was changed every day. Cultures were grown for 10 days before denudation.

2.3.6.1.3. Denudation

To denude cells, cultures were first washed in PBS. Extraction buffer comprised of 20mM NH_4OH (ammonium hydroxide) and 0.5% Triton X-100 in PBS, was applied

for 2 mins until no cells could be identified by microscope (cell lysis is virtually instantaneous). Extraction buffer was partially removed, and the cultures washed several times with PBS containing calcium and magnesium (ThermoFisher Scientific). Residual DNA was digested with DNAse I (ThermoFisher Scientific), at 10µg/ml in PBS containing calcium and magnesium for 30 mins at 37ºC. CDMs were stored at 4ºC in PBS containing calcium and magnesium, with 1% P/S and Fungizone (ThermoFisher Scientific) at 1µg/ml.

2.3.6.2. Plating experimental cells on CDM

CDMs were washed with PBS containing calcium and magnesium, and then washed in serum-containing medium three times. Experimental cells were detached as described in 2.3.1., and reseeded at the desired density. CDMs were prepared for imaging as described in 2.8.3.2.

2.3.7. HD culture

2.3.7.1. Plating

Cells were detached as described in 2.3.1., and resuspended at a density of 3.3 $x10^5$ cells/ml. Drops were plated on the inside of a 10cm petri dish lid with ~ 30 drops of 30µl each (10,000 cells per drop). The dish was filled with PBS to create a humidity chamber. The lid was inverted smoothly and placed atop the dish. HDs were incubated for 5 days before use. A video demonstrating the plating of HDs is shown by Foty, 2011, although note that the cell density and size of HDs are different from those used herein.

2.3.7.2. Manipulation and imaging

Drops were moved by mouth pipette. The end of glass pasteurs were smoothed by placing briefly in a flame, and rotated to smooth and shrink the hole slightly. The HDs were inverted, and then moved individually by suction. Drops were left to begin attaching in the media transferred with the drop by mouth pipette, for 30 mins at 37ºC. Whilst cells were incubating, matrigel was prepared (Corning). Matrigel was kept on ice, and mixed 1:5 with warmed cell culture media. Matrigel solution was

placed atop HDs to cover the bottom of the dish (100µl in a 24-well dish). Matrigel solution was left to set for 30 mins at 37^{o}C, before the well was filled with media. Cultures were allowed to attach for at least 4 hrs before imaging.

2.3.8. Cells for live imaging

2.3.8.1. Vital stains

Cells were stained for imaging experiments using vital dyes from Vybrant (ThermoFisher Scientific), according to the manufacturer's instructions. Cells were resuspended at a density of $1x10^{6}$ cells/ml in serum-free media, then incubated for ~20 mins with 5µl of staining solution at 37^{o}C. Cells were centrifuged at 13,000rpm for 3 mins, and all liquid removed. Cells were resuspended in media to wash, and centrifuged again. This wash step was repeated twice more. Cells were reseeded at the desired density, and experiments performed the following day. For nuclear visualisation, cells were stained with a Hoescht dye suitable for live cells (NucBlue, ThermoFisher Scientific) 30 mins prior to imaging. NucBlue was added at 5µl/ml media.

Absorbance and emission spectra are as follows for the dyes; DiI has an absorbance of 549nm (nanometres) and emission at 656nm, DiO has an absorbance of 484nm and emission at 501nm and DiD has an absorbance of 644nm and emission at 665nm. NucBlue has an absorbance at 360nm and emission at 460nm.

2.3.8.2. Plating

Cells were plated onto 24-well glass bottom dishes (Iwaki) for confocal microscopy. For experiments creating a edge, a sterile plastic tube was placed in a well, and pressed down to create a seal. Media was pipetted into the tube to check for leaks. 50,000 cells were plated inside the ring and allowed to attach. The tube was removed prior to imaging.

2.4. RNA methods

2.4.1. RNA isolation

All RNA was stored at -80^{o}C, immediately following preparation.

2.4.1.1. Cells in culture

Cells were detached as described in 2.3.1. Once detached, cells were centrifuged and trypsin EDTA solution removed. Cells were lysed in the appropriate volume of buffer RLT Plus (Qiagen). At this point, samples were either frozen at -80^{o}C, or processed through the RNA isolation kit (RNeasy Plus micro/mini Kit (Qiagen)). RNA quantity and quality was analysed using a nano-spectrometer (Nanodrop, ThermoFisher Scientific).

2.4.1.2. Primary cells

RNA was prepared from primary cells that were isolated via FACS (fluorescence-activated cell sorting) experiments, see 2.6.3. RNA quality and quantity was analysed using a 2100 Bioanalyzer (Agilent Technologies). The Bioanalyzer was run by Agnes Gallacher of the IGMM core technical services. Briefly, 1.5µl of RNA sample was heated for 2 mins at 70^{o}C. After heating, sample was placed on ice before being run on Bioanalyzer according to the manufacturer's instructions.

2.4.2. cDNA synthesis

2.4.2.1. For general use

cDNA (complementary DNA) was generated using the Reverse Transcription System (Promega) according to the manufacturer's instructions. An equal amount of RNA was loaded in to the reactions (per experiment), and the volume adjusted as appropriate with dH_2O.

2.4.2.2. Primary cells for RNA-sequencing

For RNA-sequencing, cells were sorted via FACS as described in 2.6.3. Due to the small number of primary cells collected, a more sensitive cDNA synthesis kit was used. The Ovation RNA-Seq System V2 from NuGen, is specifically designed to amplify cDNA from total RNA from samples that have a low starting material (~500pg), or have suffered some degradation.

2.4.3. Reverse transcription PCR

Primers for rtPCR (reverse transcription PCR) were designed to span exon-exon junctions to distinguish between cDNA and possible gDNA (genomic DNA) contamination. Reactions were mixed as described in 2.2.7.

RtPCRs were generally carried out using a 'Touchdown' protocol to enable several primers with different Tms (melting temperatures) to be run in tandem;

Initial Denaturation	95°C	5 mins	
Denaturation	94°C	30 sec	10 cycles
Annealing	68°C (-1°C on each cycle)	30 sec	
Extension	72°C	45 sec	
Denaturation	94°C	30 sec	25 cycles
Annealing	58°C	30 sec	
Extension	72°C	45 sec	
Final Extension	72°C	5 mins	

2.5. Protein methods

2.5.1. Protein isolation from cells

Cells were grown to confluence in a 6-well plate. Media was removed, and cells were washed in PBS. 100µl of 1X Cell Lysis Buffer (Cell Signalling Technology) plus 1mM PMSF (phenylmethanesulfonylflouride, ThermoFisher Scientific), plus protease inhibitor (1 tablet per 10ml, Roche), was added per well. This was incubated on ice for 10 mins. Disposable cell scrapers were used to detach cells from the well,

Table 2.2. rtPCR primers used in this thesis

Target	Forward primer	Reverse primer	Band size
Cdh1 (E-cadherin)	AACAGGCCAGAGTTTACCCA	GGGTAACTCTCTCGGTCCAG	245bp
Cdh2 (N-cadherin)	GGAGACCCTACAGGAAGGT	GTCACAGACACAGTGGCTGTC	188bp
Gapdh	TGTCGTGGAGTCTACTGGTG	CCCTTCCACAATGCCAAAGT	238bp
Keratin 1	TCAGAAGGAAGGTGGACTCG	CAATGTCTTGCTGGAGGGC	225bp
Keratin 2	CCCATCTTCCAGGCCTACAT	GCAGCTCTGTCTTGTCCATG	220bp
Keratin14	GACCAAGTTTGAGACGGAGC	GCGTCCATCTCCACATTGAC	219bp
KIT	GAACAGGACCTCGGCTAACA	GCCATTTATGAGCCTGTCGT	220bp
mKITL	CAGAGTCAGTGTCACAAAACCA	TACAAGCGAAATGAGAGCCG	157bp
P63	GTTGGAGCAAGGGGGACATT	GGGTTTCTATGAAACGCTGGA	524bp
sKITL	CCGAAGAGGCCAGAAACTAGA	CTTTGCGGCTTTCCCTTTCT	156bp

and the contents were transferred to a centrifuge tube. Lysates were sonicated for 3x30 secs (Bioruptor, Diagenode), then centrifuged at 14,000g (g-force) for 15 mins at 4^{o}C. The supernatant was transferred to a fresh tube, and stored at -80^{o}C.

2.5.2. Protein separation

Protein samples were separated by molecular weight by SDS-PAGE (sodium dodecyl sulphate-polyacrylamide gel electrophoresis), using the NuPAGE Novex gels from Invitrogen. Equal amounts of protein for each sample, plus 1X sample reducing agent and 1X sample loading buffer (both Invitrogen), were heated to 72^{o}C for 10 mins. Samples were loaded on to a suitable gel, dependent on expected protein sizes, along with Novex Sharp Protein Standard for size comparison. For detecting KIT protein, a 4-12% Bis-Tris gel was used, combined with MOPS SDS running buffer (Invitrogen). The gel was submerged in 1X running buffer, plus 1X antioxidant (Invitrogen), and run using the XCell Surelock Mini system at 200V (volts) for 60 mins.

2.5.3. Western blotting

2.5.3.1. Transfer

After SDS-PAGE, the gel was removed from the case, and samples transferred onto nitrocellulose membranes (Hybond P, GE Healthcare) using the iBlot 2 Dry Blotting System (Invitrogen) according to the manufacturer's instructions.

2.5.3.2. Immunoblotting

After transfer, membranes were washed in TBSt (0.05% Tween-20 in TBS (tris-buffered saline)), then placed in blocking solution (5% dried skimmed milk powder (w/v)(Marvel, Premier foods) in TBSt) rocking for 1hr at room temperature. Primary antibodies (see Table 2.3.) were diluted as required in blocking solution. Membranes were then incubated in antibody mix overnight at 4^{o}C rocking. Membranes were washed in TBSt 3 times for 5 mins to remove unbound primary antibody. Next, membranes were incubated with the relevant HRP-conjugated (horseradish

peroxidase) secondary antibody (see Table 2.3.) diluted in TBSt, for 1hr at room temperature. Finally, membranes were washed 3 times in TBSt for 5 mins each.

2.5.3.3. Protein signal detection

Antibody signal was detected using the SuperSignal West Pico Chemiluminescent Substrate kit (ThermoFisher Scientific) according to the manufacturer's instructions. Protein bands were visualised and images were acquired digitally in an ImageQuant LAS 4000 (GE Healthcare), and analysed using ImageQuant TL software.

2.5.3.4. Reprobing and storage

Membranes were stripped between different primary antibodies, by incubating for 5 mins with Restore PLUS stripping buffer (ThermoFisher Scientific) followed by washing in TBSt and blocking buffer. For long-term storage, membranes were dried between Whatmann filter papers, and stored sealed in plastic at 4^{o}C. To re-use, membranes were equilibrated in transfer buffer before re-blotting using a new primary antibody. Membranes were re-used a maximum of 2 times before the western blot protocol was repeated from the beginning.

2.6. Mouse methods

Mouse husbandry and genotyping was performed by Margaret Keighren (Jackson lab, IGMM). Mice were maintained and euthanised by cervical dislocation in accordance with the facility's Home Office licence.

2.6.1. Preparation of mouse dermal cells from adults

The back torso of the mouse was shaved, and fine hairs removed using a generic depilatory cream according to the manufacturer's instructions. A patch of skin ~ 4x3cm was removed from the back by lifting the skin with blunt-ended forceps, and then cutting using surgical scissors. Placing the skin epidermal side down, fat was removed using curved forceps to scrape the surface. The defatted skin was placed in a dish containing 0.5% trypsin (Sigma-Aldrich) in PBS, and

Table 2.3. Antibodies used in this thesis

Antibody	Source	Species	Dilution (application)
Collagen IV	AbD Serotec (2150-1570)	Rabbit	1:100 (IF)
E-Cadherin	Transduction Laboratories (C20820)	Mouse	1:2500 (IF)
Fibronectin	Abcam (ab131065)	Mouse	1:500 (IF)
Fibronectin	Abcam (ab2413)	Rabbit	1:1000 (IF)
Filamin	Bethyl Laboratories Inc (BL876)	Rabbit	1:1000 (IF)
Keratin 10	Covance (PRB-159P)	Rabbit	1:500 (IF)
Keratin 5	Covance (PRB-160P)	Rabbit	1:1000 (IF)
KITL	Prof. B Wehrle-Haller	Rabbit	1:1000 (WB)
Laminin	Sigma-Alrdich (L9393)	Rabbit	1:1000 (IF)
SCF (KITL)	Abcam (ab64677)	Rabbit	1:1000 (WB) 1:100 (IF)
ECL Anti-rabbit IgG, HRP linked	GE Healthcare	Donkey	1:7500 (WB)
ECL Anti-mouse IgG, HRP linked	GE Healthcare	Donkey	1:7500 (WB)
Anti-rabbit IGG, Alexafluor 488 linked	Invitrogen	Donkey	1:500 (IF)
Anti-mouse IGG, Alexafluor 488 linked	Invitrogen	Donkey	1:500 (IF)
Anti-rabbit IGG, Alexafluor 594 linked	Invitrogen	Donkey	1:500 (IF)
Anti-mouse IGG, Alexafluor 594 linked	Invitrogen	Donkey	1:500 (IF)
Anti-rabbit IGG, Alexafluor 647 linked	Invitrogen	Donkey	1:500 (IF)
Anti-mouse IGG, Alexafluor 647 linked	Invitrogen	Donkey	1:500 (IF)

incubated at room temperature for 30 mins. The skin was cut into small pieces, and incubated in digestion medium (0.2 Wünsch units/ml Liberase TL (Roche) in DMEM) for 1hr at 37ºC, mixing occasionally. Sample was then treated with DNase by adding skin pieces to solution containing 0.05% DNase (ThermoFisher) and 5% FCS in PBS, and incubated for 5 mins at room temperature.

2.6.2. Preparation of mouse melanoblasts from embryos

For embryos age E13.5 and E14.5, melanoblasts were isolated by first dissecting the skin as demonstrated in Mort *et al.*2014. This method begins by dissecting the embryo to just the torso, and then uses a toothbrush bristle secured in a bamboo stick to gently sweep the skin away without damage. For embryos at E12.5, the skin is impossible to remove with this method. Instead, the embryo was dissected down the middle of the belly, and as much of the innards removed as possible with curved forceps. Skin samples were then transferred to a solution of 10mM EDTA (Sigma-Aldrich) in PBS and incubated for various times according to the embryonic stage (45 mins at E14.5, 30 mins at E13.5, 20 mins at E12.5). Sample was centrifuged gently (300rpm) and liquid removed. Samples were then incubated in digestion medium (0.2 Wünsch U/ml Liberase DL (Roche) in DMEM) for 30 mins at 37ºC, mixing occasionally.

2.6.3. FACS preparation and process

After final digestion steps outlined in 2.6.1. and 2.6.2., cells were prepared for FACS to obtain single cells. This was achieved by taking the sample through a needle series from 19G-25G, at each stage ensuring sample flowed with ease. Samples were passed through a 40µm cell strainer (Corning). Samples were centrifuged, and resuspended in appropriate volume of PBS (based on pellet size –usually 1ml) in FACS tubes (Corning). FACS experiments were run by Elisabeth Freyer of the IGMM core technical services team.

For RNA sequencing, cells were sorted directly into 1.5ml tubes (Eppendorf) containing 350µl buffer RLT.

2.7. Histology

Histology methods 2.7.1. and 2.7.2. refer to investigations into 3D COCA samples. Methods were developed in association with Allyson Ross of the IGMM core technical services team.

2.7.1. Wax processing

2.7.1.1. Sample fixing and preparation

All media was removed from inside and outside inserts. Samples were fixed in 4% PFA (paraformaldehyde) (ThermoFisher Scientific) for 5 mins. Fix was applied outside the insert first, and then applied dropwise down the side of the inside well, to protect the delicate COCA layers. Fix was removed, and samples dehydrated in an EtOH series from 10%-70%. Samples were stored in 70% EtOH until used further.

2.7.1.2. Wax embedding

Samples were dehydrated further by washing 3 times in 100% EtOH. After the final wash, the PCF membrane was cut out of the plastic mount using a needle. Care was taken at every stage to ensure the cell layer faced upwards and did not physically touch any surface. The membrane was transferred to a glass embryo dish. Samples were cleared using fresh xylene. Samples were incubated at room temperature for 10 mins in xylene a further two times. On the third xylene change, samples were incubated at 60^{o}C. The samples were then immersed in molten wax (paraffin) for 3 changes of 10 mins at 60^{o}C. After the final change, the sample was embedded in a small plastic mould, allowing a thin layer of wax to set on the bottom first to ensure sample would not settle at the bottom. A plastic cassette was placed on top to stop wax shrinkage. Once set, the wax was cut and trimmed to allow cutting at right angles. The block was mounted on a wooden chuck.

2.7.1.3. Cutting and mounting

Sections were cut at 4µm on a microtome using disposable blades, and floated on a water bath at 50^{o}C to stretch. Sections were mounted on Superfrost Plus slides

(Menzel-Gläser, ThermoFisher Scientific). Once mounted, samples were left to dry overnight at room temperature. Samples were sealed to the slides by baking in a 60^{o}C oven for 2hrs before use.

2.7.1.4. Wax removal and rehydration

Wax was removed by placing slides in 3x5 min changes of xylene, followed by 3x5min changes in 100% EtOH. To rehydrate, slides were placed in 2 mins changes through an EtOH series from 90%-30%, before washing in tap water.

2.7.2. Haematoxylin and eosin staining

Slides were stained in haematoxylin for 2 mins, then washed in tap water. Samples were differentiated in acid/alcohol (1%HCl (hydrochloric acid) in 70%EtOH) for a few seconds, before washing in tap water. Slides were blued in saturated lithium carbonate solution for a few seconds, and washed well in tap water. Slides were stained in eosin for 1.5 mins, and then rinsed in water. Finally, slides were rinsed in 100% EtOH. To mount, slides were taken through 2 changes of 100% EtOH and 3 changes of fresh xylene of 5 mins each. Slides were mounted in DPX (Sigma), and left to dry.

2.7.3. Immunocytochemistry

Antigen retrieval was performed by bringing slides to a near boil in citrate buffer (10mM citrate, 0.1% Tween-20, 1mM EDTA, pH 6.0), for 15 mins in a microwave oven. Slides were cooled, then washed in PBS and blocked in 10% donkey serum in PBS for 1hr. Slides were incubated in primary antibody diluted in TBST (TBS plus 0.1% Triton X-100) overnight at 4^{o}C (Table 2.3.). Slides were then washed in PBS, and then incubated with secondary antibodies diluted in TBST for 1hr at room temperature (Table 2.3.). Control slides were also prepared using only the secondary antibodies on a sample to ensure signal is specific to the primary antibody. Slides were washed in PBS. DAPI was added for 5 mins at 2µg/ml before mounting in ProLong gold (ThermoFisher Scientific).

Where immunocytochemistry was performed directly on cells, or CDMs, samples were fixed directly on glass surface, and antigen retrieval was not necessary. All other steps were performed as described, directly in the plates. To mount, ProLong gold was dropped onto a clear coverslip which was then placed atop the sample.

2.8. Microscopy

2.8.1. Light microscopy

2.8.1.1. Fluorescence imaging

Epifluorescent images were acquired using a Photometrics Coolsnap HQ2 CCD camera and a Zeiss Zeiss Axioplan II fluorescence microscope with Plan-neofluar objectives (Carl Zeiss, Cambridge, UK), a Mercury Halide fluorescent light source (Exfo Excite 120, Excelitas Technologies) and Chroma #83000 triple band pass filter set (Chroma Technology Corp., Rockingham, VT) with the excitation filters installed in a motorised filter wheel (Ludl Electronic Products, Hawthorne, NY). Image capture was performed using Micromanager (https://open-imaging.com/).

2.8.1.2. Brightfield colour imaging

Brightfield images were acquired using a Micropublisher 5MP cooled colour CCD camera (Qimaging, Surrey, BC, Canada) mounted on a Zeiss Axioplan II fluorescence microscope with Plan-neofluar or Plan Apochromat objectives (Carl Zeiss, Cambridge, UK). Image capture was performed using Micromanager (https://open-imaging.com/).

2.8.2. Confocal microscopy

Images were acquired on a Nikon Confocal A1R confocal microscope. The microscope is equipped with 405nm diode, Argon laser and 561 and 648nm laser lines, and four Photomultiplier tubes. Data was acquired using NIS Elements AR software (Nikon Instruments Europe, Netherlands). Images were scanned at various intervals, dependant on experiment. The Nikon A1R confocal microscope comprises a Nikon Eclipse TiE inverted microscope with Perfect Focus System. The scan head

contains both a high resolution galvano scanner and high speed resonant scanner for live cell imaging.

2.8.3. Live imaging and assembly

Live imaging was performed on the A1R confocal microscope as above. Environmental control of the cultured cells was maintained during imaging with an incubation chamber incorporating temperature and humidified CO_2 control (Solent Scientific Ltd., Segensworth, UK). Images were captured at various rates dependent on experiment, typically experiments lasting longer than 6 hrs were imaged every 15 mins, unless otherwise indicated. Live imaging was performed with cells in their normal media, supplemented with 25mM HEPES buffer (4-(2-hydroxyethyl)-1-piperazineethanesulfonic acid) (Sigma-Aldrich).

2.8.3.1. Stratified COCA culture live imaging assembly

Detailed assembly of the chamber for both the original and inverse orientations of the 3D COCA culture can be seen in Figure 3.3.

2.8.3.1.1. Original orientation

A lumox membrane was secured to the individual black chamber using an O-ring. The tube of the black clip was filled with a 0.8% agarose in PBS mix and left to cool. The membrane was carefully cut out using a fine needle, whilst holding the edge with surgical forceps. The membrane was inverted, and placed cell side down, in the middle of the lumox membrane. It was secured in place using the black clip, and the whole well filled with media.

2.8.3.1.2. Inverted orientation

A lumox membrane was secured to the individual black chamber using a plastic O-ring. The temporary upper chamber was removed, and the majority of the agarose removed. The insert was inverted and placed in the chamber, with the cells facing downwards at the lumox membrane. The well was filled with media.

2.8.3.2. CDM imaging assembly

Cells were plated as described in 2.3.6.2., at least 8 hrs before experiments. Chambers were prepared by first coating the bottom surface of the inner chambers protruding ring (which holds the magnet) with silicon grease (RS pro), being careful to ensure the grease would not spread onto the coverslip once pressed. The CDM coverslip was removed from media, and the edge briefly blotted on tissue paper. The coverslip was placed in the outer chamber, CDM facing upwards, in the small groove which ensures it lies flush with the metal. Next, the inner chamber was placed atop, and pressed down to seal. The magnet was transferred to the inner chamber to complete the assembly. The well was filled with media, and incubated at 37^{o}C for 30 mins before imaging to check the chamber was secure. Imaging CDMs was performed on the A1R as described. For timelapse imaging, an automated stage function to escape and refocus between wells had to be added, to ensure the lens cleared the chamber casing sufficiently when moving. To do this, the command 'StgMoveZ(500,0)' was executed after every capture.

2.9. *In Silico* analysis

2.9.1. Image analysis

Analysis of imaging data was performed on the open source platform Fiji (https://imagej.net/Fiji). Custom scripts were prepared by Dr Richard Mort for identifying cell areas and measuring ratio of sfGFP:Cherry (super-folder green fluorescent protein). Cell tracking was performed using the TrackMate plugin (Tinevez et al., 2017). The free program 'chemotaxis and migration tool' from Ibidi was used to plot cell migration tracks (http://ibidi.com/xtproducts/en/Software-and-Image-Analysis/Manual-Image-Analysis/Chemotaxis-and-Migration-Tool).

2.9.2. Statistics

Statistical analyses were performed using Microsoft Excel. The appropriate test was informed and executed using a statistical guide by Dytham (2011). Throughout this thesis, $P<0.05$ is considered significant.

Chapter 3
Assay development and characterisation

This chapter will discuss the development and characterisation of the various assays that have been used during this project. Many of these are based on standard techniques that have novel modifications, in order to recycle them for specific experiments. The assays described in this chapter are based on a few cell lines that were readily available, but they would be easily applicable to other cell lines. Further, it is important to note that these assays were designed with an integrated approach in mind, and are therefore designed to be used in concert with one another. Thus from the 'basic' approaches described herein, different experimental combinations can produce different platforms dependent on the scientific question.

3.1. Modelling melanoblasts and the surrounding environment

The development of the assays relied on the use of six different cell lines. These are broadly split into the 'environment' cells i.e. those cells used to create the environment with which the pigment cells interact, and the melanoblast/melanoma lines (MLs) which were the experimental focus.

3.1.1. Modelling the melanocyte external environment

3.1.1.1. COCA cells

To model the epidermis, COCA cells which were described by Segrelles *et al.* (2011) were used in co-culture assays. They are a line of immortalised keratinocytes, developed from the dorsal skin of 2 month old C57BL6/DBA mice. These cells can be grown in culture to a high passage number, and the authors showed that the cells retain the capacity to form the core components of an epidermis. *In vitro,* this process

first requires growing a confluent monolayer of cells. This monolayer is then supplied with a high calcium containing medium and is raised to an ALI in order to begin the differentiation and stratification processes. They were also able to show through *in vivo* grafting experiments, that COCA cells could reform the fully stratified epidermal skin layer when implanted back into immunodeficient mice. The main differences observed between the *in vivo* and *in vitro* experiments, was slight alterations in the expression pattern of keratin-10, loricrin and filaggrin in the *in vitro* culture. These proteins should all be expressed continuously in the suprabasal layers, however they appear patchy by immunofluorescence (IF) staining in the *in vitro* cultures. This may indicate that the keratinocytes are not fully differentiating evenly across the membrane, and probably reflects the culture method and conditions rather than a failure of the cell line.

3.1.1.2. NIH3T3 fibroblasts

To model the dermal environment, the standard fibroblast line NIH3T3 were cultured (Todaro and Green, 1963). This line has been used to produce CDMs previously (Chlenski et al., 2011), so offer a positive control. CDMs and their production is detailed in section 3.1.3. NIH3T3 cells express KIT shown by experiments using an AP-tag in research by Flanagan and Leder (1990).

3.1.1.3. Sl/Sl fibroblasts

The $Kitl^{Sl}$ mutation was discussed in Chapter 1.3. Briefly, $Kitl^{Sl}$ mice have a large deletion in the region of *Kitl*, which causes a complete or near complete deletion of the protein coding region; fibroblasts isolated from this line accordingly lack expression of KITL (Sarvella and Russell, 1956). Later, Flanagan and Leder used the $Kitl^{Sl}$ fibroblast cells to prove the receptor/ligand relationship between *W* and *Sl* mutant mice, which had long been linked phenotypically (Flanagan and Leder, 1990). Kit^{Sl} mice are embryonic lethal, with death caused by anaemia (Flanagan and Leder, 1990).

3.1.2. Modelling melanoblasts, melanocytes and melanoma

3.1.2.1. B16F10 melanoma cells

The B16 mouse melanoma line was isolated in 1954 from a spontaneous tumour that arose in a C57/BL6 mouse (Teicher, 2011). As discussed in Chapter 1.4., subclones of the B16 line have different metastatic properties, with B16F10 showing high metastasis and invasion *in vivo*.

3.1.2.2. Melb-a melanoblasts

Melb-a cells were initially isolated and immortalised in 1995, and were the first melanoblast cell line to be cultured long term *in vitro* (Sviderskaya, Wakeling and Bennett, 1995). The definition of melanoblasts at this time was unclear, as the stages between cells exiting the NC and becoming pigmented melanocytes were not understood. In this study, cells of NC origins were isolated from the skin and melanoblasts were defined as cells which were unpigmented but could subsequently become pigmented. However, the population that was isolated, was comprised of two differing populations in relation to *Tyr* expression (fundamentally, at the point of isolation, these cells remained unpigmented). They continued to remain unpigmented during the expansion phase, when they were grown on a layer of XB2 keratinocyte feeder cells. However, when differentiated, they did produce pigment, and were then considered melanocytes. The authors describe how all, or nearly all, cloned melb-a cells contain DCT despite differences in *Tyr* expression. To provide some clarification, this paper finally defines melanoblasts as “any unipotent precursor of melanocytes, where melanocytes are cells that make melanin via tyrosinase”.

Due to the culturing methods post-isolation, it is unlikely that these cells remain as pure melanoblasts exhibiting the same behaviours as their *in vivo* relatives. To label them melanoblasts therefore, is potentially misleading, and these cells should be thought of as ‘melanoblast-like’ more appropriately; this is investigated further in Chapter 6.

3.1.2.3. Melb-s1 melanoblasts

Melb-s1 melanoblasts were also isolated by Sviderskaya *et al.*, using the same technique developed in the melb-a paper. This cell line however, is isolated from

mice carrying a mutation in Ednrb - Ednrb^{s} (Sviderskaya, Easty and Bennett, 1998). This mouse is used to model Hirschprungs disease, which is characterised by a failure of the peripheral nervous system to colonise the gut in humans, leading to reduced innervation and thereby, digestion problems (Howard, 1972). The peripheral nervous system (PNS) is also derived from the NC. As well as issues with the PNS, Ednrb^{s} mice lack pigmentation in their extremities and often present with a white belly spot. Melanoblasts isolated from these mice are reported to be morphologically normal but have changed behaviour *in vivo*, including reduced proliferation and invasive properties.

3.1.2.4 Melb-m5 melanoblasts

Melb-m5 cells are the third melanoblast cell line used herein created by Sviderskaya *et al*., from mice with a mutation at the *misty* locus (Sviderskaya et al., 1998). The *misty* mutation is a spontaneous mutation that arose in the 1940s, in the DBA/J mouse strain (Wooley, 1941). The misty locus is located on chromosome 4, and is historically well-known as an anchor locus used in chromosome mapping. A homozygous mutation in the *Dock7* gene leads to mice which have a diluted/paler coat colour, a white belly spot and white tips of their appendages (Blasius et al., 2009). In this mutant, data shows some problems which are attributed to late melanoblast development, rather than their ability to migrate and proliferate in the early stages.

3.1.3. CDMs

The biological community has long been aware of the importance of the extracellular environment, and that when studying cell behaviour, the individual cell is being influenced by a multitude of external factors. CDMs are, as the name suggests, ECMs produced by a cell culture *in vitro*. Many areas of research are increasingly focussing on the contribution of the environment to cell behaviour, including research looking at the cancer micro-environment, glial cell contribution to neurological disease and even in its contribution to stem cell niche maintenance and regulation. A detailed protocol for producing CDMs has been published recently (Kaukonen et al., 2017), however the protocol has been described by members of the

same group previously (Jacquemet et al., 2013). The CDM is produced by growing cells in a fully confluent monolayer over a number of days on a gelatin coated surface. Ascorbic acid (essentially Vitamin C), is supplied regularly to help stabilise the ECM that the cells produce naturally. The cells are then completely removed from the matrix by extraction with NH_4OH, which removes all cell components but leaves the CDM intact. CDMs are extremely fragile, so must be treated with extreme care. The protocol takes ~2 weeks to grow the cultures (dependent on the cell line), and they have a relatively short shelf-life of 1 month, so, it is perhaps not surprising that they are underused in favour of their commercially available counterparts.

Previous work has concentrated in the use of fibroblast cell lines to create CDMs. The reasons for this are extensive, including the fact that fibroblasts are easy to handle in culture, they grow quickly and are not adversely affected when confluent. *In vivo*, fibroblasts are a core component of many connective tissues, providing structure, ECM and biochemical support to specialised cell types (Alberts et al., 2002). The epidermis however, is composed primarily of keratinocytes. In order to model the epidermal environment specifically, COCA cells were used to produce novel CDMs.

Several commercial products are available, ranging from purely 3D support structures, to synthetic protein matrices, to culture chamber coatings. Coating cell culture chambers with various proteins is a popular method, the most commonly used substrates include collagen and fibronectin which are abundant proteins in the ECM.

During the development of the HD migration protocols discussed later in this chapter, the assay was performed using matrigel. Unfortunately, matrigel introduces significant problems, namely that the manufacturers are unable to specify exactly what is contained within the matrigel, and that there is significant batch-to-batch variation (Hughes, Postovit and Lajoie, 2010). In all experiments, the same batch of low growth factor matrigel was used throughout to try and address these problems, but reproducibility between groups remains an issue. Further, matrigel is produced from mouse sarcoma tissue, and may not be appropriate to use in conjunction with other species. Although organically produced, the matrix produced by these

sarcomas is not necessarily similar in composition to the dermis or epidermis. This highlighted the need for a more reliable, and more specific substrate.

3.1.4. 3D model - hanging drop cultures

Hanging drop (HD) cultures are an excellent, easy method that are widely recognised as much more physiologically relevant than 2D culture methods. Two main advantages are that there is no interaction with an artificial surface, and it is entirely 3D. With no artificial surface to adhere to, the cells can only interact with each other. It is a logical conclusion that cell behaviour on any artificial surface, such as glass and plastic may not be biologically representative at all. Introducing a 3D culturing technique eliminates the requirement for these surfaces, and may induce interesting behavioural changes. HDs also force cells to interact with gravity, so characteristics relating to spatial organisation and adhesion can be examined.

3.2. Assays to study cell behaviour

3.2.1. COCA cells act as an epidermal substitute

Initial experiments were designed using the COCA cell line (Segrelles et al., 2011). In order to recapitulate the epidermal conditions during mid-gestation development, experiments were performed when the cell line had been cultured for 1 week at an ALI. This stage consists of a confluent monolayer that is beginning to differentiate. *In vivo*, the epidermis is a single cell layer (not including the periderm) until stratification begins around E15 (Sotiropoulou and Blanpain, 2012). Stratification occurs due to a change in cell plane division, which becomes perpendicular to the basal membrane (Smart, 1970). The aim was to combine this developing culture with the various MLs, then use timelapse imaging to observe cell behaviour patterns under different conditions. We hypothesised that the MLs would migrate throughout the culture

3.2.1.1. Histological analysis of COCA cell line

To demonstrate that the 3D COCA membrane could be successfully prepared, and to further assess the *in situ* expression of epidermal markers, histological and IF analyses were performed.

Figure 3.1.A. shows the COCA keratinocyte line *in vitro* culture at passage 32. The next image (Figure 3.1.B.) demonstrates the staining kit (provided with media) used to check that a confluent monolayer has been formed; confirming this is important as achieving a confluent layer is crucial to successfully differentiating the culture. H&E staining in Figure 3.1.C. demonstrates the 3D appearance of the culture after 1 week at the ALI. At this stage, the keratinocyte cells are beginning to stratify; their shape has become long and flat, and they are multi-layered.

Some key markers of keratinocyte differentiation are shown by IF staining in Figure 3.2.; Collagen VI is the core component of the basement membrane, where it provides an organised structure for support (Paulsson, 1992). IF staining revealed strong expression on the basal aspect of the COCA cell layer, but clearly underneath the cells themselves. The staining appears slightly blurred; this is no doubt due to the presence of the PCF membrane, on which the cells are grown. This confirms that the cells have developed a continuous basement membrane, probably incorporated within the PCF membrane. The presence of this structure is essential to the epidermis (Breitkreutz, Mirancea and Nischt, 2009; LeBleu, MacDonald and Kalluri, 2007). E-cadherin is an essential protein in cell-cell junction formations. It is highly expressed in the epidermis, as the junctions between keratinocyte cells have to provide an impenetrable barrier to the outside environment (Alberts, Johnson and Lewis, 2002). K5 is a Type II keratin (basic/neutral) that is expressed in the basal keratinocytes of the epidermis. It partners with K14, and together these form an important marker of the basal cell layer in stratified epithelia. They are also one of the earliest markers of keratinocyte differentiation (Kurokawa et al., 2011). In the COCA culture, K5 is expressed continuously along the basal layer, indicating the epidermis is beginning to differentiate. K10 is also a marker of the suprabasal epidermal keratinocytes (Kurokawa et al., 2011). Higher magnification reveals that K10 is indeed expressed

specifically in the basal layer of keratinocytes. All four proteins examined are localised to the correct location, and demonstrate that epidermal differentiation is occurring in the 3D culture. These patterns were observed in triplicate biological repeats.

3.2.1.2. RNA expression profile of COCA cell line

To further examine the differentiation process, the transcriptional expression profile was assessed at various stages of the culture. This was achieved by rtPCR, and compared to RNA in skin samples obtained from embryonic mice and mouse pup skin. The skin used for comparison was not separated by cell type, so is comprised of not only keratinocytes, but also melanoblasts/melanocytes, so express some RNAs that are not expected in the COCA cells. The results are summarised in Table 3.1, and data can be seen in Appendix A. K1, K2, K14 and p63 were used as markers of the stages of epidermal development. The transcription factor p63 is the earliest specific marker of the keratinocyte lineage (Green, Easley and Iuchi, 2003), and is expressed by the COCA cells at all stages. K14 is also expressed continually through the stages. K2 is a marker of terminal differentiation in the upper spinous and granular layers of the epidermis; the COCA cultures do not express this marker, even after 2 weeks of differentiated growth. K1 marks keratinocyte differentiation, indicating cells which have lost their capacity to divide, and is accompanied by a downregulation of K14 in those cells.

K1 begins to be expressed by the COCA cultures after 2 weeks at the ALI, signifying the development into a stratified epithelium. Like E-cadherin, P-cadherin is a cell-cell adhesion molecule, however it is expressed specifically in basal epithelium (Nose and Takeichi, 1986). It shows strong RNA expression at all stages. Finally, the expression of the sKITL and mKITL were tested, to determine whether the COCA cultures could support MLs. Expression of both ligand was consistent throughout the stages of the culture.

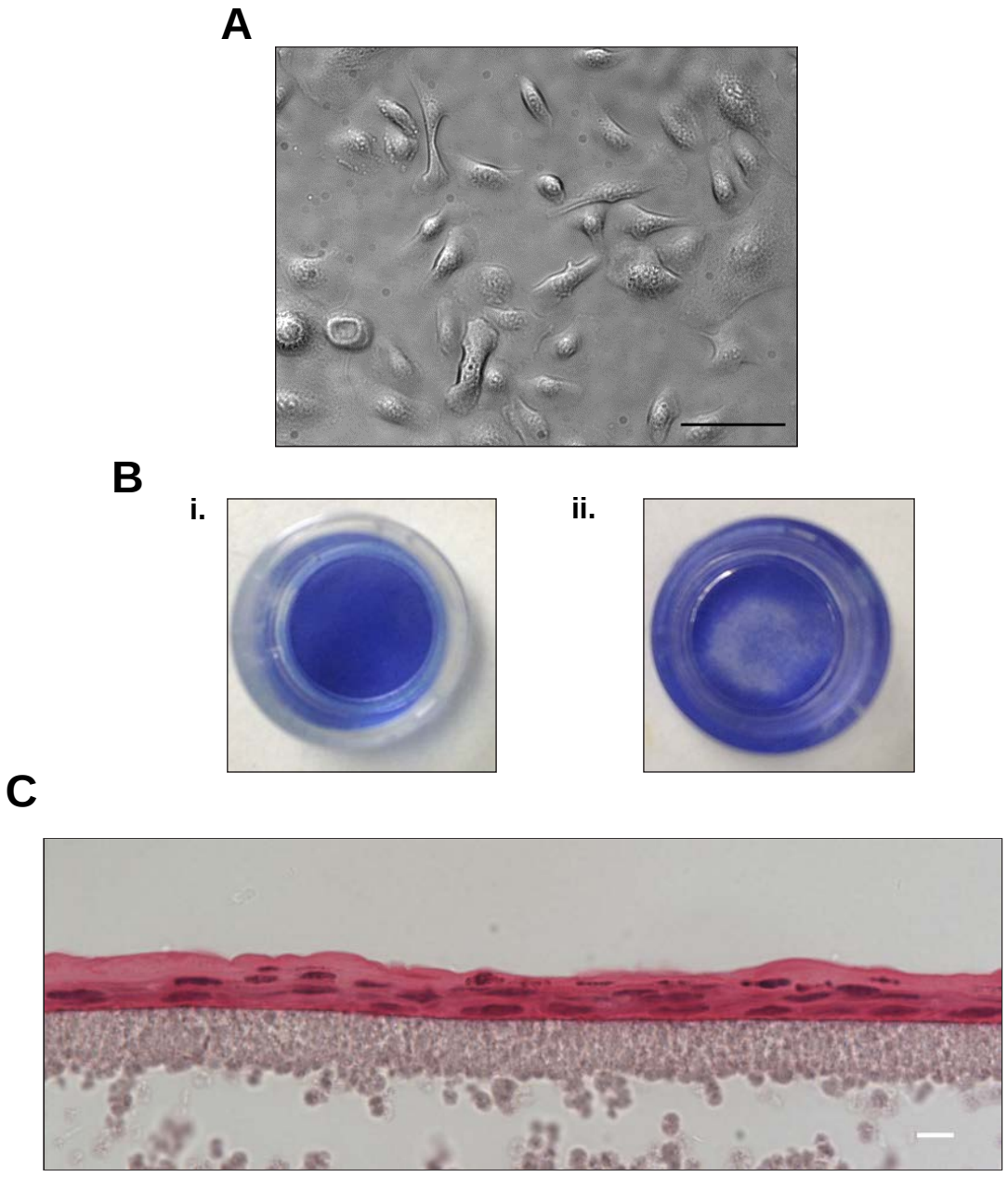

Figure 3.1. COCA cells at various stages of culture. A. COCA cells in 2D culture. Scale bar represents 100µm. **B.** Millipore PCF membranes are plated with 200,000 cells and grown for ~3 days. The cells are not visible by light microscopy, so the membrane is stained to check whether a full monolayer has formed. **i.** shows a membrane grown in the original orientation, which is fully confluent. **ii.** shows a membrane grown in the inverse orientation, where cells are not yet confluent in the middle. **C.** H&E staining of COCA cultures differentiated at an ALI for 10 days. Cells are starting to form layers, with some areas 3 cells deep. Below the cell layer is the Millipore PCF membrane. Scale bar represents 10 µm.

Table 3.1. RNA expression profile of COCA cells determined by rtPCR assays

Gene	COCA cells	1wk ALI	2wk ALI	E14.5 skin	P15 skin	Marker of
K1	-	-	+	+	+	Differentiation
K2	-	-	-	-	+	Terminal differentiation
K14	+	+	+	+	+	Basal cells of epithelium
p63	+	+	+	+	+	Keratinocytes
mKITL	+	+	+	+	+	-
sKITL	+	+	+	+	+	-
E-cadherin	+	+	+	+	+	Cell-cell adhesion
P-cadherin	+	+	+	+	+	Basal cells of epithelium

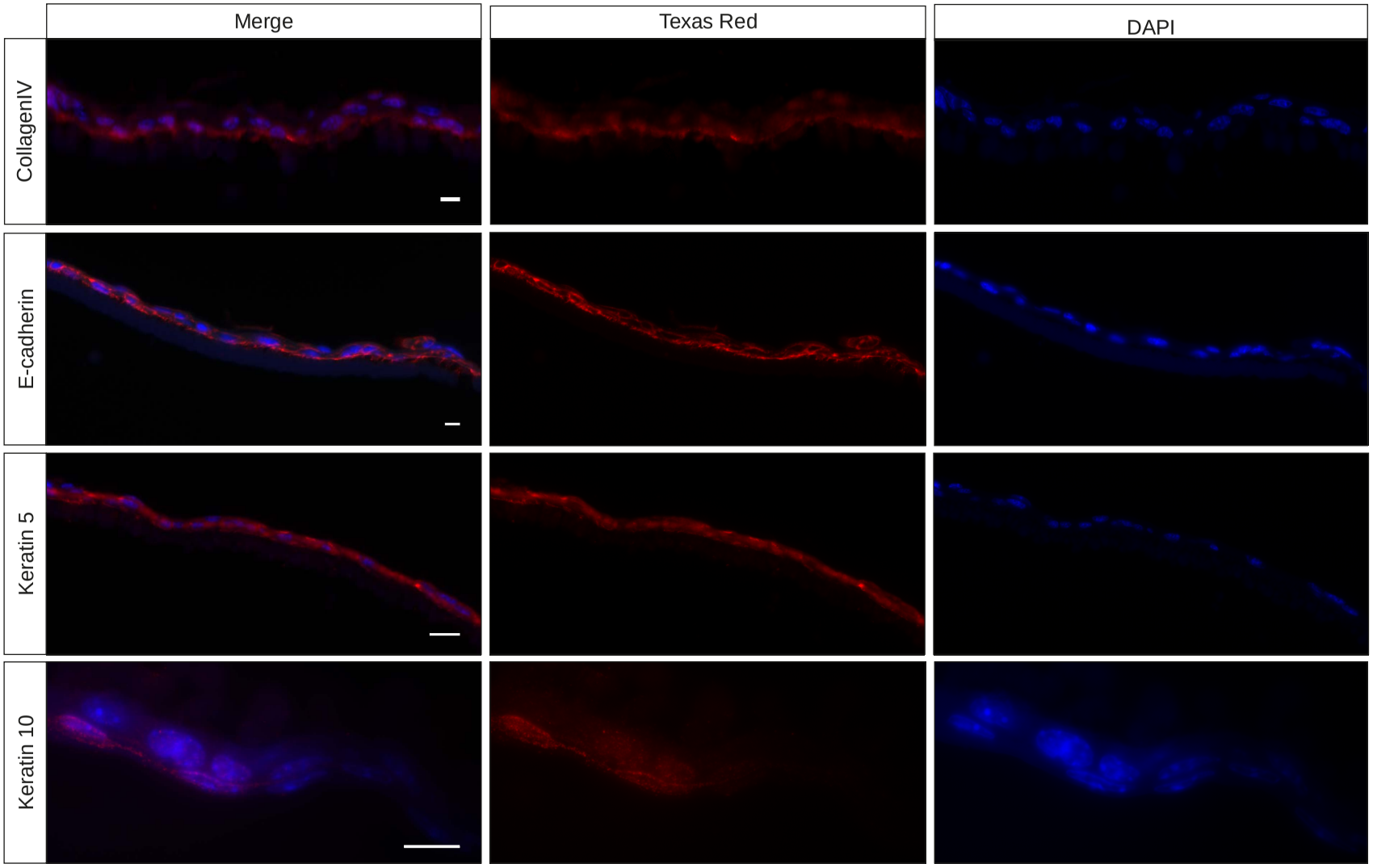

Figure 3.2. **IF staining of COCA membranes after 7 days at an ALI.** Scale bars represent 10μm for each row.

3.2.1.3. Timelapse imaging of COCA cell line in co-culture with MLs

To analyse migration of MLs in the COCA cultures, live timelapse imaging of the cultures was required, and so it was necessary to devise a method of inverting the cells, while maintaining the growing conditions. To do this, a technique was developed based on the system used by Mort *et al.* (Mort, Hay and Jackson, 2010); using a lumox membrane to act as both a coverslip, and as the permeable part of the air-liquid surface. As demonstrated in Figure 3.3. there are two orientations possible with this culture. Each is suitable for live cell imaging, however the inverted orientation shown in Figure 3.3.A.ii. proved to be the more reliable and reproducible; the membrane does not have to be physically cut out of the plastic mount; avoiding this step bypasses complications of disturbing the cells, or losing the membrane in the air flow of a laminar flow hood. Also, the membrane remains fully stretched and flat - once cut out, it is difficult to ensure the membrane is flat and does not move, as the only factor holding it in place is the downwards pressure of the clip. In order to grow cells on the inverse orientation, firstly, a new chamber to hold the media/cells is created from the bulb of a sterile standard plastic pastette. Secondly, in order to eliminate air pockets and stabilise the mounts in the media, the bottom chamber is filled with a media/agarose mixture. This also allows new media to diffuse to the cells, in two ways - by over-filling the chamber with the agarose/media mixture, the structure is lifted slightly so there is space for media to enter, and also by preventing air bubbles forming at the membrane.

At the epidermal stage which corresponds to the developmental stage *in vivo* (1 to 2 cell layers thick: 1-week differentiation ALI), the MLs in this culture do not move. Vital lipophilic dyes were used to stain cells as described in Chapter 2.3.8. In Figure 3.3.B., COCA cells are labelled blue with DiD, and melb-a cells are labelled green with DiO. Timelapse imaging these cultures shows that the cells still look viable and are ‘shuffling’ around in the culture, but there is no net migration as would be observed *in vivo* or *ex vivo*. This was repeated multiple times, but no migration was observed. An example of this can be seen in Video 3.1., which is the timelapse of the cells shown in Figure 3.B.

3.2.1.4. Pigmentation of COCA cell line in co-culture with MLs

An interesting feature that arose following these co-culture experiments was the observation of pigment in the cultures after growing at the ALI for >1.5weeks. Figure 3.4.A.i and ii. show two examples, in photographs taken of pigmented cultures. In Figure 3.4.A.i., a pigmented membrane grown in the inverted orientation has been inverted on a lumox membrane in preparation for imaging. In Figure 3.4.A.ii. a pigmented culture grown in the original orientation remains in the mount. Figure 3.4.B. shows confocal imaging from a timelapse series, with a section of cells around a pigmented patch magnified. In this culture, B16F10 cells are labelled red with DiI, while COCA cells are unlabelled. These images demonstrate that the pigment is not contained within the B16F10 cells. This result was consistent across numerous experiments. In melanogenesis, melanin is transferred to the surrounding keratinocytes. Attempts to conclude whether this was occurring in these samples histologically proved unsuccessful, as the majority of the top layer of cells became detached from the culture when any fix was applied. This upper layer was clearly visibly detached, and it proved impossible to rescue the cultures beyond this stage.

3.2.2. CDMs

CDMs were produced from fibroblast and keratinocyte cells in order to model the extracellular dermal and epidermal environments. The three lines are the commonly used NIH3T3 fibroblast line, fibroblasts isolated from $Kitl^{Sl}$ mice and the keratinocyte COCA cells.

3.2.2.1. In situ protein expression in CDMs

In order to assess the integrity of the CDMs and compare their composition, the CDMs were stained for key basement membrane and epidermal markers. Figure 3.5. shows the results of Van Gieson staining on each CDM. Van Gieson staining is used to label collagen (all types), as well as nuclei and other tissue. Collagen is very highly expressed in the CDM produced by all three cell lines. Staining of the COCA CDMs is very strong, stronger than in the other lines, indicating a high collagen presence in the epidermis. It is likely that a high proportion of this is composed of

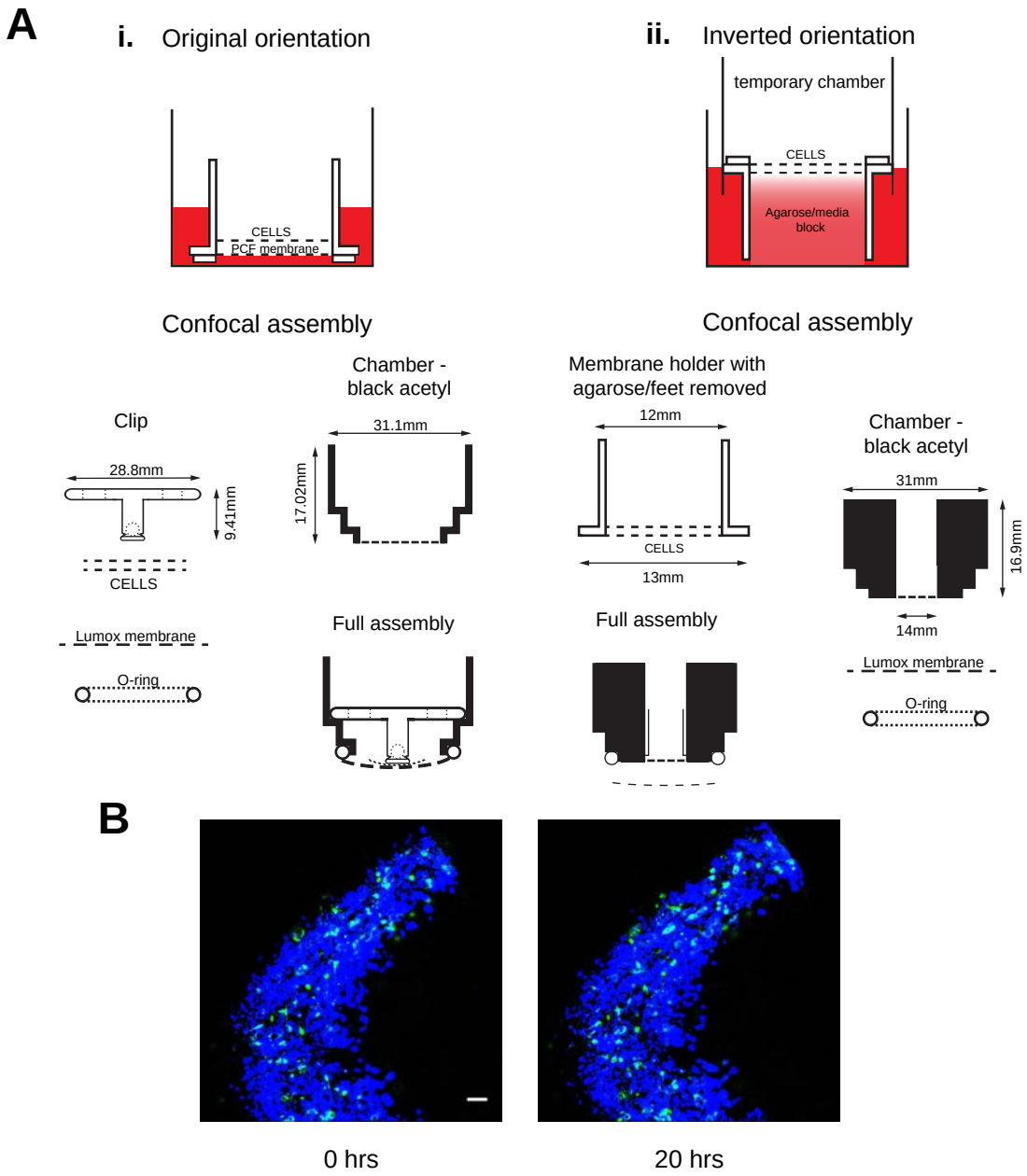

Figure 3.3. COCA 3D culture imaging. Schematic of culture chamber assembly with cells at the ALI. Two orientations were tested for optimising imaging. **i.** The membrane is grown in the plastic well and media is removed from the middle to create the ALI. To assemble the imaging platform, the membrane is cut out, inverted, then sandwiched between the clip and a lumox membrane. This set-up is described in detail in Mort *et al.* 2014. **ii.** In the inverted orientation, a section of plastic pastette, creates a temporary chamber on the reverse side of the membrane. The under side is filled with an agarose/media mix to hold the casing off the bottom of the well to allow media to touch the agarose, and to eliminate any air pockets. For imaging, the plastic pastette is removed and the whole plastic structure is turned over to fit into an alternative imaging chamber. The plastic feet of the casing must be cut off. In both orientations, a lumox membrane is used to seal the chamber whilst maintaining an ALI, this is secured in place using a plastic O-ring. The chambers are inserted into the perpex casing described in Figure 3.7.A. **B.** Timelapse images acquired 20 hrs apart by confocal microscopy of COCA cells (blue) in co-culture with melb-a cells (green). There is no measureable movement of cells in this time (this also is observed in other ML co-cultures). Scale bar represents 50 µm.

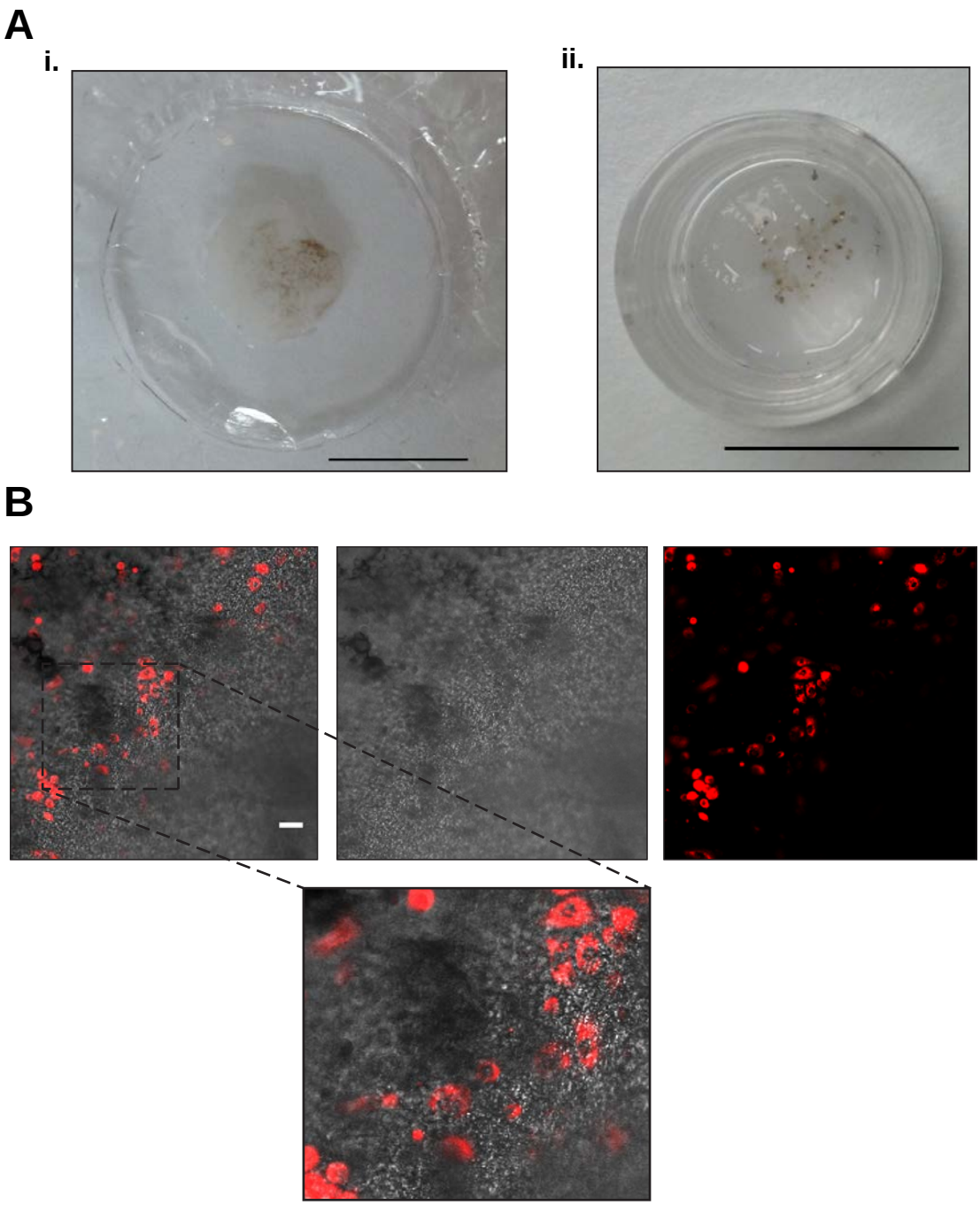

Figure 3.4. Pigmentation of 3D COCA cultures. A. **i.** Photograph of a pigmented culture on a lumox membrane. This culture is B16F10 cells, plated in a ratio of 1:10 with COCA cells, and grown for 10 days at the ALI. **ii.** Photograph of a pigmented culture within the plastic casing. This culture is also B16F10 cells in a 1:10 ratio. This culture was grown for 14 days. Scale bars represent 1cm. **B**. Confocal images showing B16F10 cells labelled in red by DiI, in co-culture with COCA cells. Black pigment is clearly visible in the transmitted light channel. The grainy texture covering the transmitted light channel is the PCF membrane.The black pigment and B16F10 cells do not colocalise, indicating that pigment has travelled away from the pigment producing B16F10 cells. It is possible the pigment is situated within the COCA keratinoytes, which are confluent over the whole membrane. Scale bar represents 50 µm.

collagen IV, which as discussed, is a core component of the basement membrane (and is demonstrated by IF in Figure 3.6.). Further, this staining also shows that the CDMs have been successfully removed of any nucleic matter, or any other cell tissue. This provides confidence that the cultures taken forward for staining, or live cell imaging, are indeed composed solely of the ECM expressed by the environment cells. It is also a quick, reliable method to check that the CDMs are intact after the denudation process.

Figure 3.6.A. shows the results of IF experiments, again comparing deposition of key ECM proteins. The CDM protocol describes how leaving the media change to every other day, will increase the deposition of fibronectin in the matrix (Kaukonen et al., 2017). Fibronectin is primarily present in the connective tissue comprised of fibroblasts and in the skin, fibronectin is mainly found in the dermis, and at the dermal-epidermal junction (Fyrand, 1980). NIH3T3 and Sl/Sl CDMs express fibronectin in the expected fibrillar pattern. IF experiments were performed in parallel with secondary antibody-only controls to ensure that the staining is genuine. There was no visible deposition of fibronectin in the COCA CDMs. Laminin is a core component of basal membranes (Aumailley and Smyth, 1998). Staining of NIH3T3 and Sl/Sl CDMs again follows the expected fibrillar pattern, associated with the collagen network. In the COCA CDM, laminin staining appears non-uniform and speckled.

3.2.2.2. KITL

KITL is essential for melanoblast survival (Yoshida et al., 1996). The soluble isoform, sKITL, is glycosylated and integrated into the ECM (Morrison-Graham, West-Johnsrud and Weston, 1990). To determine the KITL status of the CDM producing cell lines, total protein was isolated and detected via western blotting. Figure 3.6.B. shows a western blot of protein extracted from the three environment cell lines, probing for KITL. KITL is predicted to have a molecular weight of around 32kDa (kilodalton) (Reber, Da Silva and Frossard, 2006). This western blot used a custom antibody kindly provided by Professor B. Wehrle-Haller. Although there are

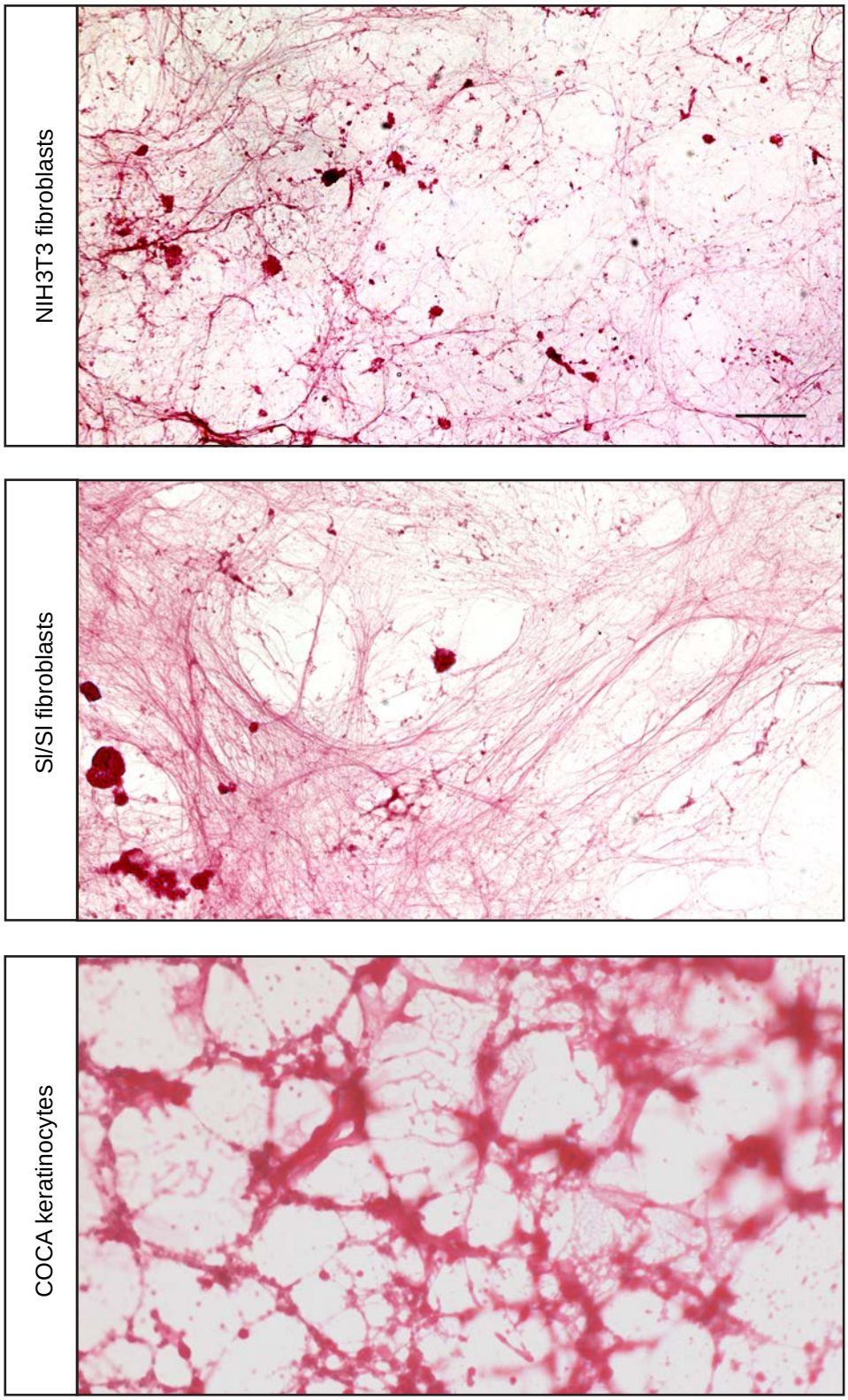

Figure 3.5. Van Gieson staining of CDMs produced from NIH3T3, Sl/Sl and COCA cells. The Van Gieson staining method marks all isoforms of collagen in red, nuclei in blue and other tissues in yellow. The COCA culture showed high collagen staining. All three cultures showed collagen staining consistent with the fibrillar structure expected. No blue or yellow staining shows that cells have been successfully removed from the matrix during the denudation process. Scale bar represents 20 μm.

some additional bands, this antibody successfully demonstrates the lack of KITL in the Sl/Sl line.

3.2.2.3. Chamber for confocal imaging of CDMs

In an effort to increase the throughput of CDM experiments, a new imaging chamber was designed and manufactured with the IGMM technical workshop. After exploring several routes and numerous prototypes, the final design is a small magnetised chamber which houses 6 individual 13mm coverslips. This allows multiple experiments to run at once, and makes it possible to recover the CDM coverslip post-imaging. The chamber is based on a standard 6-well culture plate. Thus, any standard fit plastic lid can be used to cover the chamber for sterility, and it also fits into standard size confocal microscope stage inserts. The chamber schematic can be seen in Figure 3.7. with exact measurements. Essentially, the CDM-bearing coverslip is sandwiched between an inner and outer chamber, secured with a ring magnet and further sealed with silicon grease. A video of the equipment assembly is available in Video 3.2. (filmed by Craig Nicol and Len Hay). This system has proved to be watertight, suitable for confocal microscopy and non-damaging to the exposed part of the delicate CDM. This equipment is very versatile, and suitable for securing any thin, watertight membrane/glass/plastic etc. specimen of interest.

In designing the chamber, there were several factors to consider. For confocal microscopy, the glass coverslip must sit as close to the bottom edge of the chamber as possible. Conversely, the metal plate at the bottom needed to be thick enough for the magnet to adhere strongly. Therefore, we opted to use a sloped gradient to the opening in the centre, providing both the strength, and shallow depth required. This does mean that when capturing images in a multi-point timelapse experiment, the microscope must have the ability to automatically escape and refocus in order the move between wells.

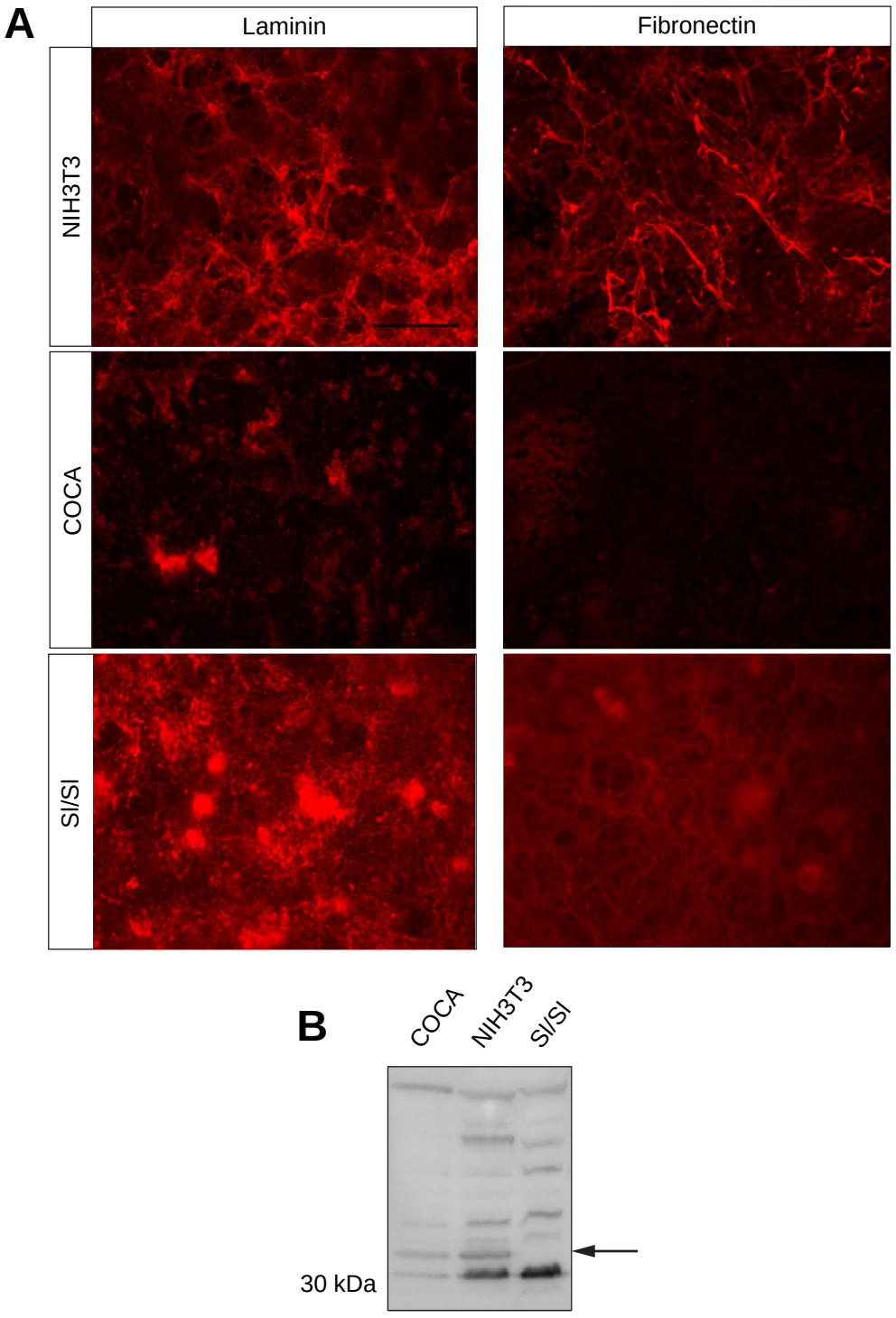

Figure 3.6. IF staining of CDMs and Sl/Sl validation. A. Fibronectin and laminin staining is strong in both NIH3T3 and Sl/Sl CDMs, showing the expected fibrillar pattern consistent with ECM. Fibronectin staining on COCA CDMs appears weak. Laminin staining appears non-specific on COCA CDMs; when compared to NIH3T3 and Sl/Sl CMDs, there is also some uncharacteristic granular staining. Scale bars represent 50µm. **B.** Western blot of protein isolated from COCA, NIH3T3 and Sl/Sl fibroblasts, probing for KITL expression. KITL has a predicted molecular weight of ~30 kDa. The arrow indicates the missing band in the Sl/Sl line, which confirms the absence of KITL in these cells.

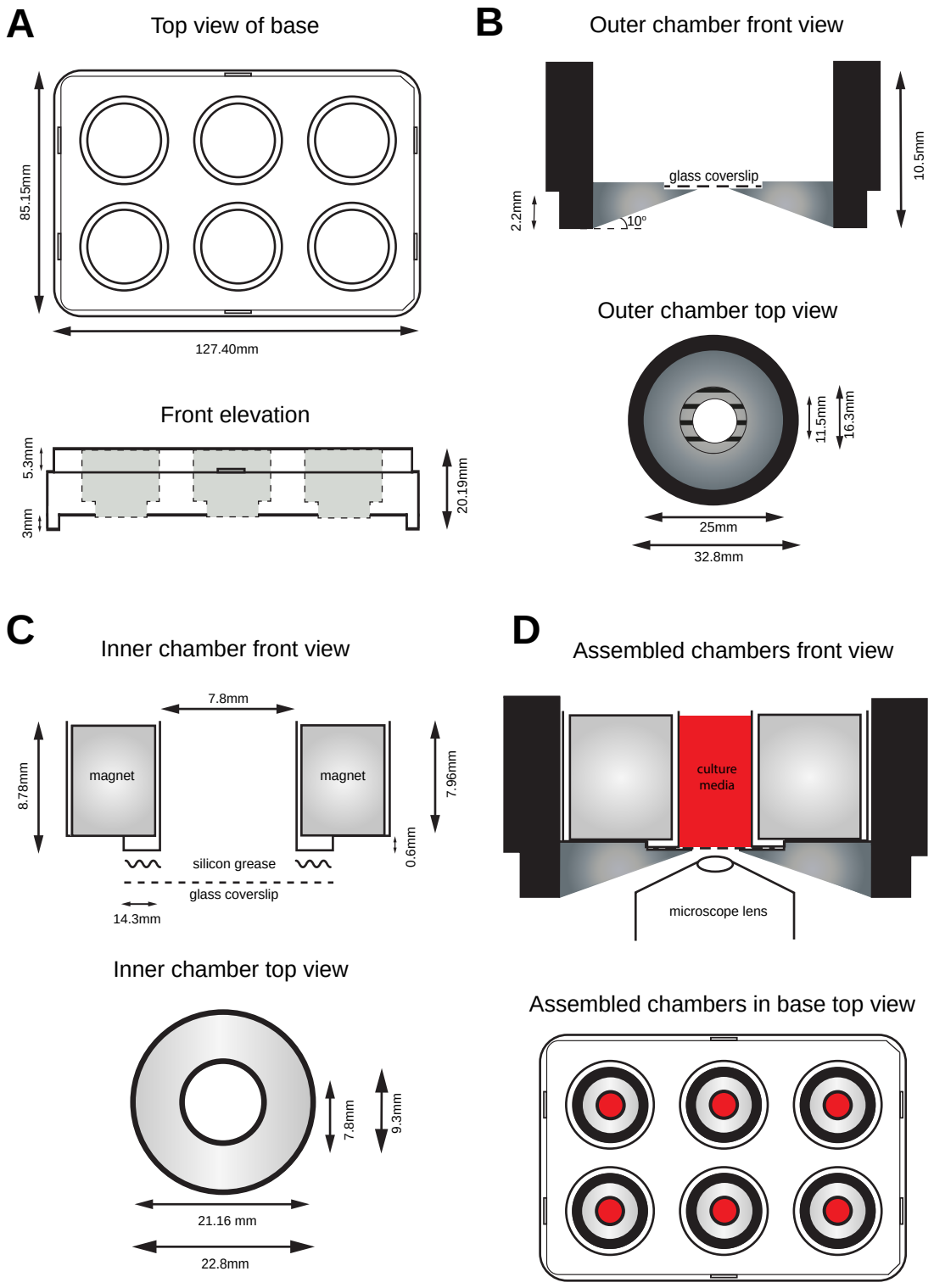

Figure 3.7. Schematics showing assembly of CDM imaging chamber. A. The outer casing is based upon a standard 6-well plate design and made from perspex. **B.** Outer chamber in which the glass coverslip sits in a small recess for stability, and to allow the magnet to sit flush with the base. The base of this chamber is magnetic metal, seen in the lower figure with the coverslip recess. **C.** The inner chamber houses the magnet, keeping it separated from the culture. **D.** Fully assembled equipment with culture media filling the wells. The CDM coverslip sits at the bottom of this aspect, close to an inverted microscope lens.

3.2.3. HD cultures

Another approach to examining cells in a more physiologically relevant 3D culture was to use the commonly described HD technique. HD cultures were produced from all 4 MLs and grown for 5 days. At this point a defined aggregate of cells can be seen. These cultures are then re-inverted, and plated on various surfaces to observe the subsequent behaviours of the cells over time. The formation and delamination (discussed later) of the HDs is highly reproducible, and was performed routinely.

3.2.3.1. Optimising the culture

Before any migration experiments were performed, it was observed that there was a difference in the structure of the aggregates formed between the cell lines. To investigate this further, the number of cells plated into the culture was optimised, to determine whether this would have a large impact on the structures produced. See Figure 3.8. for images taken of each cell line. These images are taken when the drop is still inverted i.e. they have not been disturbed at all for 5 days. The melanoblast lines melb-s1 and melb-m5 behaved in a similar manner, creating small, compact aggregates, throughout the series of dilutions. They begin to lose their compact shape when numbers plated reach ~12,000 cells. Melb-a cells are less compacted, with more cells appearing unattached at the border of the aggregate. The B16F10 cell line was most strikingly affected, with a very clear switch of non-adherence to adherence between 6,000-7,000 cells plated. This could be an interesting effect of the cancer cell line, indicating a threshold level of cells at which a tumour might start to develop. To maintain equality, and satisfy all four ML lines, 10,000 cells were routinely plated for subsequent experiments.

3.2.3.2. Co-culturing HDs

Attempts were made to produce HDs with the COCA cells, with the intention of co-culturing MLs and environment populations in the same drop to observe their interactions, and how they would organise themselves. This proved impossible. Firstly, COCA cells in a HD did not form an aggregate, and instead formed a layer of cells along the ALI, which dissipated immediately upon inversion of the drop. This is

perhaps not surprising for a number of reasons; keratinocytes are, crucially, polar at an ALI and they form a sheet of cells *in vivo* rather than a mass. However, there should be tight junctions formed between neighbouring keratinocytes – perhaps this is not the case when the cells are only one layer thick. Secondly, when the co-cultures were attempted, the MLs would no longer form an aggregate either.

3.2.3.3. Requirement for an ECM

Once formed, HD aggregates were handled and transferred via mouth micro-pipette. This technique allowed for a high amount of precision, vital for the delicate aggregates. Some of these aggregates were used for live time-lapse imaging studies. In these imaging experiments, half of the HDs were covered with a matrigel:media (1:5) solution, while the other half had no matrigel. Aggregates with no matrigel did not migrate in any of the cells lines. This was repeated several times, to ensure that the aggregate was not simply floating in the media as can occur, but that there was no migration when attached to the surface. Whether the necessity of the matrigel is down to the ECM proteins it provides, or the physical structure it provides for attachment is unclear. Later experiments combined HD cultures with CDMs, and these proved able to support the MLs in the same manner as the matrigel, thereby negating the reliance on matrigel (presented in Chapter 4.3.).

3.2.4. 2D assays

Studying cell behaviour *in vitro* is most commonly achieved using 2D assays. Although there is a strong focus on moving to more 3D models, these ‘simple’ assays are still useful in providing basic cell characteristics.

3.2.4.1. Visualising cells in vitro

These assays make use of the vital dyes DiI, DiO and DiD from ThermoFisher, which are easily incorporated into the cell, are non-toxic and last for over 72 hrs through multiple generations. These dyes were used in combination with NucBlue, a vital nuclear dye. Using these dyes in combination allowed different lines to be

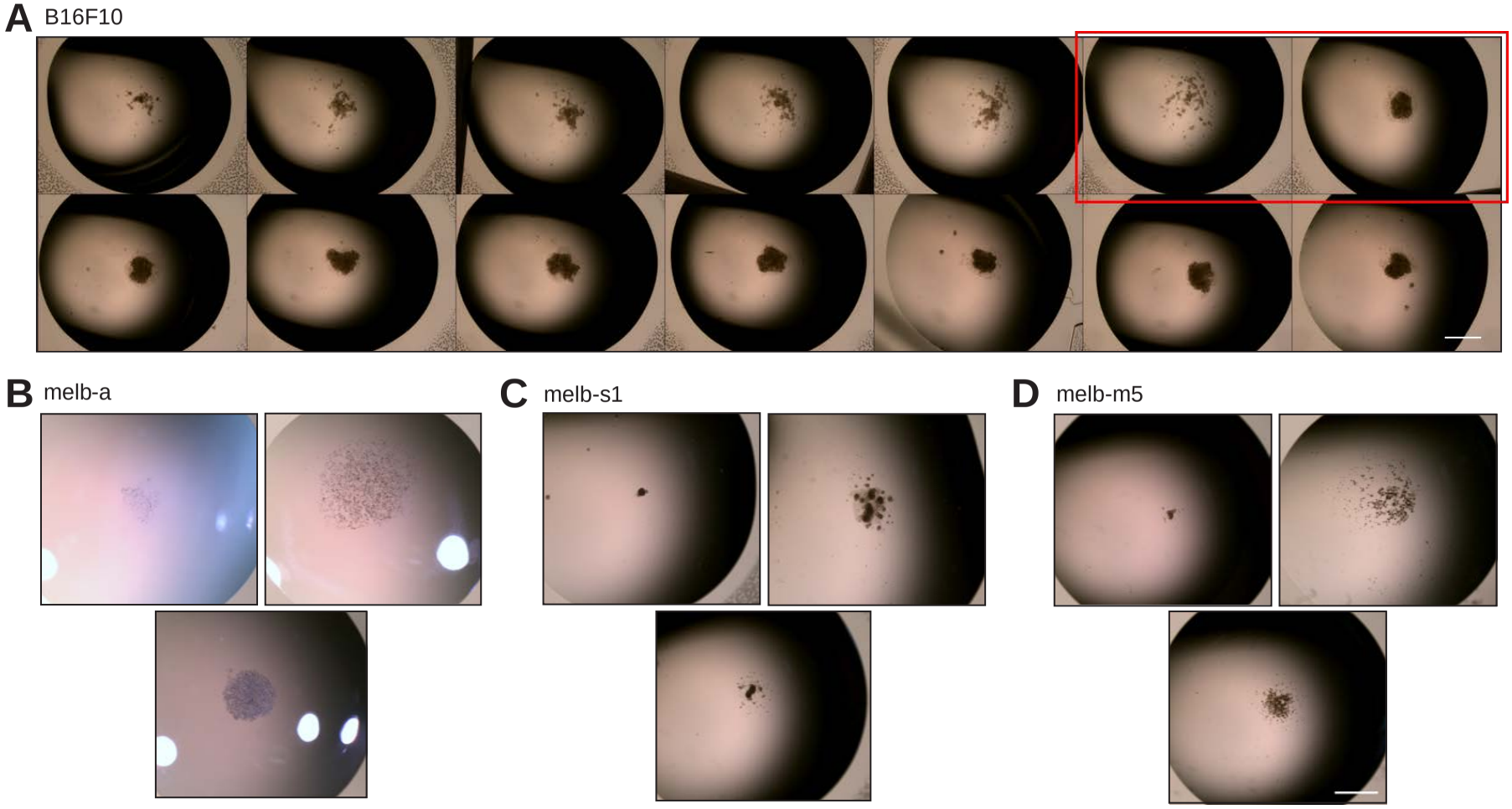

Figure 3.8. Optimisation of cell number in the HD assay. Various numbers of cells plated in a drop. Ranging from 1,000 cells to 14,000 cells (not all shown). Each drop is 30µl media, scale bars represent 500µm. Drops are imaged from above, whilst hanging from petri dish lid. **A.** B16F10 cells. Panels are 1,000 cells to 14,000 cells from left to right. The dramatic shift from scattered cells to dense aggregate is shown in the red box between 6,000 (L) and 7,000 cells (R). **B-D.** Melanoblast lines. All panels are: top 1,000 cells (L) then 14,000 cells (R) and bottom 10,000 cells.

imaged together, or can also be used to visualise a subset of cells in a dense population. Although only the 3 basic colours (red, green and blue) were used here, the dyes can be mixed to give an even wider range e.g. mixing DiI (red) and DiD (blue) will give purple (Gan et al., 2000). This is useful as tracking cells at high density can become inaccurate when the cells are moving atop one another. Examples of the use of these labels can be seen in Chapter 4.

3.2.4.2. Creating a leading edge

A commonly used 2D technique in migration experiments is the scratch assay. This simple assay consists of cells grown in a monolayer, then a scratch is made along the surface. This simulates a wound, to which the surrounding cells respond. There are two problems with using this technique to model NC developmental migration; firstly, in melanoblasts there is only a single side moving outwards, rather than two sides trying to re-join; cells on either side of the trunk migrate independently of one another, patterns are not consistent between the two sides (Huszar, Sharpe and Jaenisch, 1991). Secondly, a wound/scratch induces many inflammatory pathways e.g. cytokines being released by nearby dying cells. Therefore, creating a more natural edge within a culture was desirable. To achieve this, cells were plated within a silicon ring attached to the imaging surface. A neat edge of cells is created when the ring is removed, which have not been exposed to influential factors before beginning their migration. Examples of these cultures can be seen in Figure 4.1.

3.3. Discussion

3.3.1. Co-culture of MLs with COCA cells proved unsuitable for experiments on cell behaviour

When COCA and ML cells were cultured together and then stratified, imaging showed that the ML lines were not migratory. There may be at least three reasons for this, and perhaps all three may be contributing factors. Firstly as mentioned previously, in order to bring the COCA culture to the ALI to differentiate, the layer of cells must first be confluent. This may simply lead to there being no space for the

MLs to move through. In a related point, an important factor that this culture cannot incorporate is the expansion of the skin during development. Experiments performed *in vivo* have both a growing domain, and a gradient of cell concentration, such that at E14.5, there is a higher concentration of cells at the dorsal aspect than at the ventral, although this is not true in *ex vivo* cultures, which do show migration (Mort, Hay and Jackson, 2010). Melanoblasts migrate along this axis naturally as they exit the NC at the dorsal aspect in order to populate the whole trunk. Lastly, the inverted nature of the experimental equipment to maintain compatibility with confocal imaging, may lead to the delicate epidermal layers being 'squashed' together. In this case, any space that the MLs were migrating through in culture, may have been lost during imaging.

The observation of pigmentation in the differentiated cultures confirmed that the MLs were still viable in the culture, at the stage where they were no longer moving (as observed by timelapse imaging). This was an interesting prospect as a system to study the transfer of pigment between an adult melanocyte and a neighbouring keratinocyte. It could also be a more simple case that the MLs were producing and releasing pigment that was not being taken up by keratinocytes. This is commonly seen in culture of these cell lines, the growth medium is often heavily pigmented with released melanin. Indeed, in order to prevent differentiation i.e. pigmentation of the melanoblast lines, these cells are maintained at low confluency. As described by Sviderskaya *et al*., the melanoblast lines are no longer considered as 'melanoblasts' once pigmentation begins, so it is also possible that the process to differentiate the keratinocyte culture, has the same effect on the melanoblasts. In order to determine whether this system could be used to study melanin transfer, further histological studies should be undertaken to establish where the melanin is residing.

Although the co-culture model did not produce the imaging results that were desired, there were some positive outcomes. Importantly, the COCA line was found suitable as an epidermal mouse line for future combination with the MLs. RtPCR and IF studies demonstrated the expression of both sKITL and mKITL. They also showed clear markers of epidermal differentiation stages, supporting the use of COCA as an epidermal tissue substitute.

Ultimately however, these co-culture live imaging experiments proved unsuitable for our desired use and the project direction was adjusted. The rest of this thesis will instead concentrate on other techniques for incorporating the environmental stimuli using other methods.

3.3.2. CDMs produced from dermal and epidermal cells show variable levels of ECM proteins

In order to study cell behaviour in the epidermis specifically, CDM production was attempted from the keratinocyte line COCA. This endeavour was successful, and allows the opportunity to perform experiments from two angles; with fibroblast derived CDMs representing the dermal environment, and COCA CDMs representing the epidermal environment. Reasons for looking at cell behabiour on the different CDMs is highlighted by the differences in their compositions; keratinocyte CDMs were shown to be composed mainly of collagen fibres, whilst fibroblast CDMs were richly deposited with laminin and fibronectin. The epidermis is known to have a unique extracellular composition, which was highlighted by the IF staining.

3.3.3. HD cultures resemblance to NC explant cultures

Historically, studies into NC expansion have been performed *ex vivo*, where the NC is dissected out at ~E8.5, and then maintained in culture for a number of days (Huang et al., 1998). Cells of the NC migrate outwards in a characteristic pattern. When HDs were plated and left to migrate, they did so in a pattern strikingly similar to the *ex vivo* neural tube cultures, and this perhaps can serve as a model for NC migration *in vitro*. This will be discussed further in terms of migration in Chapter 4. *In vivo*, cells disseminate from the NC via EMT mechanisms (discussed in Chapter 1.1.2.). The possibility of this occurring in these HD cultures is also explored in Chapter 4 and 6.

Chapter 4

Dynamic behaviours of cultured cells

At the cellular level, there are many aspects of behaviour that can be modelled to characterise a cell population. Tracking cell movement allows observation of several behaviours, including migration speed, persistence of direction and distance travelled. *In vivo*, these behaviours are carefully controlled during development to ensure cells populate the embryo correctly, while in cancer metastasis, the ability of a cell to migrate is central to the disease progression (Aman and Piotrowski, 2010). In melanoblast development there are several distinct stages that are of particular interest, including: the dissemination from the NC as the melanoblast precursors begin their development; the cells crossing the basement membrane at around E12.5 to populate the epidermis; the mass migration and population expansion to colonise the entire embryo, and finally, the localisation of melanoblasts to the hair follicle (Mort, Jackson and Patton, 2015). Once in the hair follicle, the establishment of a stem cell pool and melanocytes in skin homeostasis are key areas of research. Examining characteristics of dynamic cell behaviours *in vivo* is difficult for a number of reasons, as discussed in Chapter 1.4. In essence, the ability to maintain an uncompromised tissue *ex vivo* and be able to examine the cells behaviour within the tissue in real-time is technically challenging. There are models which are able to overcome these issues, however they are not without other limitations. For example, the *ex vivo* skin culture system developed by Mort *et al.* is used in a short time frame due to the inability to separate the embryonic skin pre-E13.5 and the skin becoming thicker post-E14.5 which makes imaging difficult (Mort *et al.*, 2014). Current methods using *in vivo* or *ex vivo* migration studies are unable to dissect some important factors, for example, it is not possible to examine individual cells in isolation, or to manipulate the population density. *In vitro* cell assays can be used to complement the current models, by quantifying some of those parameters which are difficult to observe, and also by providing a large volume of data that may be required to extract subtle behaviours.

To model melanoblast and melanoma (MLs) behaviour *in vitro*, several different immortalised cell lines were used, which were introduced in detail in Chapter 3.1. Firstly, four experimental ML cell lines were used; melb-a, melb-s1 and melb-m5 to model melanoblasts and B16F10 to model melanoma. Melb-a cells are a wildtype melanoblast cell line (Sviderskaya, Wakeling and Bennett, 1995), melb-s1 cells carry a mutation in the EdnrB gene (Sviderskaya, Easty and Bennett, 1998) and melb-m5 cells are derived from mice with mutations at the *misty* locus (Sviderskaya et al., 1998). The B16F10 mouse melanoma line is highly metastatic *in vivo* and invasive *in vitro* (Gehlsen and Hendrix, 1986). To model the extracellular environment, CDMs were produced from NIH3T3 fibroblasts, Sl/Sl fibroblasts and COCA keratinocytes, as detailed in Chapter 3. NIH3T3 fibroblasts have been used before to create CDMs, and were used as a positive control of technique as well as a model for the dermal environment (Chlenski et al., 2011). Sl/Sl fibroblasts from the Kit^{Sl} mutant lack expression of KITL (Sarvella and Russell, 1956). COCA cells were the first immortalised line of mouse keratinocytes that retain the ability to differentiate *in vitro* (Segrelles et al., 2011), and are used herein to model the epidermal environment. Results from Chapter 3.2.2. and Figures 3.5. and 3.6. demonstrated different compositions in key ECM proteins of the fibroblast derived and keratinocyte derived CDMs, which may impact upon cell behaviour.

The experiments developed and used in this thesis concentrate on modelling the migration of melanoblasts from the NC during early development. The assays were introduced in Chapter 3, and this chapter will continue by using those assays to explore the behaviour of the cell lines under various culture conditions.

4.1. Dynamic cell behaviour in 2D

Cells in culture are highly dynamic and exhibit several measurable behaviours. The focus herein is on the migratory properties of the cell lines, although these cultures are also suitable for examining their proliferative and morphological properties.

2D cell migration experiments were performed to characterise basic characteristics of velocity and persistence. In order to visualise the cells in culture, cells were

synthetically labelled using the commercially available lipophilic tracers DiI, DiO and DiD. These tracers do not affect cell viability, and are incorporated into the plasma membrane where they persist through many generations (Honig and Hume, 1986). Examples of labelled cells in culture can be seen in Figure 4.1. and in Video 4.1. This figure also demonstrates the two cultures in which cell migration was compared – the standard whole field (WF) plating, and the leading edge (LE) plating method. To create a leading edge, cells are plated within a silicon ring, which is removed immediately prior to imaging. Figure 4.1.B. shows an example of an LE culture with melb-a cells labelled with DiI, DiO and DiD in a timelapse sequence. Cells move into the empty space over time as illustrated.

Individual cells are tracked through a timelapse imaging experiment using the Fiji plugin 'TrackMate' (Tinevez et al., 2017). Four main measurements are taken from the cell tracking data: the velocity, the accumulated distance, the Euclidean distance and the persistence. The velocity is calculated as the distance moved in μm per minute. Accumulated distance is the total distance a cell travels during a track. The Euclidean distance is the distance the cell travels from the origin of the track, in a straight line. The persistence is a measure of how straight a cells migratory pathway is. It is calculated by dividing the Euclidean distance by the accumulated distance; the closer to 1 the persistence value, the straighter the track, while a cell moving more randomly will have a persistence value closer to 0. Cell migration persistence (or directionality) is an important factor during cell migration that is influenced by extrinsic migration factors such as chemoattractants and mechanical cues (Petrie, Doyle and Yamada, 2009). Cells and organisms vary their migratory persistence depending on the collective behaviour required. For example in mouse, melanoblasts migrate in a predominantly undirected manner when colonising the epidermis (Mort et al., 2016), this may have evolved as a mechanism to guarantee even pigmentation of the coat to avoid predation. Conversely, amoeba alternate between persistent and anti-persistent behaviour in the search for food as a mechanism to efficiently cover the area they are exploring (Miyoshi, Masaki and Tsuchiya, 2003).

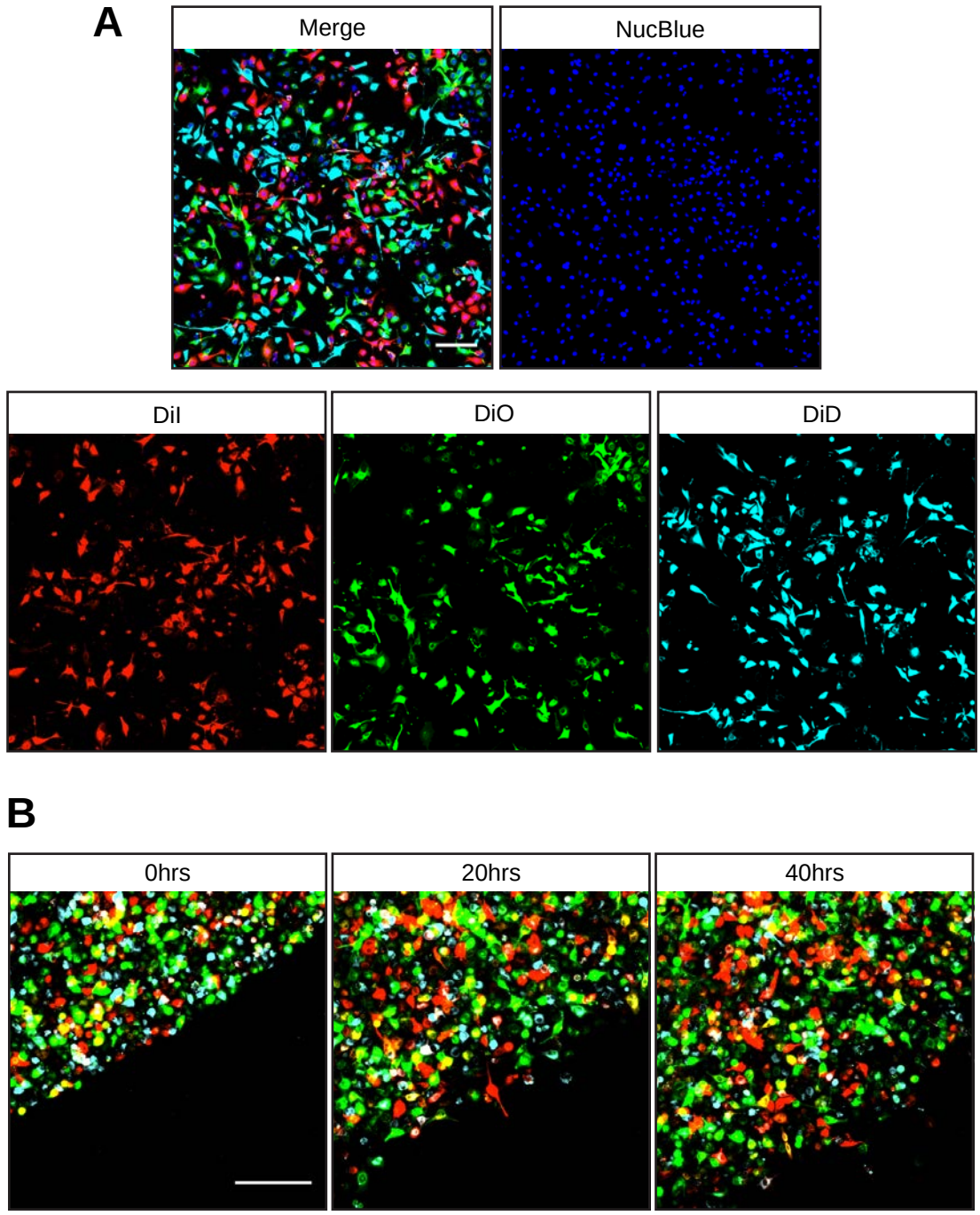

Figure 4.1. Vital dyes used in combination to label cells in WF and LE culture. A. Melb-a cells in a WF culture are labelled with DiI, DiO and DiD, and the nucleus is labelled with NucBlue. A single flask is split in three - each group is labelled with a different colour due, then all three are recombined into a single culture. NucBlue is added to the imaging media ~30 mins before the experiment. **B.** Labelled melb-a cells are plated in a silicon ring to create the LE culture. The ring is removed immediately prior to imaging, and cells begin migrating into the empty space. In this timelapse, cells were followed for 40 hrs, and imaged every 30 mins. Scale bars represent 100µm.

In the following results, each cell type group is composed of cell tracks combined from a number of individual experiments, to provide technical and biological replicates (at least three). The number of cell tracks is indicated under each graph. From a single timelapse sequence, all cells which remain in the frame for at least 50% of the sequence were considered for tracking. This ensured that enough measurements were obtained for a track to accurately represent the velocity and persistence. The mean values were compared between replicates before pooling to ensure similarity, and a normal distribution was confirmed.

4.1.1. ML cells exhibit four main patterns of migratory pathway

To begin characterising the migratory patterns of the ML lines, cells were plated in WF cultures and timelapse imaging was performed. Tracking data shows that migration behaviours of the ML cell lines in culture is heterogeneous in terms of the patterns of pathway followed. Within a single culture, four main patterns of trajectory were identified, and are presented in Figure 4.2. These trajectories were all isolated from a single melb-s1 WF culture, but are identifiable in all ML lines, and also in both WF and LE cultures. The first is a 'stop-start' behaviour (Figure 4.2.A.), where cells have periods of high migration followed by periods of low migration. These cells accumulate most of their travelled distance in short bursts. The second behaviour (Figure 4.2.B.) is highly migratory, in which cells migrate a long distance (accumulated) but do not venture far from their original location, so have a low persistence. The third behaviour includes cells which migrate extensively throughout the track (Figure 4.2.C.). These cells travel furthest from their origin, and consequently have a higher persistence. Finally, are cells which are migrating very little (Figure 4.1.D.). Cells in this category are still highly dynamic with changing shape, but do not move away from their origin.

A further observation in the LE cultures, is the emergence of single highly migratory cells from the rest of the population, in the manner of the 'third behaviour' described above. These cells exhibit what might be considered 'exploratory' behaviour by emerging first and furthest into the space. If the LE cultures are allowed to migrate

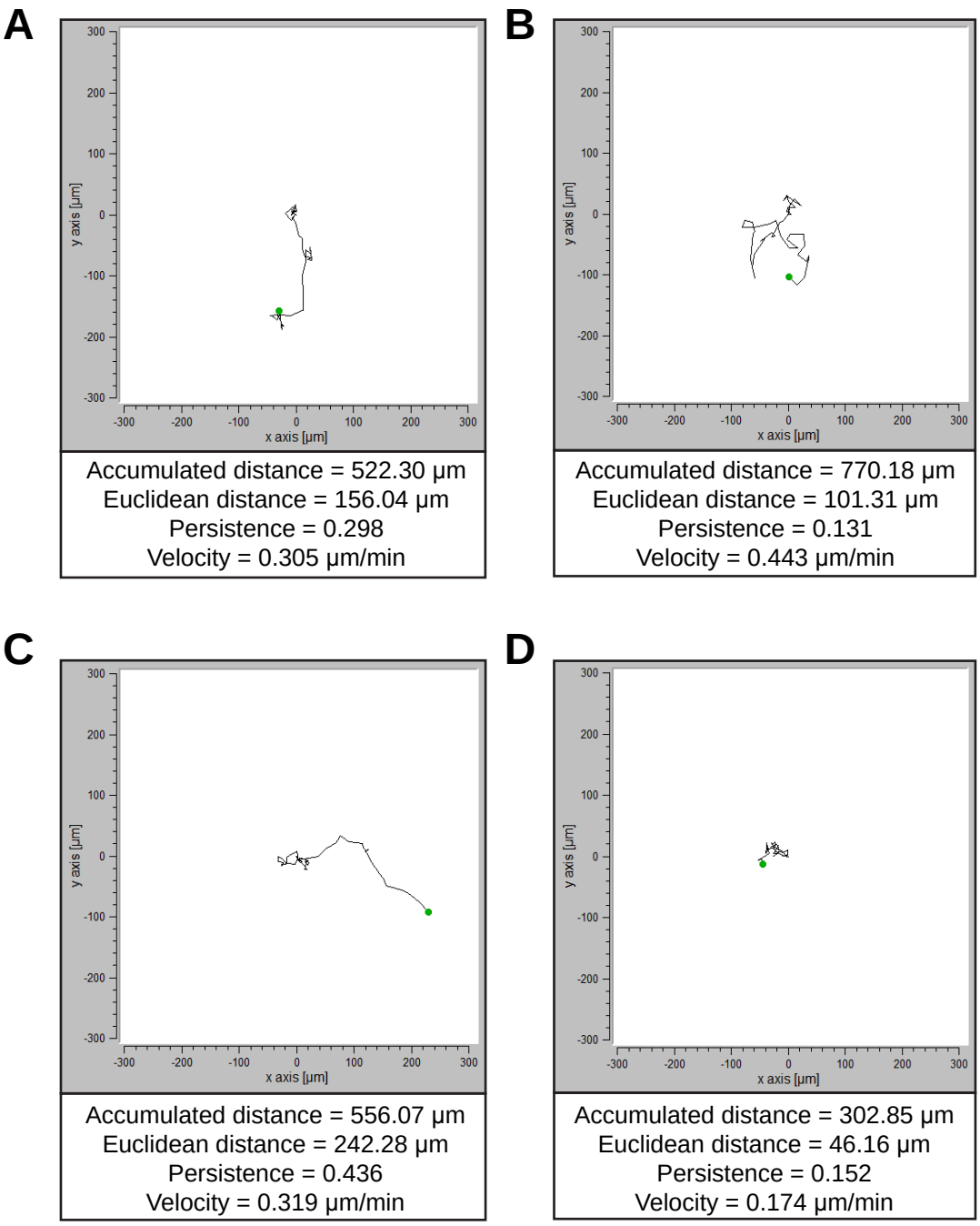

Figure 4.2. Cell trajectories vary within cultures as demonstrated by individual cell tracks in a melb-s1 WF culture. Four individual cell trajectories are represented, showing some typical migratory patterns of cells within a single melb-s1 culture. Cells were imaged every 30 mins, over a 30 hr timelapse experiment. All cells begin migration at point (0,0), and the green spot represents the final cell position. **A.** Cell 1 has sections at the start, middle and end of the track where the cell stops and moves around a single location for multiple frames, before migrating in the same direction again. **B.** Cell 2 migrates the fastest, and accumulates a large distance, but does not move far from its origin. **C.** Cell 3 migrates steadily away from its origin, and has the most persistent migration path. **D.** Cell 4 has both a small accumulated and Euclidean distance, and migrates very little from its origin.

for longer, the remaining population will reach the same distance, and those early migrating cells reintegrate with the rest of the population. Video 4.2. shows a timelapse sequence of B16F10 cells migrating in the LE culture, with cell nuclei marked by NucBlue and the migratory tracks overlaid, with 3 cells in the lead exhibiting this behaviour. The tracks are coloured on a 'heat' scale of blue to red based on relative mean migration velocity – the red tracks of the cells that emerge first are migrating the fastest, while those cells still in the main population have blue tracks indicative of slower velocity. Although these cells are seen in all four cell lines, they are not seen in every experiment.

4.1.2. Plating cells in leading edge cultures causes the population to preferentially spread into the space

To measure collective cell migration in the ML cell lines, cultures were prepared in the LE culture method as described above. It is hypothesised that in cultures with no external migration influences, a cell population would spread evenly in all directions. Figure 4.3. shows the population spread of all four ML cell lines in WF and LE cultures. All cell tracks are plotted from the origin (0,0), with green dots representing the final cell position, and the red lines representing x=0 and y=0. In WF cultures, cells show isotropic spreading; the population spreads evenly in both axes, indicating no bias towards any particular direction as expected. Contrarily, it is shown in LE culture that cells will migrate into the empty space. To measure this as a spread in the population, and determine if spreading occurs preferentially in the direction of the empty space, the same analysis was performed. Cell population spread in LE culture shows a positive shift on the y-axis, meaning more tracks are migrating in that direction. As the images used in this analysis are oriented so the cells are negative in y to the edge (i.e. cells begin at the bottom of the image and migrate upwards), it is shown that the cells are migrating into the empty space preferentially. This effect is particularly obvious in the presented B16F10 and melb-m5 cultures, although it does occur in all four cell lines. Migration to left and right still occurs evenly. This shows local anisotropic spreading as expected, however, this only applies to this field of view. If the whole population were to be measured i.e. encompassing the entire circle

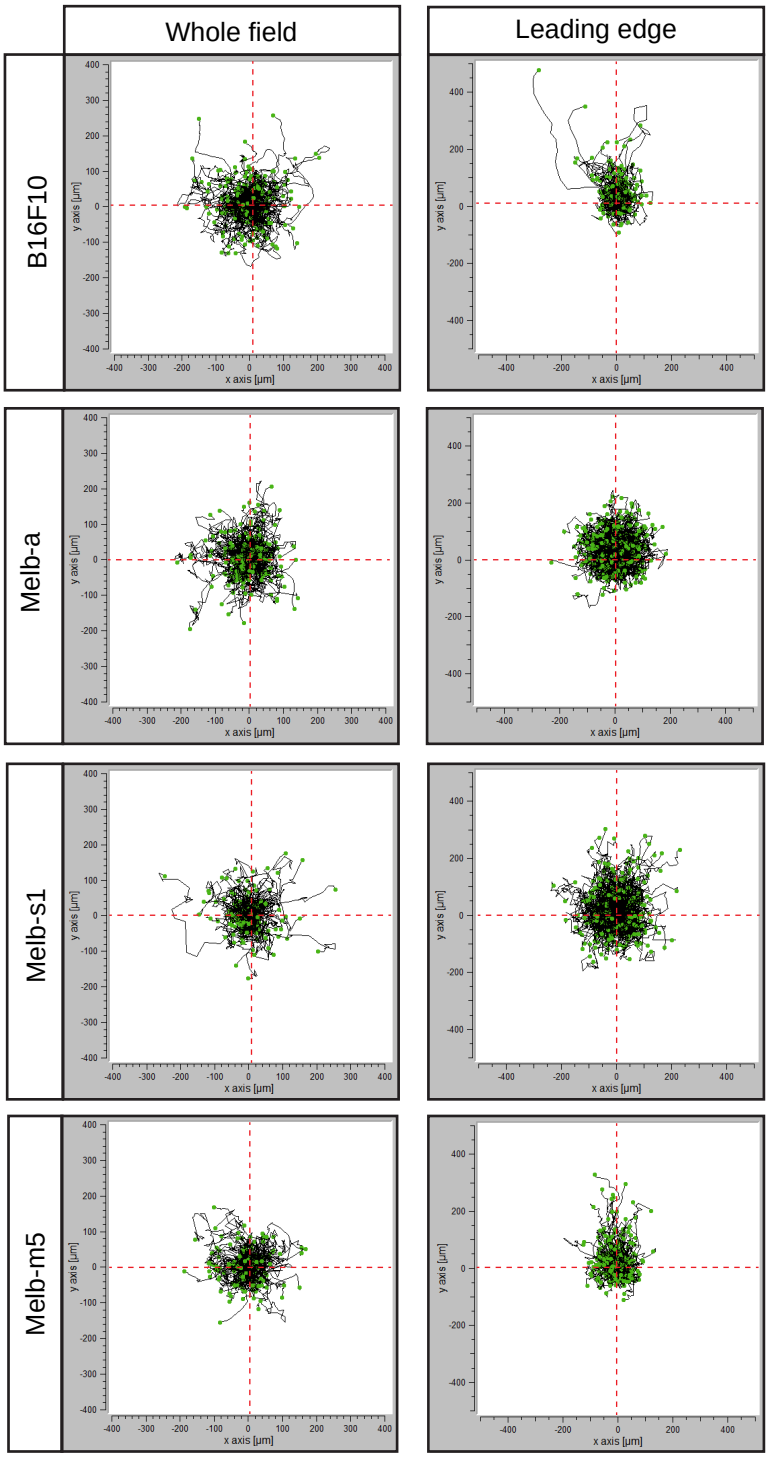

Figure 4.3. Cell population spatial spread in WF and LE cultures. The left panels show cells which are migrating in a WF culture, and in the right panels are cells migrating in the LE culture. Tracks originate at (0,0), and the final cell position is represented by a green dot. The red lines represent the x=0 and y=0 axes. Experiments are oriented so the empty space is above the migrating culture in each image - forward movement into the space is thereby positive on the y axis. Cells in WF culture migrate evenly in both x and y, with some cells migrating further than others, and many finishing tracks close to the origin. In the LE cultures, there is a general spread of the populations into the empty space as shown by a positive shift on the y axis. The populations remain evenly distributed in x.

of cells, spreading may be isotropic again as cells migrate into the empty space in all directions equally.

4.1.3. Cell lines migrate slower than melanoblasts in vivo

To examine the velocity of cell migration, cells in culture were tracked through timelapse imaging experiments. Melanoblasts migrate at ~0.5 μm/min during development, as calculated by *ex vivo* skin cultures (Mort, Hay and Jackson, 2010). In these cultures, the melanoblast cells and B16F10 cells migrate slower than *in vivo* melanoblasts on average.

The migration velocity of cells in WF and LE culture are shown in box and whisker plots in Figure 4.4.A. The mean velocities of each cell line is also listed for comparison. A one-way analysis of variance test (ANOVA) was performed to investigate whether there were differences between the groups; do individual cell lines change velocity between WF and LE culture, and are there differences between the cell lines in WF and LE cultures (separately)? We hypothesised that cells in LE culture would migrate faster than cells in WF culture, due to an increase in cell diffusion into a lower area of cell concentration. We further hypothesised that the melb-a cells would migrate fastest, as they are closest to wildtype cells, with the B16F10 melanoma cells at around the same speed. We expected the melb-s1 cells to be the slowest, as the mutation in this line leads to known behavioural changes. Finally, we hypothesised that the melb-m5 cell line, which results in reduced pigmentation, would have similar behaviour to the melb-a wildtype cells.

One-way ANOVA showed significant differences between the groups; both between the cell lines and between the culture methods. To determine which groups were significantly different, pairwise t-tests were performed between each combination and corrected for multiple testing using the Bonferroni method. Significant differences are discussed further.

4.1.3.1. B16F10 and melb-s1 cells have different migration speeds when cultured by LE

B16F10 cells in LE culture showed a significant decrease ($P = 0.0425$) in migration velocity when compared to cells in WF culture (0.257 (n=202) and 0.229 µm/min (n=141) respectively). Melb-s1 cells showed a significant increase in migration speed ($P = 4.715 \times 10^{-10}$); in WF culture, cells migrated with a speed of 0.323 µm/min and in LE culture this increased to 0.402 µm/min. Melb-a cells migrated with speeds of 0.437 and 0.405 µm/min in the WF and LE cultures, which showed no significant difference. Similarly, melb-m5 cells showed no significant difference with cells in WF migrating at 0.256 µm/min and cells in LE migrating at 0.282 µm/min.

4.1.3.2. Melb-a and melb-s1 cells migrate faster than B16F10 or melb-m5 cells

Comparisons between the different cell lines revealed significant differences in migration velocity. Overall, melb-a and melb-s1 cells migrated faster than B16F10 and melb-m5 cells in both culture methods. B16F10 and melb-m5 cells migrate at a similar speed in WF culture (0.257 and 0.256 µm/min), but melb-m5s migrate significantly faster than B16F10s in LE culture (0.229 and 0.282 µm/min, $P = 0.0008$). Melb-a cells migrate significantly faster than melb-s1 cells in WF culture (0.437 and 0.323 µm/min, $P = 6.085 \times 10^{-13}$), but the difference is not significant when compared in LE culture (0.405 and 0.402, $P = 0.809$).

4.1.4. Culturing B16F10 and melb-m5 cells in WF culture vs. LE culture changes cell persistence

In the LE cultures, cells move out into the empty space, but whether the cells are actively migrating in this direction is unknown. There may be a baseline level of persistence that cannot be observed in a WF culture as they are limited spatially by the presence of other cells. However, we hypothesised that the difference in culture methods should have no effect on the persistence of the cell lines, as *in vivo* cells diffuse randomly (Mort et al., 2016). This culture method may also be interesting to observe cell behaviour at the leading edge, in contrast to cells in the main population.

As discussed, cell persistence is the measure of how direct a cell's track is between the start and end point; cells migrating randomly will have a very indirect path between the start and end points, whilst cells migrating towards something will have a more direct path. The results of this experiment are shown in Figure 4.4.B.i. and ii. The same statistical tests were applied to compare both intra- and inter-cell line; a 1-way ANOVA was performed followed by pairwise testing if a significant *P*-value was obtained.

The 1-way ANOVA revealed a significant difference between the culture methods in B16F10 and melb-m5 cells, and also a difference between the persistence of cell lines in LE culture. There was no significant differences in the persistence between cell lines in WF culture. B16F10 and melb-m5 cells shows a significant increase in persistence when cultured in LE. B16F10 cells increased from a persistence of 0.251 to 0.375 ($P = 2.506 \times 10^{-10}$). Melb-m5 cells increased from a persistence of 0.211 to 0.337 ($P = 1.502 \times 10^{-6}$). Melb-a and melb-s1 cells show no change in persistence between the culture methods as hypothesised, and accordingly, the increase in persistence in B16F10 and melb-m5s creates a significant difference between the groups when all cell lines are compared in LE culture. In LE culture, B16F10 cells migrate more persistently (0.375) than melb-a cells (0.278, $P = 3.334 \times 10^{-15}$) and melb-s1 (0.226, $P = 1.363 \times 10^{-14}$). Melb-m5 cells also migrate more persistently than melb-s1 cells (0.226, $P = 1.725 \times 10^{-5}$). There was a slight significant difference between the persistence of B16F10 and melb-m5 cells ($P = 0.0134$).

4.1.5. Treatment with exogenous sKITL changes cell dynamics

KIT/KITL signalling is essential during melanoblast development for survival, migration and proliferation (Yoshida et al., 1996), as discussed in Chapter 1.3. The KIT receptor is expressed on the cell surface of migrating melanoblasts, while KITL is found in the surrounding environment (Hirobe, 2005). KIT signalling is observed during different stages of melanoblast development, including during delamination from the NC (Wehrle-Haller and Weston, 1995) and later on in localisation to the hair follicle (Jordan and Jackson, 2000a). KIT signalling has also been shown to

A i.

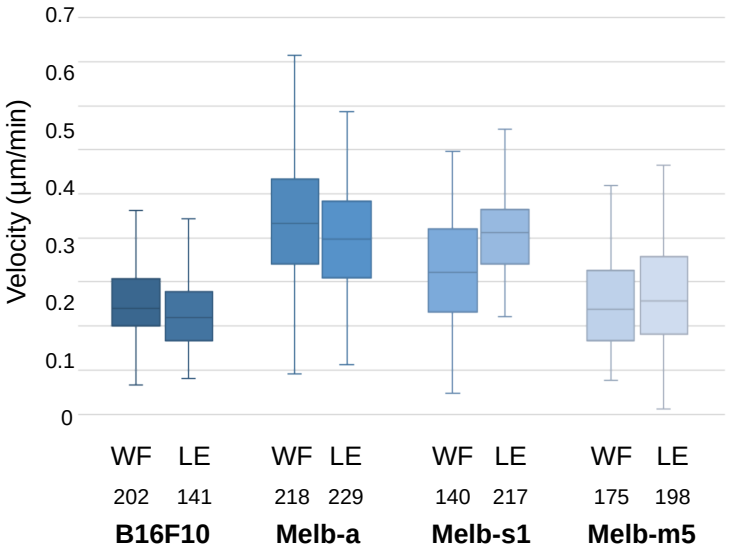

n= number of tracks analysed

ii.

Cell and culture method	Mean velocity (µm/min)
B16F10 WF	0.257
B16F10 LE	0.229
melb-a WF	0.437
melb-a LE	0.405
melb-s1 WF	0.323
melb-s1 LE	0.402
melb-m5 WF	0.256
melb-m5 LE	0.282

B i.

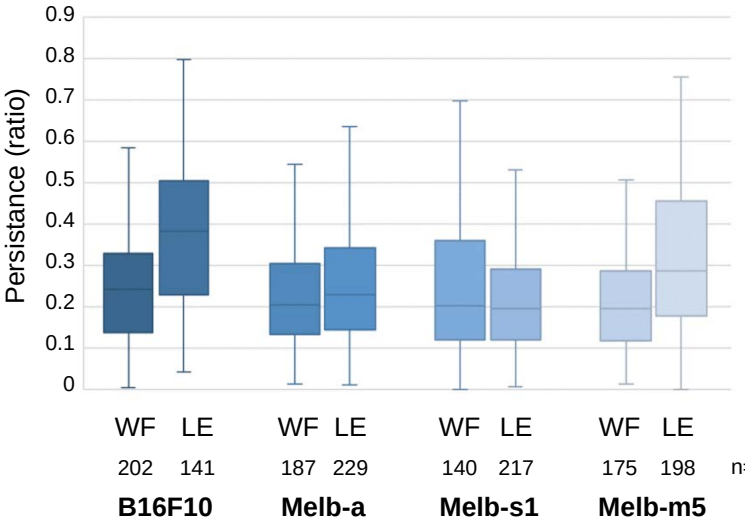

n= number of tracks analysed

ii.

Cell and culture method	Mean persistance
B16F10 WF	0.251
B16F10 LE	0.375
melb-a WF	0.238
melb-a LE	0.278
melb-s1 WF	0.240
melb-s1 LE	0.225
melb-m5 WF	0.211
melb-m5 LE	0.337

Figure 4.4. Cell migration velocity and persistence in WF and LE cultures. A. i. Cell track velocities are measured in µm/min. For each cell line, the left box is cells in WF culture, and the right box is cells in LE culture. Significant differences between the groups are discussed in the text. The number of tracks analysed in each case is indicated below the plot. All cell lines exhibit a wide range of velocities, with melb-a and melb-s1 cells moving the fastest. **ii.** The mean average velocity of each cell line in the two culture methods. All cells migrate in the range of 0.22-0.44 µm/min. **B.i.** The persistence of cell tracks was measured for each condition. It indicates how direct a cells path is along its migration route. Movement in a straight line is calculated as 1, and complete random movement is calculated as 0. B16F10 and melb-m5 cells show an increase in persistence between the WF and LE culture. Significant differences are discussed in the text. **ii.** The mean average persistence of cell tracks in each culture.

affect migration, proliferation and survival in other cells lines, such as mast cells and haematopoietic precursor cells (Meininger et al., 1992; Okumura et al., 1996).

In melanoblast development, there has been no evidence of a chemotaxis gradient involving KITL, although it has chemokinetic properties demonstrated by increased melanoblast localisation to hair follicles with the addition of exogenous sKITL (Jordan and Jackson, 2000a). The ML cell lines were assayed in a WF culture with a concentration series of exogenous sKITL, to determine if there were any changes to their migration profiles. Over 150 individual cell tracks were included for analysis in each sample group, excepting melb-m5 cells treated with 50ng/ml sKITL (n=114). We hypothesised that increasing concentrations of sKITL would increase both velocity and persistence in culture.

4.1.5.1. Melb-a and melb-m5 cells migrate faster in the presence of high concentrations of sKITL

Exogenous sKITL was added to fresh medium and supplied to the cell culture immediately before imaging. The melanoblast cell lines are grown in sKITL containing medium at 20ng/ml from initial isolation (Sviderskaya et al., 1998; Sviderskaya, Easty and Bennett, 1998; Sviderskaya, Wakeling and Bennett, 1995), while B16F10 cells are not. Figure 4.5.A. shows the result of cell tracking in different concentrations of sKITL. A 1 way ANOVA was performed on each cell group to determine whether the changes in migration were significant, then pairwise comparisons were performed where appropriate with Bonferroni correction for multiple testing. ANOVA testing showed significant differences in migration in all cell lines at different concentrations of sKITL.

B16F10 cells shows a slight increase in migration rate at 50ng/ml (0.384µm/min) which was significantly faster than at 0, 20 and 100ng/ml (P = 0.0083, P = 0.0006, $P = 8.76 \times 10^{-7}$). Melb-a cells show a general trend of increase in velocity in line with the increase in sKITL concentration. There was no significant difference between 0ng, 20ng or 50ng, but at 100ng/ml, melb-a cells migrated significantly faster in all comparisons (0-100ng $P = 9.56 \times 10^{-40}$, 20-100ng $P = 6.7 \times 10^{-32}$, 50-100ng $P = 9.0 \times 10^{-46}$). 0.607µm/min was the fastest migration observed in these migration

experiments. Melb-s1 cell migration was significantly higher between 0ng/ml and 20ng/ml (P = 0.0012). No other significant changes were seen. Similar to melb-a cells, melb-m5 cells showed a significant increase in migration velocity at 100ng/ml sKITL (0-100ng $P = 8.07 \times 10^{-24}$, 20-100ng $P = 1.33 \times 10^{-26}$, 50-100ng $P = 2.102 \times 10^{-21}$). Migration velocity increased to 0.351µm/min from ~0.25µm/min at the lower concentrations.

4.1.5.2. Increasing sKITL concentrations has a variable effect on cell persistence

Increasing levels of sKITL had no significant effect on the cell migration persistence of B16F10 cells. There were significant effects in all 3 melanoblast lines, however no obvious trend is apparent. Figure 4.5.B. shows the cell persistence values. Melb-a cell migration persistence increased significantly with the increase in concentration until 50ng/ml (0-20ng P = 0.001, 0-50ng $P = 3.55 \times 10^{-8}$, 20-50ng P = 0.006), but at 100ng/ml, the persistence fell slightly (not significant). Melb-s1 cells showed a higher persistence at 20ng/ml compared to 0 and 100ng/ml (0-20ng P = 0.041, 20-100ng $P = 4.26 \times 10^{-5}$). Melb-m5 cells had the lowest persistence at 20ng/ml, and the highest persistence at 100ng/ml, which was significantly different ($P = 8.9 \times 10^{-5}$).

4.2. HD cultures as a model for EMT

In Chapter 3.2., it was described how the HD aggregates became interesting as a model after it was observed that cells migrating from the drop did so visually in a manner that was strikingly reminiscent of cells exiting the NC in explant cultures (Huang et al., 1998). EMT is the process cells must undergo to leave the NC, and is characterised by the cadherin switch, along with the expression of typical markers including *Snai1* and *Snai2* (Theveneau and Mayor, 2012; Wheelock et al., 2008). The process is integral to allowing cells to dispel their connections to their neighbouring cells and migrate away from the NC (Theveneau and Mayor, 2012). Equally, it may be assumed that the opposite action of taking cells from culture and into the HD would cause a mesenchymal-epithelial transition. The formation of the HD aggregates was discussed in Chapter 3.2., in particular related to the requirement

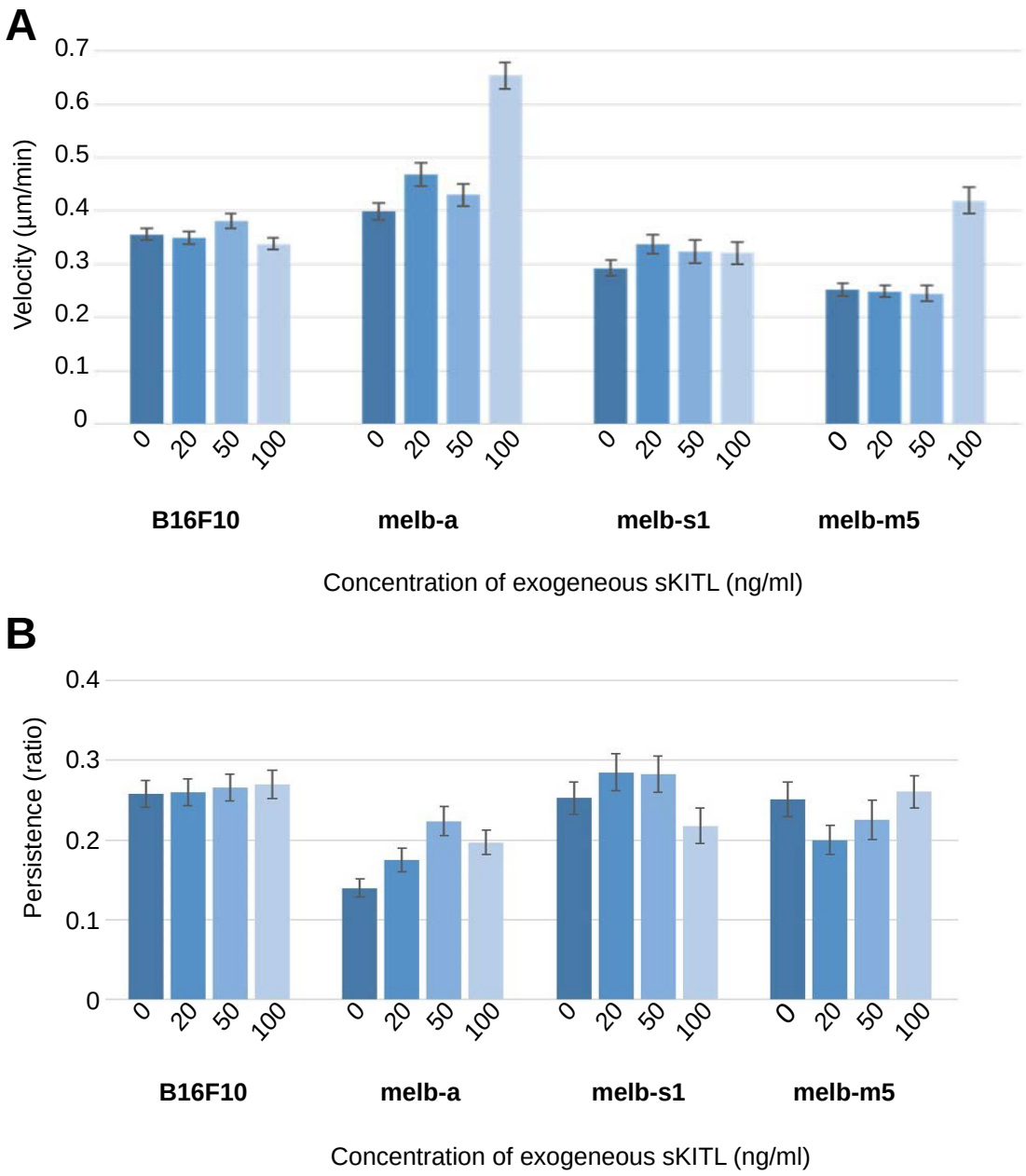

Figure 4.5. The effect of exogenous sKITL on the velocity and persistence of cells in culture. Cells were supplied with fresh culture media immediately before imaging, containing increasing concentrations of sKITL as shown. Cells migrating in a WF culture were tracked, and the values for velocity and persistence were measured. Error bars show the 95% confidence interval. **A.** The migration velocities of the cell lines are shown with each treatment. Melb-a cells show a general increase in migration velocity with increasing sKITL concentration, with a large increase at 100ng/ml. Melb-m5 cells also showed an increase in velocity at 100ng/ml of sKITL. B16F10 and melb-s1 cells showed small differences in velocity, although there was no clear trend of increasing or decreasing velocity correlated to the change in concentration. Significant differences between the groups are discussed in the text. **B.** The persistence of cell migration was calculated as a ratio between the accumulated and Euclidean distance. Changes in persistence were seen in the melanoblast cell lines between treatment groups, however there was no general trend of increase or decrease correlated to the change in concentration. Significant differences are discussed in the text.

of a threshold number of cells (Figure 3.8.). In further investigations of this culture method, two main interests were followed. Firstly, what are the characteristics of the HD aggregate when plated? Secondly, has EMT occurred in the cells which have migrated from the aggregate?

4.2.1. Melanoblast cells migrate sooner than melanoma cells

When plated on a surface, cells from the aggregate migrate away after notably different time periods. Figure 4.6. shows a HD example from each cell line, immediately after plating and at the end of the experiment 67 hrs later. The right hand column indicates the approximate time after plating at which cells begin to migrate. Images were taken 30 mins apart, leaving room for an ~30 min margin of error for this timing. Melb-a and melb-s1 cells migrate from the HD shortly after the beginning of imaging, ~ 6 and 7 hrs after plating respectively. Melb-m5 cells take around 13 hrs to migrate from the HD aggregate. B16F10 cells take much longer to emerge, around 34 hrs post-plating. This timing is variable by some hrs between different experiments, however cells were never seen emerging before ~24 hrs. Melb-a and melb-s1 cells consistently migrate very early in the experiment. Videos of the migrating HDs shown in Figure 4.6., can be seen in Video 4.3. (B16F10), Video 4.4. (melb-a) and Video 4.5. (melb-s1). Video 4.6. shows melb-m5 cells migrating in a shorter sequence (22.5 hrs). In this video, two aggregates are shown, with cells migrating out of the aggregate after varying times; cells emerge from the aggregate on the right after ~13 hrs, while on the left cell emerge after ~19 hrs demonstrating heterogeneity. All of the cultures have been plated with matrigel in a 1:10 ratio with culture media as described in Chapter 2.3.7.

4.2.2. Cells migrating from the drop are mainly unpigmented

Images in Figure 4.6. and 4.7.B. demonstrate that the HDs of all lines are pigmented, while the majority of the cell cells migrating away from the aggregate are not. Indeed, one of the key features that identifies the aggregate forming is the pigmented mass which can be seen by eye. This suggests that the population within the drop is heterogeneous, with different migration vs. pigmentation properties. In the adult

mouse tail skin, pigmented melanocytes reside in the interfollicular epidermis. A population of amelanotic melanocytes were recently also identified within this space, which were distinct from other MSCs in the hair follicles (Glover et al., 2015). The emergence of non-pigmented cells from the pigmented HD presents an interesting model in this regard, as a mixture of pigmented and non-pigmented cells has been achieved in the same model which exhibit different behaviours.

4.2.3. Cadherin switching of HDs

In the classic EMT model, migratory cells downregulate expression of *Cdh1* (E-cadherin) and upregulate the mesenchymal *Cdh2* (N-cadherin) (Maeda, Johnson and Wheelock, 2005). To investigate the characteristic cadherin switch which defines classic EMT, IF experiments were performed on cultures which were fixed between 24-48 hrs after plating. This window was chosen to allow the observation of both migrating cells and cells still in the HDs in the same experiment. Images were acquired with a z-stack to account for the different focal planes in which these populations sit, allowing images to be obtained from both the migrated cells and cells still in the aggregate. The immunostaining proved inconclusive, so other methods including qPCR would be suggested to improve the understanding of EMT in the HD model. The imaging results from these staining are shown in Appendix C. Negative controls were performed with secondary antibody staining only, all of which show no staining.

4.3. CDMs as environmental substrate models

CDMs were created in an attempt to model the changing extracellular environment of the migrating melanoblasts. NIH3T3 and Sl/Sl fibroblasts were developed to model early migration in the dermis, and the keratinocyte line COCA was developed to model migration in the epidermis. Sl/Sl fibroblasts derived from the Kit^{Sl} mutant which have no expression of KITL (confirmed by western blotting, Figure 3.6.), were used to produce CDMs to investigate the effects of tethered KITL on cell migration behaviours. The assembly and culture of CDMs was discussed in Chapter 3.1., where it was shown that the stabilised matrix contains some essential

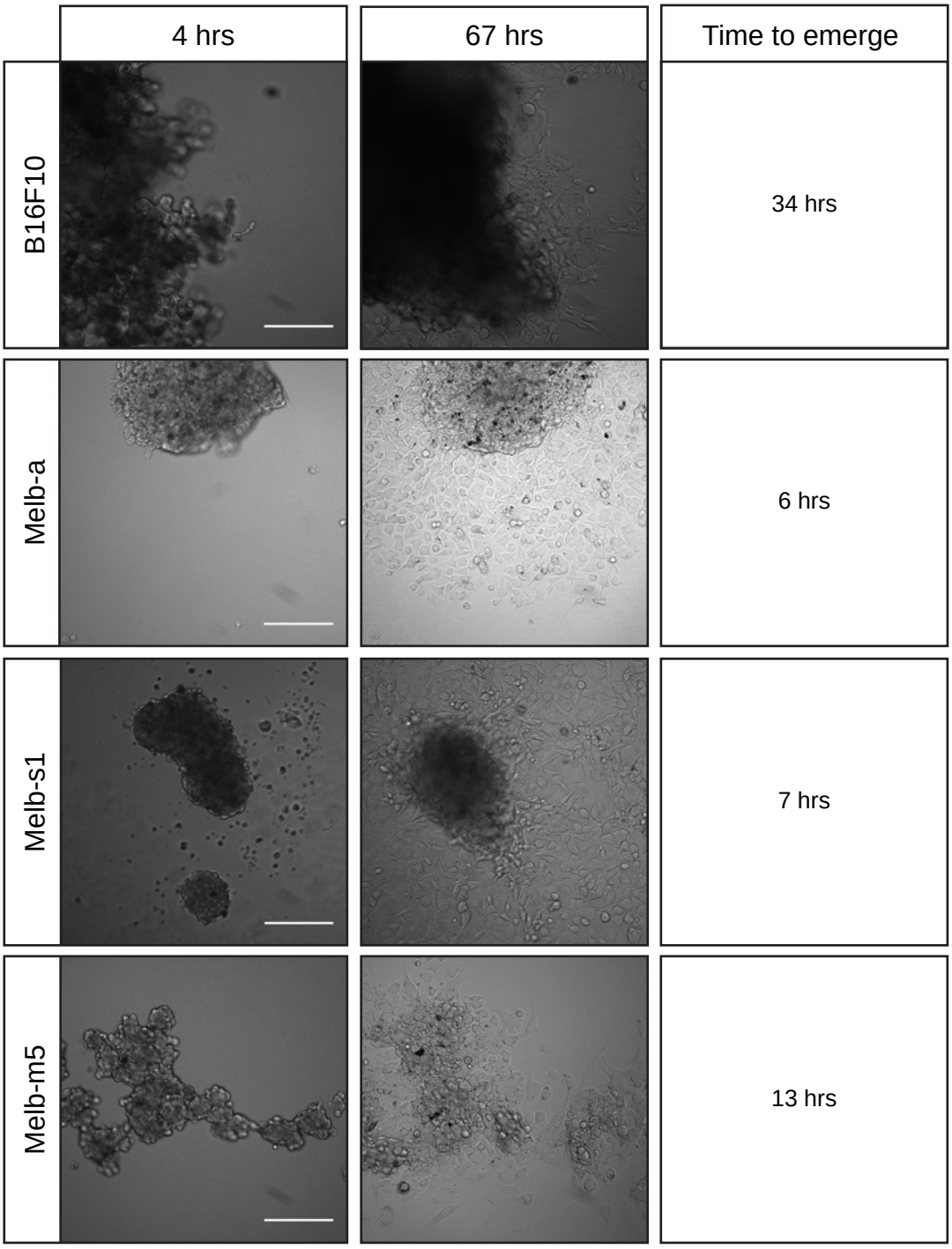

Figure 4.6. Cells in the HD emerge from the aggregate at different times. The panel shows HDs plated on glass with matrigel, imaged every 30 mins for 67 hrs. Images on the left show the aggregate at the first time point, ~ 4 hrs after plating. Images on the right show the aggregate at the end of imaging, ~ 67 hrs after plating. The final column shows the approximate time that individual cells are identifiable as they emerge from the aggregate. There is some variation of this between experiments. B16F10 cells took notably longer than the melanoblast cell lines. Melb-a cells emerge the soonest, with melb-s1 cells emerging not long after. Melb-m5 cells take around double the time of the others to emerge. Scale bars represent 100μm.

environmental components including collagen.

4.3.1. CDM in live-imaging

To integrate the CDMs into the confocal imaging platform, a specialised chamber was designed and engineered in the IGMM workshop in collaboration with Len Hay (Figure 3.7.). This chamber allows a CDM grown on a coverslip to form the base of an imaging well, onto which experimental cells can be plated. Three CDMs were produced from different lines to model both the dermal and epidermal environment; NIH3T3 cells model the dermis, while COCA cell model the epidermis. Images from preliminary timelapse imaging experiments are shown in Figure 4.7. B16F10, melb-a and melb-s1 cells were labelled with DiI and plated at low-mid confluence on the CDMs. In Figure 4.7.A.ii., B16F10 cells are shown plated on a COCA CDM, whose integrity can be confirmed by brightfield. These cultures proved unsuitable for migration experiments, and require further refinement to the methodology in relation to the culture conditions in the microscope chamber. Observations from these early experiments however, indicate that the cells are highly dynamic on the CDMs, particularly in changing morphologies; cells appear to have lots of branching structures extending outwards from the cell body. Interaction with the CDM can also be observed in the brightfield channel; where migration was observed, cells appear to 'pull' the matrix with them in the direction of migration, before releasing and migrating onwards.

4.3.2. HDs can migrate on CDMs without matrigel

The HD experiments have relied heavily on the use of matrigel to allow cell migration, as described in Chapter 3.2.3.3. See Video 4.7. for an example of the failure of cells to migrate in the absence of matrigel; a melb-a HD is plated into a glass well, and imaged every 30 mins over a 21 hr timelapse sequence. In order to remove the requirement for matrigel in these experiments, HD aggregates were plated onto CDMs. HD aggregates were plated and the cultures were left for 72 hrs to allow for cell migration to occur, before fixation. Figure 4.7.B. shows a melb-a HD which has been plated on a COCA CDM. DAPI staining of the nucleus shows

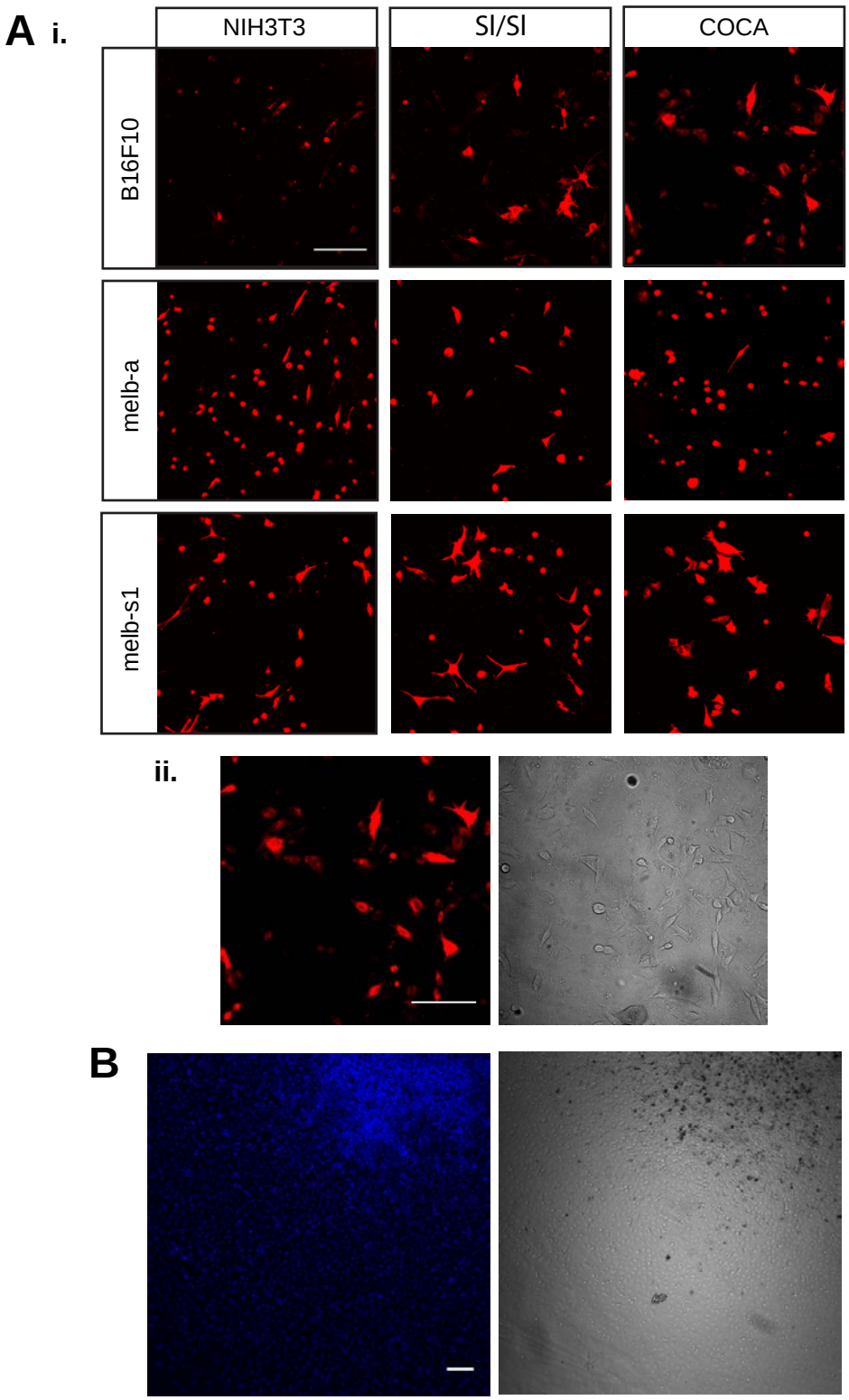

Figure 4.7. Culturing cell lines on CDMs. A.i. B16F10, melb-a and melb-s1 cells were labelled with DiI and plated onto CDMs from the three environment lines - NIH3T3, Sl/Sl and COCA. **ii.** A closer view of B16F10 cells on a COCA CDM show that the CDM is intact in the brightfield channel. **B.** A melb-a HD has migrated on a COCA CDM; migrated cells fill the field of view, confirming that cells can successfully migrate on a CDM without matrigel. Cells in the HD were allowed to migrate for 72 hrs before fixing and staining with DAPI. All scale bars represent 100µm.

that cells have migrated to fill the whole view. The cell confluence makes it impossible to identify the CDM underneath, however all cultures were checked for integrity of the matrix before use.

4.4. Discussion

In this Chapter, assays to study cell behaviour were used to investigate the migration of melanoblast and melanoma cells *in vitro.*

4.4.1. Cell migration is heterogeneous within a cultured cell population

The measured levels of migration velocity and persistence in the cell lines exhibited a large variation within a culture. This is demonstrated by extracting individual cell tracks in Figure 4.2. For example, the migration velocity differences between the cell in B. and D. is striking, and suggests populations of cells within the cultures which have become distinct, in terms of their migration profiles. The continued culture of cell lines has potential to lead to clonal expansion of sub-populations with distinct characteristics. This is also true within the LE cultures, where cells identified as 'exploratory' were identified which migrated furthest and fastest out into the empty space. Whether these cells are genuinely different, and present a sub-population of highly migratory cells is unknown. It is possible that being close to the edge is a favourable position which induces this behaviour through signals including mechanical cues or contact inhibition of locomotion.

4.4.1.1. The effect of sKITL on cultured cell migration is heterogeneous

The process of cell migration is well researched at both the individual, and collective cell level. The mechanical action of cell migration is also well understood, and involves complicated spatial and temporal organisation of cytoskeletal components. Cell migration is broadly split into intrinsic actions, or due to extrinsic factors such as chemoattractants, electric fields and mechanical cues (Petrie, Doyle and Yamada, 2009). In other cell models, the influence of KIT signalling on migration is well understood as discussed previously (Meininger et al., 1992), and would be described

as an extrinsic factor. The significant impact KIT signalling has on migration in melanoblasts is known at several distinct stages. However, the mechanism of action, and the mechanism of how the different isoforms of KITL contribute toward survival and migration separately is not elucidated.

Increasing the concentration of sKITL in the culture media on the different cell lines produced varied responses. Given the critical role that KIT signalling plays in melanoblast biology, more consistent trends shared between the melanoblast lines may have been expected. These lines are maintained in sKITL containing medium, which should maintain their dependence on KIT/KITL signalling. Of the four cell lines, melb-a showed the greatest response to the change in sKITL. This may reflect the level of KIT receptor expression in the different lines. As the wildtype line, it is encouraging that this line maintains responsiveness after many generations in culture. At the highest concentrations of sKITL, melb-a migration velocity was significantly increased, while persistence was unaffected, while at the lowest concentration, the migratory persistence in these cells was significantly lower, while velocity was unaffected. These contrasting behaviours at the extremes of sKITL concentration indicate multiple functions of sKITL in the migratory behaviour. It is possible that the behaviours accredited to KIT signalling are based on a gradient model. Models of signalling cascades which confer different cell properties based on their expression levels are known. Indeed, MITF, the master regulator of melanocyte biology is thought to act in a ‘rheostat’ model, with different behaviours attributed to high and low expression (Strub et al., 2011). It is possible that a greater effect would be observed in combination with the LE culture.

4.4.2. Migration behaviours can be influenced by population density in vitro

The main interesting differences are those observed between the WF and LE culture method within a cell line. Clearly, there is a response from the cell population as demonstrated by the migration of cells into the area preferentially, however melb-a and melb-s1 cells both showed only very moderate changes in either cell migration velocity or persistence. B16F10 and melb-m5 cells showed a noticeable and

significant increase in track persistence when cultured in the LE, however, the analysis cannot say that the increase in persistence is specifically in the direction of the empty space. There is still migration in the x axis, and some away from the edge. This method may be able to expose intrinsic differences between the cell lines that are not observable in the WF culture. This is especially true of the B16F10 melanoma line, which is described as highly metastatic and invasive (Fidler and Nicolson, 1976; Gehlsen and Hendrix, 1986). The exploratory cells which emerge from the LE culture could represent a metastatic sub-population that is only observable when cells are presented with environments of extreme difference in cell population density to either side. In the LE culture, this would be the population of cells within the ring, and the empty space, while in cancer it may be representative of the tumour mass, and the adjoining tissue/blood vessel to which the metastatic cell migrates.

On the other hand, cells within these culture may not exhibit their true migratory properties or reach their full migration potential due to differences in culture densities. At high densities, cell movement may be impaired, and different local densities may cause migration between areas, so unseen factors that are external to the field of view may be present. Density was controlled only in so far as the number of cells seeded within a well, however this is not a guarantee that cells will attach uniformly across the surface. A method of creating a cell gradient across a well was trialled however, it was not very effective. In the LE cultures, cells often attached in clumps at the silicon ring, creating a ‘wall’ of cells that was unsuitable for experimentation.

4.4.3. HD assays in isolation

The HD assay has been shown to be visually similar to that of a neural tube explant. However, an important difference between the *in vitro* assays and melanoblast cell migration *in vivo*, is the number of cells. As discussed previously, only ~ 98 melanoblast fated cells are specified from the NC during development (Luciani et al., 2011). In the HD cultures, 10,000 melanoblast/melanoma cells are plated per

aggregate. Collective cell migration behaviours are undoubtedly different in populations with such a large difference in number.

Immunostaining of HD and migrated cells investigating the cadherin-switch proved inconclusive across the cell lines. Within the HD, N-cadherin failed to stain the centre, although this is also true of DAPI. Whether the lack of staining is attributable to a genuine lack of expression by those cells deep within the aggregate, or poor penetration by the antibody is unknown. Sectioning the HDs and performing IF at this point prior to migration would be advantageous to ascertain the cadherin composition in the middle. E-cadherin stained the cell aggregates effectively, however some expression was still observed in the migrating cells. Expression of cadherin proteins is well documented, and typically appears as bright staining at cell-cell adhesions as would be expected. This pattern was not seen in these experiments, even at higher magnification, casting doubt on the success of the immunostaining protocol. Again, a sectioned layer of a HD may provide a more suitable substrate, for imaging deep inside the aggregate.

The possibility of EMT occurring is explored further in Chapter 6 using RNA sequencing.

4.4.4. Future directions

4.4.4.1. Tracking migration in HD migratory cells

It was demonstrated that cells in the HD could migrate outwards from the aggregate in the presence of either matrigel or a CDM. Whether the substrates are necessary due to growth factors, or structural ECM components is unknown, although a combination of both has been shown to be important in mammary epithelial cells (Roskelley and Bissell, 1995). There are numerous studies reporting different cell morphologies and behaviours when cultured in 2D vs. 3D environments. One such study by Cukierman *et al*. examined the effect on human fibroblast behaviour of 3D matrices derived from either tissue or cells compared with mechanically compressed 3D tissue/cell matrices, 3D collagen gel lattices and 2D ECM component coated surfaces. The 3D tissue/cell derived matrices were significantly more effective at

facilitating cell-cell adhesion, and behaviourally cells showed increased migration velocities and proliferation rates (Cukierman et al., 2001). These differences further highlight the importance of both the 3D structure and the ECM proteins. A similar approach could be followed to ascertain the contribution of the 3D structure vs. the ECM proteins herein, using mechanically flattened CDMs or collagen coated surfaces for comparison. To continue this work, performing cell tracking on the migrating cells would be advantageous, and to include these in a comparison with 2D cells in WF and LE cultures. Achieving this would require some modifications to the timelapse sequences shown here. Firstly, the incorporation of the lipophilic labels and/or NucBlue to the HD would help follow single cells through the time lapse series; this could be further aided by only colouring a small percentage of the original cells. It is not known however, if the dyes would still effectively label cells after 5 days in the HD and then through the 3 day imaging required. Second, the imaging frequency would need to be to be increased to allow accurate migration tracking. To capture all four cell lines migrating for a sufficient length of time, images were only captured every 30 mins. This leaves a large time frame for migration events to be missed; between two adjacent time points, the distance the cell moves is a straight line, and it is only by adding all these straight lines between time points that a track is established. So in these cells, which have been shown to migrate with low persistence, a 30 min unrecorded time period could include lots of migration. Not acquiring this data could lead to skewed measurements of both velocity and persistence.

4.4.4.2. Integrating CDMs

Culturing cells in combination with CDMs has great potential to incorporate a physiologically relevant substrate that could model different times of melanoblast development. Preliminary imaging experiments show that CDMs are able to replace the use of matrigel in the HD experiments. However, to undertake migration studies on CDMs, there remain some technical obstacles to overcome. In order to keep cells alive during cell migration experiments, a heated chamber was placed around the microscope. Coupled with repeated laser exposure, media from the wells evaporated quickly. This is compounded by the small well that is created in order to house the

magnet fastening, which allows only room for ~1ml of media. The initial solution was to simply place another glass coverslip over the top of the well, however this proved ineffective, probably due to the lack of CO_2 dissolving into the media, despite the humidification of the chamber. Replacing media during the timelapse is impractical; moving the culture plate will invariably change the imaging position, and adding media directly into the wells is potentially hazardous if spills happen on the equipment. A potential solution could be securing the top of each well with a gas-permeable lumox membrane (commercially available).

It must be noted that although potentially highly useful, the production of CDMs is technically difficult and labour intensive. The cultures take ~2 weeks to grow (dependent on cell line), and following the exact methodology did not consistently produce intact CDMs. Once a satisfactory product is obtained, CDMs are extremely delicate - care must be taken to not aspirate liquid too close and pipetting must be gentle, and directed to the side. When combining with the other assays described here, only the standard WF culture is straightforward. The mouth micro-pipetting method used to transfer HDs allows fine control of the aggregate, however, placement is controlled by hand and there is a high chance of accidentally touching the CDM coverslip when gently dispelling the aggregate. Indeed, in non-CDM HD cultures, touching the surface while gently dispelling through the mouth pipette is the best way to ensure the aggregate attaches to the surface and remains whole. No method was developed to combine the CDM with the LE culture, which would be of significant scientific interest. Examining the diffusion profiles of melanoblasts on dermal vs. epidermal CDMs could yield interesting differences.

4.4.4.3. Mathematical modelling

Many of the differences observed both inter- and intra- cell lines in the migration experiments reached statistically significant levels, however the impact on the cell biology must be considered carefully. For example, melb-a cells migration speed increased from 0.323 to 0.397μm/min between the WF and LE cultures – is this a biologically relevant increase that has any impact? A powerful tool to aid in answering questions of biological relevance lies in the integration of *in silico*

mathematical modelling. Many of these small changes in migration velocity and persistence are mainly useful when input into mathematical modelling, to examine outcomes with varied parameters. In a 2D model of cell migration, cell migration was examined using parameters obtained by *ex vivo* imaging of melanoblasts (Mort et al., 2016). By changing values of cell migration and cell proliferation, it was shown that chimeric patterns of coat pigmentation could be achieved using a single diffusion based model. Further, the same diffusion model could be applied to parameters taken from Kit^{Wv} melanoblasts, and a failure to completely colonise the ventral area was observed, simulating the creation of a belly spot. It was further shown that in melanoblast migration, the rates of cell proliferation had the greatest effect on the final pigmentation outcome, over migration velocity. In the diffusion based model, a higher rate of proliferation drives diffusion of cells to colonise the entire area. The LE cultures described here provide an excellent model to simulate a similar effect *in vitro*. In particular, the melb-a and melb-s1 cells which showed very little change in migration velocity or persistence between WF and LE culture, demonstrate that migration into the empty space is due to another factor. Given the findings from the diffusion model, it is assumed that the cells are diffusing into the empty space passively, whilst continuing their normal migratory behaviours.

The power of the modelling in these experiments is undeniable – slight changes to cell behaviours including migration, proliferation and persistence can be computed to measure outcomes multiple times without the need for repeated laboratory experiments.

Chapter 5
Interactions of KIT/KITL

The biochemical and signalling properties of KIT and KITL have been discussed previously (Chapter 1.3.). Briefly, KITL binds KIT as a dimer pair, inducing KIT receptors to form a dimer pair in turn, which is the activated form of the receptor (Lemmon et al., 1997). The cascade of downstream signalling is complex, involving the MAPK and PI3K pathways among others (Vosseller et al., 1997; Whitmarsh, 2007). This signalling is vital in melanoblast development for both survival and migration (Wehrle-Haller and Weston, 1995), but is usually studied in the haematopoetic and gamete cells. Despite a wealth of knowledge on KIT and KITL interactions at the mechanistic and biochemical level, there is relatively little known about how the signalling actually contributes to survival and migration behaviours.

Fluorescently tagged forms of *Kit* and both major isoforms of *KitL* were stably introduced into NIH3T3 fibroblast cells using the Flp-In system. This chapter will concentrate on examining those cells lines. Two tags were introduced per protein: the first is either NeonGreen (KITL) or Cherry (KIT), and the second is a fluorescent timer tag which can be used to observe protein kinetics. NeonGreen is reported to be the brightest green protein currently available (Bajar et al., 2016; Shaner et al., 2013). As NeonGreen and Cherry can be separated spectrally, they are suitable for co-culture studies.

The design of the KITL fluorescent proteins was based on previously described constructs from the research group of Professor Bernard Wehrle-Haller (Paulhe et al., 2009; Wehrle-Haller and Imhof, 2001), who also kindly provided the Kit_Cherry construct for this project. Using sequences obtained from this group, new fluorescent markers were incorporated, and the entire constructs were cloned into the Flp-In vectors for transfection into a stable NIH3T3 host cell line. In the KITL constructs, fluorophores are inserted between exon 5-6, as the tail region of *Kitl* contains an

essential targeting sequence which directs the protein to the basolateral surface of the expressing cell (Wehrle-Haller and Imhof, 2001). The design of the timer tag proteins were based on a system designed by Khmelinskii *et al* (2012); it is composed of the KIT or KITL protein, fused to sfGFP and Cherry so that all three are transcribed as a single protein. See Figure 5.1. for a schematic of the relevant constructs. SfGFP and Cherry mature at different rates, so the amount of fluorescence in each channel directly relates to the rate of protein production. Newly synthesised protein will be marked in green (sfGFP), as it matures and fluoresces very quickly once transcribed. Older protein will be marked in red (Cherry), as it takes longer to mature - so fluorescence of Cherry is delayed by comparison. The ratio of fluorescence between the two colours can eventually be used to estimate the turnover rate of the protein of interest. See Figure 5.1.C. for a schematic from Khmelinskii *et al.* illustrating the behaviour of the timer tag proteins.

5.1. Generation of fluorescent cell lines

5.1.1. Genetic manipulation techniques

The Flp-In system from Thermo-Fisher Scientific is a standard technique for the insertion of genetic material into a mammalian genome, using their unique FRT/Flp recombinase application. An FRT site is integrated into the genome of interest randomly or targeted by homologous recombination. This integration is selected, and the line is checked for single integration events. Modifications can be made in the gene of interest, within an expression plasmid that contains another FRT site. When this plasmid is transfected into the base cell line with the POG44 plasmid (which produces Flp-recombinase), the FRT sites ‘flip’ and the expression plasmid is inserted into the genome at this site. This method ensures that modifications are made in the same locus consistently and that only a single integration occurs – both of which provide much needed consistency. An original aim of this project was to create new Flp-In compatible cell lines with the COCA line and the MLs, for the purpose of introducing KIT/KITL constructs respectively. This was attempted both by homologous recombination and by the CRISPR-Cas9 system.

The CRISPR-Cas9 system was introduced in 2013 by the Zhang group, and has quickly become the new standard in genetic manipulation (Ran et al., 2013b). Using an innate defence system isolated from bacterial cells, the enzyme makes double stranded breaks at a specified point, determined by a guide RNA. This break can be repaired by one of two ways – either non-homologous end-joining (NHEJ), or, if a repair template is also introduced, by homology directed repair (HDR). The aim was to introduce the Flp-In FRT site into the ROSA26 locus. Unfortunately both of these methods proved unsuccessful in creating new host lines. In the CRISPR-Cas9 system, it is known that inserting DNA into cells in culture is difficult as recombination with the repair template by HDR appears to be very low efficiency (Ran et al., 2013a; Rong et al., 2014). It is probable that in both cases, the large size of the CAG/FRT fragment that was to be inserted contributed to the difficulties experienced. We continued the project using an already established clonal NIH3T3 Flp-In cell line, which has a non-targeted FRT site integration, and had been used successfully in the laboratory previously.

5.1.2. Tandem fluorescent timer proteins

Fluorescent timer proteins have been described in the past with only limited effectiveness, despite their huge potential to study protein kinetics (Terskikh et al., 2000). In the original methods, the fluorescent protein used would be one which changed colour over time e.g. from red to green. The major problem with this method was that these proteins were highly likely to dimerise, thereby impacting on the behaviour of the protein of interest (Khmelinskii et al., 2012). A modern method which was devised to counter this issue was followed herein. As described, these tags work under the principal that different fluorescent proteins have different maturation rates. Instead of using a single protein that changes colour, there are two entirely different fluorescent proteins which are well-separated on the emission spectrum. These proteins are both fused with the protein of interest, and the observation is the younger protein of interest marked with the faster maturing fluorescent protein, and the older protein marked by the slower. A model combination was used in the paper, with sfGFP for the fast folding protein, and Cherry for the slow folding protein.

SfGFP matures and fluoresces within mins of first synthesis (Pédelacq et al., 2006), whilst Cherry matures at ~40 mins (Merzlyak et al., 2007).

5.1.3. Vector generation

5.1.3.1. Modifications to Flp-In

A modification was made to the commercially available pcDNA5/FRT vector to improve protein expression. The CMV promoter was replaced with a CAG promoter. CAG is a stronger promoter, and does not become silenced over time (Miyazaki et al., 1989).

PcDNA5/FRT was linearised with NheI and MfeI, removing the CMV promoter. A polylinker was inserted, designed to destroy the MfeI site, whilst inserting a MCS (multiple cloning site). CAG was excised from a suitable laboratory plasmid (pCAG_FUCCI) using SalI (blunt end) and EcoRI. PcDNA5/FRT+polylinker was linearised with StuI (blunt end) and MfeI (complimentary ends to EcoRI) which had been included in the MCS. These fragments were cleaned, ligated and transformed as described in the Methods.

5.1.3.2. KIT/KITL cloning

To study the interactions of KIT and KITL, a number of different fluorescent constructs were cloned. These constructs were designed to both visualise the activity of the proteins individually, and also to view their interactions with one another. The fluorophores mNeonGreen, sfGFP/Cherry and *sKITL/mKITL* were synthesised by GeneArt and manufactured to specification, with the correct restriction sites surrounding the sequences. The overall construct structures can be seen in Figure 5.1. In each plasmid, the gene of interest (GOI) portion is replaced with either *KIT* or *sKITL* or *mKITL* fused to the fluorescent protein sequence. The combination of plasmids generated in shown in Figure 5.1 B. Each plasmid required several cloning steps, which were confirmed at each stage by restriction digest. Additional checks by sequencing the plasmids was not performed, and confirmation of the success was determined by the evidence of fluorescence after transfection. As described, the fluorescent tag is located at the 3’ end of *KIT*, but in *KITL* constructs, the fluorophore

is located between exons 5-6 (Wehrle-Haller and Imhof, 2001). Vector maps are shown in Appendix B.

The cloning steps to create the vectors are described herein;

A plasmid containing *Kit* (cKit_Cherry_pcDNA3) was kindly provided by Prof B. Wehrle-Haller (University of Geneva). *Kit* was excised from this plasmid, and inserted into the pcDNA5/FRT_CAG plasmid along with fluorescent tags. CKit_Cherry_pcDNA3 was linearised with EcoRI and XhoI, and a polylinker was inserted to create a new MCS. NeonGreen and sfGFP/Cherry fluorophores were excised from their GeneArt plasmids using MluI and BssHII. CKit_Cherry_pcDNA3+polylinker was cut with MluI, and the fluorophores were ligated. Finally, cKit_Cherry_pcDNA3+fluoro and pcDNA5/FRT_CAG were cut with HindIII and XhoI. These fragments were ligated to create pcDNA5/FRT_KIT_sfGFP/Cherry, and pcDNA5/FRT_KIT_mNeonGreen. In order to visualise KIT and KITL together *in vitro*, another plasmid was created by excising the original cKit_cherry sequence and inserting this into pcDNA5/FRT. The cloning steps were the same as above, without ligating in a new fluorophore. The final plasmid was named pcDNA5/FRT_KIT_Cherry.

PcDNA5/FRT_CAG and m/sKITL GeneArt plasmids were digested using NheI and KpnI. These fragments were ligated together to create pcDNA5/FRT_mKITL and pcDNA5/FRT_sKITL. Next, the fluorophores were excised from their GeneArt plasmids using MluI and BssHII. PcDNA5/FRT_sKITL and pcDNA5/FRT_mKITL were digested with MluI, and the fluorophores were ligated.

5.1.3.3. Cell line generation

Co-transfection of the POG44 plasmid and Flp-In fluorescent vector, using lipofectamine, successfully generated all of the required combinations, and cell viability using this method was very good. All constructs show bright, consistent expression that is easily trackable by imaging. The combinations of cell lines are shown in Table 5.1., along with the abbreviated names that will be used to refer to the protein produced by each construct.

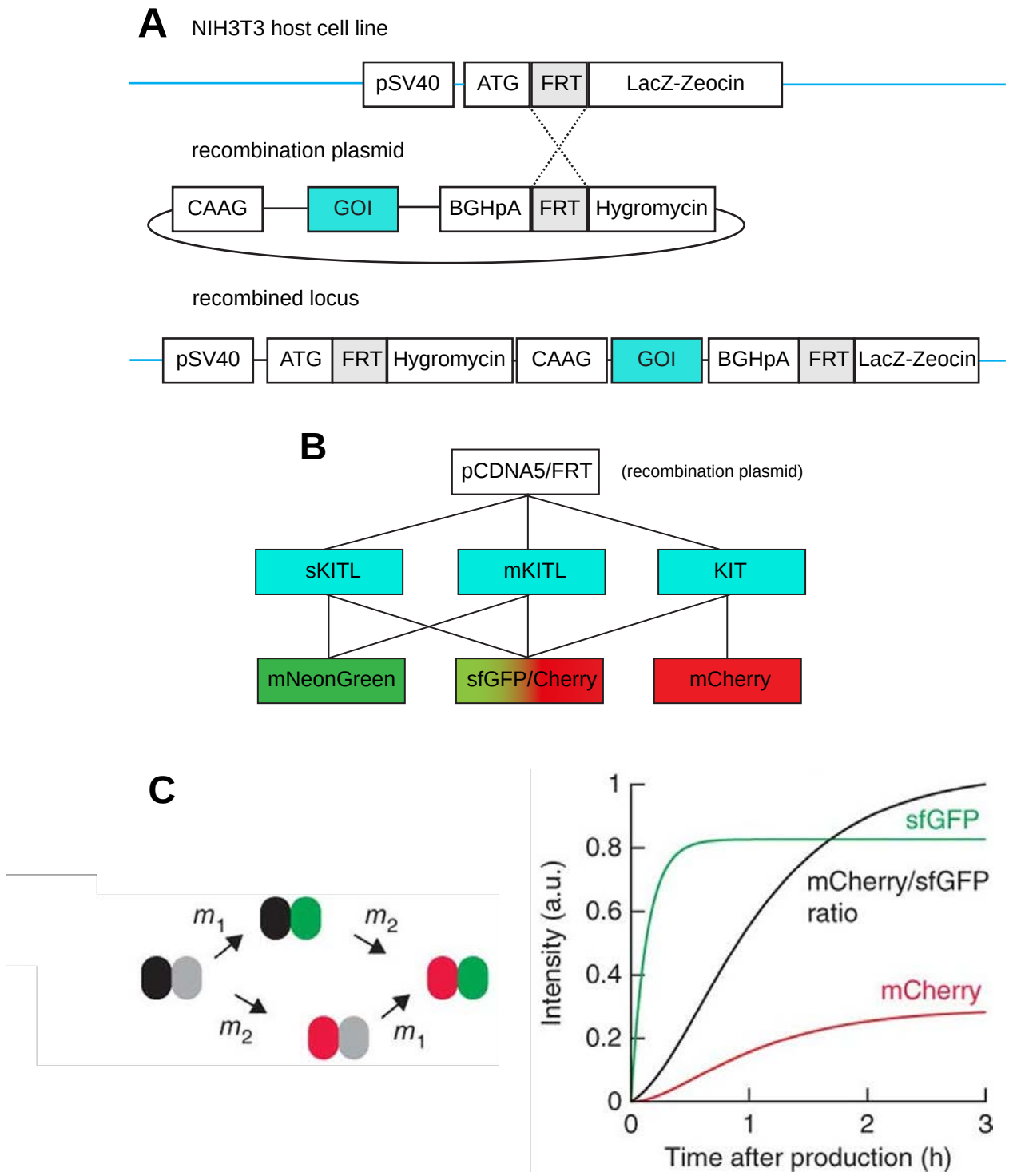

Figure 5.1. Integration of fluorescent constructs. A. The Flp-In host cell line contains a stably integrated FRT site. The GOI is cloned into the recombination plasmid alongside another FRT site. Transfection of the recombination plasmid with the Flp-recombinase expressing plasmid POG44, induced integration of the GOI into the genome. **B.** Combination of the GOI and fluorescent proteins produced in this thesis. Different combinations allow KIT and KITL to be imaged in co-culture experiments. **C.** Behavior of a tandem fusion of mCherry (black, red) and sfGFP (gray, green) with the maturation rate constants (m1, m2). Fluorescence intensity curves are normalized to the brightness of sfGFP. Ratios are normalized to the maximum in each plot. Taken from Khmelinskii *et al.* 2012.

Table 5.1. Description of fluorescent constructs in NIH3T3 cells.

Name of cell line	Description	Fluorophore
KIT_TD	KIT receptor fused to timer tag	sfGFP and Cherry
KIT_C	KIT receptor fused to Cherry	Cherry
sKITL_TD	Soluble KIT ligand fused to timer tag	sfGFP and Cherry
sKITL_NG	Soluble KIT ligand fused to NeonGreen	NeonGreen
mKITL_TD	Membrane KIT ligand fused to timer tag	sfGFP and Cherry
mKITL_NG	Membrane KIT ligand fused to NeonGreen	NeonGreen

5.2. Fluorescent construct localisation

5.2.1. sKITL

5.2.1.1. sKITL is enriched at the cell membrane and in the perinuclear region

The sKITL_TD line shows strong ubiquitous localisation across the whole cell, with occasional enrichment at the cell membrane. Enrichment along the cell membrane appears to be linked to cell morphology – cells observed with cell membrane associated localisation appear to be elongated, with no protrusions, although not all cells with this morphology exhibit this localisation. This is demonstrated in Figure 5.2.A. where two cells in the panel show this characteristic pattern. The other cell in this panel is wider and has an irregular shape in comparison, and does not show specific green fluorescence surrounding the cell. Figure 5.2.B. shows a time-lapse series of the same cells, with each image taken 2 mins apart.

Very bright signal is detected in the green channel at various points along the cell membrane, in a changing pattern that is unpredictable between frames. This dynamic

green fluorescence occurs at the distal tips of cells, and indicates the appearance of new protein at these sites. Signal in the red channel is mainly localised to the perinuclear region, although there is some localisation throughout the cytoplasm.

Figure 5.2.C. shows the single colour construct sKITL_NG. sKITL_NG localisation generally resembles that of sKITL_TD, although the perinuclear compartment is much less dominant. There is still bright localisation in the region, but the area is much smaller.

5.2.1.2. sKITL_NG is localised to attachment filaments

In sKITL_NG cells, there is strong localisation in fibrillar structures protruding from the cell body. Firstly, in the retraction fibres that appear during mitosis to tether the rounded cell to the surface (Lancaster and Baum, 2011). Figure 5.2.D. and Video 5.1. show two examples of this. Figure 5.2.D. shows a time-lapse series of a cell undergoing mitosis, with images captured every 5 mins. At the beginning, the mitotic cell resembles others in the culture, with strong green sKITL localisation throughout. In the following frames, the cell rounds up as it prepares to divide. Long projections, thought to be the retraction fibres, marked by green fluorescence extend from the cell, to the area it has just vacated. Video 5.1. shows another mitotic cell with the retraction fibres surrounding the rounded cell, identified in the yellow circle. These structures were observed consistently in mitotic cells. Secondly, sKITL_NG marks fibrillar structures in non-mitotic cells. These structures resemble filopodia, are highly dynamic and often appear connecting two cells for multiple frames. Examples of this can also be seen in many of the cells in Video 5.1.

5.2.2. mKITL

5.2.2.1. mKITL is enriched at the cell membrane and in the perinuclear region

mKITL localisation varied between the two constructs (Figure 5.3.). mKITL_TD is localised throughout the cell, and appears enriched at the cell membrane. The older

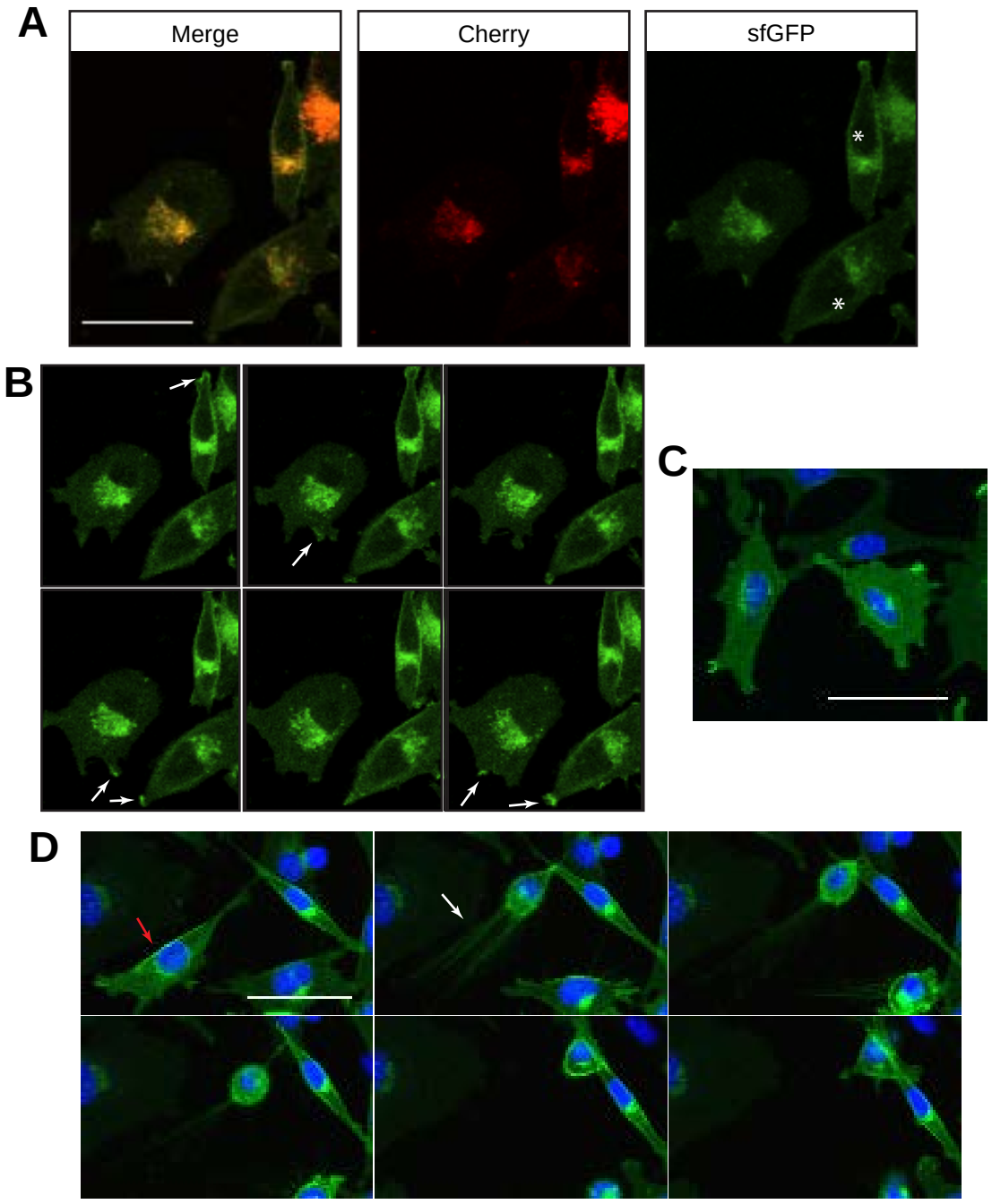

Figure 5.2. Localisation of sKITL constructs A. sKITL_TD shows localisation across the whole cell. SfGFP shows some enrichment at the membrane (in cells indicated by stars), and at distal tips. Cherry localises mainly to the perinuclear region. **B.** White arrows indicate new protein in a series of timelapse images of the same cells (L-R), taken 2 mins apart. Localisation of young protein in sfGFP is dynamic and transient at the end of protruding tips. This pattern is not seen in the red channel. **C.** sKITL_NG cells in culture. Bright fluorescence of green is seen throughout the cell, with enhancement at distal tips in a similar manner to sKITL_TD. The perinuclear compartment appears much smaller. The nucleus is stained with NucBlue. **D.** In a timelapse series of sKITL_NG culture (L-R), a mitotic cell is attached to the glass surface by fibrillar protrusions, which are marked in green. The red arrow indicates the cell which is about to divide, and the white arrow shows the sKITL marked protrusions. These protrusions retract with the cell over the next frames as it rounds up, then divides. Scale bars represent 50μm.

protein, marked by Cherry, is concentrated in the perinuclear region. mKITL_NG localisation is very limited in comparison. It also marks the perinuclear region and the immediate cytoplasm, but does not effectively mark any dynamic cell extensions past the main cell body. Adjusting the microscope settings does reveal localisation further towards the membrane, but at weak levels that are unsuitable for imaging in comparison to the rest of the cell. The localisation pattern of the older, red mKITL_TD protein and mKITL_NG are comparable. As in the sKITL constructs, localisation around the nucleus is characteristic and suggests that the older mKITL_TD may be being targeted to this area. Similar localisation by mKITL_NG could indicate that a large amount of the protein is being sequestered before it can reach the membrane.

5.2.2.2. mKITL is localised to in filopodia and attachment filaments

mKITL_TD is localised in cellular protrusions at the front of the cell, which are presumed to be filopodia although this was not successfully determined (Figure 5.3.C.). The structures can be seen in variable numbers, protruding out of the cell membrane in multiple cells. Often they appear to connect to neighbouring cells and remain in contact through multiple time frames. In a similar manner to sKITL, mKITL is also localised in filaments appearing out of the rear of the cell. Figure 5.3. demonstrates these structures, which are clearly marked by green fluorescence, and are extremely dynamic. This also demonstrated in Video 5.2., which follows the same cells for a few frames.

5.2.3. KIT

5.2.3.1. KIT is localised throughout the cell

KIT_TD is localised throughout the cell, although the appearance of the two colours is quite different (Figure 5.4.A). SfGFP is seen throughout the cytoplasm, and is sometimes enriched at the cell membrane. Cherry has a speckled appearance, and similarly to other timer tag constructs, it mainly appears near the nucleus. However, the area it covers appears larger and extends further into the cytoplasm than the perinuclear region. Red fluorescence is not seen at the membrane. Again, this

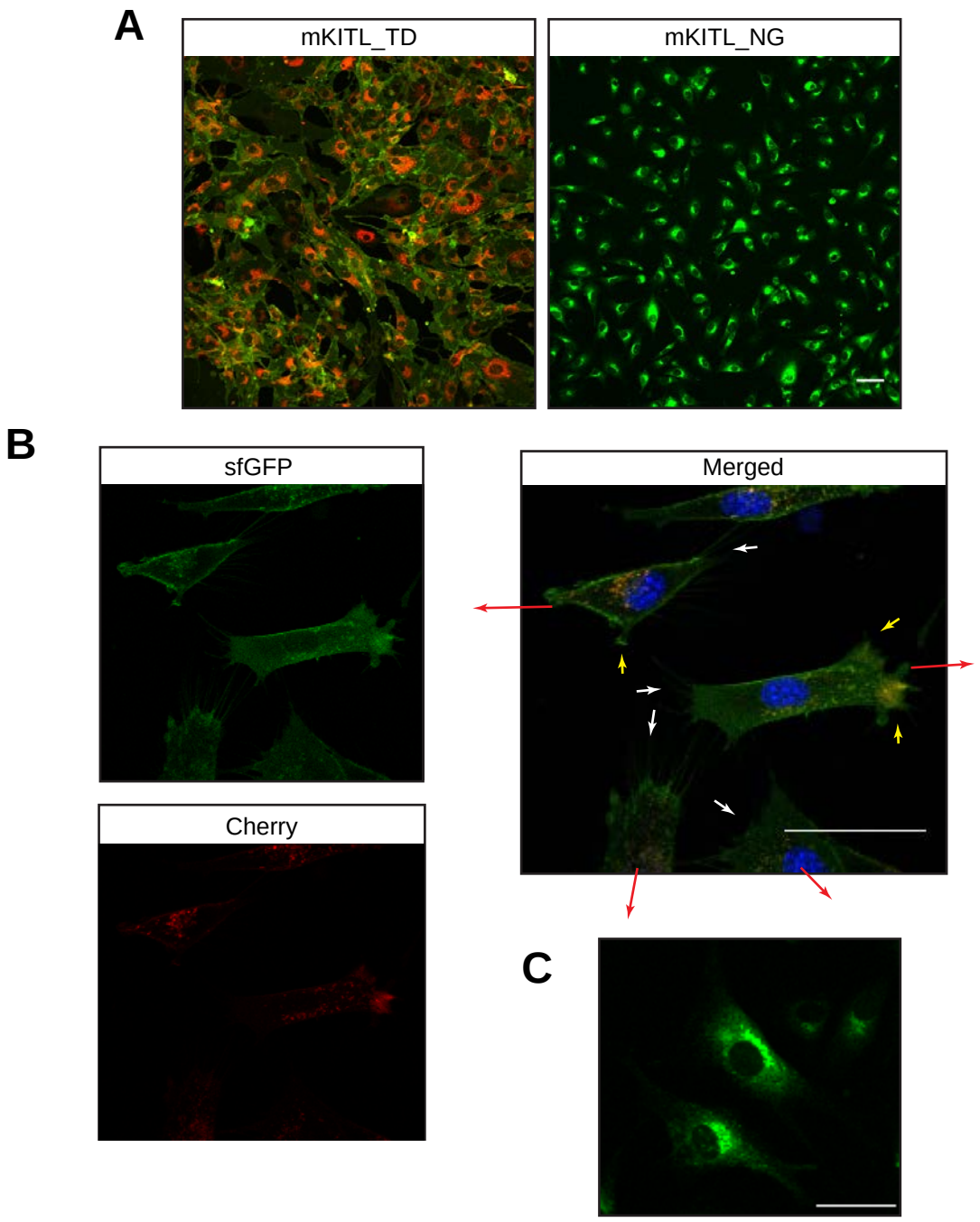

Figure 5.3. Localisation of mKITL constructs; fluorescence localisation patterns vary between mKITL_NG and mKITL_TD. A. Whole field images of each cell line, plated at the same density. As the constructs differ only in the fluorophore, we expect the same localisation within the cell. **B.** Higher magnification shows mKITL_TD is localised throughout the cell. SfGFP is enriched at the membrane, while Cherry is dominant around the nucleus. Numerous small protrusions from the membrane are marked by mKITL_TD. In the merged panel, white arrows indicate the area of protrusions to the rear of the cell, yellow arrows indicate protrusions to the front of the cell, and the red arrows indicate the direction of cell movement. **C.** A magnified view of mKITL_NG cells shows protein is localised primarily in the perinuclear area and in the immediate cytoplasm, but does not effectively label the cell membrane. Some cells show very little expression of the fluorophore, as can be seen in the two cells in the top right quadrant. All scale bars represent 50μm.

suggests that the older protein is being targeted inwards as it ages. KIT_C localisation broadly matches the localisation patterns of both green and red protein in KIT_TD (Figure 5.4.C). Red fluorescence is observed throughout the cytoplasm in low amounts, and appears enriched and speckled in the perinuclear region.

5.2.3.2. KIT shows transient localisation at distal tips of cell protrusions

Occasionally in KIT_TD cells, bright green fluorescence is observed at the tips of protrusions from the cell body, or at the tips of elongated cells (Figure 5.4.B.). This localisation is dynamic between time frames. It has been suggested that upon detection of KITL in the environment, KIT receptors cluster in the area to maximise signalling (Tabone-Eglinger et al., 2014); this bright localisation of green could indicate a clustering of KIT receptors. This is not a mixed culture, but the fluorescent KIT receptors may be reacting to endogenous KITL protein. The location on the tips of extending structures could be significant; KIT may also be associated with structural cytoskeletal components.

5.3. KIT/KITL kinetics

To ascertain the turnover of sKITL, mKITL and KIT, tandem fluorescent protein timers using sfGFP and Cherry were developed. SfGFP matures quickly, while Cherry matures more slowly. In a pool of proteins, newly synthesised molecules are green after synthesis, then gradually gain red fluorescence as the protein matures. The ratio of green to red is, therefore, an indicator of the relative age of the protein pool, and can be used to estimate turnover rates (Khmelinskii et al., 2012).

5.3.1. Validation of tandem fluorescent protein timers

5.3.1.1. Cycloheximide treatment blocks new protein production

To validate the timer tag constructs, and show that the fluorescence is related to the age of the protein pool, protein production was blocked using the transcriptional inhibitor cycloheximide (CHX) (Schneider-Poetsch et al., 2010). We hypothesised that this would lead to an older protein pool i.e. increased Cherry fluorescence

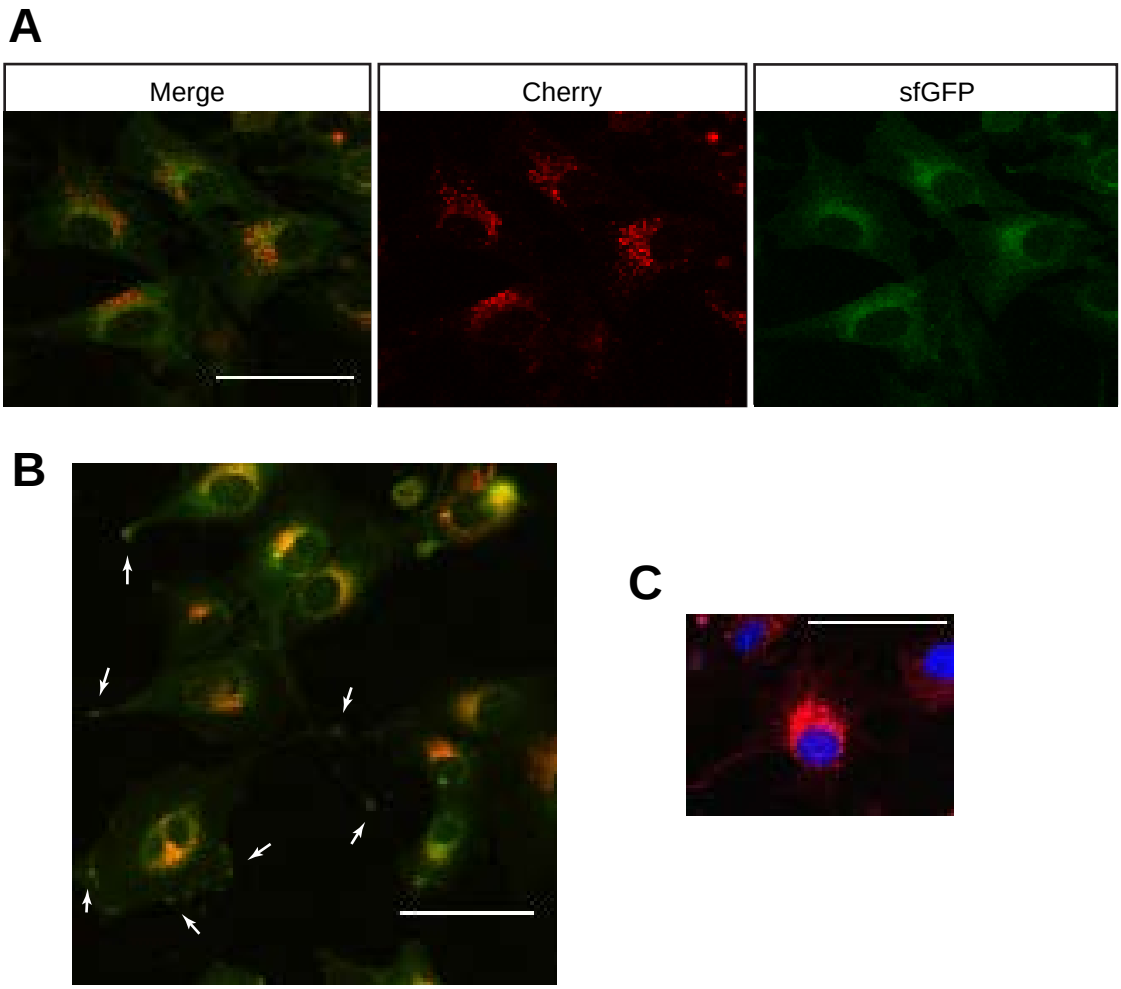

Figure 5.4. Localisation of KIT constructs. A. KIT_TD is localised throughout the cell. SfGFP can be seen in the cytoplasm to the edges of the cell, and is occasionally enriched at the membrane. Cherry has a speckled appearance, and is enriched near the nucleus. **B.** In KIT_TD cells, bright green fluorescence is sometimes observed at the ends of cell protrusions. This is seen in several cells in this image; white arrows indicate bright sfGFP signal. **C.** KIT_C localisation resembles KIT_TD, with fluorescence throughout the cell. There is some localisation to the membrane, but the brightest fluorescence is in the perinuclear region. The nucleus is shown in blue, marked by NucBlue. Scale bars represent 50µm.

and a higher ratio. These imaging experiments were performed by Stephanie Wright, under the supervision of Dr Richard Mort at the University of Lancaster. mKITL_TD cells were treated with various concentrations of CHX, and the ratio between sfGFP and Cherry was measured as described. Results from these experiments are shown in Figure 5.5. The ratiometric images and the graph show that the age of the protein pool has been shifted with the addition of CHX. This shift is shown to be significant by 1-way ANOVA ($P = 3.5 \times 10^{-20}$), and pairwise t-tests were used to assess differences between the groups.

There was a significant increase in the age of the protein pool between all cells treated with CHX and the negative control cells in the cytoplasmic compartment; 0µM-2µM $P = 1.642 \times 10^{-6}$, 0µM-5µM $P = 2.416 \times 10^{-8}$, 0µM-10µM $P = 2.363 \times 10^{-12}$. This was accompanied by a significant increase in the ratio between the untreated cells and all the CHX treated cells in the perinuclear region; 0µM-2µM $P = 9.179 \times 10^{-5}$, 0µM-5µM $P = 1.039 \times 10^{-5}$, 0µM-10µM $P = 1.257 \times 10^{-8}$. Increasing the concentration of CHX elicited no significant effect on the age of the protein pool after 2µM.

5.3.1.2. Treatment with exogenous sKITL increases turnover of KIT_TD

Experiments with the KIT_TD cells further confirms the validation of the timer tags as described above. Treating KIT_TD cells with exogenous sKITL was performed, with the hypothesis that an increase in ligand availability would increase the rate of receptor turnover. These imaging experiments were also performed by Stephanie Wright, under the supervision of Dr Richard Mort at the University of Lancaster.

KIT_TD cells were treated with a low concentration of exogenous sKITL for 24 hrs before imaging, then the ratio between sfGFP and Cherry was measured as described. Results from these experiments are shown in Figure 5.6.

The addition of sKITL induces a significant shift in the ratio of fluorescence. In both the cytoplasm and perinuclear regions, there is a significantly reduced ratio, indicating more green/less red fluorescence; cytoplasm $P = 0.0028$, perinuclear $P = 3.28 \times 10^{-6}$. This correlates with a younger KIT_TD protein pool, which is being

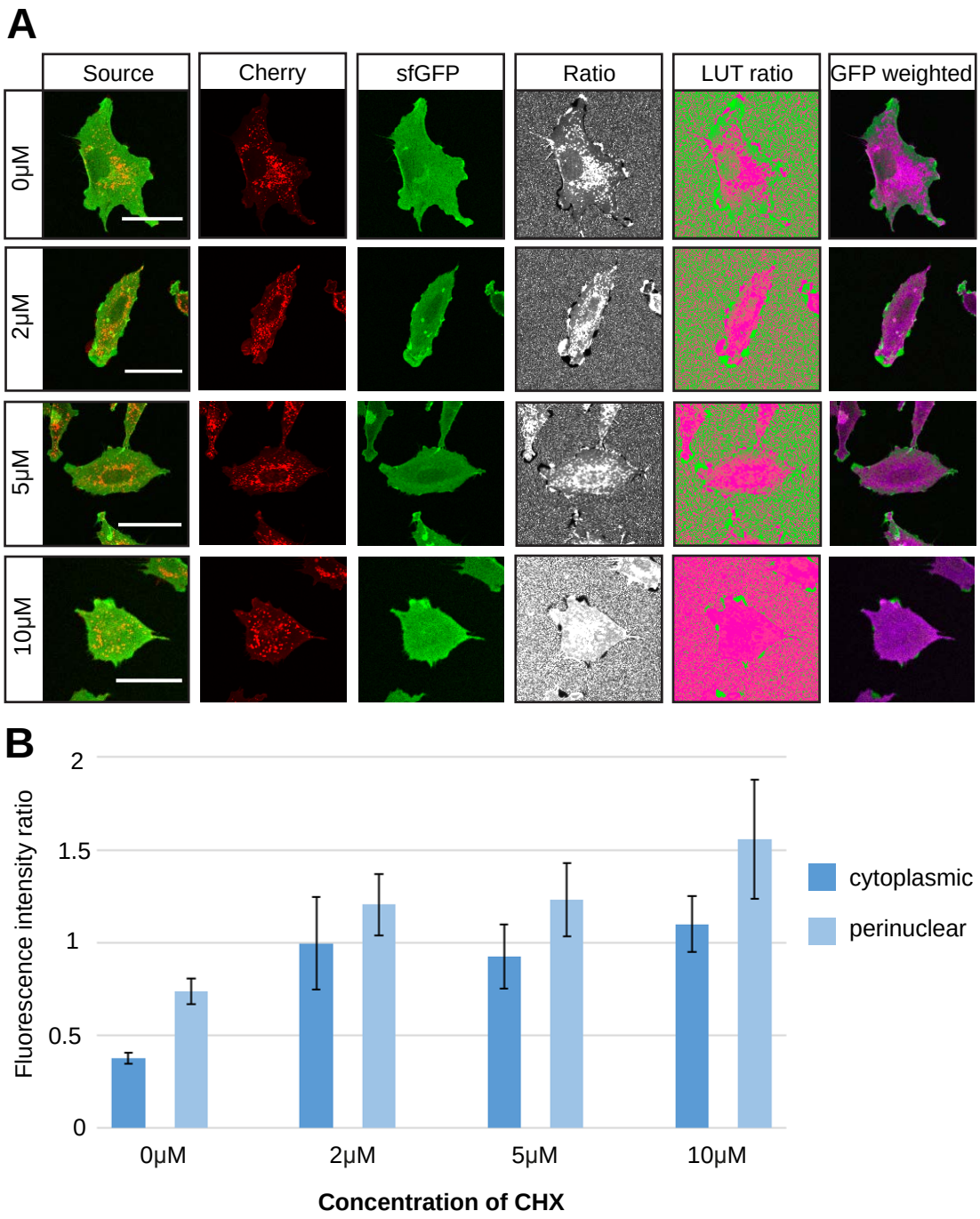

Figure 5.5. mKITL_TD production can be blocked by CHX treatment. A. The ratiometric images panel shows mKITL_TD cells treated with increasing concentrations of CHX. From left to right the panels show; the original source image, followed by the source image separated into the green and red channels. The fluorescence intensity of each channel is calculated and displayed as a ratio in the next panel - this is the image on which fluorescence intensity measurements are made. Next, and LUT (look up table) is applied, which colours the image based on the fluorescence intensity. This is mulitplied by the GFP channel to create the final GFP-weighted image. The GFP-weighted image shows that there is a shift in the ratio towards red throughout the cell, indicating an older protein pool. Scale bars show 50μm. **B.** Quantification from the ratiometric images shows the ratio between sfGFP:Cherry in the cytoplasmic and perinuclear regions. There is an increase in fluorescence in both compartments with the addition of CHX. Significant differences are discussed in the text. The error bars show the 95% confidence interval.

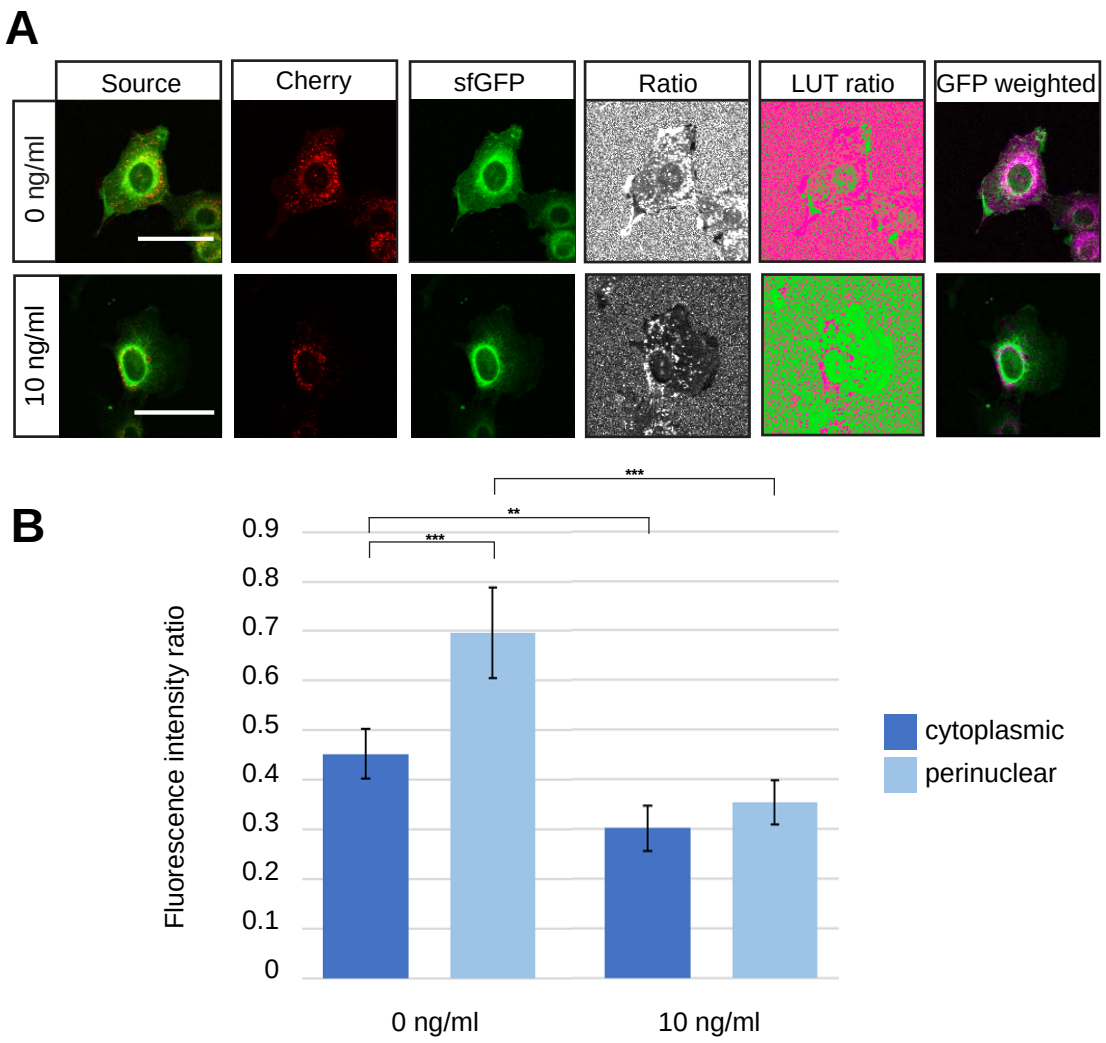

Figure 5.6. KIT_TD protein turnover increases with addition of exogenous sKITL. A. The ratiometric imaging data from cells treated with 10ng/ml sKITL vs. a negative control. The panels are as described in Figure 5.5. The GFP weighted image shows that there is a shift in the ratio towards green throughout the cell when treated with sKITL, indicating a younger protein pool. Scale bars show 50µm. **B.** The fluorescence ratio was measured in the cytoplasm and perinuclear region. There is a significant decrease in the relative age of the KIT_TD protein pool in the presence of sKITL as demonstrated by a lower ratio in both compartments. Although the perinuclear region still has the higher ratio in cells treated with 10ng/ml sKITL, it is no longer significantly higher compared to the cytoplasmic region (P = 0.127). Error bars show the 95% confidence interval.

turned over faster to in response to abundant ligand.

5.3.2. Ratios of sfGFPCherry vary across the cell in all constructs

In all three protein fusions, the ratio of green/red varied across the cell, demonstrating that the proteins move extensively within the cell over their lifetime. This has been alluded to when discussing localisation of the proteins, and now a more thorough analysis follows. Refer to Figure 5.7. for a full comparison of the ratios between compartments, and cell lines. The ratio is given as an integer, where 0 represents fully green, and the higher the number, the more red is present, resulting in a yellow colour on a composite image. Figure 5.7.B. shows the ratiometric analysis performed to obtain the measurements. A 1-way ANOVA was performed to assess whether any significant differences existed between the groups, then pair-wise t-tests were performed as appropriate. ANOVA testing showed that there were significant differences in compartment localisation in all three timer tag cell lines (KIT_TD $P = 4 \times 10^{-12}$, sKITL_TD $P = 5.6 \times 10^{-14}$, mKITL_TD $P = 4 \times 10^{-18}$).

In all three lines, the youngest protein is dominant in the cytoplasmic compartment as shown by the small ratios; KIT_TD = 0.383, sKITL_TD = 0.299, mKITL_TD = 0.344. The cytoplasm and cell membrane were considered as one unit in the analysis, as much higher resolution imaging would be required to discriminate between the two.

The pool of protein residing in the perinuclear region is significantly older in comparison, in each construct, as demonstrated by the higher ratio; KIT_TD = 0.717 ($P = 3.372 \times 10^{-9}$), sKITL_TD = 0.547 ($P = 2.755 \times 10^{-13}$), mKITL_TD = 0.735 ($P = 6.654 \times 10^{-13}$). The whole cell ratio lies roughly in the middle of values for cytoplasmic and perinuclear regions. Where possible, the ratio should therefore be measured separately in the different compartments.

In comparisons between the cell lines, the sKITL_TD protein has the lowest ratio in all areas, indicating a younger protein pool. mKITL_TD protein has whole cell and

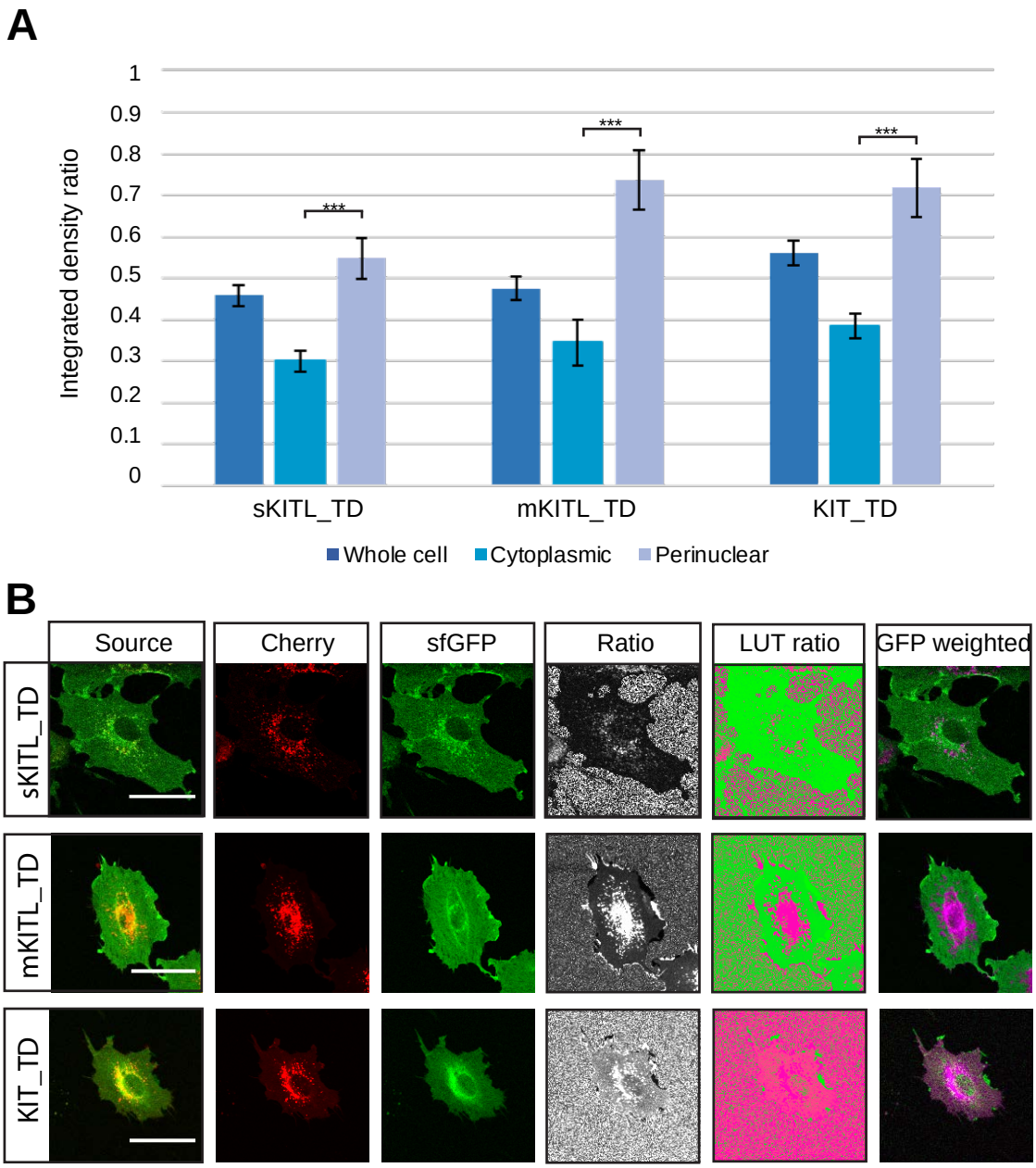

Figure 5.7. The ratio of green to red in tandem fluorescent protein timers is used to estimate the relative age of the protein pool. A. Graph shows the ratios of sfGFP:Cherry protein in the cellular compartments for each cell line. A younger protein pool has more sfGFP, and is represented closer to 0, while an older protein pool has more Cherry, and is represented closer to 1. In each case, the overall pool of protein is youngest in the cytoplasmic compartment and oldest in the perinuclear region. This reflects the observations from imaging. Error bars show the 95% confidence interval. **B.** Images from the analysis steps are shown with a single cell representation of each cell line. Observations from the graph are reflected in this final image; sKITL_TD cells show the highest sfGFP fluorescence, indicative of a younger protein pool. The perinuclear regions contain the oldest protein, shown by the higher amount of Cherry. The KIT_TD protein pool is older in the cytoplasm than in either KITLs. Scale bars represent 50μm.

cytoplasmic ratios similar to that of sKITL_TD with no significant differences, however the perinuclear compartment has a much higher ratio of 0.547 vs. 0.735 ($P = 1.03 \times 10^{-5}$). sKITL_TD has a significantly lower ratio in every area compared to KIT_TD; cytoplasm $P = 1.45 \times 10^{-5}$, perinuclear $P = 3.45 \times 10^{-4}$ and whole cell $P = 4.08 \times 10^{-7}$. mKITL_TD and KIT_TD showed no significant differences in ratios in either the cytoplasmic and perinuclear compartments, but did show a significant difference when the whole cell was measured ($P = 1.05 \times 10^{-4}$).

5.4. KIT and KITL interaction

To determine whether the fluorescent ligands are being cleaved from the membrane and incorporated into other cells in culture, co-culture experiments were performed NIH3T3 cells do not endogenously express KIT protein (Wang et al., 2000), so fluorescent sKITL or mKITL cannot normally be transferred into these cells. In the following mixed culture experiments, all green fluorescence observed in KIT_C cells must originate from the KITL_NG cells. Therefore, any cells which are both red and green are KIT_C cells, whilst any only green cells are KITL_NG cells. Furthermore, any green fluorescence must have entered the cells through the KIT_C receptors. In the mixed cultures with melb-a and B16F10 cells, any fluorescence must also originate from the KITL_NG cells, but enters through endogenous KIT receptors.

5.4.1. sKITL transfer to other cells in mixed cultures

5.4.1.1. sKITL_NG can be transferred to KIT_C cells

Figure 5.8. shows sKITL_NG localised in KIT_C cells, with those cells indicated by white arrows in all channels. Fluorescence in KIT_C cells compared to sKITL_NG cells appears less bright as expected. This was quantified and plotted in Figure 5.8.B., and it was shown that there was significantly less fluorescence in the KIT_C cells ($P = 1 \times 10^{-7}$). Colocalisation of fluorescent red and green proteins can be seen in composite images as yellow pixels. However, when there is a difference in the fluorescent intensity at seen here, a more accurate method to determine whether proteins are colocalised must be performed. sKITL and KIT colocalisation was

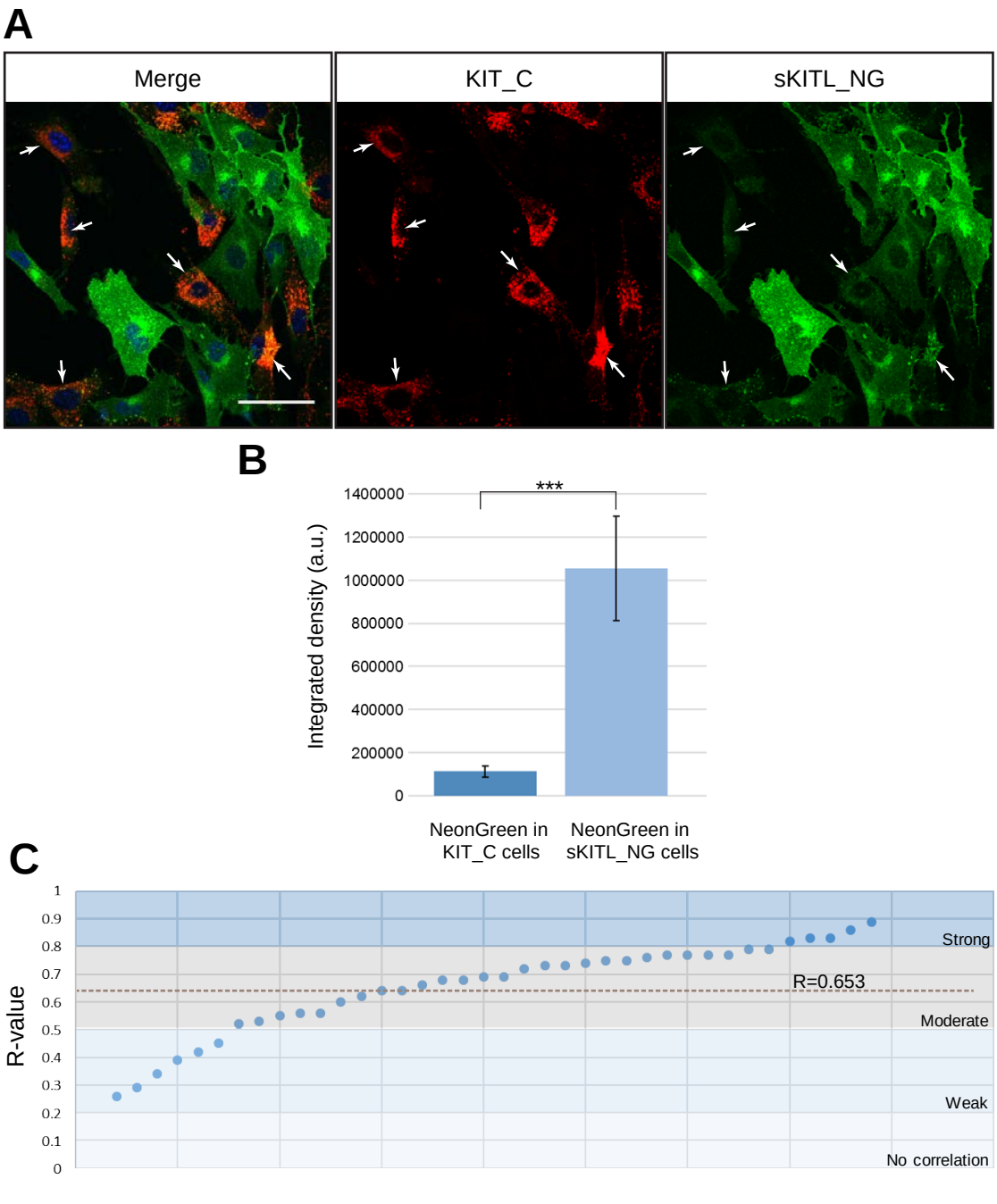

Figure 5.8. sKITL is taken up by other NIH3T3 cells and colocalises with fluorescent KIT receptor. A. Images show a mixed culture of NIH3T3 cells - one line expressing sKITL_NG and the other expressing KIT_C. The arrows in the merged panel show cells with both red and green fluorescence. No Cherry signal is detected in the sKITL_NG cells. Scale bar represents 50µm. **B.** The integrated density of NeonGreen fluorescence was measured - those which were producing sKITL_NG, and those which were not (i.e. KIT_C). The level of green signal in KIT_C cells is lower than in sKITL_NG cells in the same culture ($P=1x10^{-7}$). Error bars show the 95% confidence interval. **C.** Colocalisation between KIT and sKITL in KIT_C cells was assessed using Pearson's correlation coefficient (R). There is a moderate positive correlation between the localisation of green and red protein across the whole cell (mean R=0.653 +/-0.160). The graph shows the range of R values from a subset of cells, and demonstrates that the variation among results places them in different categories of correlation significance.

measured in the KIT_C cells, using the Pearson's correlation co-efficient. This tests fluorophore correlation in terms of pixel overlap, on a scale from 1 (perfect positive correlation) to 0 (no correlation) to -1 (perfect negative correlation), the positive aspect can be seen in Figure 5.8.C. The average correlation was determined for the data set as R = 0.653, which indicates a moderate level of positive correlation. However, the array of R-values taken into account for the average vary greatly within the small range of R-values. Many of the cells show weak correlation, whilst a few show strong correlation. Overall, there is a positive correlation, indicating there is colocalisation between the proteins, but the strength of correlation varies by cell. Colocalisation of the proteins would indicate the ligand/receptor have bound and been internalised.

5.4.1.2. sKITL_TD can be transferred to melb-a and B16F10 cells

To confirm that the KITL constructs could be taken up through endogenous KIT receptors, KITL_TD expressing NIH3T3s were put in mixed cultures with melb-a and B16F10 cells. The level of fluorescence observed may also give an indication of the abundance of receptors available for binding. The melb-a or B16F10s were coloured using DiI, which was demonstrated in Chapter 3. Images from a melb-a mixed culture can be seen in Figure 5.9.A., with a melb-a cell outlined in white for easy identification. The levels of sKITL in both the sKITL_TD producing cells and the melb-a or B16F10 cells was analysed by calculating the integrated density (Figure 5.9.B.). When the levels of fluorescence were quantified, the NIH3T3 cells expressing the construct had the highest levels as expected. Melb-a cells had significantly less fluorescence than the NIH3T3 cells ($P = 0.001$), and B16F10s had even less fluorescence ($P = 4 \times 10^{-4}$). This is interesting, as the B16F10 cell line is not dependent upon sKITL in culture, whilst melb-a cells are maintained with sKITL supplemented medium.

To assess the age of the proteins in each cell type, the sfGFP:Cherry ratio was measured as described above (see Figure 5.9.C.). Due to the extremely low fluorescence in the B16F10 cells, measuring the ratio was unachievable in these cells. The ratio in melb-a cells was significantly higher than in the sKITL_TD cells,

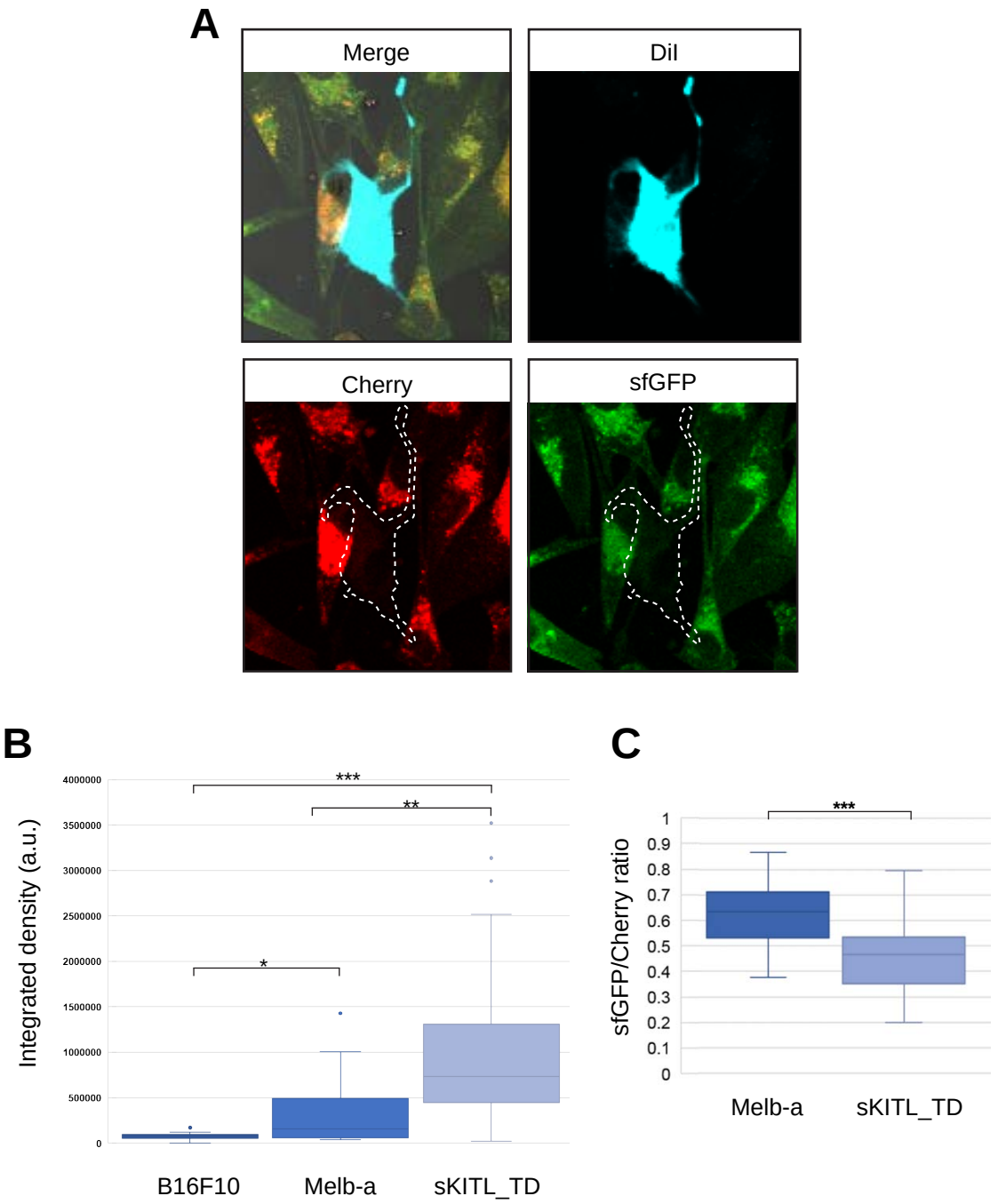

Figure 5.9. Melb-a and B16F10 cells can uptake fluorescent sKITL. A. A melb-a cell is marked by DiI in co-culture with sKITL_TD cells. The melb-a is outlined in white to demonstrate its position in other channels. SfGFP and Cherry are both faintly visible in the cell. Scale bar represents 50µm. **B.** Integrated density was measured for each cell type to determine the amount of fluorescence, then compared between cell lines. Integrated density was significantly lower in melb-a and B16F10 cells in comparison to sKITL_TD ($P = 0.001$, $P = 4x10^{-4}$ respectively). There was also significantly less fluorescence in B16F10 cells in comparison with melb-a ($P = 0.032$). **C.** The ratio of the red and green protein in melb-a and sKITL_TD cells was compared. The sKITL_TD protein localised to melb-a cells had a significantly higher ratio ($P = 1.02x10^{-7}$), indicating that the melb-a had less green and more red protein present. Box and whisker plots show the minimum, maximum, interquartile range and mean of the data set.

indicating an older protein pool had been internalised as would be expected ($P = 1.02 \times 10^{-7}$). The donor cells, are constantly producing new protein, whereas the melb-a/B16F10 cells can only uptake protein that is presented.

5.4.2. mKITL transfer to other cells in mixed cultures

5.4.2.1. NeonGreen can be transferred to KIT_C cells

Figure 5.10. demonstrates the ability of fluorescent mKITL to be transferred to KIT_C cells.

Initially, the mKITL_NG in the KIT_C cells does not have the same localisation pattern as in the cells producing the protein; there is no pronounced perinuclear localisation and protein is evenly distributed across the whole cell with some speckling. Over the time course, localisation of mKITL_NG increases within the KIT_C cells, and the perinuclear localisation appears much stronger. This suggests that the perinuclear localisation is due to high amounts of the protein.

The levels of NeonGreen fluorescence were quantified in the different cell lines at the start and the end of the imaging time course. The quantification can be seen in Figure 5.10.B. After 4 hrs in culture, there is a significant difference between the amount of fluorescence in the mKITL_NG expressing cells and the KIT_C cells as may be expected ($P = 9.28 \times 10^{-6}$). This difference decreases over the time course, as significantly more mKITL_NG is found in the KIT_C cells after 8.5 hrs ($P = 3.136 \times 10^{-5}$).

Localisation between the proteins was measured, again using Pearson's co-efficient (R). Refer to Figure 5.8.C for position of R values in terms of the correlation significance. After 4 hrs in culture, there is no colocalisation of the proteins, as demonstrated by an R-value of 0.06389. By 8.5 hrs, there is a strong correlation between the red and green proteins, with an R-value of 0.84.

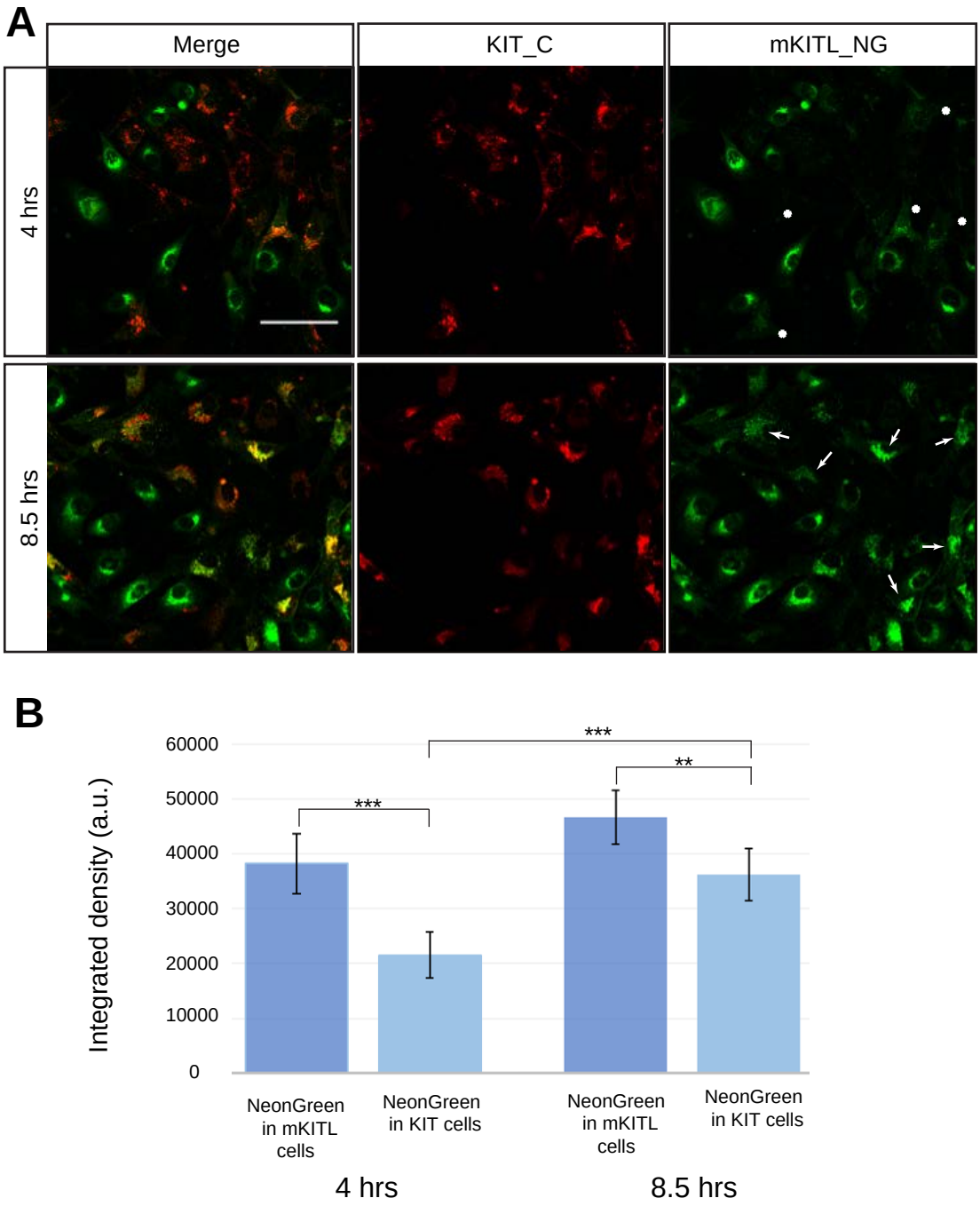

Figure 5.10. mKITL_NG is taken up by KIT_C cells, and changes localisation over time. **A.** Images from timelapse experiments shows that mKITL_NG is taken up by KIT_C cells, as green fluorescence is visible in the red cells. Cells were imaged 4 hrs after plating in culture together (time points are indicated as time post-plating). At 4hrs, low green fluorescence in the KIT_C cells is evenly distributed; dots indicate KIT_C cells which are also positive for mKIT_NG. After 8.5 hrs, as levels of fluorescence within the KIT_C cells increases, arrows indicate examples of areas where perinuclear localisation has increased. **B.** The level of mKITL_NG was quantified at the beginning and end of imaging in both mKITL_NG and KIT_C cells. There was a significant difference between the levels of fluorescence in each cell type at both time points, although the significance decreased after 8.5 hrs (4 hrs $P = 9.28 \times 10^{-6}$, 8.5 hrs $P = 3.66 \times 10^{-3}$). There was a significant increase in the amount of NeonGreen fluorescence in KIT_C cells over the time course ($P = 3.14 \times 10^{-5}$). Error bars show the 95% confidence interval.

5.4.2.2. mKITL_TD can be transferred to melb-a cells

As with sKITL, the ability of mKITL_TD to be transferred into melb-a cells was determined. Figure 5.11.A. shows the presence of mKITL_TD in melb-a cells which are outlined in white. Fluorescence is faintly visible in these cells, primarily in the perinuclear compartment. The level of total fluorescence was measured by integrated density, results of which are shown in Figure 5.11.B. There is a highly significant difference ($P = 1.33 \times 10^{-30}$) between the integrated density measured in melb-a cells and the mKITL_TD producing cells. This is clear from the imaging, as fluorescence in both channels is very faint. To determine whether the protein found in the cells was of a similar age, the sfGFP:Cherry ratio was measured as before. The results in Figure 5.11.C. show that the melb-a cells had a significantly higher ratio, indicating an older protein pool is present as described for sKITL_TD.

5.4.3. KITL transfer through conditioned medium

Conditioned medium experiments were performed to determine whether fluorescent KITL is effectively cleaved from the membrane, and is able to be transferred in the absence of donor cells. KITL cells were grown in fresh culture medium for 24 hrs to create a conditioned medium. The media was removed, and filter sterilised before adding to KIT_C cells followed by imaging. Figure 5.12. shows KIT_C cells cultured in media conditioned by sKITL cells in 5.12.A.i. and from mKITL cells in 5.12.B.i. The images show the first frame from a time-lapse series, and are taken ~30-40 mins after addition of the conditioned media. The amount of fluorescence was assessed over time, to determine whether the KITL in the media was being taken up by the cells as would be expected. The average fluorescence intensity is plotted by time in Figure 5.12.A.ii. and B.ii. for sKITL and mKITL respectively.

sKITL_NG fluorescence increases slightly over the first hour, before beginning a steady decline over the time course. At the start of the culture, the fluorescence is distributed evenly across the cell, however this becomes more speckled over time and this localisation quickly appears increased around the perinuclear region. mKITL_NG fluorescence declines steadily over the 4 hrs, with a slight increase in

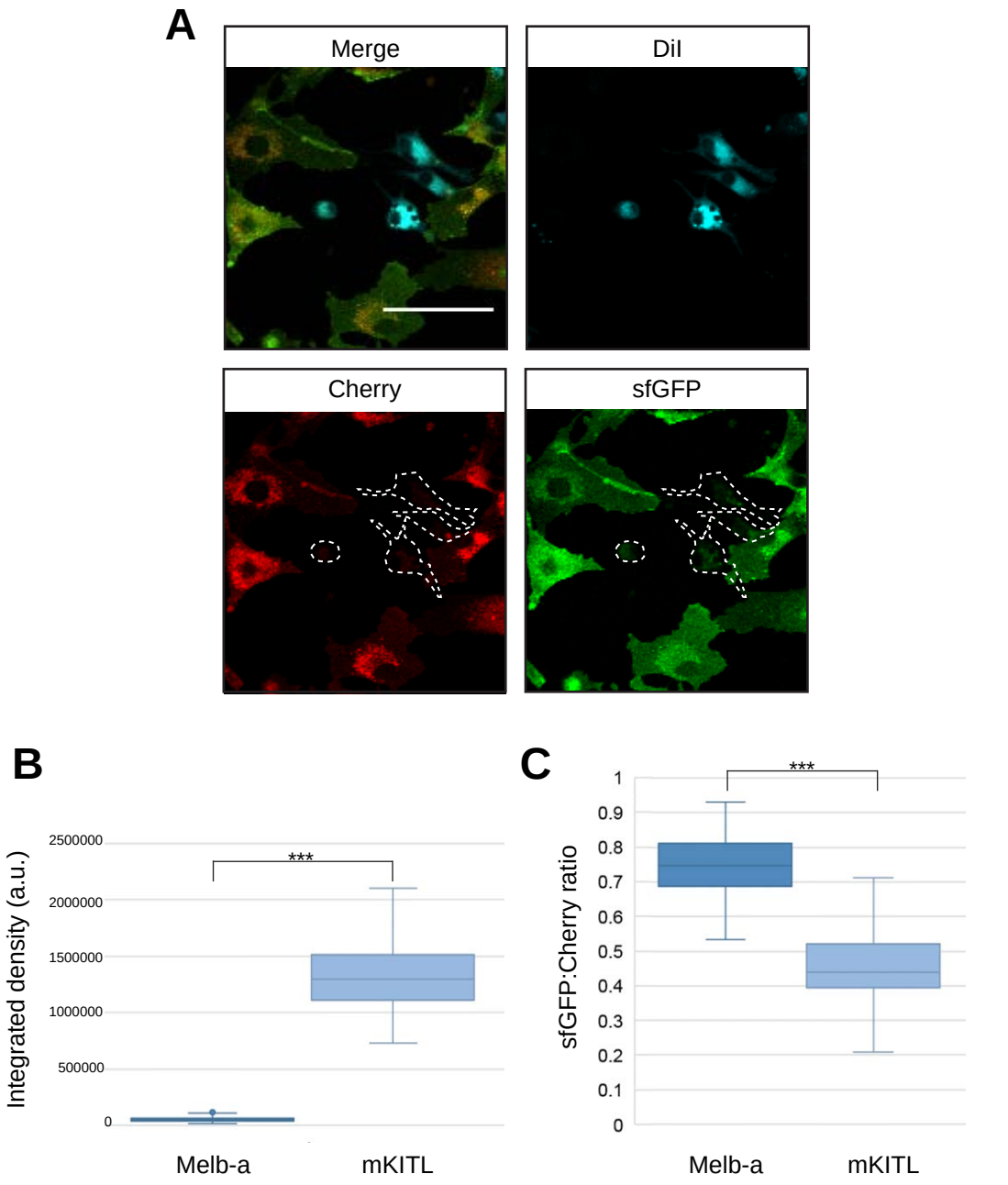

Figure 5.11. Melb-a cells can uptake fluorescent mKITL. A. Melb-a cells are marked by DiI in co-culture with mKITL_TD cells. The melb-a cells are outlined in white to demonstrate their position in other channels. SfGFP and Cherry are both faintly visible in the melb-a cells. Scale bars represent 50μm. **B.** The amount of fluorescence in the different cells was measured and quantified by integrated density. There is a significant difference between the integrated density in the melb-a and mKITL_TD cells ($P = 1.33x10^{-30}$). **C.** The age of the protein pools in the different cells was measured. The fluorescence in melb-a cells has a significantly higher ratio than the mKITL_TD cells, indicating an older protein pool.

rate between 2 and 3 hrs. In both sKITL and mKITL cultures, the fluorescence of KIT_C decreased over time. The rate of decrease is greatest during the first hrs, and then slows down over the rest of the time course. KIT_C fluorescence does not decline in this way in KIT_C only cultures. The reasons for this were not clarified, although it could be hypothesised that the excess of ligand has caused saturation of the receptors. Once bound and internalised, the complex may be degraded as discussed. Consequently, in levels of high ligand availability, the receptors may not be able to re-establish in large quantities at the membrane due to constant ligand binding and degradation.

5.5. Discussion

5.5.1. Localisation patterns of KITL support associations with actin

Results suggest that both sKITL and mKITL may be associated with actin-based structural components. Structural and cytoskeletal plasticity is vital during cell migration to change the cell attachments which will allow forward motion. Migratory cells exhibit classical front-rear polar morphologies which are well studied. The main structures in non-invasive cells are highly dynamic, and are formed and regulated by actin polymerisation (Alblazi and Siar, 2015). Lamellipodia form at the leading edge of the cell, and are thought to be the driving force of cell migration by attaching the cell body to the surface and pulling it forward (Yamaguchi and Condeelis, 2007). Many lamellipodia form, and the frontal morphology is often described as a 'ruffling' effect (Suraneni et al., 2012). Also at the front of the cell, filopodia are 'spike-like' protrusions which extend into the environment (Suraneni et al., 2012). Filopodia are essential for migrating cells where they are described as an environmental probe (Mattila and Lappalainen, 2008). The localisation pattern of mKITL constructs resemble filopodia extending into the environment. At the rear of the cell, the tail is attached to the surface (Lodish et al., 2000). Movement of the rear is dependent upon microtubule reorganisation to retract the tail of the cell towards the cell body, thereby creating a net forward movement (Ganguly et al., 2013). Again, both sKITL and mKITL were observed in these attachments to the rear.

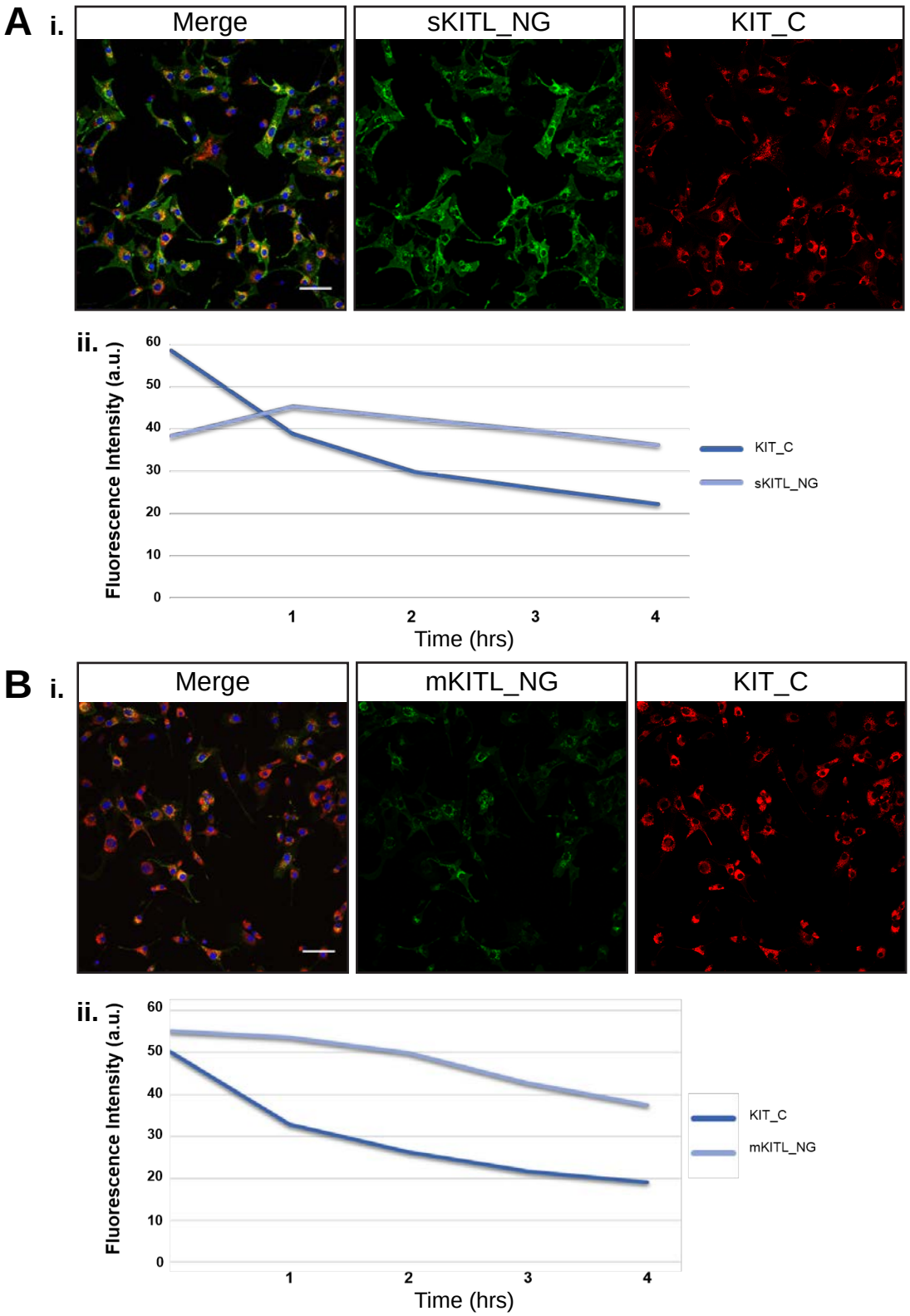

Figure 5.12. KITL in conditioned medium is taken up by KIT_C cells. KIT_C cells were supplied with conditioned medium siphoned from **A.** sKITL_NG cells and **B.** mKITL_NG cells. Scale bars represent 50µm. **A ii.** The amount of sKITL_NG and KIT_C were quantified over 4 hrs. KIT_C declines steadily, while sKITL_NG intensity rises over the first hour in culture before beginning to decline. **B. ii.** The amount of mKITL_NG and KIT_C were quantified over time. mKITL_NG intensity declines steadily, but initially at a slower rate than KIT_C.

In the literature, there are few instances of links between KITL and actin. A study by Ballestrem *et al*. (Ballestrem et al., 2000) used KITL to successfully induce lamellipodium formation in melb-a cells, which was critical to allow cell migration. Tabone-Eglinger *et al.* investigated the clustering roles of mKITL with KIT, and described association with F-actin at the cell membrane, although it was not sustained for long after initial cluster formation (Tabone-Eglinger et al., 2014).

Alternatively, KITL may be associated with the filopodia-like structures known as cytonemes (Kornberg and Roy, 2014). These structures were used to describe a direct-delivery model of morphogens during development, where signals are transferred through direct contact to ensure cell-specificity (Ramírez-Weber and Kornberg, 1999). This model was proposed to be a mechanism for achieving a morphogen concentration gradient in *Drosphila* (Ramírez-Weber and Kornberg, 1999).

5.5.2. Dynamic localisation of KIT and KITL at the membrane may show clustering of complexes

The clustering of KIT and KITL has been demonstrated previously in mKITL/KIT studies described by Tabone-Eglinger *et al*. Bright, dynamic localisation of KITL and KIT was observed at the cell membrane, and at the distal tips of protruding appendages. In KITL cells, this was accompanied by generally strong localisation at the membrane and frequent instances of bright localisation at the membrane. These events did not appear as frequently in the KIT cells, although this may be a consequence of the different fluorophores. Areas where cells overlapped or where cells extend protrusions into other cells, fluorescence of sfGFP or NeonGreen does appear brighter, however there was no obviously brighter fluorescence specifically at touching membranes, where KIT and KITL would interact. To determine whether this indicates a higher local concentration of protein and review this localisation more conclusively, fixing these cultures and imaging at high resolution would be beneficial. If these events were indeed clustering of the ligand and receptor, then these constructs would provide a useful method of observing the real-time dynamics in more detail.

5.5.3. Localisation of older KIT and KITL supports models where degradation of the complex occurs after signalling

In all of the cell lines, strong fluorescence was observed in the perinuclear compartment. The localisation of proteins around the nucleus is characteristic of lysosomal degradation. It suggests that a large portion of the older red sKITL_TD is being degraded. The fate of KITL after activation of KIT has not been conclusively demonstrated; there are conflicting reports as to the fate of the KIT/KITL complex once activation of the downstream pathways has begun. It has been shown that the KIT signalling complex can be internalised and trafficked in endosomes. It is also known that downregulation of KIT signalling can be achieved through receptor ubiquitination, leading to lysosomal degradation (Masson et al., 2006). However, it has also been shown that mKITL at least, lacks the localisation signal allowing targeting for endocytosis, thereby prolonging its time bound to the membrane for signalling (Wehrle-Haller and Imhof, 2001). This is an important feature which distinguishes sKITL and mKITL, as they produce different downstream signalling events, related to the duration of receptor activation (Miyazawa et al., 1995). However, the lack of signal on the ligand may not be relevant once the mKITL is eventually cleaved from the membrane and internalised along with the KIT receptor. Imaging data from the timer tag proteins in particular would support that there is internalisation and degradation of the proteins, due to an older protein pool in the perinuclear region where endocytic recycling occurs. Conversely, consistent localisation of the sfGFP fluorophore at the cell membrane suggests that new protein production is responsible for maintaining signalling.

It must be considered that this localisation may be a consequence of highly overexpressed proteins or due to an interfering presence of the fluorophore, and not a true event. Data from the timer tag proteins suggest a movement to this area by the older protein, rather than sequestering after translation. Further, the fluorescent proteins are all monomeric so not likely to dimerise, and are tested in combination with other proteins to show that they are useful as fusion proteins (Khmelinskii et al., 2012). The placement of fluorophores in all three constructs followed previously published sequences in which the fluorescent KIT and KITL proteins are known to

have accurate localisation properties. However, the timer tag proteins are pH sensitive, with sfGFP showing less stability than Cherry at low pHs, so it follows that in the lysosomes/endosomes, Cherry fluorescence would be dominant (Khmelinskii and Knop, 2014).

5.5.4. Fluorescent KITL is transferable between cells

The experiments described. are important to demonstrate that the KITL proteins are able to interact with the KIT receptors. The presence of fluorophores in cells which were not expressing the construct was the main method of achieving this, through mixed cultures and conditioned media. Both sKITL and mKITL was found in conditioned medium, and was able to enter KIT_C cells successfully. Fluorescence was also transferred in low amount melb-a and B16 cells, which express endogenous KIT. To further confirm these results, an experiment combining the KITL expressing NIH3T3s with general, non-KIT expressing NIH3T3s could be performed. No fluorescence should be apparent in these cells in either a mixed culture, or if cultured with conditioned medium.

The decrease of KIT_C over the time course in the conditioned media experiments is important to consider for control reasons. It is potentially concerning that the levels reduce as KIT_C should be produced consistently throughout by the stably transfected cells. It suggests that the rate or level of KIT/KITL signalling is not stable, and that there is a discrepancy between the level of overexpression of the KITL and KIT constructs. This may be exacerbated if KIT_C is also interacting with endogenous KITL, in addition to the over expressed fluorescent KITLs. Alternatively, the observations may indicate the saturation of the receptor with ligand, so the level of KIT_C may plateau to a base level, sometime after the 4 hrs imaged; although the levels are still decreasing at 4 hrs, the rate of decrease is slower than in the first hour. In the conditioned media experiments, media is only added ~ 20 mins before imaging whereas in mixed cultures, the cells are plated together for at least 4 hrs (usually over 16 hrs) before imaging to allow for attachment. The levels of receptors may have ‘balanced’ before imaging in the mixed culture experiments.

5.5.5. Manipulating the age of the protein pool can be quantified

Experiments using CHX and exogenous sKITL show that the ratio between green/red fluorescence in the timer tag protein constructs can be shifted in line with expected outcomes; treatment of mKITL_TD cells with CHX blocked new protein translation, so the age of the protein pool increased. Treatment of KIT_TD cells with exogenous sKITL increased the turnover rate of KIT_TD, so the age of the protein pool decreased. These validation steps show that the calculated ratios relate directly to the turnover of the protein, and validate the constructs for use in further protein kinetic experiments.

5.5.6. Future directions

Some experiments for developing the current findings have already been suggested specifically in the relevant sections. There are further studies which could greatly advance and promote the use of these cell lines and/or constructs as viable models to observe KIT/KITL proteins *in vitro*.

Higher resolution imaging, perhaps super-resolution, could be used to identify localisation patterns more accurately. At high resolutions, colocalisation of KIT and KITL in specific compartments, including at the membrane, could be investigated. Higher resolution imaging would also be more accurate in determining colocalisation occurrences.

The power of mathematical modelling has been described in Chapter 4 in relation to cell migration studies. Similarly, modelling can be used to incorporate protein dynamics to observe cell behaviour. In order to parametrise such a model, quantitative protein dynamics are required. Abundance of the proteins as well as their rates of production and degradation, are important baseline measurements. Further, the duration of downstream signalling events would be an important consideration. The timer tag proteins described here provide an interesting model to explore some of these features. The quantity of protein is needed to calculate turnover rates, but unfortunately, fluorescence intensity is not an accurate method of quantifying levels

of protein expression. It is mainly useful within the same construct to say if something appears brighter or dimmer, and if so higher or lower protein expression can be assumed, but is not comparable between different cell lines. Western blotting or ELISA experiments could be performed to establish the abundance of protein, and then turnover rates by calculating the ratio between tagged and endogenous protein. However, to date, there are no commercial antibodies able to differentiate between the two isoforms of KITL.

Within this project, attempts were made to introduce the Flp-In system into the relevant cell lines using homologous recombination and CRISPR-Cas9. Introducing fluorescent KIT and KITL constructs into melb-a and COCA cells respectively would be extremely advantageous. The NIH3T3 cell line is mainly applicable as a dermal cell equivalent, which produces KITL. This is especially true for examining KIT, as NIH3T3 cells endogenously produce KITL, which may be causing unknown complications as the ligand and receptor are both expressed in the same cell. Similarly, another interesting target cell line for introduction of the KITL constructs would be the Sl/Sl line used in the CDM assays, which do not produce endogenous KITL (Flanagan and Leder, 1990).

Chapter 6

Differential gene expression during melanoblast development and between culture methods

Examining the gene expression profile of cells through RNA sequencing is a powerful technique used to investigate differences in gene expression across the entire genome, and can be applied in various biological questions. It can be used to identify cell-specific markers and processes down to the individual cell in single-cell RNA-sequencing. In development and disease progression, it can reveal changes that lead to certain biological actions and behaviours. RNA sequencing is highly reliant on the development of the sequencing technology, which is becoming increasingly accurate and accessible.

Within this project, there were two distinct streams to the RNA sequencing experiments. The first experiment concentrated on examining the temporal development of primary melanoblasts, at ages previously unreported; the use of a new mouse line allowed the isolation of melanoblasts from E12.5, which is the earliest reported. Other studies have included microarray at E15.5 (Colombo et al., 2011), and a combination of rtPCR/qPCR (quantitative PCR) at E14.5, E16.5 and in MSCs (Colombo et al., 2011; Osawa et al., 2005). Between the ages of E12.5 to E14.5, there are important biological events including massive expansion of the population, mass migration through the trunk and crossing the dermal-epidermal basement membrane (Mort, Jackson and Patton, 2015). See Chapter 1.1. for a detailed narrative.

The previous chapters have concentrated on using *in vitro* cell lines as a model for melanoblasts, including the wildtype melanoblast line, melb-a (Sviderskaya, Wakeling and Bennett, 1995). It is hypothesised that by taking a cell from the *in vivo*

environment to *in vitro* culture, and ultimately to an immortal line, there will be changes to various aspects of the cells behaviour, expression pattern and identity. In this case, the RNA sequencing data is used to explore how accurately melb-a cells reflect *in vivo* melanoblasts. Melb-a cells were cultured in HDs to explore the effects of culturing in a 3D model on cell behaviour. Results presented in Chapter 3.2.2 and Chapter 4.2., suggest that this method of culture induces EMT. RNA sequencing provides an excellent tool to explore this hypothesis, particularly as methods such as western blotting and immunostaining proved impractical tools due to the experimental conditions. Melb-a cells which have been cultured using the HD method are also included to ascertain the effects of changing the growing conditions, as well as melb-a cells that have been plated and allowed to migrate away from the cell mass.

6.1. Sample collection and processing

6.1.1. Fluorescent primary melanoblasts – a novel melanoblast line

A novel mouse line which was targeted and developed by Dr Richard Mort, was used to collect primary melanoblasts. See Figure 6.1. for schematics of the constructs and identification of melanoblasts *ex vivo* using this model (data provided by Dr Richard Mort). The *Pmel-CMN* line was created to address issues of specificity surrounding current melanoblast models which traditionally use *DCT* or *Tyr* to drive reporters. Both DCT and TYR are expressed in other populations of NC lineage (Battyani et al., 1993; Jiao et al., 2006), which is problematic for isolating melanoblasts, particularly at the youngest ages. Pmel17 has been previously identified as an early marker of the melanoblast lineage and offers an excellent alternative (Baxter and Pavan, 2003).

The *Pmel-CMN* mouse was cloned and targeted as shown in Figure 6.1.A.; exon 11 of *Pmel17* was cloned and fused to a CreERT2-f2a-mKate2-t2a-H2bCerulean (CMN) cassette, using the t2a self cleaving peptide. The cassette was designed to express CreERT2, membrane localised Kate2 and nuclear localised Cerulean, as well

as wildtype PMEL. The construct was targeted in mouse embryonic stem cells to the *Pmel17* locus and a positive clone identified by long range PCR across the 5' and 3' homology arms. A mouse line was generated by blastocyst injection of the *Pmel-CMN* ES cell line. Figure 6.1.B-D. show melanoblasts from *Pmel-CMN* lines visualised by *ex vivo* culture. In Figure 6.1.B., *Pmel-CMN* skin at E14.5, H2BCerulean was detected, but there was no expression of mKate2. No expression of H2BCerulean was observed in the underlying nerves, unlike in *Tyr::CreA* and *Tyr::CreB* mice (Delmas et al., 2003). In Figure 6.1.C.i. and ii., mice were crossed to *R26R-YFP* mice to facilitate lineage tracing. Tamoxifen was administered at E10.5, and skin was imaged at E14.5; a population of cells is labelled with YFP. Again, no expression was detected in the underlying nerves. Finally, Figure 6.1.D. shows an image of labelled melanoblasts in a whole mount embryo.

6.1.1.1. FACS isolation

FACS data of the isolation of primary melanoblasts from these mice is shown in Figure 6.2. For each age category, 3 separate litters were collected, and used for biological repeats.

The dissociation protocol for FACS analysis is detailed in Chapter 2.6. Briefly, the head and appendages were removed, leaving the trunk intact. The skin was detached using methods described in detail by Mort *et al*.(2014), before dissociation in EDTA and collagenase solutions. Once single cell suspensions were achieved, FACS analysis was performed and cells were collected directly into buffer for the RNA extraction protocols. As cells were collected directly to maximise RNA yield, their purity was not checked by double sorting.

For FACS analysis and separation, the collected populations were based on a non-fluorescent control litter shown in Figure 6.2.A., and gatings were kept well separated from the non-fluorescent populations. Cells were first sorted on the forward and side scatter profiles to remove dead cells, clumps and debris. The number of cells obtained from the primary melanoblasts cell sorts are detailed in Table 6.1.

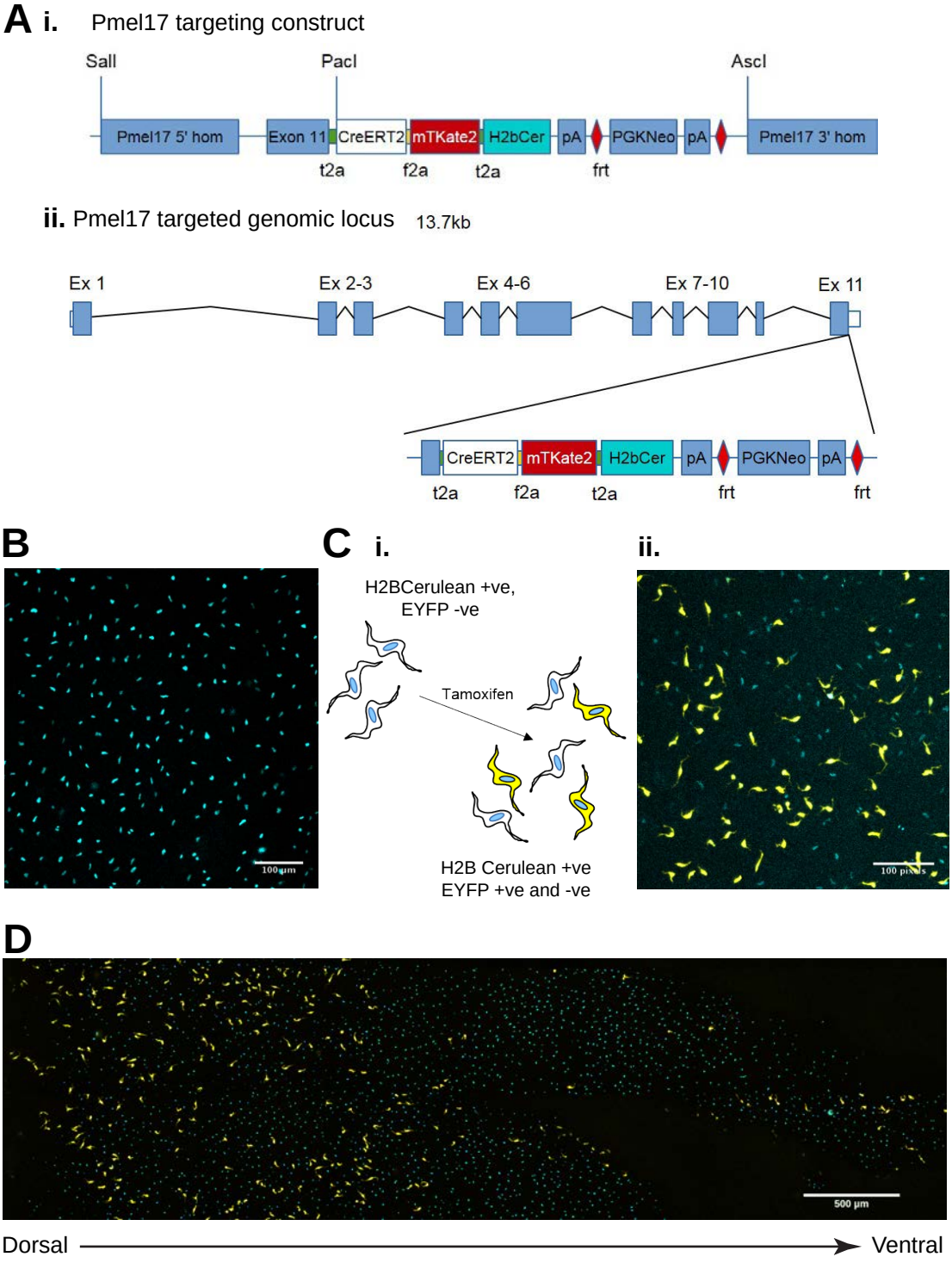

Figure 6.1. A novel melanoblast reporter line *Pmel-CMN*. Data from Dr Richard Mort. **A.i.** Exon 11 of *Pmel* was cloned and fused to a CreERT2-f2a-mKate2-t2a-H2bCerulean (CMN) cassette using the t2a self cleaving peptide. **ii.** The construct was targeted in mouse embryonic stem cells to the *Pmel* locus. **B.** In E14.5 embryonic skin from *Pmel-CMN* mice H2BCeruelan could be detected in melanoblasts but no expression of mKate2 was evident. **C.i.** *Pmel-CMN* mice were crossed with *R26R-YFPR* mice. Tamoxifen was administered at E10.5 and they were imaged at E14.5. **ii.** A subpopulation of cells morphologically identifiable as melanoblasts was labelled with YFP. **D.** In whole mount embryos, YFP labelled melanoblasts could be seen throughout the epidermis from the dorsal to ventral aspect.

6.1.1.2. E12.5

At around E12.5, melanoblasts which have been migrating in the dermis from E10.5, begin to invade the epidermis by crossing the basement membrane (Nishikawa et al., 1991). At the E12.5 time course, it was anticipated that the brightness of the Cerulean fluorophore would prove problematic; rapid proliferation at this time means that the fluorophore, which is bound to histone 2B, has little time to accumulate in the cell before mitosis. To avoid this, the *Pmel-CMN* line was crossed onto the CreERT2 inducible, floxed YFP reporter mouse – *R26R-YFP* (Srinivas et al., 2001). Melanoblasts are then double-marked in both YFP and CFP (cerulean fluorescent protein); PMEL expressing cells are marked by CFP and melanoblast lineage cells are marked by YFP. 4-OHT (4-hydroxytamoxifen) was used to activate the CreERT2 at E11.5, around 24 hrs before dissection. Binding of 4-OHT to the mutated oestrogen receptor of CreERT2 causes its translocation to the nucleus, thereby allowing the Cre recombinase to recombine the loxP sites around the stop codon on the *R26R-YFP* allele; removal of the stop codon allows transcription and translation of the YFP fluorophore (Feil, Valtcheva and Feil, 2009; Srinivas et al., 2001). Sorting for YFP/CFP +/+ fluorescent cells is then possible via FACS. Figure 6.2.B. shows the FACS sort from one biological repeat of the E12.5 age. The populations shown in P4 and P2 are the main interest for this project, as these are the PMEL expressing cells i.e. early melanoblasts. P2 are also melanoblasts, but recombination by CreERT2 appears to be fairly low, as only an average of 34% of the total population of melanoblasts (i.e. P4 vs. P2+P4) are labelled with YFP. Regardless, for extra confidence in isolating a pure melanoblast population, only double positive cells sorted into P4 were considered for sequencing.

6.1.1.3. E13.5 and E14.5

At E13.5 and E14.5, melanoblasts are migrating throughout the epidermis to colonise the entire trunk of the embryo (Luciani et al., 2011). Unlike the E12.5 embryos, the E13.5 and E14.5 embryos were not anticipated to require the *R26R-YFP* lineage reporter, as testing the CFP fluorescence via FACS showed that it was bright enough in heterozygous $Pmel^{+/CMN}$ embryos. *Pmel-CMN* males were crossed to laboratory

standard CD1 females, in order to increase litter size and maximise the number of melanoblasts obtained. Again, the FACS results in Figure 6.2.C. and D. show clear populations of CFP+ cells which express PMEL and represent the melanoblast population.

6.1.2. Cultured cells

There are two main questions surrounding the immortalised melanoblast cell line in this chapter. Firstly, do melb-a cells provide a good model for studying melanoblasts? Secondly, do the different culturing methods/statuses change the expression profile of the cells? In particular, do they reflect typical changes seen in EMT/MET processes? As stated, the three categories of cultured cells that were sequenced are: 'melb-a cells'; 'melb-a cells HDs'; and 'melb-a cells migrated from a HD'. Refer to Chapter 3.2. and 4 for information and visual representation of these cultures. For the 3 biological repeats, a single flask of melb-a cells was split and passaged twice before considered as a repeat. At this point, three separate flasks were used to set up HD cultures. For each of these three repeats, half of the cultures were harvested after 5 days for the 'melb-a HD' category. The other half were plated onto a glass surface and cells allowed to migrate away from the cell mass for 24 hrs. Then, the remaining cell's mass was dislodged and removed by microdissection, before the cells that had migrated and adhered to the surface were harvested. As mentioned previously, the HDs require the aid of matrigel (if not plated on a CDM) in order to migrate, so this must be taken into consideration.

6.1.3. RNA quality control

RNA was isolated and prepared as detailed in Chapter 2.3. Before processing to cDNA, the RNA was analysed on an Agilent Bioanalyser. The electrophoretically separated peaks of 18S and 28S species of rRNA (ribosomal RNA) are used to determine sample quality, and produce an RNA integrity number (RIN). This gives a good indication of the quality of cDNA that may be produced (Schroeder et al., 2006).

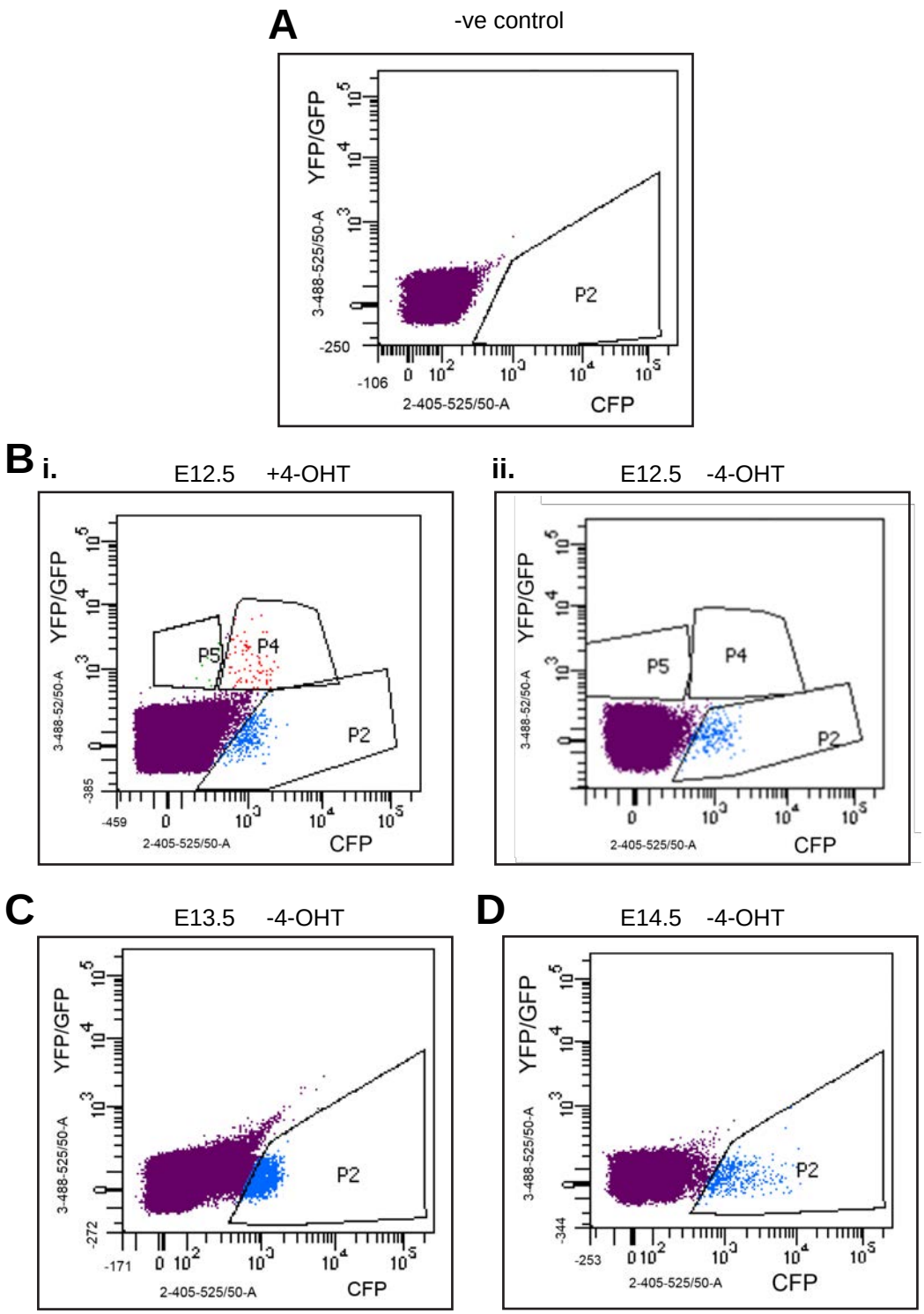

Figure 6.2. Isolation of primary melanoblasts by FACS analysis. FACS plots showing one biological replicate (one pooled litter) from each sample age. YFP/GFP fluorescence is plotted over CFP fluorescence. **A.** A non-fluorescent E13.5 CD1 negative control mouse. All future FACS gatings were based on this control to minimise mouse culling. The P2 labelled population in all plots are CFP+ cells which are expressing PMEL. **B.i.** A litter of E12.5 embryos of the *Pmel*$^{+/CMN}$*;R26FPR* line. **ii.** An E12.5 4-OHT negative control. The additional labelled populations at E12.5 are: P4 - PMEL+/YFP+ cells which are expressing PMEL and are lineage traced by YFP, and P5 - PMEL-/YFP+ cells which are not expressing PMEL and are lineage traced by YFP. **C.** A litter of E13.5 embryos. **D.** A litter of E14.5 embryos.

Generally, a RIN of below 8 is considered degraded and poor quality, however the majority of the samples were used with scores below this; this is a common problem when using primary tissue or cells. The NuGen cDNA synthesis kit that was used is specifically designed to improve synthesis from both low RNA amounts and poor RNA quality. The RIN scores for the primary cells are shown in Table 6.1. For the cultured cells, use of the NuGen kit was not required, as cell numbers and RNA quality were not an issue.

cDNA quality and integrity was confirmed by Edinburgh Genomics before progressing to the library preparation. The libraries were sequenced using the Illumina Hi-Seq 4000 platform.

Table 6.1. Quantitative data of primary melanoblast samples in RNA sequencing.

Sample	Number of cells	RIN	RNA concentration pg/µl	cDNA concentration ng/µl
E12.5_1	2,900	6.4	4,517	259.8
E12.5_2	1,300	9.1	406	177.1
E12.5_3	890	5.5	54,586	200.2
E13.5_1	29,000	7.3	3,486	262.1
E13.5_2	40,000	8.5	20,000	279.9
E13.5_3	25,000	8.3	45,000	324.2
E14.5_1	28,000	6.0	20,715	306.5
E14.5_2	36,000	7.3	10,000	272.2
E14.5_3	13,000	4.3	11,776	272.7

6.2. RNA sequencing

Each RNA sequencing experiment returned >30million reads per sample. RNA sequencing analysis was performed in collaboration with Dr Phillipe Gautier from the IGMM Bioinformatics Analysis Core, using standard analysis tools and packages, run in R software; data quality was assessed using FastQC, then run through the TopHat and Bowtie tools for alignment and labelling. Read count analysis was performed using the R package DESeq which uses raw input without normalisation, and is considered more accurate than Cufflinks in the community and in some reports (Zhang et al., 2014). Results not satisfying both a significance value of <0.05 and a log fold change of <-2 and >2 were discarded. The gene expression data was examined both by looking for the most changed gene expression between samples, and also by extracting candidate genes identified through the literature which are involved in pathways or processes of interest. Simple lists of the top 20 upregulated and downregulated genes for each pair-wise comparison between the primary cells are shown, ordered by log2 fold change. GO terms (gene ontology) were also used to examine what functions the changed genes are associated with. To examine GO terms, the entire genes list was separated into upregulated vs. downregulated before input into the PANTHER classification tool (freely available at http://pantherdb.org/). GO term analysis can be performed under several key ontologies, however herein, the biological functions of the groups is the principal interest. Genes may identify with multiple GO terms. GO term enrichment was also performed to assess if any particular groups were prevalent (freely available at http://www.geneontology.org/page/go-enrichment-analysis). This enrichment analysis determines if a set of genes are associated with a certain GO term, at a higher frequency than would be expected. Heat maps are also used to visualise changes in expression between the sample groups.

The melb-a_migrated repeat 1 sample was discounted early into processing due to extremely poor alignment to the genome at only 24.7%. All other samples had concordant pair alignment of around 50%. Although this was still considered poor, it left enough reads to do viable downstream analyses, as advised by Dr Gautier. The majority of published RNA-sequencing projects report concordant pair alignment of

>80%. Reasons for the low alignment are not known. Multiple attempts were made to increase the alignment rate in the analysis, including data trimming based on read-quality. However, the increases in alignment rate were minimal. Manipulating the data before processing is generally avoided in order to preserve as many true reads as possible, so ultimately the raw inputs were used in favour of the trimmed inputs.

6.2.1. PCA clustering

A principal component analysis (PCA) was performed on all the raw data, which gives a statistical analysis of the variance between samples. Ideally, biological repeats should cluster closest together, indicating their similarity to one another.

The first PCA is presented in Figure 6.3.A. and demonstrated that there were problems with some of the samples; samples E12.5_2, E13.5_3 and E14.5_3 were all located far away from the other samples on the plot. The sequences and alignment results of these samples were examined closely. These samples showed a low exonic alignment rate, which may be concurrent with gDNA contamination. This was unexpected, as the pre-processing data for these samples indicated an adequate level and quality of RNA which was not dissimilar to the other biological samples. Regardless, the PCA and other tests strongly supported the removal of these samples from the data set.

The PCA was repeated once these samples had been removed, the results of which are shown in Figure 6.3.B. In this plot, the primary melanoblasts are clearly clustered together, as are the melb-a cells. Further, the different ages in the primary cells cluster convincingly, although the data is limited to only two biological repeats. The cultured cells cluster less convincingly by type, with a sample each from melb-a cells and melb-a HD appearing closer to each other than their other repeats. However, in two repeats from each sample, results appear extremely close together. Indeed, in the melb-a migrated group, the biological repeats are indistinguishable as they lie atop one another. This PCA was considered successful, and supportive of further analysis of the dataset.

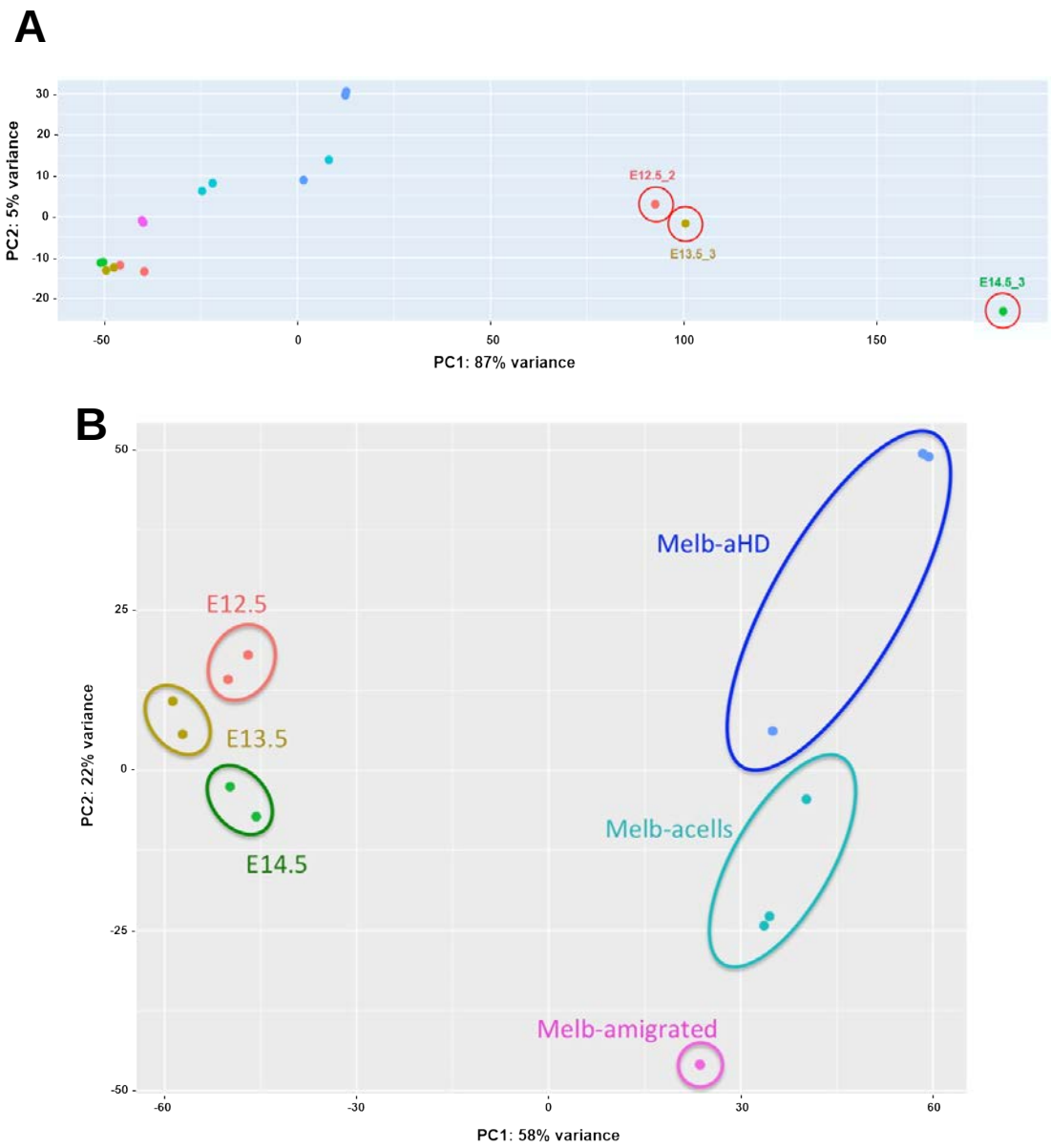

Figure 6.3. PCA plots of RNA sequencing data. A. The original PCA highlighted problems with multiple samples. These samples, shown encircled in red, were removed from the analysis following further investigation. The affected samples were: E12.5_2, E13.5_3, E14.5_3 and melb-a migrated_1 (discarded before the original PCA and not shown). **B.** The PCA was repeated after removing the outliers. The samples cluster convincingly into primary vs. cultured cells, and further into the biological repeats within the sample groups.

6.2.2. Top changes in gene expression - pairwise comparisons

The full set of genes for each pairwise comparison can be found in Appendix D on the accompanying CD.

6.2.2.1. Primary cells

6.2.2.1.1. E12.5 to E13.5

The top 20 upregulated genes between the E12.5 and E13.5 samples can be seen in Table 6.2. As mentioned previously, to examine the top overall GO terms, the entire set of upregulated or downregulated genes was used, and not limited to the top 20 results. GO term analysis shows categories which may be expected to change between these ages in line with developmental processes; biological adhesion, localisation, locomotion, cell communication and cell cycle processes.

In Table 6.2, some individual genes have previously reported associations to melanocyte biology. *Ccl2* is a known target in cancer, and indeed in melanoma progression, as an important chemokine component (Lim et al., 2016). *Dsc3* is involved in embryonic development and cell adhesion as a member of the cadherin family (Den et al., 2006), and has also been described in skin cancers, particularly in those of the epidermis (Chen et al., 2012). *Dkk1* has a wide range of functions through Wnt signalling both during embryonic development (Lieven, Knobloch and Rüther, 2010) and in hair follicle formation (Lei et al., 2014). *Map3k14* is directly involved in MAPK signalling.

GO term enrichment revealed gene enrichment in the following principal categories: collagen fibril organisation which had a 7.9 fold enrichment in the data set, positive regulation of cell motility which had a 2.38 fold enrichment, positive regulation of locomotion which had a 2.3 fold enrichment, regulation of cell migration which had a 2.14 fold enrichment and cell adhesion which had a 2.26 fold enrichment. GO enrichment on the downregulated data set returned only two significantly enriched GO term groups: noradrenergic neuron development was enriched >100 fold, and sympathetic nervous system development was enriched 26.84 fold.

Table 6.2. Top 20 upregulated genes between E12.5 and E13.5.

Values are ordered by log2 fold change. The values in columns 3 and 4 are raw read counts, averaged over the biological repeats. Values have been rounded to 3d.p.. The adjusted p-values (padj) are also shown. The final column shows GO terms associated with the gene. Only 2 GO terms are listed per gene, those with more are denoted with a *. (All tables of up/downregulated genes follow this format).

Name	Biotype	E12.5	E13.5	log2 FoldChange	padj	Associated GO terms
Cpa3	Protein coding	0	2049.858	9.187	5.73×10^{-14}	regulation of angiotensin levels in blood proteolysis
Cpxm2	Protein coding	0	721.999	8.431	3.53×10^{-12}	proteolysis
Zfp385b	Protein coding	1.056	857.068	7.942	2.48×10^{-12}	apoptotic process intrinsic apoptotic signalling pathway by p53 class mediator
Ccl2	Protein coding	0	351.743	7.556	5.24×10^{-9}	MAPK cascade positive regulation of endothelin cell proliferation *
Dsc3	Protein coding	0	322.773	7.381	2.47×10^{-8}	in utero embryonic development cell adhesion *
Prr16	Protein coding	0	300.405	7.302	3.64×10^{-8}	positive regulation of transcription positive regulation of cell size

Rgag1	Protein coding	0	266.503	7.116	$1.30x10^{-7}$	biological process
Osr2	Protein coding	2.151	637.472	7.082	$3.14x10^{-12}$	cell differentiation positive regulation of cell proliferation *
Adam33	Protein coding	1.642	590.941	6.862	$1.70x10^{-9}$	regulation of cell proliferation proteolysis *
Pparg	Protein coding	0	261.979	6.796	$1.59x10^{-6}$	negative regulation of transcription from RNA polymerase II promoter signal transduction *
Dkk1	Protein coding	0	227.437	6.718	$2.03x10^{-6}$	hair follicle development cell morphogenesis involved in differentiation *
Inhbb	Protein coding	0	228.574	6.675	$2.90x10^{-6}$	regulation of MAPK cascade response to mechanical stimulus *
Map3k14	Protein coding	0	209.613	6.673	$2.36x10^{-6}$	MAPK cascade protein phosphorylation *
S100a6	Protein coding	2.151	543.294	6.654	$5.05x10^{-9}$	ion transmembrane protein
Dpt	Protein coding	7.393	2105.690	6.582	$2.24x10^{-7}$	cell adhesion collagen fibril organisation *
Cd14	Protein coding	0	200.184	6.545	$5.44x10^{-6}$	receptor mediated endocytosis response to molecule of bacterial origin *
Abca8a	Protein coding	2.190	488.782	6.503	$1.31x10^{-9}$	lipid transport transmembrane transport

Mfap5	Protein coding	1.604	364.420	6.427	7.12×10^{-8}	definitive haemopoiesis supramolecular fibre organisation
Hdc	Protein coding	0.547	246.759	6.352	1.52×10^{-6}	histamine biosynthetic process cellular amino acid metabolic process
Thy1	Protein coding	11.342	1485.905	6.345	3.10×10^{-12}	regulation of cell-matrix adhesion

Table 6.3. Top 20 downregulated genes between E12.5 and E13.5.

Name	Biotype	E12.5	E13.5	log2 FoldChange	padj	Associated GO terms
Slfn1	Protein coding	329.144	0.284	-7.763	7.87×10^{-11}	cell cycle arrest negative regulation of transcription from RNA polymerase II promoter *
Gm14226	Protein coding	585.505	1.041	-5.687	4.43×10^{-4}	biological process viral life cycle
Pklr	Protein coding	199.689	2.460	-5.385	5.39×10^{-6}	response to cAMP response to hypoxia *
Tmprss11f	Protein coding	933.622	17.9116	-5.266	5.80×10^{-10}	proteolysis
Insm1	Protein coding	209.144	3.8478	-4.763	3.04×10^{-4}	cell differentiation nervous system development *
Tmem179	Protein coding	412.978	6.306	-4.685	1.513×10^{-3}	biological process
Pkp2	Protein coding	202.292	5.614	-4.564	2.86×10^{-5}	desmosome assembly single organismal cell-cell adhesion *
Tmem74b	Protein coding	776.009	25.387	-4.564	1.40×10^{-7}	biological process
Myom2	Protein coding	400.258	5.171	-4.490	6.29×10^{-3}	actin filament organisation striated muscle contraction *

Phox2b	Protein coding	769.369	9.932	-4.485	6.53 x10^{-3}	neuron migration NC cell migration involved in autonomic nervous system development *
Shh	Protein coding	97.778	2.396	-4.4540	6.04 x10^{-4}	pattern specification process NC cell migration *
Pdzph1	Protein coding	259.511	0.631	-4.388	1.98x10^{-2}	biological process
Tmem63c	Protein coding	309.120	10.248	-4.228	5.47x10^{-4}	ion transport cation transmembrane transport
Fignl2	Protein coding	189.703	5.298	-4.206	2.68x10^{-3}	regulation of double-strand break repair via homologous recombination
Trim71	Protein coding	1353.784	55.639	-4.204	1.29x10^{-5}	neural tube closure G1/S transition of mitotic cell cycle *
Slc23a4	Protein coding	164.558	3.248	-4.198	9.62x10^{-3}	biological process transmembrane transport
Lrrc10b	Protein coding	693.945	32.454	-4.149	1.87x10^{-7}	biological process
Fezf2	Protein coding	237.611	1.262	-4.134	3.07x10^{-2}	axon guidance locomotory behaviour *
Prss44	Protein coding	327.947	0.347	-4.0817	3.83x10^{-2}	proteolysis
Nat14	Protein coding	560.165	15.800	-3.979	1.18x10^{-2}	transcription, DNA-templated biological process

6.2.2.1.2. E13.5 to E14.5

Table 6.4. shows the top 20 upregulated genes between E13.5 and E14.5, where many known melanoblast factors emerge. The top upregulated gene is *Tryp1*, *Oca2* is at number 10, *Dct* is at number 16 and *Mc1r* is at number 18. These are all key genes in the melanogenesis pathway. *Serpinb5* is essential during embryonic development and basement membrane formation, and although its function is unclear it is known to influence cell adhesion to laminin (Gao et al., 2004). *Ceacam2* is involved in binding to the ECM. It has no previous reports of links to melanocyte development, however its closely related family member, *Ceacam1*, has strong links to metastatic events in melanoma (Turcu et al., 2016). *Gm14226* makes another appearance in this list, although it is shown to increase by a log fold change of 2.670, instead of a log fold change of -5.687 as between E12.5 and E13.5. *Calm4* encodes a calmodulin protein, involved in calcium ion binding which is known to appear in the epidermis during development, although associated with the suprabasal keratinocytes (Lessard et al., 2015), which are not present at this time point (Sotiropoulou and Blanpain, 2012). *Mlana* is the gene encoding for a melanocyte specific antigen (Kawakami et al., 1994) and is expressed at all 3 time points with high read frequency. *Syt4* is another gene involved in calcium ion binding and is associated with vesicle activities in neurons, but not melanocytes. However, another synaptotagmin gene, *Syt7*, has been associated with the transfer of melanosomes in the mature melanocyte (Wäster et al., 2016).

GO term analysis for the upregulated genes returned only 40 genes with associated terms. The largest group was ‘metabolic activities’ which separated fairly evenly into protein, lipid, carbohydrate and nucleobase-containing activities. ‘Cellular processes’ was another main category, and within this cell communication and cell cycle were identified. GO enrichment shows a greater than 100 fold enrichment for genes associated with melanin biogenesis and pigmentation.

In Table 6.5. the top 20 downregulated genes between E13.5 and E14.5 are shown. The top downregulated gene *Csmd3* encompasses over 1.2Mb (megabase) on the genome, and is associated with dendritic development (Mizukami, Kohno and

Hattori, 2016). *Mgp* is linked to the ECM, where it prevents mineralisation of the matrix in a locally controlled manner (Murshed et al., 2004). Downregulation of this factor would suggest a specific role, as it is ubiquitously expressed but only known to be active in areas of mineralisation. *Slc6a1* encodes a key transporter for the neurotransmitter GABA (Carvill et al., 2015). *Syt1* shows a downregulation of -4.572 fold in comparison to the upregulation of its family member *Syt4*. Both genes have similar associated roles in vesicular trafficking, and further share another member of this large family (*Syt14L*) which is believed to act through a shared C2 domain to control melanocyte differentiation (Yoo et al., 2013).

Go term analysis for the downregulated genes included 291 genes. The largest group was ‘binding’ and more specifically ‘protein binding’. Several growth factors were included in this group including *Fgf1, Fgf18, Gdf6* and *Otor*. GO term enrichment of the downregulated genes resulted in many significant terms associated with neuronal biology. Some examples include: positive regulation of synapse assembly which had an 11.2 fold enrichment, synapse organisation which had a 9.87 fold enrichment, axon guidance which had a 5.15 fold enrichment, and positive regulation of neuron differentiation which had a 3.72 fold enrichment. Lastly, cell adhesion showed a 3.73 fold enrichment.

Table 6.4. Top 20 upregulated genes between E13.5 and E14.5

Name	Biotype	E13.5	E14.5	log2 FoldChange	padj	Associated GO terms
Tyrp1	Protein coding	736.750	23450.566	4.239	5.86×10^{-14}	pigmentation melanin metabolic process *
Ano3	Protein coding	41.740	806.048	3.453	1.14×10^{-7}	lipid transport detection of mechanical stimulus *
Bpifc	Protein coding	3.113	385.476	3.424	9.43×10^{-5}	(molecular function - lipid binding)
Akr1c13	Protein coding	4.914	226.468	3.410	4.52×10^{-5}	xenobiotic metabolic process oxidation-reduction process
Serpinb5	Protein coding	19.045	481.601	3.400	7.11×10^{-6}	morphogenesis of an epithelium ECM organisation *
Hcar2	Protein coding	5.479	216.042	3.174	2.48×10^{-4}	apoptotic process negative regulation of lipid catabolic process *
Ceacam2	Protein coding	59.440	607.849	2.976	1.16×10^{-8}	viral process negative regulation of brown fat cell proliferation *
E330034G19Rik	Protein coding	76.446	889.439	2.959	3.01×10^{-6}	positive regulation of proteasomal ubiquitin-dependent protein catabolic process
Gsta1	Protein coding	12.087	191.738	2.725	1.576×10^{-3}	glutathione metabolic process response to stilbenoid

Oca2	Protein coding	75.488	1164.318	2.684	2.105 x10^{-3}	melanocyte differentiation melanin biosynthetic pathway
Gm14226	Protein coding	1.694	94.988	2.670	5.91 x10^{-3}	biological process viral life cycle
Calm4	Protein coding	0.565	228.425	2.665	6.419 x10^{-3}	cellular response to leukaemia inhibitory factor
Ggt6	Protein coding	0.000	122.747	2.605	8.356 x10^{-3}	proteolysis glutathione metabolic process
Gm26752	lincRNA	1.129	102.460	2.521	1.208 x10^{-2}	-
Cubn	Protein coding	1482.160	10979.672	2.487	4.77 x10^{-5}	transport receptor mediated endocytosis *
Dct	Protein coding	26783.332	185169.471	2.472	7.11 x10^{-6}	melanin biosynthetic pathway developmental pigmentation *
Mlana	Protein coding	1280.510	8495.173	2.413	1.57 x10^{-5}	(cellular compartment – melanosome)
Mc1r	Protein coding	692.140	5015.972	2.386	4.25 x10^{-4}	melanin biosynthetic pathway pigmentation *
Syt4	Protein coding	1303.012	10595.723	2.380	2.03 x10^{-3}	regulation of vesicle fusion cell differentiation *
Efcab6	Protein coding	17.109	232.162	2.374	1.36 x10^{-2}	biological process regulation of transcription, DNA-templated

Table 6.5. Top 20 downregulated genes between E13.5 and E14.5

Name	Biotype	E13.5	E14.5	log2 FoldChange	padj	Associated GO terms
Csmd3	Protein coding	345.805	1.402	-5.368	6.28 x10^{-15}	regulation of dendrite development
Mgp	Protein coding	339.971	2.834	-5.060	2.34 x10^{-14}	cell differentiation ossification *
Slc6a1	Protein coding	314.165	0.488	-4.851	2.26 x10^{-10}	neurotransmitter transport response to organic substance *
Ube2ql1	Protein coding	390.888	6.582	-4.741	6.28 x10^{-15}	-
Rgs8	Protein coding	342.307	1.859	-4.708	2.66 x10^{-10}	G-protein coupled receptor signalling pathway regulation of dopamine receptor signalling pathway *
Nrsn2	Protein coding	249.683	0.000	-4.630	4.51 x10^{-9}	biological process
Mapk8ip2	Protein coding	335.444	0.457	-4.601	4.84 x10^{-9}	MAPK cascade dendrite morphogenesis *
Syt1	Protein coding	366.321	5.211	-4.572	1.20 x10^{-11}	detection of calcium ion cell differentiation *
Ren1	Protein coding	169.697	0.488	-4.457	9.43 x10^{-9}	kidney development regulation of MAPK cascade *

Fmo1	Protein coding	913.123	23.920	-4.454	5.98 x10^{-15}	response to osmotic stress organic acid metabolic process *
Cntn2	Protein coding	678.221	4.631	-4.433	8.77 x10^{-9}	microtubule cytoskeleton organisation neuron migration*
Ralyl	Protein coding	168.867	0.000	-4.348	5.58 x10^{-8}	biological process
Mapk10	Protein coding	782.967	15.936	-4.231	8.92 x10^{-10}	MAPK cascade
Asb9	Protein coding	164.962	0.000	-4.217	2.19 x10^{-7}	protein ubiquitination intracellular signal transduction *
Gdf6	Protein coding	257.605	1.951	-4.181	9.82 x10^{-8}	apoptotic process positive regulation of neuron differentiation *
Nap1l2	Protein coding	229.994	2.346	-4.170	5.47 x10^{-8}	nucleosome assembly regulation of stem cell division *
A2m	Protein coding	485.450	13.713	-4.043	8.92 x10^{-10}	stem cell differentiation pregnancy *
Msc	Protein coding	347.567	8.563	-3.992	1.18 x10^{-8}	palate development transcription, DNA-templated *
Trpm3	Protein coding	425.621	9.631	-3.984	2.94 x10^{-8}	ion transport protein tetramerisation *
Snhg11	Protein coding	1062.845	10.361	-3.969	1.02 x10^{-6}	biological process

6.2.2.2. Melb-a cells through culture

Analysis of the melb-a cell line in culture revealed many differences in RNA expression between the culture techniques. However, displaying the results as for the primary cells proved unsuitable; in lists of the top changed genes, high fold change between the groups was observed primarily due to a read count of 0 (or very low numbers) in one sample. This leads to any expression in the comparison sample being deemed immediately a very high fold change, even if there is still a low read count. There is some debate as to the relevance of very low read counts; some researchers believe anything above 0 can only arise if the RNA is accurately detected, where others suggest some background levels may compromise the accuracy, however they provide no guide as to what minimum read count is acceptable. For example, in the comparison between melb-a cells and melb-a HD cells, the top differentially expressed gene is *Cox6a2* which has read counts of 41.519 and 0.488 respectively. This is a 4.816 fold change, that is highly significant, but as the read counts are still very low, the biological relevance is in question. In comparison to other gene expression in the melb-a HD cells, there are other genes such as *Dct* which has a read count of 8908.328. Therefore, genes were chosen for discussion that were deemed to have read count changes that could be biologically relevant.

6.2.2.2.1. Melb-a vs. melb-a HD

The first comparison is between melb-a cells and cells cultured for 5 days in the HD.

6.2.2.2.1.1. Higher expression in melb-a cells

Of the genes with higher expression in melb-a cells vs. melb-a HD cells, many are reported to have general metabolic functions. Cells grown in the HD are not encouraged to proliferate by passaging, and are limited in their growth potential which may be reflected in these gene absences or downregulations. *Trim46* has known links to cell migration through microtubule formation and organisation (van Beuningen et al., 2015). Downregulation of this factor is understandable, as the HD cells are relatively static within the confinement of the drop. The transcription factor *Fos* has highly complex biology, and is associated with numerous functions in both

normal and cancerous activities. Its expression is known in EMT, with expression linked to loss of cell polarity and metastatic events (Eger et al., 2000). Lower expression of *Fos* in HD cells may therefore be concurrent with MET.

118 genes were included in the GO term analysis for genes expressed in higher levels in melb-a cells. 'Cell communication' was a major group, accounting for 53 gene hits, which mainly consisted of signalling molecules. GO enrichment returned significantly higher number of genes associated with tRNA (transfer RNA) aminoacylation for protein translation, with a fold enrichment of 42.8, and intrinsic apoptotic signalling pathway in response to endoplasmic reticulum stress, with a fold enrichment of 26.15. A significant number of the genes in this list relate to developmental expression. *Ascl1* is used as a cell specific marker of pulmonary neuroendocrine cells, which are believed to be of NC origin (Guillemot et al., 1993). *Evx2* is a known player in neuronal development, involved in specifying excitatory neurons (Juárez-Morales et al., 2016). *Evx2* also identifies as a Hox gene in vertebrate limb development (Hérault et al., 1996). *Meltf* is known in melanoma and has been linked to ECM disassembly and being a negative regulator of cell spreading through substrate adhesion (Suryo Rahmanto, Dunn and Richardson, 2007), both of which reflect the physical change in the culture method. *Nptx2* is another neuronal protein involved in the neuronal synapse (Xiao et al., 2017), although there are no published links to early development. *Pthlh* is a regulator of chondrocyte differentiation, another NC lineage cell (Minina et al., 2002). *Lhx2* is a transcription factor involved in many different processes linked to the NC including nervous system development as early as the neural tube closure (Liu, Helms and Johnson, 2004), to hair follicle formation (Folgueras et al., 2013).

6.2.2.2.1.2. Higher expression in melb-a HD cells

Some interesting genes were identified as being upregulated in the melb-a HD cells. *Dusp1* is associated with both environmental stress, which is appropriate for the culture method, and also with inhibition of cell proliferation (Shen et al., 2017). *Evx2* is believed to be associated with development and specifically limb morphogenesis (Goodman et al., 2002; Slavotinek et al., 1999). *Lhx2* is associated with cell lineage development, including gliogenesis and derivation of haematopoetic progenitor cells

(Chen et al., 2015; de Melo, Clark and Blackshaw, 2016). Finally, *Ascl1* has been shown to have involvement in neural cell fate decisions and migration (Parras et al., 2002).

GO terms analysis of genes with higher expression in melb-a HD cells consisted of 1479 genes in total. The largest single GO term association by 239 genes, was with 'cell communication' and 'signal transduction' indicating a highly active and dynamic population. As expected, 'developmental processes' formed a large group of genes, broken down into GO terms that associated with NC lineage cells including neuronal development, and skeletal system development. GO term enrichment returned a large number of significantly enriched terms, a few of which are listed: positive regulation of neutrophil chemotaxis whic had a fold enrichment of 6.2, spinal cord development which had a fold enrichment of 3.7, neuron fate commitment which had a fold enrichment of 3.7, dorsal/ventral pattern formation which had a fold enrichment of 3.4, and cell adhesion which had a fold enrichment of 1.7.

6.2.2.2.2. Melb-a vs. melb-a migrated

The second comparison is between melb-a cells, and those which have migrated from the HD.

6.2.2.2.2.1. Higher expression in melb-a cells

Firstly, those genes which show higher expression in melb-a cells. *Muc4* is a glycoprotein involved in preventing cell-adhesion, and although there are references to its actions in epithelial tissue, the epidermis is not a major site of expression (Carraway et al., 2002). *Reln* is a gene with a wide variety of functions, mainly explored in the brain, but related to cell adhesion and motility (Berthier-Vergnes et al., 2011).

2405 genes were entered for GO analysis. Grouping using GO terms shows a fairly generic metabolic and cell signalling landscape of genes which are found in higher amounts in melb-a cells. GO enrichment returned many significant results, although mainly with a low fold enrichment. Some of the terms showing higher fold

enrichment include: sodium ion transmembrane transport which had a fold enrichment of 3.7, positive regulation of synapse assembly which had a fold enrichment of 2.9, calcium ion transmembrane transport which had a fold enrichment of 2.5, and homophilic cell adhesion via plasma membrane adhesion molecules which had a fold enrichment of 2.8.

6.2.2.2.2.2. Higher expression in melb-a migrated cells

Syt4 also features highly as upregulated in the melb-a migrated samples, and its functions have been discussed previously. *Foxr2* is associated with EMT in some cancers (Lu et al., 2017). *Itga4* is a fibronectin receptor, playing roles in cell adhesion and migration (Chigaev et al., 2003). *Map1b* is mainly described in neurons, being involved in actin and microtubule based reorganisation of the cytoskeleton during dendrite retraction (Bouquet et al., 2007). Interestingly, *Pmel* features at number 23 on the list of top differentially expressed genes, with a log fold increase of 8.374, which was highly significant.

For GO term analysis, 1400 genes were included. 159 genes identified with 'cellular organisation or biogenesis' indicating a high amount of internal changes, consistent with the dendritic processes that are extended during migration. 98 genes are linked to mitosis, showing a highly proliferative population. 509 genes associated with generic metabolic processes. As before, GO term enrichment returned a high number of significantly increased GO terms in the data set, but with low fold enrichment, including: kinetochore organisation which had a fold enrichment of 9.7, and DNA replication initiation which had a fold enrichment of 8.2.

6.2.2.2.3. Melb-a HD vs. melb-a migrated

The final comparison within the cultured cell groups is between cells in the HD and those which have migrated from the HD.

6.2.2.2.3.1. Higher expression in melb-a HD cells

Muc4 and *Reln* were noted for their roles in cell-cell adhesion and motility. *Flt1* is a tyrosine kinase involved in cell migration, and also in the MAPK pathway (Wang et al., 2011). *Scn11a* is well researched, as the protein it produces is a voltage-gated

sodium ion channel that is found mutated in some patients with lack of pain sensation (Leipold et al., 2013). *Rxfp1* is a relaxin receptor which is a vital hormone found during pregnancy, which has functions of ECM and collagen degradation (Samuel, Lekgabe and Mookerjee, 2007).

GO term analysis returned 5672 genes, with a wide range of GO term associations. 'Response to stimulus' encompassed 1216 genes, with many of those associating to 'response to stress', this is presumably due to limited nutrient and oxygen supply in the small volume of media. Over 300 genes identified were transcription factors. Nearly 900 genes were involved in cell-cell communication via signal transduction, including many G-protein coupled receptors and growth factors. 306 genes associated to 'cellular component organisation or biogenesis', indicating a high level of internal changes. In a similar manner to the other cultured cells, GO enrichment found many enriched GO terms with significant but low fold enrichment. These include: homophilic cell adhesion via plasma membrane adhesion molecules which had a fold enrichment of 2.14, and sodium-independent organic anion transport which had a fold enrichment of 3.03.

6.2.2.2.3.2. Higher expression in melb-a migrated cells

Syt4 is again one of the highly differentially expressed genes, with a fold change of 8.91 (to a read count of >20,000). *Foxr2* is a proto-oncogene associated with cell proliferation (Li et al., 2016). *Pmel* is listed as the 6th highest differentially expressed gene, with a fold increase of 8.25.

Of the 1358 genes found more highly expressed in the melb-a migrated cells, the majority were attributed to either 'metabolic functions' or 'cellular processes'. Within these categories, 'cell cycle', 'cell communication' and 'nucleobase-containing compound metabolic processes' were the main groups. GO term enrichment again showed a large list of enriched terms. Included in this list were: pigment metabolic processes which had a fold enrichment of 3.22, and response to UV which had a fold enrichment of 2.55.

6.2.2.3 Primary cells vs. cultured cells

The primary cells were compared with each of the three cultured cells, to identify gene groups that have changed the most. Firstly, between the primary cells and melb-a cells, GO enrichment showed very few terms which were enriched by more than a fold change of 1. Those which were enriched in the primary cells include: exogenous drug catabolic process which had a fold enrichment of 4.63, and xenobiotic metabolic process which had a fold enrichment of 3.59. There were many more enriched in the melb-a cells at higher fold changes including: regulation of photoreceptor cell differentiation which had a fold enrichment of 6.22, regulation of prostatic bud formation which had a fold enrichment of 8.29, and specification of nephron tubule identity which also had a fold enrichment of 8.29.

Secondly, a comparison was made between primary cells and those in the HD. Go enrichment for the primary cells again showed very few enriched areas, and those which are above 2 fold enrichment were the same as above. GO term analysis of genes expressed higher in the melb-a HD cells revealed enrichment in areas including: retinal rod cell differentiation which had a fold enrichment of 14.08, anterior/posterior axon guidance which had a fold enrichment of 11.26, and positive regulation of keratinocyte proliferation which had a fold enrichment of 7.04.

Lastly, when comparing the primary cells with the melb-a migrated cells, the gene with the highest differential expression was *Ednrb*, with a log fold change of 13.243. *Enrb* is critical for early melanoblast migration (Lee, Levorse and Shin, 2003), but the melb-a cell line are not cultured with endothelin (the ligand) in the media. GO term analysis of genes expressed highly in the primary cells showed many areas of enrichment including: NC cell migration which had a fold enrichment of 2.83, positive regulation of neutrophil chemotaxis which had a fold enrichment of 3.21, negative regulation of axon guidance which had a fold enrichment of 3.71, planar cell polarity pathway involved in neural tube closure which had a fold enrichment of 4.73, and regulation of prostatic bud formation which had a fold enrichment of 6.15. On the reverse, the list of GO terms which were enriched in the melb-a migrated cells was much smaller, and often linked to general metabolic processes. Some

examples include: kinetochore organisation which had a fold enrichment of 7.16, post replication repair which had a fold enrichment of 5.45, and apoptotic mitochondrial changes which had a fold enrichment of 3.47.

6.2.3. Changes in known melanocytic genes

In this section, heat maps are used to display changes in gene expression. Heat maps display the relative levels of expression in each group - it is important to remember that the expression is relative, so even if a gene appears in blue, it may still be expressed, just at a lower level than other groups in warmer colours. Correspondingly, each line should be considered individually, and not read in a columnar direction. This information should be considered for all heat maps presented.

Key genes involved in melanocyte biology were extracted from the data sets and displayed in Figure 6.5. Several genes increased across the primary cell time course including *Pmel*, *Mcr1*, *Slc24a*5, *Oca2* and *Tyrp1*. Increases in *Mc1r*, *Slc24a5*, *Oca2* and *Tryp1* co-ordinate with establishment of the melanogenesis pathway. *Ednrb* has documented functions in the migration of early melanoblasts. Lee *et al*, used X-gal staining of *Ednrb* mutant mice to demonstrate that the critical time point for this action was between E10.5 and E12.5 (Lee, Levorse and Shin, 2003). In these data, which may be considered more sensitive than staining, expression of *Ednrb* is still high at E12.5, but is even higher at E14.5 indicating *Ednrb*'s role may not finish so early. Only one gene has expression that lowers through the time series - *Tal1*. *Tal1* functions upstream of *Kit*, and is shown to be a positive regulator of *Kit* transcription in haematopoiesis (Krosl et al., 1998). At E12.5 and E13.5 there is certainly concurrent expression of *Tal1* and *Kit*, however the dip in *Kit* expression at E13.5 does not correspond to changes in *Tal1*.

Comparing expression across the primary cells and different culture methods shows some interesting differences. *Pmel* expression in melb-a cells and those in the HD is very low, with reads of ~ 8 and 11 respectively, whereas the melb-a migrated cells show expression levels between that of E13.5 and E14.5. Melb-a migrated cells show a similar expression pattern to the E14.5 cells in particular. Notable differences

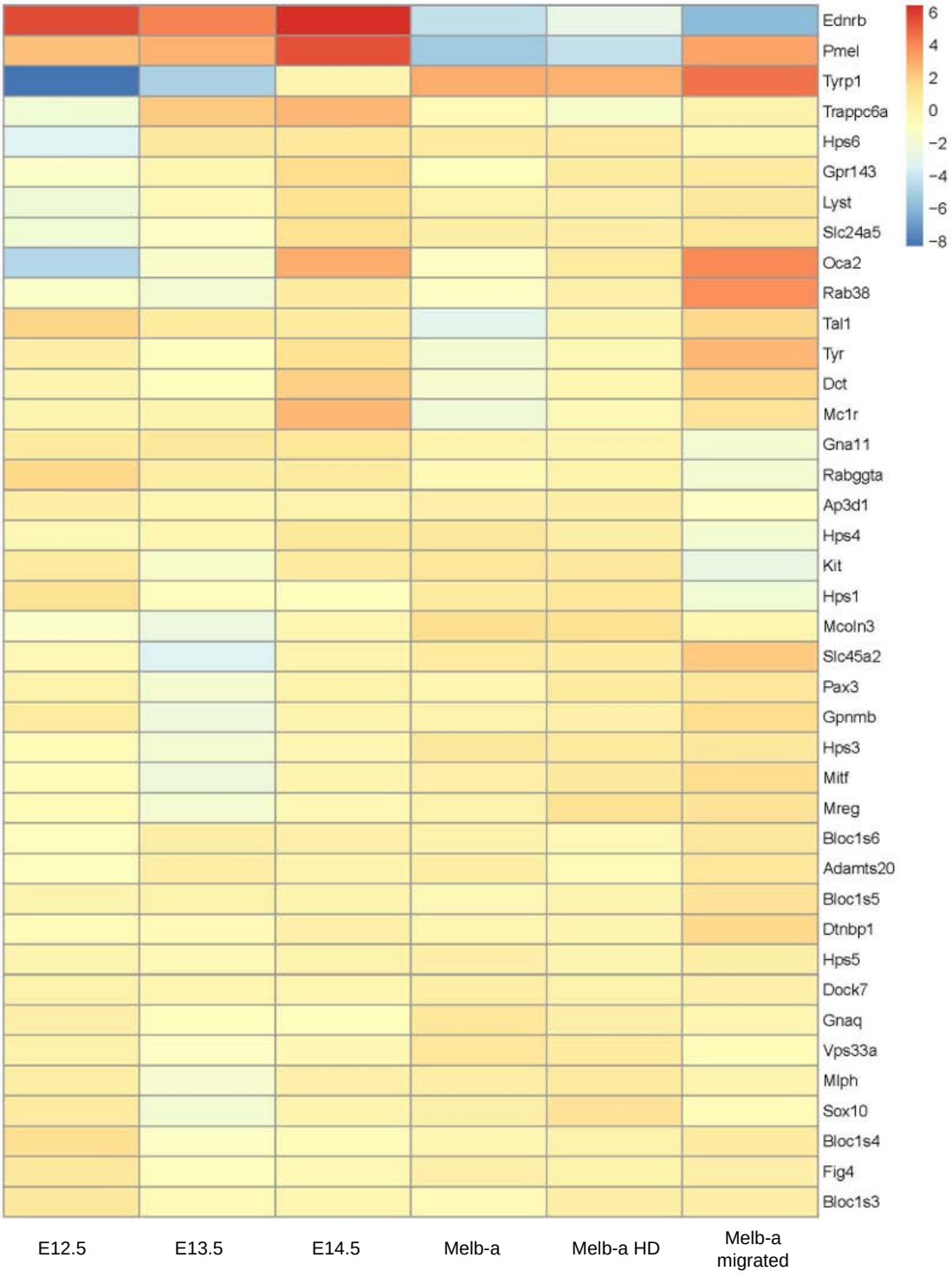

Figure 6.4. Gene expression variation in known melanocyte genes. The heatmap shows the relative expression levels of various genes that have been linked to melanocyte biology, including genes important during development and also later in melanogenesis. The key on the right indicates the scale of colour assigned based on the relative gene expression from normalised counts.

between these groups are in *Ednrb* (which none of the cultured cells express to a high level), *Kit* and *Tyrp1*. Cells in the HD have lower expression in both melanogenesis genes such as *Tyr* and *Dct*, and also in melanoblast developmental genes including *Pmel*, *Pax3* and *MITF*, despite the fact that they are pigmented in culture.

6.2.4. Changes in known EMT/MET genes

In the tables of top 20 upregulated/downregulated genes, some EMT markers have already been identified and discussed. For a fuller picture of EMT gene expression, a number of associated genes were chosen, and their expression are shown in Figure 6.6. EMT is a highly complex process, so this list is by no means a complete list of genes involved. The primary focus of this gene set is to establish whether the HD culture process could be used to model NC EMT.

The progression of EMT has been discussed in detail in Chapter 1.1.2. In summary, to transition between epithelial and mesenchymal states, cells undergo a complete reprogramming of their cell architecture to change their adhesion to neighbouring cells and allow them to move. This happens during development and in cancers; cells leaving the NC must emerge from the crest to migrate around the embryo, and for a cancer to metastasise cells must leave the primary tumour.

EMT is a well-studied event in different biological settings, and as such, the genetic network is fairly well understood, if not completely. Cells in the NC express classic markers such as *Sox, Zeb, FoxD3, Snai1* and *Snai2* genes. Behind these are multiple signalling pathways of EMT-inducing transcription factors, including Wnt, FGF and BMP. Their overall aim is to reduce the expression of cell adhesion proteins, primarily E-cadherin, and induce transcription of cell migration proteins. If EMT is occurring in these cultures, we might expect to see some of these markers in the melb-a migrated samples.

Firstly, there are many EMT genes which are positively changed in the melb-a migrated samples. Most importantly, there is a downregulation of E-cadherin (*Cdh1*), the hallmark of EMT events. There was a slight upregulation of *MITF*, a master

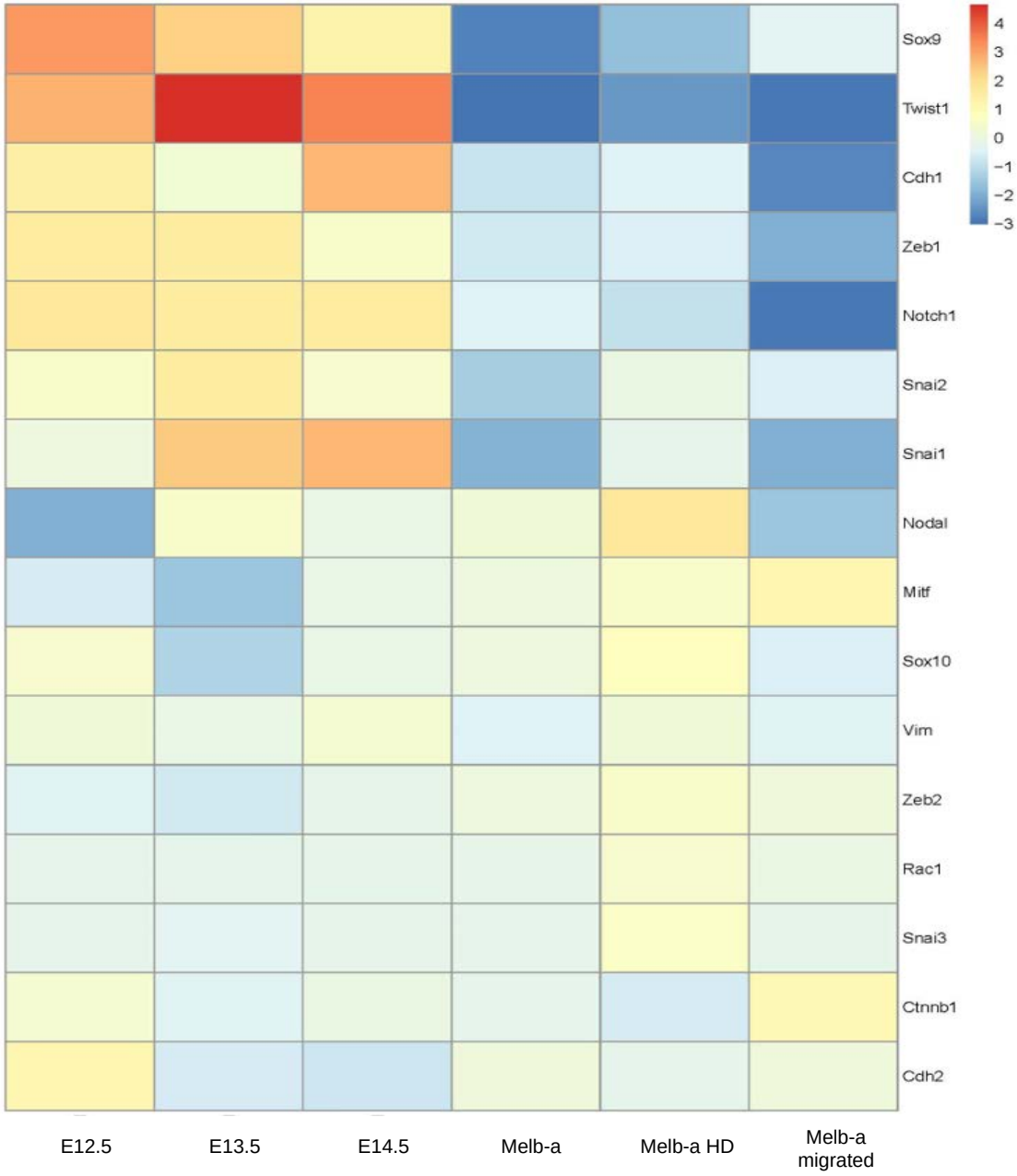

Figure 6.5. Gene expression variation in known EMT/MET genes. The heatmap shows the relative expression levels of various genes that have been implicated in EMT biology.

regulator in melanocyte biology. There was upregulation of β-catenin (*Ctnnb1*) in the Wnt signalling pathway

However, on the negative side, there are many genes which are shown to be central to EMT which either have the opposite change in expression, or no change in expression. There was no change in the expression of *Snai1* or *Snai3*, and a slight upregulation in *Snai2*. *Zeb1* was downregulated, while there was no change in *Zeb2*. There was no change in *Twist1*, downregulation of *Nodal*, and downregulation of *Notch1*. There was no change in the expression of the Vimentin gene, which is a classic marker for mesenchymal cells.

On the other side, we would expect some MET markers in the HD cultures, having taken mobile cells in culture to the aggregate. Although the EMT/MET states are simple opposites of one another, the process controlling MET is different, and not merely a reduction in those genes which induce EMT. In all the genes that were chosen, there was a downregulation between melb-a cells and melb-a HD cells, which is opposite to the expected result. The genes of interest are *Akt1*, *Egfr*. *Fgfr2*, *BMP2* and *BMP7*. There was also no upregulation of E-cadherin.

6.2.5. Changes in keratinocyte associated genes

During examination of the E14.5 samples in particular, it was noted that several genes which are involved in keratinocyte biology were highly expressed. Figure 6.7. shows some candidates which were selected as genes known to play specific roles within keratinocytes.

The E14.5 sample stands out as having relatively high expression in several genes, including keratins, loricrin and dermokine. Expression of these genes increased over the E12.5-E14.5 time course to moderate levels.

There is very little to no expression of these genes in the cultured cells. In particular, melb-a migrated samples showed mainly no expression, with the exception of *Pkp2* which is expressed moderately with a read count of 483. *Pkp2* produces a component

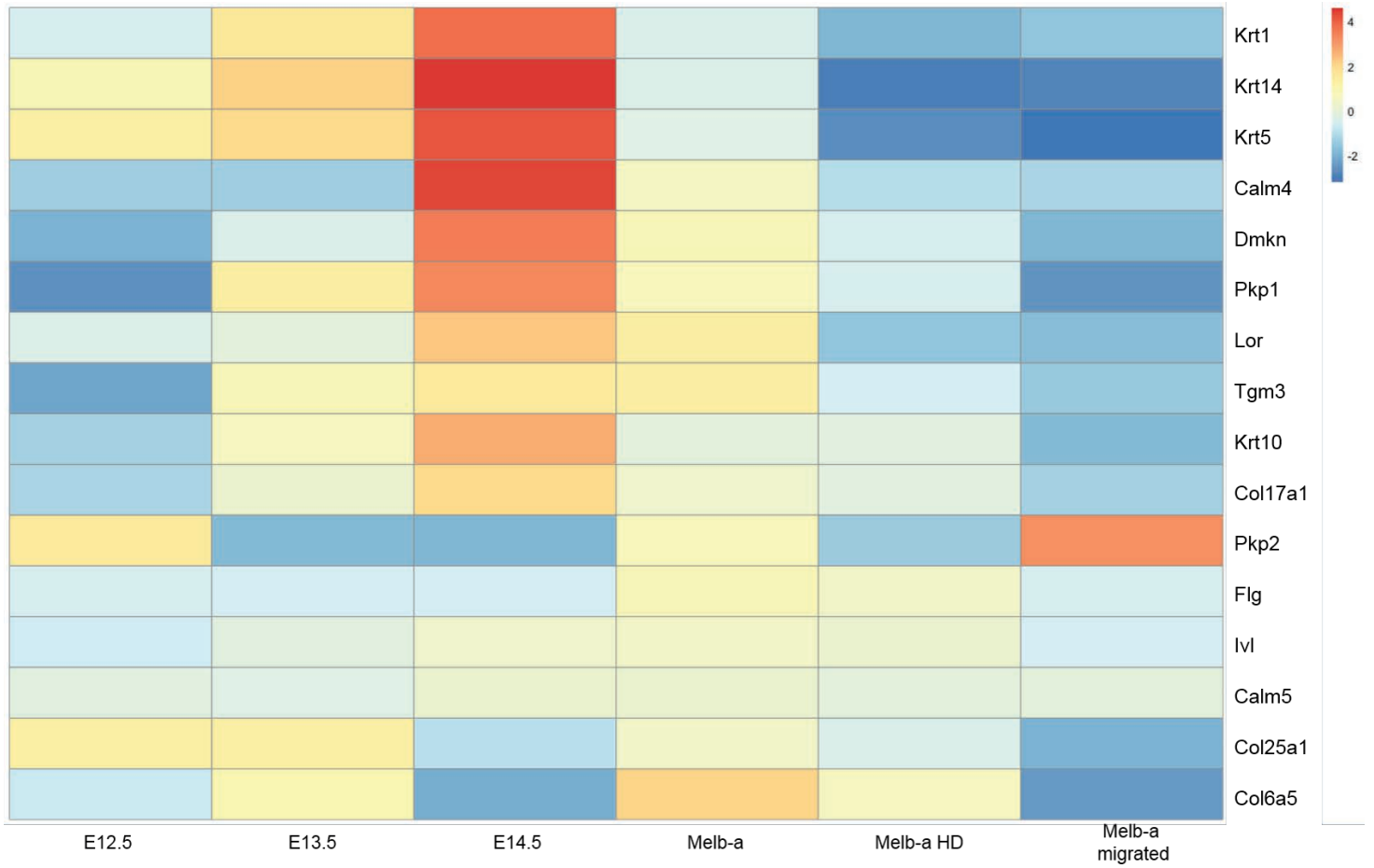

Figure 6.6. Gene expression variation in genes related to keratinocyte development. Several genes which are known as keratinocyte genes were identified in high amounts, particularly in the E14.5 samples. This may indicate problems in the methodology, for example contamination from keratinocytes, or they may be genuine genes expressed in the melanoblast population.

of the desmosome, a cell-cell attachment structure. This is unexpected as these migratory cells are moving outwards and ultimately away from their neighbours. Melb-a cells expressed all of these genes, but all at read counts lower than 36 which is very little expression. These counts were even lower in the HD cells.

6.2.6. Crossing the basement membrane

A major biological event which occurs near the time points examined, is the migration of the melanoblasts from the dermis to the epidermis across the dermal-epidermal basement membrane, occurring at around E12.5. There is mass expansion of the epidermal population as it continues colonising the embryo, but whether dermal melanoblasts continue contributing to this growth is unclear (Luciani et al., 2011). As discussed in Chapter 1.2.2., basement membranes are highly organised structures separating different tissues, and are the basis of several vital biological processes. In development, melanoblasts cross the barrier to reach their main destination, whilst in melanomas, early metastasis events are predominantly concerned with breaching this membrane in the opposite direction so as to access other parts of the body. A heatmap with genes implicated in breaching the basement membrane can be found in Figure 6.7.

Breaching the basement membrane has historically been thought to be achieved through locally degrading the membrane, due to apparent degradation of collagen IV (Kelley et al., 2014). However, more recently, advancements in the study of invadopodia have led to alternate theories. The most likely theory is that there are a combination of events, where some degradation of the membrane occurs to allow the invadopodia to gain access to the membrane to attach and begin infiltration. Due to the difficulties of studying such a small structure, research relies heavily on *in vitro* methods, and the primary animal model is *C.elegans*. Some genes which have known associations with this process across various species are displayed.

Dcc is a probable candidate gene for involvement for a number of reasons. It is known to be involved in the secondary migration of NC cells, specifically peripheral nerves of the enteric nervous system (Hagedorn et al., 2013). It also acts to direct

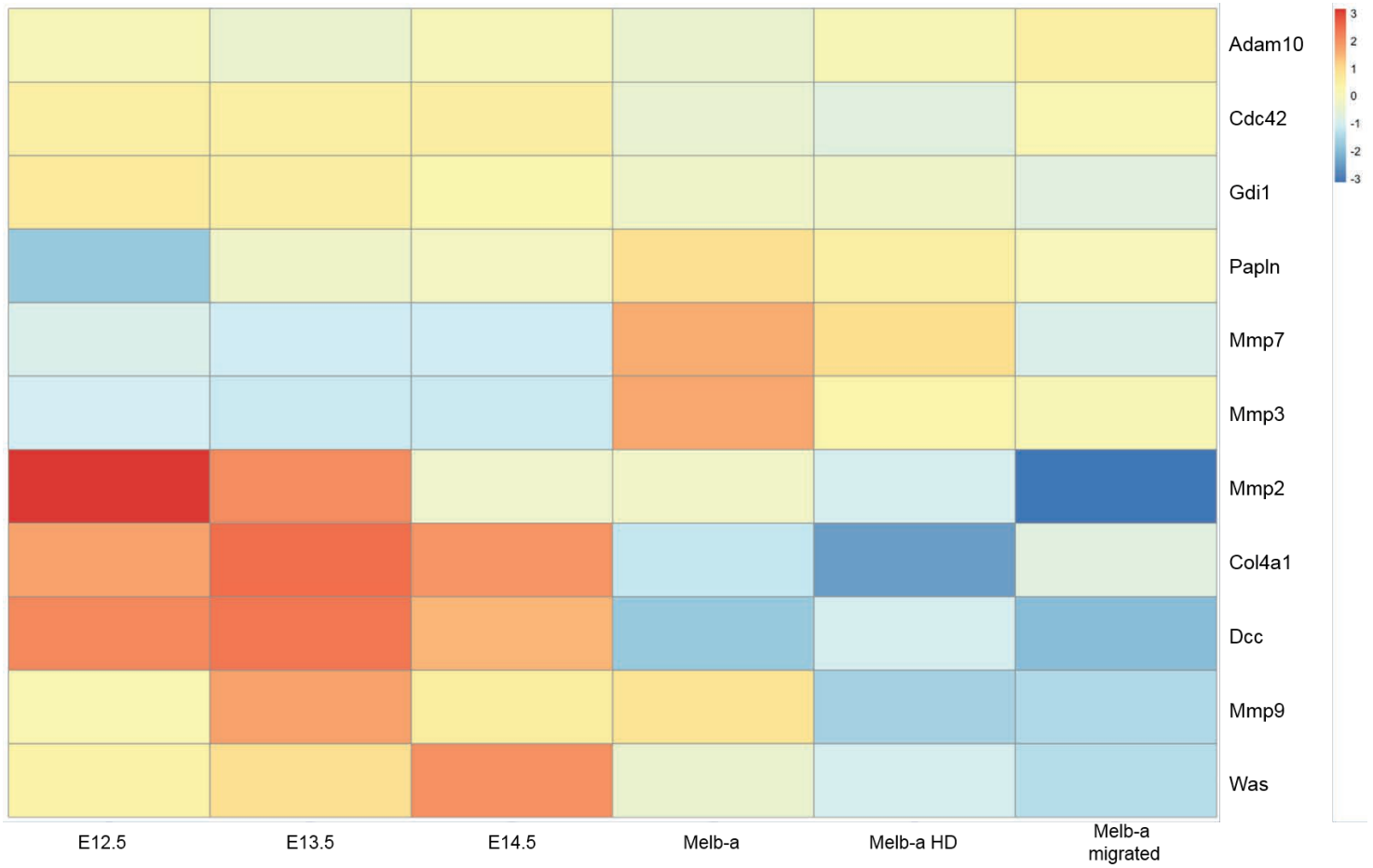

Figure 6.7. Expression variation in genes implicated in breaching the basement membrane during development. Melanoblasts cross the dermal-epidermal basement membrane from around E12.5. Different species have evolved different mechanisms to achieve basement membrane infiltration, and are either chemical or mechanical. Genes identified in both methods are represented here.

invadopodia during the important breach of the membrane in *C.elegans* (Morrissey, Hagedorn and Sherwood, 2013). A number of MMPs are expressed in high levels. The heat map shows 4 specifically, but the large family has over 20 members, all of which are concerned with the breakdown of the ECM. *Mmp2*, which is predominantly concerned with the breakdown of collagen IV, is found expressed around E12.5, although using MMP inhibitors has been shown to have no impact on melanoblast migration (Li et al., 2011).

There is little expression of these genes in the cultured cells, with only melb-a cells showing elevated levels of Mmp7 and Mmp3. These MMPs both fulfil general protease activities, and are not specifically related to the basement membrane.

6.3. Discussion

6.3.1. Early temporal development

6.3.1.1. Early melanoblasts express genes typically associated to other cells

There is a general movement towards the idea that melanocytes in the epidermis are performing more functions than merely pigmentation. Isolated populations of melanoblasts are found in places where they do not make sense biologically with their currently attributed functions of pigmentation e.g. in the heart and in the ear (Meyer zum Gottesberge, 1988; Mjaatvedt et al., 2005). The RNA sequencing results support this trend, with the appearance of keratinocyte and immune system genes as examples. The contribution of melanoblasts and melanocytes to regulating their microenvironment, including the surrounding cells, would be an interesting line of questioning.

It is known that adult melanocytes express immune factors, and there is mounting evidence that melanocytes play a role in the immune response in the skin (Hong et al., 2015). There is evidence of this as early as E13.5, when *Ccl2* appears as a highly upregulated gene for example.

High expression of several keratinocyte-related genes in the E14.5 group are noteworthy. Many of the genes on the list, for example *Dmkn* and *Lor*, are strictly associated with terminal differentiation of keratinocytes. At E14.5 keratinocytes are still present as a single basal layer and do not even begin stratification, which is required for differentiation, until around E15. Furthermore, there is a steady increase in the expression of these factors from E12.5 showing that there is some expression from even earlier. Attributing their expression to contamination in the sample is therefore implausible, and should be taken as true results. The interplay between melanoblasts and the epidermis are hugely important in skin homeostasis, and the appearance of these keratinocyte genes, suggests that the connections are there before the structures have even formed. The main argument against melanoblasts being an important regulatory element in epidermal development is that in disorders where melanocytes are not present, a functional epidermis still forms.

6.3.1.2. Melanoblasts continue downregulating genes of other NC lineages

Downregulation of several neuronal linked genes, including *Cntn2, Slc6a1* and *Csmd3,* between E13.5 and E14.5 indicates that there is continued diverging pathways of the melanoblasts from the peripheral nerves, long after the cells have disseminated from the NC. It is surprising that there are genes which are firmly linked to specific neuronal functions, such as axon growth, are still expressed at all at these stages.

Conversely, upregulation of key melanogenesis genes by E14.5 confirms that the cells which were isolated are melanoblast fated. It also shows that the melanogenesis machinery is already activating at this early age, despite pigmentation not being apparent at this point.

6.3.1.3. New candidates in melanoblast developmental processes

Several genes with no strong links to melanocyte biology emerged from this research, including *Syt4* and *Otor*. These may be good candidates for further research in different areas. *Otor* is thought to be highly tissue specific to the cochlea and the

eye (both areas in which cranial melanoblasts are found). It has also been found to have inhibitory growth properties in melanoma cells (Robertson et al., 2000). Downregulation of *Otor* to nearly 0 by E14.5 after relatively high expression at both E12.5 and E13.5 suggest it could be a regulator of melanoblast proliferation. No references to *Otor* knock-out models were discovered in a literature search; this may be an interesting gene to target in a knock out model. Synaptotagmins appeared in the gene lists multiple times. As mentioned, *Syt4* is associated with calcium dependent vesicular exocytosis. It may be a good candidate for study in relation to melanosome transfer to the keratinocytes, as other members of this family have been linked to melanocyte biology previously.

6.3.2. Varying culture methods

A question that emerged during experimental procedures was that of determining if cultured melanoblasts could be converted to different models through culture methods alone?

6.3.2.1. Melb-a cells in the HD express genes associated with different NC lineages

Reverting to a more NC like state is supported by the appearance of a number of genes, including *Ascl1*, *Evx2*, *Nptx2*, *Pthlh* and *Lhx2*. Some of these genes are described in the literature as highly specific to cell lines other than melanocytes. For the first three genes mentioned, these are all major factors in neuronal biology, but not all peripheral nerves. *Pthlh* is a negative regulator of chondrocyte differentiation (Minina et al., 2002). As has been evidenced many times, there are complex links between the cells of NC descent. Expression of these genes uniquely in this culture may support the theory that cells in the HD have regressed towards a more NC like state. Although expressional evidence of EMT/MET processes is low, there are definite changes which support a reversion to a precursor state.

Although not many known genes emerged during the comparison between melb-a and melb-a migrated cells, the large number of genes which were significantly different between the two groups does indicate that culturing in the HD has a

profound effect. This is supported by the expression changes within the HD, which when examining the PCA were the least like the other cell lines.

6.3.2.2. Evidence of stress in HD culture

Signs of stress in the HD were quite high as may be expected. The cells in the middle of the mass in particular will be at risk of hypoxia and nutrient deficiency. Unfortunately, it is not possible to reduce the amount of time cells are confined to the HD as the aggregate does not form properly before day 4. This should be addressed in any future experiments; there are sophisticated culture chambers which allow media change without disturbing the cells.

6.3.2.3. Evidence of EMT in migratory cells

For the melb-a migrated sample, cells were left to migrate for 24 hrs before harvesting. This was due to experimental observations across the cell lines that the B16 cells took much longer to migrate than the melanoblast cell lines. Melb-a cells began to emerge from the aggregate ~ 5/6 hrs after being plated, while the B16s took 24+ hrs. This may be due to differences in EMT between developmental cells and cancerous cells - the process is not assumed to be identical. In the literature, there is little/no information on how long the EMT process takes, or how long the relevant genes are expressed for. It is a transient event, but there are several timing questions that affect the interpretation of this data. Do all cells undergo EMT at the same time, or is there a proximity effect based on how close to the migratory surface the cell is? How long after initial separation do the migratory cells express EMT signatures? Is 24 hrs too long after the event to capture the expected changes? In reality, dissembling this complex network depends on many factors of timing, and as such the results are difficult to conclude one way or another. As an example, in these results, the collagen genes listed are downregulated in the melb-a migrated samples. Collagen I is known to promote EMT events, but appears two-steps upstream from *Snai1* activity. To complicate further, the melb-a migrated cells are made of a mixed population of any cells that remain attached once the HD has been removed; cells that have migrated at the front of the population may have a different profile than those just emerging from the aggregate. However, there are many indications that the

culture system is potentially a good model with some experimental adjustments, including timing of sample collection, and further dissecting the sample to different distance of cell migration. Overall, the downregulation of E-cadherin in the migrated sample serves as the crucial indicator that EMT has occurred. It is likely that the network of genetic events that lead to this change have simply been missed. Upregulation of *Loxl2*, *Epha3* and *Il13ra1* are just some of the additional genetic upregulations which support this further.

The gene expressions of *Sox, Snai1, Snai2* etc. are all discussed in relation to 'pre-migratory NC cells'. Presumably, this means immediately before the cells begin migrating. Unfortunately, this is not the population captured by these culture methods - to capture the canonical EMT changes of the NC, the aggregate should be harvested at the point where cells are just beginning to migrate. Sampling cells at different times after migration begins would also be beneficial.

6.3.3. Different culture methods to study different aspects of melanocyte biology

Using GO term analysis and GO enrichment highlighted differences between cells *in vitro* and those *in vivo*. In every comparison, the primary cells showed higher expression of genes involved in interacting with other body systems. This is a crucial point that cells in culture cannot achieve, and one of the biggest positive arguments for using animal models; recreating the entire environment is unrealistic. The impact of the interactions which are lost must be assessed when using *in vitro* methods. In this case, loss of hundreds of olfactory genes for example is deemed acceptable, but changes in genes relating to locomotion would cause problems.

In comparing the primary cells to those in culture, there are also differences between the culture methods. Overall, the melb-a migrated cells appear to have the most relevant expression patterns to the primary cells based on some key genes in melanocyte biology, although they had the highest number of differentially expressed genes overall. The expression *of Pmel, Tal1, Tyr* and *Dct* at levels comparable to the primary melanoblasts distinguished the melb-a migrated cells in this category.

However, this was also the only culture method where there were many areas in which the primary cells showed large fold enrichments. In both the melb-a and melb-a HD comparisons to primary cells, the cultured cells did not show many significant areas where they had lost expression. The lack of *Ednrb* expression by the melb-a migrating cells is of some concern as a model of early melanoblast migration from the NC as *Ednrb* is critical during these stages. Its absence suggests either compensatory mechanisms, as the cells are clearly still migrating. It could also be an issue of timing, similar to that discussed above. Alternatively, cells in culture may lose their dependence on growth factors they are not exposed to. In the melb-a cells and melb-a HD cells vs. primary cells analysis, there were not many areas in which the primary cells showed enrichment, but the cultured cells did, and often in areas that allude to them losing their specificity to the melanocyte lineage. Many of the other melanocyte genes were expressed at similar levels between all 3 cultures. Melb-a HD cells had the lowest level of expression in the melanogenesis genes and the lineage markers *Pmel, Dct* and *Tyr*, again suggesting the possibility that the HD method returns cells to a more NC like state. In terms of genes that are associated with keratinocyte biology, there was no cultured cell group that matched the primary cells in particular. The melb-a cells express most of the genes at levels below 50 reads, indicating very low expression. In the vast majority of these genes, expression lowered even further in the HD cultures and the melb-a migrated cells. There were low levels of expression in E12.5 and E13.5 age groups, with an increase to moderate expression by E14.5. There was little similarity between the primary cells and the cultured cells with relation to basement membrane breaching genes. This is not unexpected, as this is not a biological factor that the cultured cells are faced with.

Chapter 7

Conclusion

7.1. The transition from 2D to 3D

The original aim of this project was to develop an entirely self-sufficient 3D model in which to observe melanoblast behaviour. The system was designed to provide a novel way to visualise, primarily, melanoblast migration in the epidermal layer of the skin. This system was not successful, and is not recommended for further use. It did highlight the challenges of 3D cell culture. To incorporate the 3D environment into a melanoblast development model, there are several vital components to be considered including; a concentration gradient of melanoblast cell density, an expanding keratinocyte population which is differentiating and stratifying, an intact epidermal-dermal basement membrane, and the unique ALI component. We showed that using a differentiating and stratifying immortalised keratinocyte line was insufficient to replicate these conditions. The majority of research aimed at developing 3D models is conducted using human samples, and is focussed on treating diseases. The inclusion of melanocytes in these models is therefore usually only undertaken if there is a phenotypical change in pigmentation that researchers want to explore. The use of these models in studying a fully formed epidermis/dermis, and the development of the melanocyte lineage has therefore been unexplored.

An exciting approach to creating model systems is the use of pluripotent stem cells – either induced pluripotent stem cells (iPSCs) or embryonic stem (ES) cells. The generation of iPSC derived melanocytes has been described by numerous groups (Fang et al., 2006; Mica et al., 2013; Nissan et al., 2011; Yang et al., 2011). Fundamentally, during the melanocyte generation, iPSCs can be identified as melanocyte precursors by the presence of MITF and SOX10 before melanin production begins. One human skin equivalent (HSE) *in vitro* model created using iPSCs was reported by Gledhill *et al.* (2015), and incorporates keratinocytes, melanocytes, and fibroblasts. In this stratified model, the melanocytes do localise to

the basal layer, and are able to form a functional pigmentation unit with the keratinocytes. However, the model is created in several stages which are not reminiscent of the development of the skin. First, a collagen matrix is seeded with the iPSC fibroblasts for 7 days. Next the iPSC keratinocytes and melanocytes are seeded onto the matrix and incubated for 7 days. Finally, the culture is lifted to the ALI which induces stratification of the model. This example highlights how co-culture methods still rely on some form of artificial matrix and also use fully differentiated cells, rather than their precursors as would be relevant herein. Growing iPSCs requires precise control of growth factors, which are unique to each cell line, so the ability to combine the cells before they are fully differentiated in this model is unknown. Alternatively, there are iPSC models of NC cells which could be explored (Huang et al., 2016) – if these NC cells were co-cultured within a HSE, would they develop into melanoblasts and eventually melanocytes?

7.2. Measuring protein dynamics in real time

In this project, several cell lines were generated to study KIT and KITL, and their interactions. One of the principal aims was to incorporate fluorescently tagged versions of these proteins into the appropriate cell line for use in live imaging i.e. KIT into keratinocytes and KITLs into melanoblasts. This was unsuccessful, and an alternative NIH3T3 fibroblast cell line was used. Although interesting data was obtained, including confirmation that sKITL has a faster turnover than mKITL, the study is greatly limited by the use of an unrelated cell line. The use of ES cells for the generation of cell lines would be highly beneficial, as it is generally agreed that ES cells are easier to target, rather than manipulating immortalised cells in culture. Once targeted, ES cells could be induced to form melanocytes or keratinocytes using established protocols, thereby creating the desired cell lines for experimentation.

Tandem fluorescent timer proteins can be manipulated *in vitro,* and these proteins present an exciting resource with which to observe protein kinetics in real time. We also generated fluorescent KIT and KITL constructs, which produce proteins that are able to interact in the expected manner. These proteins would be recommended for further study using sophisticated imaging techniques, including super resolution.

7.3. Changing cell behaviour through culture methods

We showed through both live imaging and RNA sequencing, that changes can be induced in cultured cell lines through the use of culture methods alone. RNA sequencing showed that culturing techniques have a profound effect on the expression profile, so researchers must be exacting in their methodologies when using cells *in vitro*. For example, in the melb-a migrated samples, although expression of pigmentation genes was comparable to primary melanoblasts, they have less expression of key gene groups, for example planar cell polarity genes, which would be critical for the orientation of the melanoblast and it is probable that their loss would greatly affect cell behaviour. We showed that culturing cells in the HD assay induces the loss of expression of melanocyte markers, thereby suggesting a reversion to a more NC like state. This model has great potential, as it omits any chemical interference to achieve this state, and may be a model of EMT/MET transition.

7.4. Differences between primary cells and cultured cells - the NC3Rs factor

Ultimately, one of the main aims of this project was to determine the value of using *in vitro* models when compared to *in vivo* systems. The use of CDMs, HD assays and 2D assays were successful and interesting when exploring single behaviours, but were unable to compensate for extrinsic factors which influence cell behaviours *in vivo*. We showed for example, that migration of cell *in vitro* was slower than *in vivo*. We show using RNA sequencing, that the melb-a cell line, which is a widely used melanoblast line, is more appropriately termed melanoblast-like, due to large changes in the expression profile. We conclude that while *in vitro* experiments can be used to compliment and advise animal experiments, this project has not achieved a complete replacement for the use of animal models in melanoblast development research.

References

Adameyko, I., Lallemend, F., Aquino, J.B., Pereira, J.A., Topilko, P., Müller, T., Fritz, N., Beljajeva, A., Mochii, M., Liste, I., Usoskin, D., Suter, U., Birchmeier, C. and Ernfors, P. (2009) 'Schwann Cell Precursors from Nerve Innervation Are a Cellular Origin of Melanocytes in Skin', *Cell*, 139(2), pp. 366–379.

Adameyko, I., Lallemend, F., Furlan, A., Zinin, N., Aranda, S., Kitambi, S.S., Blanchart, A., Favaro, R., Nicolis, S., Lubke, M., Muller, T., Birchmeier, C., Suter, U., Zaitoun, I., Takahashi, Y. and Ernfors, P. (2012) 'Sox2 and Mitf cross-regulatory interactions consolidate progenitor and melanocyte lineages in the cranial neural crest', *Development*, 139(2), pp. 397–410.

Alberts, B., Johnson, A. and Lewis, J. (2002) 'Cell-cell adhesion', in *Molecular Biology of the Cell*.

Alberts, B., Johnson, A., Lewis, J., Raff, M., Roberts, K. and Walter, P. (2002) 'Fibroblasts and Their Transformations: The Connective-Tissue Cell Family', in *Molecular Biology of the Cell*.

Alblazi, K.M.O. and Siar, C.H. (2015) 'Cellular protrusions--lamellipodia, filopodia, invadopodia and podosomes--and their roles in progression of orofacial tumours: current understanding.', *Asian Pacific Journal of Cancer Prevention*, 16(6), pp. 2187–91.

Aman, A. and Piotrowski, T. (2010) 'Cell migration during morphogenesis', *Developmental Biology*, 341(1), pp. 20–33.

Aumailley, M. and Smyth, N. (1998) 'The role of laminins in basement membrane function.', *Journal of Anatomy*, 193(1), pp. 1–21.

Bajar, B.T., Wang, E.S., Lam, A.J., Kim, B.B., Jacobs, C.L., Howe, E.S., Davidson, M.W., Lin, M.Z. and Chu, J. (2016) 'Improving brightness and photostability of green and red fluorescent proteins for live cell imaging and FRET reporting.', *Scientific Reports*, 6, p. 20889.

Balch, C.M., Soong, S.-J., Gershenwald, J.E., Thompson, J.F., Reintgen, D.S., Cascinelli, N., Urist, M., McMasters, K.M., Ross, M.I., Kirkwood, J.M., Atkins, M.B., Thompson, J.A., Coit, D.G., Byrd, D., Desmond, R., Zhang, Y., Liu, P.-Y., Lyman, G.H. and Morabito, A. (2001) 'Prognostic Factors Analysis of 17,600 Melanoma Patients: Validation of the American Joint Committee on Cancer Melanoma Staging System', *Journal of Clinical Oncology*, 19(16), pp. 3622–3634.

Ballestrem, C., Wehrle-Haller, B., Hinz, B. and Imhof, B.A. (2000) 'Actin-dependent lamellipodia formation and microtubule-dependent tail retraction control-directed cell migration.', *Molecular Biology of the Cell*, 11(9), pp. 2999–3012.

Barge, A., Ruggiero, F. and Garrone, R. (1991) 'Structure of the basement membrane of corneal epithelium: quick-freeze, deep-etch comparative study of networks deposited in culture and during development.', *Biology of the Cell*, 72(1–2), pp. 141–7.

Bashamboo, A., Taylor, A.H., Samuel, K., Panthier, J.-J., Whetton, A.D. and Forrester, L.M. (2006) 'The survival of differentiating embryonic stem cells is dependent on the SCF-KIT pathway', *Journal of Cell Science*, 119(15), pp. 3039–3046.

Battyani, Z., Xerri, L., Hassoun, J., Bonerandi, J.J. and Grob, J.J. (1993) 'Tyrosinase gene expression in human tissues.', *Pigment Cell Research*, 6(6), pp. 400–5.

Baxter, L.L. and Pavan, W.J. (2003) 'Pmel17 expression is Mitf-dependent and reveals cranial melanoblast migration during murine development', *Gene Expression Patterns*, 3(6), pp. 703–707.

Beadling, C., Jacobson-Dunlop, E., Hodi, F.S., Le, C., Warrick, A., Patterson, J., Town, A., Harlow, A., Cruz, F., Azar, S., Rubin, B.P., Muller, S., West, R., Heinrich, M.C. and Corless, C.L. (2008) 'KIT Gene Mutations and Copy Number in Melanoma Subtypes', *Clinical Cancer Research*, 14(21), pp. 6821–6828.

Bell, M. (1967) 'Ultrastructure of differentiating hair follicles', in *Advances in Biology of Skin.* , pp. 61–81.

Bellone, G., Silvestri, S., Artusio, E., Tibaudi, D., Turletti, A., Geuna, M., Giachino, C., Valente, G., Emanuelli, G. and Rodeck, U. (1997) 'Growth stimulation of colorectal carcinoma cells via the c-kit receptor is inhibited by TGF-β1', *Journal of Cellular Physiology*, 172(1), pp. 1–11.

Belmadani, A., Jung, H., Ren, D. and Miller, R.J. (2009) 'The chemokine SDF-1/CXCL12 regulates the migration of melanocyte progenitors in mouse hair follicles', *Differentiation*, 77(4), pp. 395–411.

Bennett, D. (1956) 'Developmental analysis of a mutation with pleiotropic effects in the

mouse', *Journal of Morphology*, 98(2), pp. 199–233.

Bernex, F., De Sepulveda, P., Kress, C., Elbaz, C., Delouis, C. and Panthier, J.J. (1996) 'Spatial and temporal patterns of c-kit-expressing cells in WlacZ/+ and WlacZ/WlacZ mouse embryos.', *Development*, 122(10), pp. 3023–33.

Berthier-Vergnes, O., Kharbili, M. El, de la Fouchardière, A., Pointecouteau, T., Verrando, P., Wierinckx, A., Lachuer, J., Le Naour, F. and Lamartine, J. (2011) 'Gene expression profiles of human melanoma cells with different invasive potential reveal TSPAN8 as a novel mediator of invasion', *British Journal of Cancer*, 104(1), pp. 155–165.

Bialas, M., Borczynska, A., Rozwadowska, N., Fiszer, D., Kosicki, W., Jedrzejczak, P. and Kurpisz, M. (2010) 'SCF and c-kit expression profiles in male individuals with normal and impaired spermatogenesis', *Andrologia*, 42(2), pp. 83–91.

Bibel, D.J., Aly, R. and Shinefield, H.R. (1992) 'Antimicrobial activity of sphingosines.', *The Journal of Investigative Dermatology*, 98(3), pp. 269–73.

Bidaud, C., Salomon, R., Van Camp, G., Pelet, A., Attié, T., Eng, C., Bonduelle, M., Amiel, J., Nihoul-Fékété, C., Willems, P.J., Munnich, A. and Lyonnet, S. (1997) 'Endothelin-3 gene mutations in isolated and syndromic Hirschsprung disease.', *European Journal of Human Genetics*, 5(4), pp. 247–51.

Blanpain, C., Lowry, W.E., Pasolli, H.A. and Fuchs, E. (2006) 'Canonical notch signaling functions as a commitment switch in the epidermal lineage.', *Genes & Development*, 20(21), pp. 3022–35.

Blasius, A.L., Brandl, K., Crozat, K., Xia, Y., Khovananth, K., Krebs, P., Smart, N.G., Zampolli, A., Ruggeri, Z.M. and Beutler, B.A. (2009) 'Mice with mutations of Dock7 have generalized hypopigmentation and white-spotting but show normal neurological function.', *Proceedings of the National Academy of Sciences of the United States of America*, 106(8), pp. 2706–11.

Blume-Jensen, P., Claesson-Welsh, L., Siegbahn, A., Zsebo, K.M., Westermark, B. and Heldin, C.H. (1991) 'Activation of the human c-kit product by ligand-induced dimerization mediates circular actin reorganization and chemotaxis.', *The EMBO Journal*, 10(13), pp. 4121–8.

Blume-Jensen, P., Janknecht, R. and Hunter, T. (1998) 'The kit receptor promotes cell survival via activation of PI 3-kinase and subsequent Akt-mediated phosphorylation of Bad on Ser136.', *Current Biology*, 8(13), pp. 779–82.

Blume-Jensen, P., Rönnstrand, L., Gout, I., Waterfield, M.D. and Heldin, C.H. (1994) 'Modulation of Kit/stem cell factor receptor-induced signaling by protein kinase C.', *The Journal of Biological Chemistry*, 269(34), pp. 21793–802.

Boissy, R.E., Trinkle, L.S. and Nordlund, J.J. (1989) 'Separation of pigmented and albino melanocytes and the concomitant evaluation of endogenous peroxide content using flow cytometry', *Cytometry*, 10(6), pp. 779–787.

Bolande, R.P. (1974) 'The neurocristopathies: A unifying concept of disease arising in neural crest maldevelopment', *Human Pathology*, 5(4), pp. 409–429.

Bosenberg, M., Muthusamy, V., Curley, D.P., Wang, Z., Hobbs, C., Nelson, B., Nogueira, C., Horner, J.W., DePinho, R. and Chin, L. (2006) 'Characterization of melanocyte-specific inducible Cre recombinase transgenic mice', *Genesis*, 44(5), pp. 262–267.

Bouquet, C., Ravaille-Veron, M., Propst, F. and Nothias, F. (2007) 'MAP1B coordinates microtubule and actin filament remodeling in adult mouse Schwann cell tips and DRG neuron growth cones', *Molecular and Cellular Neuroscience*, 36(2), pp. 235–247.

Breitkreutz, D., Mirancea, N. and Nischt, R. (2009) 'Basement membranes in skin: unique matrix structures with diverse functions?', *Histochemistry and Cell Biology*, 132(1), pp. 1–10.

Bronner-Fraser, M. (1994) 'Neural crest cell formation and migration in the developing embryo.', *FASEB journal*, 8(10), pp. 699–706.

Broudy, V.C. (1997) 'Stem Cell Factor and Hematopoiesis', *Blood*, 90(4), pp. 1345–1364.

Broudy, V.C., Lin, N.L., Liles, W.C., Corey, S.J., O'Laughlin, B., Mou, S. and Linnekin, D. (1999) 'Signaling via Src family kinases is required for normal internalization of the receptor c-Kit.', *Blood*, 94(6), pp. 1979–86.

Burn, S.F. (2012) 'Detection of β-Galactosidase Activity: X-gal Staining', in *Methods in Molecular Biology*, pp. 241–250.

Byrne, C., Tainsky, M. and Fuchs, E. (1994) 'Programming gene expression in developing epidermis.', *Development*, 120(9), pp. 2369–83.

Cable, J., Jackson, I.J. and Steel, K.P. (1995) 'Mutations at the W locus affect survival of

neural crest-derived melanocytes in the mouse.', *Mechanisms of Development*, 50(2–3), pp. 139–150.

Caramel, J., Papadogeorgakis, E., Hill, L., Browne, G.J., Richard, G., Wierinckx, A., Saldanha, G., Osborne, J., Hutchinson, P., Tse, G., Lachuer, J.L., Puisieux, A., Pringle, J.H., Phane Ansieau, S. and Tulchinsky, E. (2013) 'A Switch in the Expression of Embryonic EMT-Inducers Drives the Development of Malignant Melanoma', *Cancer Cell*, 24(4), pp. 466–480.

Carraway, K.L., Perez, A., Idris, N., Jepson, S., Arango, M., Komatsu, M., Haq, B., Price-Schiavi, S.A., Zhang, J. and Carraway, C.A.C. (2002) 'Muc4/sialomucin complex, the intramembrane ErbB2 ligand, in cancer and epithelia: to protect and to survive.', *Progress in Nucleic Acid Research and Molecular Biology*, 71, pp. 149–85.

Carreira, S., Goodall, J., Denat, L., Rodriguez, M., Nuciforo, P., Hoek, K.S., Testori, A., Larue, L. and Goding, C.R. (2006) 'Mitf regulation of Dia1 controls melanoma proliferation and invasiveness', *Genes & Development*, 20(24), pp. 3426–3439.

Caruana, G., Cambareri, A.C. and Ashman, L.K. (1999) 'Isoforms of c-KIT differ in activation of signalling pathways and transformation of NIH3T3 fibroblasts', *Oncogene*, 18(40), pp. 5573–5581.

Carvill, G.L., McMahon, J.M., Schneider, A., Zemel, M., Myers, C.T., Saykally, J., Nguyen, J., Robbiano, A., Zara, F., Specchio, N., Mecarelli, O., Smith, R.L., Leventer, R.J., Møller, R.S., Nikanorova, M., Dimova, P., Jordanova, A., Petrou, S., Helbig, I., Striano, P., Weckhuysen, S., Berkovic, S.F., Scheffer, I.E. and Mefford, H.C. (2015) 'Mutations in the GABA Transporter SLC6A1 Cause Epilepsy with Myoclonic-Atonic Seizures.', *American Journal of Human Genetics*, 96(5), pp. 808–15.

Chen, J., O'Shea, C., Fitzpatrick, J.E., Koster, M.I. and Koch, P.J. (2012) 'Loss of desmocollin 3 in skin tumor development and progression', *Molecular Carcinogenesis*, 51(7), pp. 535–545.

Chen, X., Zhao, Q., Li, C., Geng, Y., Huang, K., Zhang, J., Wang, X., Yang, J., Wang, T., Xia, C., Liu, X., Meng, M., Yang, D., Zheng, Y., Du, J., Zhang, X., Chen, J., Pan, G. and Wang, J. (2015) 'OP9-Lhx2 stromal cells facilitate derivation of hematopoietic progenitors both in vitro and in vivo', *Stem Cell Research*, 15(2), pp. 395–402.

Cheung, M., Chaboissier, M.-C., Mynett, A., Hirst, E., Schedl, A. and Briscoe, J. (2005) 'The Transcriptional Control of Trunk Neural Crest Induction, Survival, and Delamination', *Developmental Cell*, 8(2), pp. 179–192.

Chigaev, A., Zwartz, G., Graves, S.W., Dwyer, D.C., Tsuji, H., Foutz, T.D., Edwards, B.S., Prossnitz, E.R., Larson, R.S. and Sklar, L.A. (2003) '$\alpha_4\beta_1$ Integrin Affinity Changes Govern Cell Adhesion', *Journal of Biological Chemistry*, 278(40), pp. 38174–38182.

Chlenski, A., Guerrero, L.J., Salwen, H.R., Yang, Q., Tian, Y., Morales La Madrid, A., Mirzoeva, S., Bouyer, P.G., Xu, D., Walker, M. and Cohn, S.L. (2011) 'Secreted Protein Acidic and Rich in Cysteine Is a Matrix Scavenger Chaperone', *PLoS ONE*, 6(9), p. e23880.

Ciarletta, P., Foret, L. and Ben Amar, M. (2011) 'The radial growth phase of malignant melanoma: multi-phase modelling, numerical simulations and linear stability analysis.', *Journal of the Royal Society, Interface*, 8(56), pp. 345–68.

Cichorek, M., Wachulska, M., Stasiewicz, A. and Tymińska, A. (2013) 'Skin melanocytes: biology and development.', *Postepy Dermatologii i Alergologii*, 30(1), pp. 30–41.

Colombo, S., Champeval, D., Rambow, F., Larue, L., Sophie, C., Delphine, C., Florian, R. and Lionel, L. (2011) 'Transcriptomic Analysis of Mouse Embryonic Skin Cells Reveals Previously Unreported Genes Expressed in Melanoblasts', *Journal of Investigative Dermatology*, 132(1), pp. 170–178.

Crosier, P., Ricciardi, S., Hall, L., Vitas, M., Clark, S. and Crosier, K. (1993) 'Expression of isoforms of the human receptor tyrosine kinase c-kit in leukemic cell lines and acute myeloid leukemia', *Blood*, 82(4)

Cukierman, E., Pankov, R., Stevens, D.R. and Yamada, K.M. (2001) 'Taking Cell-Matrix Adhesions to the Third Dimension', *Science*, 294(5547), pp. 1708–1712.

Curtin, J.A., Busam, K., Pinkel, D. and Bastian, B.C. (2006) 'Somatic Activation of KIT in Distinct Subtypes of Melanoma', *Journal of Clinical Oncology*, 24(26), pp. 4340–4346.

de Aberle, S.B. (1927) 'A study of the hereditary anaemia of mice', *American Journal of Anatomy*, 40(2), pp. 219–249.

Delmas, V., Martinozzi, S., Bourgeois, Y., Holzenberger, M. and Larue, L. (2003) 'Cre-mediated recombination in the skin melanocyte lineage', *Genesis*, 36(2), pp. 73–80.

Den, Z., Cheng, X., Merched-Sauvage, M. and Koch, P.J. (2006) 'Desmocollin 3 is required

for pre-implantation development of the mouse embryo', *Journal of Cell Science*, 119(3), pp. 482–489.

Dennis, L.K., Vanbeek, M.J., Beane Freeman, L.E., Smith, B.J., Dawson, D. V. and Coughlin, J.A. (2008) 'Sunburns and Risk of Cutaneous Melanoma: Does Age Matter? A Comprehensive Meta-Analysis', *Annals of Epidemiology*, 18(8), pp. 614–627.

Le Douarin, N.M. (2004) 'Neural crest cell plasticity and its limits', *Development*, 131(19), pp. 4637–4650.

Driskell, R.R., Lichtenberger, B.M., Hoste, E., Kretzschmar, K., Simons, B.D., Charalambous, M., Ferron, S.R., Herault, Y., Pavlovic, G., Ferguson-Smith, A.C. and Watt, F.M. (2013) 'Distinct fibroblast lineages determine dermal architecture in skin development and repair.', *Nature*, 504(7479), pp. 277–81.

Duchoň, J. and Matouš, B. (1967) 'Identification of two new metabolites in melanoma urine: 5-hydroxy-6-methoxyindole-2-carboxylic and 5-methoxy-6-hydroxyindole-2-carboxylic acids', *Clinica Chimica Acta*, 16(3), pp. 397–402.

Dunn, L.C. (1937) 'Studies on Spotting Patterns II. Genetic Analysis of Variegated Spotting in the House Mouse.', *Genetics*, 22(1), pp. 43–64.

Dupin, E., Glavieux, C., Vaigot, P. and Le Douarin, N.M. (2000) 'Endothelin 3 induces the reversion of melanocytes to glia through a neural crest-derived glial-melanocytic progenitor.', *Proceedings of the National Academy of Sciences of the United States of America*, 97(14), pp. 7882–7.

Durham, F.M. (1908) 'A preliminary account of the inheritance of coat colour in mice', *Rep. Evol. Com. Roy. Soc. Rep*, 4, pp. 41–53.

Dytham, C. (2011) *Choosing and Using Statistics: A Biologist's Guide*.

Eger, A., Stockinger, A., Schaffhauser, B., Beug, H. and Foisner, R. (2000) 'Epithelial mesenchymal transition by c-Fos estrogen receptor activation involves nuclear translocation of beta-catenin and upregulation of beta-catenin/lymphoid enhancer binding factor-1 transcriptional activity.', *The Journal of Cell Biology*, 148(1), pp. 173–88.

Elder, J.T., Fisher, G.J., Lindquist, P.B., Bennett, G.L., Pittelkow, M.R., Coffey, R.J., Ellingsworth, L., Derynck, R. and Voorhees, J.J. (1989) 'Overexpression of transforming growth factor alpha in psoriatic epidermis.', *Science*, 243(4892), pp. 811–4.

Fang, D., Leishear, K., Nguyen, T.K., Finko, R., Cai, K., Fukunaga, M., Li, L., Brafford, P.A., Kulp, A.N., Xu, X., Smalley, K.S.M. and Herlyn, M. (2006) 'Defining the Conditions for the Generation of Melanocytes from Human Embryonic Stem Cells', *Stem Cells*, 24(7), pp. 1668–1677.

Feil, R., Wagner, J., Metzger, D. and Chambon, P. (1997) 'Regulation of Cre Recombinase Activity by Mutated Estrogen Receptor Ligand-Binding Domains', *Biochemical and Biophysical Research Communications*, 237(3), pp. 752–757.

Feil, S., Valtcheva, N. and Feil, R. (2009) 'Inducible Cre Mice', in *Methods in Molecular Biology*. , pp. 343–363.

Ferreri, D.M. and Vincent, P.A. (2008) 'Signaling To and Through The Endothelial Adherens Junction', in *Cell Junctions*. , pp. 169–195.

Fidler, I.J. and Nicolson, G.L. (1976) 'Organ selectivity for implantation survival and growth of B16 melanoma variant tumor lines.', *Journal of the National Cancer Institute*, 57(5), pp. 1199–202.

Fitzpatrick, T.B. and Breathnach, A.S. (1963) 'The epidermal melanin unit system', *Dermatologische Wochenschrift*, 147, pp. 481–9.

Flanagan, J.G. and Leder, P. (1990) 'The kit ligand: A cell surface molecule altered in steel mutant fibroblasts', *Cell*, 63(1), pp. 185–194.

Folgueras, A.R., Guo, X., Pasolli, H.A., Stokes, N., Polak, L., Zheng, D. and Fuchs, E. (2013) 'Architectural Niche Organization by LHX2 Is Linked to Hair Follicle Stem Cell Function', *Cell Stem Cell*, 13(3), pp. 314–327.

Foty, R. (2011) 'A simple hanging drop cell culture protocol for generation of 3D spheroids.', *Journal of Visualized Experiments*, (51)

Franceschi, S., Lessi, F., Panebianco, F., Tantillo, E., La Ferla, M., Menicagli, M., Aretini, P., Apollo, A., Naccarato, A.G., Marchetti, I. and Mazzanti, C.M. (2017) 'Loss of c-KIT expression in thyroid cancer cells', *PLoS ONE*, 12(3), p. e0173913.

Fuchs, E. (2007) 'Scratching the surface of skin development', *Nature*, 445(7130), pp. 834–842.

Fyrand, O. (1980) 'Studies on fibronectin in the skin.', *British Journal of Dermatology*, 102(2), pp. 167–171.

Gan, W.B., Grutzendler, J., Wong, W.T., Wong, R.O. and Lichtman, J.W. (2000) 'Multicolor

"DiOlistic" labeling of the nervous system using lipophilic dye combinations.', *Neuron*, 27(2), pp. 219–25.

Gandini, S., Sera, F., Cattaruzza, M.S., Pasquini, P., Abeni, D., Boyle, P. and Melchi, C.F. (2005a) 'Meta-analysis of risk factors for cutaneous melanoma: I. Common and atypical naevi', *European Journal of Cancer*, 41(1), pp. 28–44.

Gandini, S., Sera, F., Cattaruzza, M.S., Pasquini, P., Picconi, O., Boyle, P. and Melchi, C.F. (2005b) 'Meta-analysis of risk factors for cutaneous melanoma: II. Sun exposure', *European Journal of Cancer*, 41(1), pp. 45–60.

Ganguly, A., Yang, H., Zhang, H., Cabral, F. and Patel, K.D. (2013) 'Microtubule dynamics control tail retraction in migrating vascular endothelial cells.', *Molecular Cancer Therapeutics*, 12(12), pp. 2837–46.

Gao, F., Shi, H.Y., Daughty, C., Cella, N. and Zhang, M. (2004) 'Maspin plays an essential role in early embryonic development.', *Development*, 131(7), pp. 1479–89.

Garraway, L.A., Widlund, H.R., Rubin, M.A., Getz, G., Berger, A.J., Ramaswamy, S., Beroukhim, R., Milner, D.A., Granter, S.R., Du, J., Lee, C., Wagner, S.N., Li, C., Golub, T.R., Rimm, D.L., Meyerson, M.L., Fisher, D.E. and Sellers, W.R. (2005) 'Integrative genomic analyses identify MITF as a lineage survival oncogene amplified in malignant melanoma', *Nature*, 436(7047), pp. 117–122.

Gehlsen, K.R. and Hendrix, M.J. (1986) 'In vitro assay demonstrates similar invasion profiles for B16F1 and B16F10 murine melanoma cells.', *Cancer letters*, 30(2), pp. 207–12.

Geissler, E.N., Ryan, M.A. and Housman, D.E. (1988) 'The dominant-white spotting (W) locus of the mouse encodes the c-kit proto-oncogene', *Cell*, 55(1), pp. 185–192.

Giebel, L.B. and Spritz, R.A. (1991) 'Mutation of the KIT (mast/stem cell growth factor receptor) protooncogene in human piebaldism', *Genetics*, 88, pp. 8696–8699.

Gilbert, S.F.S. (2000) 'The Epidermis and the Origin of Cutaneous Structures', in *Developmental Biology*.

Girdlestone, J. and Weston, J.A. (1985) 'Identification of early neuronal subpopulations in avian neural crest cell cultures.', *Developmental Biology*, 109(2), pp. 274–87.

Gledhill, K., Guo, Z., Umegaki-Arao, N., Higgins, C.A., Itoh, M. and Christiano, A.M. (2015) 'Melanin Transfer in Human 3D Skin Equivalents Generated Exclusively from Induced Pluripotent Stem Cells', *PLoS ONE*, 10(8), p. e0136713.

Glover, J.D., Knolle, S., Wells, K.L., Liu, D., Jackson, I.J., Mort, R.L. and Headon, D.J. (2015) 'Maintenance of distinct melanocyte populations in the interfollicular epidermis', *Pigment Cell & Melanoma Research*, 28(4), pp. 476–480.

Goodall, J., Carreira, S., Denat, L., Kobi, D., Davidson, I., Nuciforo, P., Sturm, R.A., Larue, L. and Goding, C.R. (2008) 'Brn-2 Represses Microphthalmia-Associated Transcription Factor Expression and Marks a Distinct Subpopulation of Microphthalmia-Associated Transcription Factor–Negative Melanoma Cells', *Cancer Research*, 68(19), pp. 7788–7794.

Goodman, F.R., Majewski, F., Collins, A.L. and Scambler, P.J. (2002) 'A 117-kb Microdeletion Removing HOXD9–HOXD13 and EVX2 Causes Synpolydactyly', *The American Journal of Human Genetics*, 70(2), pp. 547–555.

Gordon, M.K. and Hahn, R.A. (2010) 'Collagens', *Cell and Tissue Research*, 339(1), pp. 247–257.

Green, H., Easley, K. and Iuchi, S. (2003) 'Marker succession during the development of keratinocytes from cultured human embryonic stem cells', *Proceedings of the National Academy of Sciences of the United States of America*, 100(26), pp. 15625–15630.

Grüneberg, H. (1942) 'Inherited macrocytic anaemias in the house mouse', *Journal of Genetics*, 43(3), pp. 285–293.

Guillemot, F., Lo, L.C., Johnson, J.E., Auerbach, A., Anderson, D.J. and Joyner, A.L. (1993) 'Mammalian achaete-scute homolog 1 is required for the early development of olfactory and autonomic neurons.', *Cell*, 75(3), pp. 463–76.

Gupta, P.B., Kuperwasser, C., Brunet, J.-P., Ramaswamy, S., Kuo, W.-L., Gray, J.W., Naber, S.P. and Weinberg, R.A. (2005) 'The melanocyte differentiation program predisposes to metastasis after neoplastic transformation.', *Nature Genetics*, 37(10), pp. 1047–54.

Guyonneau, L., Rossier, A., Richard, C., Hummler, E. and Beermann, F. (2002) 'Expression of Cre recombinase in pigment cells.', *Pigment Cell Research*, 15(4), pp. 305–9.

Hachiya, A., Sriwiriyanont, P., Kobayashi, T., Nagasawa, A., Yoshida, H., Ohuchi, A., Kitahara, T., Visscher, M.O., Takema, Y., Tsuboi, R. and Boissy, R.E. (2009) 'Stem cell factor-KIT

signalling plays a pivotal role in regulating pigmentation in mammalian hair', *The Journal of Pathology*, 218(1), pp. 30–39.

Haftek, M., Serre, G., Mils, V. and Thivolet, J. (1991) 'Immunocytochemical evidence for a possible role of cross-linked keratinocyte envelopes in stratum corneum cohesion.', *The Journal of Histochemistry and Cytochemistry*, 39(11), pp. 1531–8.

Haftek, M., Simon, M., Kanitakis, J., Maréchal, S., Claudy, A., Serre, G. and Schmitt, D. (1997) 'Expression of corneodesmosin in the granular layer and stratum corneum of normal and diseased epidermis.', *The British Journal of Dermatology*, 137(6), pp. 864–73.

Hagedorn, E.J., Ziel, J.W., Morrissey, M.A., Linden, L.M., Wang, Z., Chi, Q., Johnson, S.A. and Sherwood, D.R. (2013) 'The netrin receptor DCC focuses invadopodia-driven basement membrane transmigration in vivo', *The Journal of Cell Biology*, 201(6), pp. 903–913.

Haglund, K., Sigismund, S., Polo, S., Szymkiewicz, I., Di Fiore, P.P. and Dikic, I. (2003) 'Multiple monoubiquitination of RTKs is sufficient for their endocytosis and degradation', *Nature Cell Biology*, 5(5), pp. 461–466.

Hajra, K.M., Chen, D.Y.-S. and Fearon, E.R. (2002) 'The SLUG zinc-finger protein represses E-cadherin in breast cancer.', *Cancer Research*, 62(6), pp. 1613–8.

Halaban, R., Moellmann, G., Tamura, A., Kwont, B.S., Kuklinska, E., Pomerantzt, S.H. and Lerner, A.B. (1988) 'Tyrosinases of murine melanocytes with mutations at the albino locus (glycosylation-deficient and protease-sensitive mutants/dopa reaction/ultrastructure)', *Cell Biology*, 85, pp. 7241–7245.

Hall, B.K. (2008) 'The neural crest and neural crest cells: discovery and significance for theories of embryonic organization', *Journal Of Biosciences*, 33(5), pp. 781–793.

Hansen, N.U.B., Genovese, F., Leeming, D.J. and Karsdal, M.A. (2015) 'The importance of extracellular matrix for cell function and in vivo likeness.', *Experimental and Molecular Pathology*, 98(2), pp. 286–94.

Hari, L., Miescher, I., Shakhova, O., Suter, U., Chin, L., Taketo, M., Richardson, W.D., Kessaris, N. and Sommer, L. (2012) 'Temporal control of neural crest lineage generation by Wnt/ -catenin signaling', *Development*, 139(12), pp. 2107–2117.

Hayashi, S., Kunisada, T., Ogawa, M., Yamaguchi, K. and Nishikawa, S. (1991) 'Exon skipping by mutation of an authentic splice site of c-kit gene in W/W mouse.', *Nucleic Acids Research*, 19(6), pp. 1267–71.

Hérault, Y., Hraba-Renevey, S., van der Hoeven, F. and Duboule, D. (1996) 'Function of the Evx-2 gene in the morphogenesis of vertebrate limbs.', *The EMBO Journal*, 15(23), pp. 6727–38.

Herranz, N., Pasini, D., Díaz, V.M., Francí, C., Gutierrez, A., Dave, N., Escrivà, M., Hernandez-Muñoz, I., Di Croce, L., Helin, K., García de Herreros, A. and Peiró, S. (2008) 'Polycomb complex 2 is required for E-cadherin repression by the Snail1 transcription factor.', *Molecular and cellular biology*, 28(15), pp. 4772–81.

Hervé, J.-C. and Derangeon, M. (2013) 'Gap-junction-mediated cell-to-cell communication', *Cell and Tissue Research*, 352(1), pp. 21–31.

Hines, S.J., Organ, C., Kornstein, M.J. and Krystal, G.W. (1995) 'Coexpression of the c-kit and stem cell factor genes in breast carcinomas.', *Cell growth & Differentiation*, 6(6), pp. 769–79.

Hirobe, T. (1984) 'Histochemical survey of the distribution of the epidermal melanoblasts and melanocytes in the mouse during fetal and postnatal periods', *The Anatomical Record*, 208(4), pp. 589–594.

Hirobe, T. (2005) 'Role of keratinocyte-derived factors involved in regulating the proliferation and differentiation of mammalian epidermal melanocytes', *Pigment Cell Research*, 18(1), pp. 2–12.

Hirota, S., Nishida, T., Isozaki, K., Taniguchi, M., Nakamura, J., Okazaki, T. and Kitamura, Y. (2001) 'Gain-of-function mutation at the extracellular domain of KIT in gastrointestinal stromal tumours', *The Journal of Pathology*, 193(4), pp. 505–510.

Hitomi, K. (2005) 'Transglutaminases in skin epidermis.', *European Journal of Dermatology*, 15(5), pp. 313–9.

Hodis, E., Watson, I.R., Kryukov, G. V, Arold, S.T., Imielinski, M., Theurillat, J.-P., Nickerson, E., Auclair, D., Li, L., Place, C., Dicara, D., Ramos, A.H., Lawrence, M.S., Cibulskis, K., Sivachenko, A., Voet, D., Saksena, G., Stransky, N., Onofrio, R.C., Winckler, W., Ardlie, K., Wagle, N., Wargo, J., Chong, K., Morton, D.L., Stemke-Hale, K., Chen, G., Noble, M., Meyerson, M., Ladbury, J.E., Davies, M.A., Gershenwald, J.E., Wagner, S.N., Hoon, D.S.B., Schadendorf, D., Lander, E.S., Gabriel, S.B., Getz, G., Garraway, L.A. and Chin, L. (2012) 'A landscape of driver

mutations in melanoma.', *Cell*, 150(2), pp. 251–63.

Hoek, K.S. and Goding, C.R. (2010) 'Cancer stem cells versus phenotype-switching in melanoma', *Pigment Cell & Melanoma Research*, 23(6), pp. 746–759.

Hong, Y., Song, B., Chen, H.-D. and Gao, X.-H. (2015) 'Melanocytes and Skin Immunity', *The Journal of Investigative Dermatology Symposium*, 17, pp. 37–39.

Honig, M.G. and Hume, R.I. (1986) 'Fluorescent carbocyanine dyes allow living neurons of identified origin to be studied in long-term cultures.', *The Journal of Cell Biology*, 103(1), pp. 171–87.

Howard, E.R. (1972) 'Hirschsprung's disease: a review of the morphology and physiology.', *Postgraduate Medical Journal*, 48(562), pp. 471–7.

Hsiao, J.J. and Fisher, D.E. (2014) 'The roles of microphthalmia-associated transcription factor and pigmentation in melanoma', *Archives of Biochemistry and Biophysics*, 563, pp. 28–34.

Huang, G.Y., Cooper, E.S., Waldo, K., Kirby, M.L., Gilula, N.B. and Lo, C.W. (1998) 'Gap Junction–mediated Cell–Cell Communication Modulates Mouse Neural Crest Migration', *The Journal of Cell Biology*, 143(6), pp. 1725–1734.

Huang, M., Miller, M.L., McHenry, L.K., Zheng, T., Zhen, Q., Ilkhanizadeh, S., Conklin, B.R., Bronner, M.E. and Weiss, W.A. (2016) 'Generating trunk neural crest from human pluripotent stem cells', *Scientific Reports*, 6(1), p. 19727.

Hughes, C.S., Postovit, L.M. and Lajoie, G.A. (2010) 'Matrigel: A complex protein mixture required for optimal growth of cell culture', *Proteomics*, 10(9), pp. 1886–1890.

Huszar, D., Sharpe, A. and Jaenisch, R. (1991) 'Migration and proliferation of cultured neural crest cells in W mutant neural crest chimeras.', *Development*, 112(1), pp. 131–41.

Hutt, K.J.J., McLaughlin, E.A. and Holland, M.K. (2006) 'Kit ligand and c-Kit have diverse roles during mammalian oogenesis and folliculogenesis', *Molecular Human Reproduction*, 12(2), pp. 61–69.

Inoue, M., Kyo, S., Fujita, M., Enomoto, T. and Kondoh, G. (1994) 'Coexpression of the c-kit Receptor and the Stem Cell Factor in Gynecological Tumors', *Cancer Research*, 54(11)

Ishida, M., Marubashi, S. and Fukuda, M. (2017) 'M-INK, a novel tool for visualizing melanosomes and melanocores', *Journal of Biochemistry*, , p. mvw100.

Jacquemet, G., Morgan, M.R., Byron, A., Humphries, J.D., Choi, C.K., Chen, C.S., Caswell, P.T. and Humphries, M.J. (2013) 'Rac1 is deactivated at integrin activation sites through an IQGAP1-filamin-A-RacGAP1 pathway.', *Journal of Cell Science*, 126(Pt 18), pp. 4121–35.

Jiang, R., Lan, Y., Norton, C.R., Sundberg, J.P. and Gridley, T. (1998) 'The Slug gene is not essential for mesoderm or neural crest development in mice.', *Developmental Biology*, 198(2), pp. 277–85.

Jiao, Z., Zhang, Z.G., Hornyak, T.J., Hozeska, A., Zhang, R.L., Wang, Y., Wang, L., Roberts, C., Strickland, F.M. and Chopp, M. (2006) 'Dopachrome tautomerase (Dct) regulates neural progenitor cell proliferation', *Developmental Biology*, 296(2), pp. 396–408.

Jordan, S.A. and Jackson, I.J. (2000a) 'MGF (KIT Ligand) Is a Chemokinetic Factor for Melanoblast Migration into Hair Follicles', *Developmental Biology*, 225(2), pp. 424–436.

Jordan, S.A. and Jackson, I.J. (2000b) 'A late wave of melanoblast differentiation and rostrocaudal migration revealed in patch and rump-white embryos', *Mechanisms of Development*, 92(2), pp. 135–143.

Juárez-Morales, J.L., Schulte, C.J., Pezoa, S.A., Vallejo, G.K., Hilinski, W.C., England, S.J., de Jager, S. and Lewis, K.E. (2016) 'Evx1 and Evx2 specify excitatory neurotransmitter fates and suppress inhibitory fates through a Pax2-independent mechanism', *Neural Development*, 11(1), p. 5.

Jung, H.-Y., Fattet, L. and Yang, J. (2015) 'Molecular Pathways: Linking Tumor Microenvironment to Epithelial-Mesenchymal Transition in Metastasis', *Clinical Cancer Research*, 21(5), pp. 962–968.

Kapur, R. and Zhang, L. (2001) 'A novel mechanism of cooperation between c-Kit and erythropoietin receptor. Stem cell factor induces the expression of Stat5 and erythropoietin receptor, resulting in efficient proliferation and survival by erythropoietin.', *The Journal of Biological Chemistry*, 276(2), pp. 1099–106.

Kaukonen, R., Jacquemet, G., Hamidi, H. and Ivaska, J. (2017) 'Cell-derived matrices for studying cell proliferation and directional migration in a complex 3D microenvironment', *Nature Protocols*, 12(11), pp. 2376–2390.

Kawakami, A. and Fisher, D.E. (2017) 'The master role of microphthalmia-associated transcription factor in melanocyte and melanoma biology', *Laboratory Investigation*, 97(6), pp. 649–

656.

Kawakami, Y., Eliyahu, S., Delgado, C.H., Robbins, P.F., Rivoltini, L., Topalian, S.L., Miki, T. and Rosenberg, S.A. (1994) 'Cloning of the gene coding for a shared human melanoma antigen recognized by autologous T cells infiltrating into tumor.', *Proceedings of the National Academy of Sciences of the United States of America*, 91(9), pp. 3515–9.

Kelley, L.C., Lohmer, L.L., Hagedorn, E.J. and Sherwood, D.R. (2014) 'Traversing the basement membrane in vivo: A diversity of strategies', *The Journal of Cell Biology*, 204(3), pp. 291–302.

Khmelinskii, A., Keller, P.J., Bartosik, A., Meurer, M., Barry, J.D., Mardin, B.R., Kaufmann, A., Trautmann, S., Wachsmuth, M., Pereira, G., Huber, W., Schiebel, E. and Knop, M. (2012) 'Tandem fluorescent protein timers for in vivo analysis of protein dynamics', *Nature Biotechnology*, 30(7), pp. 708–714.

Khmelinskii, A. and Knop, M. (2014) 'Analysis of Protein Dynamics with Tandem Fluorescent Protein Timers', in *Methods in molecular biology*. , pp. 195–210.

Kissel, H., Timokhina, I., Hardy, M.P., Rothschild, G., Tajima, Y., Soares, V., Angeles, M., Whitlow, S.R., Manova, K. and Besmer, P. (2000) 'Point mutation in Kit receptor tyrosine kinase reveals essential roles for Kit signaling in spermatogenesis and oogenesis without affecting other Kit responses', *The EMBO Journal*, 19(6), pp. 1312–1326.

Kobayashi, N., Nakagawa, A., Muramatsu, T., Yamashina, Y., Shirai, T., Hashimoto, M.W., Ishigaki, Y., Ohnishi, T. and Mori, T. (1998) 'Supranuclear Melanin Caps Reduce Ultraviolet Induced DNA Photoproducts in Human Epidermis', *Journal of Investigative Dermatology*, 110(5), pp. 806–810.

Kornberg, T.B. and Roy, S. (2014) 'Cytonemes as specialized signaling filopodia.', *Development*, 141(4), pp. 729–36.

Körner, A.M. and Pawelek, J. (1980) 'Dopachrome conversion: a possible control point in melanin biosynthesis.', *The Journal of Investigative Dermatology*, 75(2), pp. 192–5.

Kos, R., Reedy, M. V, Johnson, R.L. and Erickson, C.A. (2001) 'The winged-helix transcription factor FoxD3 is important for establishing the neural crest lineage and repressing melanogenesis in avian embryos.', *Development*, 128(8), pp. 1467–79.

Koster, M.I. and Roop, D.R. (2007) 'Mechanisms Regulating Epithelial Stratification', *Annual Review of Cell and Developmental Biology*, 23(1), pp. 93–113.

Krieg, T. and Aumailley, M. (2011) 'The extracellular matrix of the dermis: flexible structures with dynamic functions', *Experimental Dermatology*, 20(8), pp. 689–695.

Krosl, G., He, G., Lefrancois, M., Charron, F., Roméo, P.H., Jolicoeur, P., Kirsch, I.R., Nemer, M. and Hoang, T. (1998) 'Transcription factor SCL is required for c-kit expression and c-Kit function in hemopoietic cells.', *The Journal of Experimental Medicine*, 188(3), pp. 439–50.

Krystal, G.W., Hines, S.J. and Organ, C.P. (1996) 'Autocrine Growth of Small Cell Lung Cancer Mediated by Coexpression of c-kit and Stem Cell Factor', *Cancer Research*, 56(2)

Kuonen, F., Laurent, J., Secondini, C., Lorusso, G., Stehle, J.-C., Rausch, T., Faes-van't Hull, E., Bieler, G., Alghisi, G.-C., Schwendener, R., Andrejevic-Blant, S., Mirimanoff, R.-O. and Ruegg, C. (2012) 'Inhibition of the Kit Ligand/c-Kit Axis Attenuates Metastasis in a Mouse Model Mimicking Local Breast Cancer Relapse after Radiotherapy', *Clinical Cancer Research*, 18(16), pp. 4365–4374.

Kurokawa, I., Takahashi, K., Moll, I. and Moll, R. (2011) 'Expression of keratins in cutaneous epithelial tumors and related disorders--distribution and clinical significance', *Experimental Dermatology*, 20(3), pp. 217–228.

Kurzrock, R. (2003) 'Stem cell factor', in *Cancer Medicine*.

Kuzu, O.F., Nguyen, F.D., Noory, M.A. and Sharma, A. (2015) 'Current State of Animal (Mouse) Modeling in Melanoma Research.', *Cancer Growth and Metastasis*, 8(Suppl 1), pp. 81–94.

Lamouille, S., Xu, J. and Derynck, R. (2014) 'Molecular mechanisms of epithelial–mesenchymal transition', *Nature Reviews Molecular Cell Biology*, 15(3), pp. 178–196.

Lancaster, O.M. and Baum, B. (2011) 'Might makes right: Using force to align the mitotic spindle', *Nature Cell Biology*, 13(7), pp. 736–738.

Lane, D.P. (1992) 'p53, guardian of the genome', *Nature*, 358(6381), pp. 15–16.

Lang, D., Mascarenhas, J.B. and Shea, C.R. (2013) 'Melanocytes, melanocyte stem cells, and melanoma stem cells.', *Clinics in Dermatology*, 31(2), pp. 166–78.

LeBleu, V.S., MacDonald, B. and Kalluri, R. (2007) 'Structure and Function of Basement Membranes', *Experimental Biology and Medicine*, 232(9), pp. 1121–1129.

Lee, H.-O., Levorse, J.M. and Shin, M.K. (2003) 'The endothelin receptor-B is required for the migration of neural crest-derived melanocyte and enteric neuron precursors', *Developmental Biology*, 259(1), pp. 162–175.

Lei, M., Guo, H., Qiu, W., Lai, X., Yang, T., Widelitz, R.B., Chuong, C.-M., Lian, X. and Yang, L. (2014) 'Modulating hair follicle size with *Wnt10b/DKK1* during hair regeneration', *Experimental Dermatology*, 23(6), pp. 407–413.

Leipold, E., Liebmann, L., Korenke, G.C., Heinrich, T., Gießelmann, S., Baets, J., Ebbinghaus, M., Goral, R.O., Stödberg, T., Hennings, J.C., Bergmann, M., Altmüller, J., Thiele, H., Wetzel, A., Nürnberg, P., Timmerman, V., De Jonghe, P., Blum, R., Schaible, H.-G., Weis, J., Heinemann, S.H., Hübner, C.A. and Kurth, I. (2013) 'A de novo gain-of-function mutation in SCN11A causes loss of pain perception', *Nature Genetics*, 45(11), pp. 1399–1404.

Lemmon, M.A., Pinchasi, D., Zhou, M., Lax, I. and Schlessinger, J. (1997) 'Kit receptor dimerization is driven by bivalent binding of stem cell factor.', *The Journal of Biological Chemistry*, 272(10), pp. 6311–7.

Lennartsson, J. and Ronnstrand, L. (2012) 'Stem Cell Factor Receptor/c-Kit: From Basic Science to Clinical Implications', *Physiological Reviews*, 92(4), pp. 1619–1649.

Leone, D.P., Genoud, S., Atanasoski, S., Grausenburger, R., Berger, P., Metzger, D., Macklin, W.B., Chambon, P. and Suter, U. (2003) 'Tamoxifen-inducible glia-specific Cre mice for somatic mutagenesis in oligodendrocytes and Schwann cells.', *Molecular and cellular neurosciences*, 22(4), pp. 430–40.

Leptin, M. (1991) 'Twist and Snail as positive and negative regulators during Drosophila mesoderm development.', *Genes & Development*, 5(9), pp. 1568–76.

Lerner, A.B. and Fitzpatick, T.B. (1953) 'The Control of Melanogenesis in Human Pigment Cells', in *Pigment Cell Growth*. , pp. 319–333.

Lessard, J.C., Kalinin, A., Bible, P.W. and Morasso, M.I. (2015) 'Calmodulin 4 is dispensable for epidermal barrier formation and wound healing in mice.', *Experimental Dermatology*, 24(1)

Lev, S., Yarden, Y. and Givol, D. (1992) 'Dimerization and activation of the kit receptor by monovalent and bivalent binding of the stem cell factor.', *The Journal of Biological Chemistry*, 267(22), pp. 15970–7.

Levy, C., Khaled, M. and Fisher, D.E. (2006) 'MITF: master regulator of melanocyte development and melanoma oncogene', *Trends in Molecular Medicine*, 12(9), pp. 406–414.

Li, A., Dawson, J.C., Forero-Vargas, M., Spence, H.J., Yu, X., König, I., Anderson, K. and Machesky, L.M. (2010) 'The Actin-Bundling Protein Fascin Stabilizes Actin in Invadopodia and Potentiates Protrusive Invasion', *Current Biology*, 20(4), pp. 339–345.

Li, A., Ma, Y., Yu, X., Mort, R.L., Lindsay, C.R., Stevenson, D., Strathdee, D., Insall, R.H., Chernoff, J., Snapper, S.B., Jackson, I.J., Larue, L., Sansom, O.J. and Machesky, L.M. (2011) 'Rac1 drives melanoblast organization during mouse development by orchestrating pseudopod- driven motility and cell-cycle progression.', *Developmental Cell*, 21(4), pp. 722–34.

Li, X., Wang, W., Xi, Y., Gao, M., Tran, M., Aziz, K.E., Qin, J., Li, W. and Chen, J. (2016) 'FOXR2 Interacts with MYC to Promote Its Transcriptional Activities and Tumorigenesis.', *Cell Reports*, 16(2), pp. 487–497.

Liang, J., Wu, Y.-L., Chen, B.-J., Zhang, W., Tanaka, Y. and Sugiyama, H. (2013) 'The C-Kit Receptor-Mediated Signal Transduction and Tumor-Related Diseases', *International Journal of Biological Sciences*, 9(5), pp. 435–443.

Lieven, O., Knobloch, J. and Rüther, U. (2010) 'The regulation of Dkk1 expression during embryonic development', *Developmental Biology*, 340(2), pp. 256–268.

Lim, S.Y., Yuzhalin, A.E., Gordon-Weeks, A.N. and Muschel, R.J. (2016) 'Targeting the CCL2-CCR2 signaling axis in cancer metastasis.', *Oncotarget*, 7(19), pp. 28697–710.

Little, C.C. and Cloudman, A.M. (1937) 'The Occurrence of a Dominant Spotting Mutation in the House Mouse.', *Proceedings of the National Academy of Sciences of the United States of America*, 23(10), pp. 535–7.

Liu, Y., Helms, A.W. and Johnson, J.E. (2004) 'Distinct activities of Msx1 and Msx3 in dorsal neural tube development.', *Development*, 131(5), pp. 1017–28.

Lodish, H., Berk, A., Zipursky, S.L., Matsudaira, P., Baltimore, D. and Darnell, J. (2000) 'The Actin Cytoskeleton', in *Molecular Cell Biology*.

Longley, B.J. and Carter, E.L. (1999) 'SCF-KIT Pathway in Human Epidermal Melanocyte Homeostasis', *Journal of Investigative Dermatology*, 113(1), p. 139.

Lorenz, U. (2009) 'SHP-1 and SHP-2 in T cells: two phosphatases functioning at many levels.', *Immunological reviews*, 228(1), pp. 342–59.

Loring, J., Glimelius, B., Erickson, C. and Weston, J.A. (1981) 'Analysis of developmentally homogeneous neural crest cell populations in vitro: I. Formation, morphology and differentiative behavior', *Developmental Biology*, 82(1), pp. 86–94.

Loring, J.F., Barker, D.L. and Erickson, C.A. (1988) 'Migration and Differentiation of Neural Crest and Ventral Neural Tube Cells in vitro: Implications for in vitro and in vivo Studies of the Neural Crest', *The Journal of Neuroscience*, 8(35), pp. 1001–1.

Lu, S.-Q., Qiu, Y., Dai, W.-J. and Zhang, X.-Y. (2017) 'FOXR2 Promotes the Proliferation, Invasion, and Epithelial-Mesenchymal Transition in Human Colorectal Cancer Cells', *Oncology Research Featuring Preclinical and Clinical Cancer Therapeutics*, 25(5), pp. 681–689.

Luciani, F., Champeval, D., Herbette, A., Denat, L., Aylaj, B., Martinozzi, S., Ballotti, R., Kemler, R., Goding, C.R., De Vuyst, F., Larue, L. and Delmas, V. (2011) 'Biological and mathematical modeling of melanocyte development', *Development*, 138(18), pp. 3943–3954.

Ma, H.-J., Ma, H.-Y., Yang, Y., Li, P.-C., Zi, S.-X., Jia, C.-Y. and Chen, R. (2014) 'α-Melanocyte stimulating hormone (MSH) and prostaglandin E2 (PGE2) drive melanosome transfer by promoting filopodia delivery and shedding spheroid granules: Evidences from atomic force microscopy observation', *Journal of Dermatological Science*, 76(3), pp. 222–230.

MacFie, H.J., Light, N.D. and Bailey, A.J. (1988) 'Natural taxonomy of collagen based on amino acid composition.', *Journal of Theoretical Biology*, 131(4), pp. 401–18.

Mackenzie, M.A.F.F., Jordan, S.A., Budd, P.S. and Jackson, I.J. (1997) 'Activation of the Receptor Tyrosine Kinase Kit Is Required for the Proliferation of Melanoblasts in the Mouse Embryo', *Developmental Biology*, 192(1), pp. 99–107.

Maeda, M., Johnson, K.R. and Wheelock, M.J. (2005) 'Cadherin switching: essential for behavioral but not morphological changes during an epithelium-to-mesenchyme transition', *Journal of Cell Science*, 118(5)

Majumdarsb, M.K., Fengs, L., Medlockn, E., Toksozii, D. and Williamssbss, D.A. (1994) 'Identification and Mutation of Primary and Secondary Proteolytic Cleavage Sites in Murine Stem Cell Factor cDNA Yields Biologically Active, Cell-associated Protein', *The Journal of Biological Chemistry*, 269(2), pp. 1237–1242.

Marekov, L.N. and Steinert, P.M. (1998) 'Ceramides are bound to structural proteins of the human foreskin epidermal cornified cell envelope.', *The Journal of Biological Chemistry*, 273(28), pp. 17763–70.

Marinkovich, M.P., Keene, D.R., Rimberg, C.S. and Burgeson, R.E. (1993) 'Cellular origin of the dermal-epidermal basement membrane', *Developmental Dynamics*, 197(4), pp. 255–267.

Masson, K., Heiss, E., Band, H. and Rönnstrand, L. (2006) 'Direct binding of Cbl to Tyr568 and Tyr936 of the stem cell factor receptor/c-Kit is required for ligand-induced ubiquitination, internalization and degradation.', *The Biochemical Journal*, 399(1), pp. 59–67.

Mattila, P.K. and Lappalainen, P. (2008) 'Filopodia: molecular architecture and cellular functions', *Nature Reviews Molecular Cell Biology*, 9(6), pp. 446–454.

Mayer, T.C. (1973) 'The migratory pathway of neural crest cells into the skin of mouse embryos.', *Developmental Biology*, 34(1), pp. 39–46.

Mayor, R. and Theveneau, E. (2013) 'The neural crest', *Development*, 140(11), pp. 2247–2251.

McKinney, A.J. and Holmen, S.L. (2011) 'Animal models of melanoma: a somatic cell gene delivery mouse model allows rapid evaluation of genes implicated in human melanoma.', *Chinese Journal of Cancer*, 30(3), pp. 153–62.

Meininger, C.J., Yano, H., Rottapel, R., Bernstein, A., Zsebo, K.M. and Zetter, B.R. (1992) 'The c-kit Receptor Ligand Functions as a Mast Cell Chemoattractant', *Blood*, 79(4), pp. 958–963.

de Melo, J., Clark, B.S. and Blackshaw, S. (2016) 'Multiple intrinsic factors act in concert with Lhx2 to direct retinal gliogenesis', *Scientific Reports*, 6(1), p. 32757.

Merzlyak, E.M., Goedhart, J., Shcherbo, D., Bulina, M.E., Shcheglov, A.S., Fradkov, A.F., Gaintzeva, A., Lukyanov, K.A., Lukyanov, S., Gadella, T.W.J. and Chudakov, D.M. (2007) 'Bright monomeric red fluorescent protein with an extended fluorescence lifetime', *Nature Methods*, 4(7), pp. 555–557.

Meyer zum Gottesberge, A.M. (1988) 'Physiology and pathophysiology of inner ear melanin.', *Pigment Cell Research*, 1(4), pp. 238–49.

Mica, Y., Lee, G., Chambers, S.M., Tomishima, M.J. and Studer, L. (2013) 'Modeling neural

crest induction, melanocyte specification, and disease-related pigmentation defects in hESCs and patient-specific iPSCs.', *Cell reports*, 3(4), pp. 1140–52.

Milet, C. and Monsoro-Burq, A.H. (2012) 'Neural crest induction at the neural plate border in vertebrates', *Developmental Biology*, 366(1), pp. 22–33.

Miller, S.J., Aly, R., Shinefeld, H.R. and Elias, P.M. (1988) 'In vitro and in vivo antistaphylococcal activity of human stratum corneum lipids.', *Archives of Dermatology*, 124(2), pp. 209–15.

Minina, E., Kreschel, C., Naski, M.C., Ornitz, D.M. and Vortkamp, A. (2002) 'Interaction of FGF, Ihh/Pthlh, and BMP signaling integrates chondrocyte proliferation and hypertrophic differentiation.', *Developmental Cell*, 3(3), pp. 439–49.

Mintz, B. and Russell, E.S. (1957) 'Gene-induced embryological modifications of primordial germ cells in the mouse.', *The Journal of Experimental Zoology*, 134(2), pp. 207–37.

Miyazaki, J., Takaki, S., Araki, K., Tashiro, F., Tominaga, A., Takatsu, K. and Yamamura, K. (1989) 'Expression vector system based on the chicken beta-actin promoter directs efficient production of interleukin-5.', *Gene*, 79(2), pp. 269–77.

Miyazawa, K., Williams, D.A., Gotoh, A., Nishimaki, J., Broxmeyer, H.E. and Toyama, K. (1995) 'Membrane-bound Steel factor induces more persistent tyrosine kinase activation and longer life span of c-kit gene-encoded protein than its soluble form.', *Blood*, 85(3), pp. 641–9.

Miyoshi, H., Masaki, N. and Tsuchiya, Y. (2003) 'Characteristics of trajectory in the migration of Amoeba proteus', *Protoplasma*, 222(3–4), pp. 175–181.

Miyoshi, T., Maruhashi, M., Van De Putte, T., Kondoh, H., Huylebroeck, D. and Higashi, Y. (2006) 'Complementary expression pattern of Zfhx1 genes Sip1 and δEF1 in the mouse embryo and their genetic interaction revealed by compound mutants', *Developmental Dynamics*, 235(7), pp. 1941–1952.

Mizukami, T., Kohno, T. and Hattori, M. (2016) 'CUB and Sushi multiple domains 3 regulates dendrite development', *Neuroscience Research*, 110, pp. 11–17.

Mjaatvedt, C.H., Kern, C.B., Norris, R.A., Fairey, S. and Cave, C.L. (2005) 'Normal distribution of melanocytes in the mouse heart', *The Anatomical Record Part A: Discoveries in Molecular, Cellular, and Evolutionary Biology*, 285A(2), pp. 748–757.

Montone, K.T., van Belle, P., Elenitsas, R. and Elder, D.E. (1997) 'Proto-oncogene c-kit expression in malignant melanoma: protein loss with tumor progression.', *Modern pathology*, 10(9), pp. 939–44.

Morgan, B.A. (2014) 'The dermal papilla: an instructive niche for epithelial stem and progenitor cells in development and regeneration of the hair follicle.', *Cold Spring Harbor Perspectives in Medicine*, 4(7), p. a015180.

Morrison-Graham, K., West-Johnsrud, L. and Weston, J.A. (1990) 'Extracellular matrix from normal but not Steel mutant mice enhances melanogenesis in cultured mouse neural crest cells', *Developmental Biology*, 139(2), pp. 299–307.

Morrison, S.J., White, P.M., Zock, C. and Anderson, D.J. (1999) 'Prospective Identification, Isolation by Flow Cytometry, and In Vivo Self-Renewal of Multipotent Mammalian Neural Crest Stem Cells', *Cell*, 96, pp. 737–749.

Morrissey, M.A., Hagedorn, E.J. and Sherwood, D.R. (2013) 'Cell invasion through basement membrane: The netrin receptor DCC guides the way.', *Worm*, 2(3), p. e26169.

Mort, R.L., Hay, L. and Jackson, I.J. (2010) 'Ex vivo live imaging of melanoblast migration in embryonic mouse skin', *Pigment Cell & Melanoma Research*, 23(2), pp. 299–301.

Mort, R.L., Jackson, I.J. and Patton, E.E. (2015) 'The melanocyte lineage in development and disease.', *Development*, 142(4), pp. 620–32.

Mort, R.L., Keighren, M., Hay, L. and Jackson, I.J. (2014) 'Ex vivo culture of mouse embryonic skin and live-imaging of melanoblast migration.', *Journal of visualized experiments*, (87)

Mort, R.L., Ross, R.J.H., Hainey, K.J., Harrison, O.J., Keighren, M.A., Landini, G., Baker, R.E., Painter, K.J., Jackson, I.J. and Yates, C.A. (2016) 'Reconciling diverse mammalian pigmentation patterns with a fundamental mathematical model', *Nature Communications*, 7

Motohashi, T., Yamanaka, K., Chiba, K., Aoki, H. and Kunisada, T. (2009) 'Unexpected Multipotency of Melanoblasts Isolated from Murine Skin', *Stem Cells*, 27(4), pp. 888–897.

Murshed, M., Schinke, T., McKee, M.D. and Karsenty, G. (2004) 'Extracellular matrix mineralization is regulated locally; different roles of two gla-containing proteins.', *The Journal of Cell Biology*, 165(5), pp. 625–30.

Nishikawa, S., Kusakabe1, M., Yoshinaga2, K., Ogawa, M., Hayashi, S.-I., Kunisada, T., Era,

T., Sakakura1, T. and Nishikawa, S.-I. (1991) ‘In utero manipulation of coat color formation by a monoclonal anti-c-kit antibody: two distinct waves of c-kit-dependency during melanocyte development’, *The EMBO Journal*, 10(8), pp. 2111–2118.

Nishimura, E.K. (2011) ‘Melanocyte stem cells: a melanocyte reservoir in hair follicles for hair and skin pigmentation’, *Pigment Cell & Melanoma Research*, 24(3), pp. 401–410.

Nishimura, E.K., Jordan, S., hacute, An, A., Oshima, H., Yoshida, H., Osawa, M., Moriyama, M., Jackson, I.J., Barrandon, Y., Miyachi, Y. and Nishikawa, S.-I. (2002) ‘Dominant role of the niche in melanocyte stem-cell fate determination’, *Nature*, 416(6883), p. 854.

Nissan, X., Larribere, L., Saidani, M., Hurbain, I., Delevoye, C., Feteira, J., Lemaitre, G., Peschanski, M. and Baldeschi, C. (2011) ‘Functional melanocytes derived from human pluripotent stem cells engraft into pluristratified epidermis.’, *Proceedings of the National Academy of Sciences of the United States of America*, 108(36), pp. 14861–6.

Nitzan, E., Krispin, S., Pfaltzgraff, E.R., Klar, A., Labosky, P.A. and Kalcheim, C. (2013) ‘A dynamic code of dorsal neural tube genes regulates the segregation between neurogenic and melanogenic neural crest cells’, *Development*, 140(11), pp. 2269–2279.

Noonan, F.P., Recio, J.A., Takayama, H., Duray, P., Anver, M.R., Rush, W.L., De Fabo, E.C. and Merlino, G. (2001) ‘Neonatal sunburn and melanoma in mice’, *Nature*, 413(6853), pp. 271–272.

Nose, A. and Takeichi, M. (1986) ‘A novel cadherin cell adhesion molecule: its expression patterns associated with implantation and organogenesis of mouse embryos.’, *The Journal of Cell Biology*, 103(6 Pt 2), pp. 2649–58.

Oiso, N., Fukai, K., Kawada, A. and Suzuki, T. (2013) ‘Piebaldism’, *The Journal of Dermatology*, 40(5), pp. 330–335.

Oka, M., Kageyama, A., Fukunaga, M., Bito, T., Nagai, H. and Nishigori, C. (2004) ‘Phosphatidylinositol 3-Kinase/Akt-Dependent and -Independent Protection Against Apoptosis in Normal Human Melanocytes’, *Journal of Investigative Dermatology*, 123(5), pp. 930–936.

Okumura, N., Tsuji, K., Ebihara, Y., Tanaka, I., Sawai, N., Koike, K., Komiyama, A. and Nakahata, T. (1996) ‘Chemotactic and chemokinetic activities of stem cell factor on murine hematopoietic progenitor cells’, *Blood*, 87(10), pp. 4100–4108.

Olgasi, C., Dentelli, P., Rosso, A., Iavello, A., Togliatto, G., Toto, V., Liberatore, M., Barutello, G., Musiani, P., Cavallo, F. and Brizzi, M.F. (2014) ‘DNA vaccination against membrane-bound Kit ligand: A new approach to inhibiting tumour growth and angiogenesis’, *European Journal of Cancer*, 50(1), pp. 234–246.

Olivares, C., Jiménez-Cervantes, C., Lozano, J.A., Solano, F. and García-Borrón, J.C. (2001) ‘The 5,6-dihydroxyindole-2-carboxylic acid (DHICA) oxidase activity of human tyrosinase.’, *The Biochemical Journal*, 354(Pt 1), pp. 131–9.

Orfanos, C. and Ruska, H. (1968) ‘Die Feinstruktur des menschlichen Haares’, *Archiv fur Klinische und Experimentelle Dermatologie*, 231(3), pp. 264–278.

Osawa, M., Egawa, G., Mak, S.-S., Moriyama, M., Freter, R., Yonetani, S., Beermann, F. and Nishikawa, S.-I. (2005) ‘Molecular characterization of melanocyte stem cells in their niche’, *Development*, 132(24), pp. 5589–5599.

Parras, C.M., Schuurmans, C., Scardigli, R., Kim, J., Anderson, D.J. and Guillemot, F. (2002) ‘Divergent functions of the proneural genes Mash1 and Ngn2 in the specification of neuronal subtype identity.’, *Genes & Development*, 16(3), pp. 324–38.

Pasparakis, M., Haase, I. and Nestle, F.O. (2014) ‘Mechanisms regulating skin immunity and inflammation’, *Nature Reviews Immunology*, 14(5), pp. 289–301.

Paulhe, F., Wehrle-Haller, M., Jacquier, M.-C., Imhof, B.A., Tabone-Eglinger, S. and Wehrle-Haller, B. (2009) ‘Dimerization of Kit-ligand and efficient cell-surface presentation requires a conserved Ser-Gly-Gly-Tyr motif in its transmembrane domain’, *The FASEB Journal*, 23(9), pp. 3037–3048.

Paulsson, M. (1992) ‘Basement membrane proteins: structure, assembly, and cellular interactions.’, *Critical Reviews in Biochemistry and Molecular Biology*, 27(1–2), pp. 93–127.

Pédelacq, J.-D., Cabantous, S., Tran, T., Terwilliger, T.C. and Waldo, G.S. (2006) ‘Engineering and characterization of a superfolder green fluorescent protein.’, *Nature Biotechnology*, 24(1), pp. 79–88.

Petrie, R.J., Doyle, A.D. and Yamada, K.M. (2009) ‘Random versus directionally persistent cell migration.’, *Nature reviews. Molecular Cell Biology*, 10(8), pp. 538–49.

Pfaltzgraff, E.R., Mundell, N.A. and Labosky, P.A. (2012) ‘Isolation and culture of neural crest cells from embryonic murine neural tube.’, *Journal of Visualized Experiments*, (64), p. e4134.

Pickup, M.W., Mouw, J.K. and Weaver, V.M. (2014) 'The extracellular matrix modulates the hallmarks of cancer', *EMBO reports*, 15(12), pp. 1243–1253.

Pillet, F., Gibot, L., Madi, M., Rols, M.-P. and Dague, E. (2017) 'Importance of endogenous extracellular matrix in biomechanical properties of human skin model', *Biofabrication*, 9(2), p. 025017.

Pinner, S., Jordan, P., Sharrock, K., Bazley, L., Collinson, L., Marais, R., Bonvin, E., Goding, C. and Sahai, E. (2009) 'Intravital Imaging Reveals Transient Changes in Pigment Production and Brn2 Expression during Metastatic Melanoma Dissemination', *Cancer Research*, 69(20), pp. 7969–7977.

Plank-Bazinet, J.L. and Mundell, N.A. (2016) 'The paradox of Foxd3: how does it function in pluripotency and differentiation of embryonic stem cells?', *Stem Cell Investigation*, 3, p. 73.

Prasad, M.S., Sauka-Spengler, T. and LaBonne, C. (2012) 'Induction of the neural crest state: control of stem cell attributes by gene regulatory, post-transcriptional and epigenetic interactions.', *Developmental Biology*, 366(1), pp. 10–21.

Puffenberger, E.G., Hosoda, K., Washington, S.S., Nakao, K., deWit, D., Yanagisawa, M. and Chakravart, A. (1994) 'A missense mutation of the endothelin-B receptor gene in multigenic Hirschsprung's disease.', *Cell*, 79(7), pp. 1257–66.

Ramírez-Weber, F.A. and Kornberg, T.B. (1999) 'Cytonemes: cellular processes that project to the principal signaling center in Drosophila imaginal discs.', *Cell*, 97(5), pp. 599–607.

Ran, F.A., Hsu, P.D., Lin, C.-Y., Gootenberg, J.S., Konermann, S., Trevino, A.E., Scott, D.A., Inoue, A., Matoba, S., Zhang, Y. and Zhang, F. (2013a) 'Double Nicking by RNA-Guided CRISPR Cas9 for Enhanced Genome Editing Specificity', *Cell*, 154(6), pp. 1380–1389.

Ran, F.A., Hsu, P.D., Wright, J., Agarwala, V., Scott, D.A. and Zhang, F. (2013b) 'Genome engineering using the CRISPR-Cas9 system', *Nature Protocols*, 8(11), pp. 2281–2308.

Reber, L., Da Silva, C.A. and Frossard, N. (2006) 'Stem cell factor and its receptor c-Kit as targets for inflammatory diseases', *European Journal of Pharmacology*, 533(1), pp. 327–340.

Ribero, S., Glass, D. and Bataille, V. (2016) 'Genetic epidemiology of melanoma', *European Journal of Dermatology*, 26(264), pp. 335–9.

Richards, K.A., Fukai, K., Oiso, N. and Paller, A.S. (2001) 'A novel KIT mutation results in piebaldism with progressive depigmentation', *Journal of the American Academy of Dermatology*, 44(2), pp. 288–292.

Rishikaysh, P., Dev, K., Diaz, D., Qureshi, W.M.S., Filip, S. and Mokry, J. (2014) 'Signaling involved in hair follicle morphogenesis and development.', *International Journal of Molecular Sciences*, 15(1), pp. 1647–70.

Robertson, N.G., Heller, S., Lin, J.S., Resendes, B.L., Weremowicz, S., Denis, C.S., Bell, A.M., Hudspeth, A.J. and Morton, C.C. (2000) 'A Novel Conserved Cochlear Gene, OTOR: Identification, Expression Analysis, and Chromosomal Mapping', *Genomics*, 66(3), pp. 242–248.

Rong, Z., Zhu, S., Xu, Y. and Fu, X. (2014) 'Homologous recombination in human embryonic stem cells using CRISPR/Cas9 nickase and a long DNA donor template', *Protein & Cell*, 5(4), pp. 258–260.

Rönnstrand, L. (2004) 'Signal transduction via the stem cell factor receptor/c-Kit', *Cellular and Molecular Life Sciences*, 61(19–20), pp. 2535–2548.

Roskelley, C.D. and Bissell, M.J. (1995) 'Dynamic reciprocity revisited: a continuous, bidirectional flow of information between cells and the extracellular matrix regulates mammary epithelial cell function.', *Biochemistry and Cell Biology*, 73(7–8), pp. 391–7.

Russel, E.S., Thompson, M.W. and McFarland, E. (1968) 'Analysis of effects of W and f genic substitutions on fetal mouse hematology.', *Genetics*, 58(2), pp. 259–70.

Russell, E.S. (1949) 'Analysis of pleiotropism at the W-locus in the mouse; relationship between the effects of W and Wv substitution on hair pigmentation and on erythrocytes.', *Genetics*, 34(6), pp. 708–23.

Samuel, C.S., Lekgabe, E.D. and Mookerjee, I. (2007) 'The Effects of Relaxin on Extracellular Matrix Remodeling in Health and Fibrotic Disease', in *Relaxin and Related Peptides*. , pp. 88–103.

Sánchez-Martín, M., Pérez-Losada, J., Rodríguez-García, A., González-Sánchez, B., Korf, B.R., Kuster, W., Moss, C., Spritz, R.A. and Sánchez-García, I. (2003) 'Deletion of the SLUG (SNAI2) gene results in human piebaldism', *American Journal of Medical Genetics*, 122A(2), pp. 125–132.

Sarvella, P.A. and Russell, L.B. (1956) 'Steel, a new dominant gene in the house mouse with

effects on coat pigment and blood Agouti of the C3H strain', *The Journal of Heredity*, , pp. 123–128.

Scarpa, E., Szabó, A.S., Bibonne, A., Theveneau, E., Parsons, M. and Correspondence, R.M. (2015) 'Cadherin Switch during EMT in Neural Crest Cells Leads to Contact Inhibition of Locomotion via Repolarization of Forces', *Developmental Cell*, 34, pp. 421–434.

Schmoeckel, C., Stolz, W., Sakai, L.Y., Burgeson, R.E., Timpl, R. and Krieg, T. (1989) 'Structure of basement membranes in malignant melanoma and nevocytic nevi.', *The Journal of Investigative Dermatology*, 92(5), pp. 663–8.

Schneider-Poetsch, T., Ju, J., Eyler, D.E., Dang, Y., Bhat, S., Merrick, W.C., Green, R., Shen, B. and Liu, J.O. (2010) 'Inhibition of eukaryotic translation elongation by c and lactimidomycin.', *Nature Chemical Biology*, 6(3), pp. 209–217.

Schroeder, A., Mueller, O., Stocker, S., Salowsky, R., Leiber, M., Gassmann, M., Lightfoot, S., Menzel, W., Granzow, M. and Ragg, T. (2006) 'The RIN: an RNA integrity number for assigning integrity values to RNA measurements.', *BMC Molecular Biology*, 7, p. 3.

Schultz, G.S., Davidson, J.M., Kirsner, R.S., Bornstein, P. and Herman, I.M. (2011) 'Dynamic reciprocity in the wound microenvironment.', *Wound Repair and Regeneration*, 19(2), pp. 134–48.

Scott, G., Ewing, J., Ryan, D. and Abboud, C. (1994) 'Stem cell factor regulates human melanocyte-matrix interactions.', *Pigment Cell Research*, 7(1), pp. 44–51.

Segrelles, C., Holguin, A., Hernandez, P., Ariza, J., Paramio, J. and Lorz, C. (2011) 'Establishment of a murine epidermal cell line suitable for in vitro and in vivo skin modelling', *BMC Dermatology*, 11(1), p. 9.

Serbedzija, G.N., Fraser, S.E. and Bronner-Fraser, M. (1990) 'Pathways of trunk neural crest cell migration in the mouse embryo as revealed by vital dye labelling.', *Development*, 108(4), pp. 605–12.

Serre, G., Mils, V., Haftek, M., Vincent, C., Croute, F., Réano, A., Ouhayoun, J.P., Bettinger, S. and Soleilhavoup, J.P. (1991) 'Identification of late differentiation antigens of human cornified epithelia, expressed in re-organized desmosomes and bound to cross-linked envelope.', *The Journal of Investigative Dermatology*, 97(6), pp. 1061–72.

Shamis, Y., Hewitt, K.J., Carlson, M.W., Margvelashvilli, M., Dong, S., Kuo, C.K., Daheron, L., Egles, C. and Garlick, J.A. (2011) 'Fibroblasts derived from human embryonic stem cells direct development and repair of 3D human skin equivalents.', *Stem Cell Research & Therapy*, 2(1), p. 10.

Shaner, N.C., Lambert, G.G., Chammas, A., Ni, Y., Cranfill, P.J., Baird, M.A., Sell, B.R., Allen, J.R., Day, R.N., Israelsson, M., Davidson, M.W. and Wang, J. (2013) 'A bright monomeric green fluorescent protein derived from Branchiostoma lanceolatum', *Nature Methods*, 10(5), pp. 407–409.

Shen, J., Zhou, S., Shi, L., Liu, X., Lin, H., Yu, H., liang, X., Tang, J., Yu, T. and Cai, X. (2017) 'DUSP1 inhibits cell proliferation, metastasis and invasion and angiogenesis in gallbladder cancer', *Oncotarget*, 8(7), pp. 12133–12144.

Shin, K., Fogg, V.C. and Margolis, B. (2006) 'Tight Junctions and Cell Polarity', *Annual Review of Cell and Developmental Biology*, 22(1), pp. 207–235.

Slavotinek, A., Schwarz, C., Getty, J.F., Stecko, O., Goodman, F. and Kingston, H. (1999) 'Two cases with interstitial deletions of chromosome 2 and sex reversal in one.', *American Journal of Medical Genetics*, 86(1), pp. 75–81.

Smart, I.H.M. (1970) 'Variation in the plane of cell cleavage during the process of stratification in the mouse epidermis', *British Journal of Dermatology*, 82(3), pp. 276–282.

Sotiropoulou, P.A. and Blanpain, C. (2012) 'Development and Homeostasis of the Skin Epidermis', *Cold Spring Harbor Perspectives in Biology*, 4(7), pp. a008383–a008383.

Southard-Smith, E.M., Kos, L. and Pavan, W.J. (1998) 'SOX10 mutation disrupts neural crest development in Dom Hirschsprung mouse model', *Nature Genetics*, 18(1), pp. 60–64.

Srinivas, S., Watanabe, T., Lin, C.S., William, C.M., Tanabe, Y., Jessell, T.M. and Costantini, F. (2001) 'Cre reporter strains produced by targeted insertion of EYFP and ECFP into the ROSA26 locus.', *BMC Developmental Biology*, 1, p. 4.

Steven, A.C. and Steinert, P.M. (1994) 'Protein composition of cornified cell envelopes of epidermal keratinocytes.', *Journal of Cell Science*, 107 (Pt 2), pp. 693–700.

Stevens, N.G., Liff, J.M. and Weiss, N.S. (1990) 'Plantar melanoma: is the incidence of melanoma of the sole of the foot really higher in blacks than whites?', *International Journal of Cancer*, 45(4), pp. 691–3.

Strub, T., Giuliano, S., Ye, T., Bonet, C., Keime, C., Kobi, D., Le Gras, S., Cormont, M.,

Ballotti, R., Bertolotto, C. and Davidson, I. (2011) 'Essential role of microphthalmia transcription factor for DNA replication, mitosis and genomic stability in melanoma', *Oncogene*, 30(20), pp. 2319–2332.

Suraneni, P., Rubinstein, B., Unruh, J.R., Durnin, M., Hanein, D. and Li, R. (2012) 'The Arp2/3 complex is required for lamellipodia extension and directional fibroblast cell migration.', *The Journal of Cell Biology*, 197(2), pp. 239–51.

Suryo Rahmanto, Y., Dunn, L.L. and Richardson, D.R. (2007) 'The melanoma tumor antigen, melanotransferrin (p97): a 25-year hallmark – from iron metabolism to tumorigenesis', *Oncogene*, 26(42), pp. 6113–6124.

Sviderskaya, E. V, Easty, D.J. and Bennett, D.C. (1998) 'Impaired growth and differentiation of diploid but not immortal melanoblasts from endothelin receptor B mutant (piebald) mice', *Developmental Dynamics*, 213(4), pp. 452–463.

Sviderskaya, E. V, Novak, E.K., Swank, R.T. and Bennett, D.C. (1998) 'The murine misty mutation: phenotypic effects on melanocytes, platelets and brown fat.', *Genetics*, 148(1), pp. 381–90.

Sviderskaya, E. V, Wakeling, W.F. and Bennett, D.C. (1995) 'A cloned, immortal line of murine melanoblasts inducible to differentiate to melanocytes', *Development*, 121(5), pp. 1547–1557.

Tabone-Eglinger, S., Calderin-Sollet, Z., Pinon, P., Aebischer, N., Wehrle-Haller, M., Jacquier, M.-C., Boettiger, D. and Wehrle-Haller, B. (2014) 'Niche anchorage and signaling through membrane-bound Kit-ligand/c-kit receptor are kinase independent and imatinib insensitive', *The FASEB Journal*, 28(10), pp. 4441–4456.

Takayama, H., La Rochelle, W.J., Anver, M., Bockman, D.E. and Merlino, G. (1996) 'Scatter factor/hepatocyte growth factor as a regulator of skeletal muscle and neural crest development.', *Proceedings of the National Academy of Sciences of the United States of America*, 93(12), pp. 5866–71.

Talaiezadeh, A., Jazayeri, S.N. and Nateghi, J. (2012) 'Expression of c-kit protein in cancer vs. normal breast tissue.', *Contemporary Oncology*, 16(4), pp. 306–9.

Teicher, B.A. (2011) *Tumor models in cancer research*.

Terranova, V.P., Rohrbach, D.H. and Martin, G.R. (1980) 'Role of laminin in the attachment of PAM 212 (epithelial) cells to basement membrane collagen.', *Cell*, 22(3), pp. 719–26.

Terskikh, A., Fradkov, A., Ermakova, G., Zaraisky, A., Tan, P., Kajava, A. V, Zhao, X., Lukyanov, S., Matz, M., Kim, S., Weissman, I. and Siebert, P. (2000) '"Fluorescent timer" protein that changes color with time.', *Science*, 290(5496), pp. 1585–8.

Theveneau, E. and Mayor, R. (2012) 'Neural crest delamination and migration: From epithelium-to-mesenchyme transition to collective cell migration', *Developmental Biology*, 366(1), pp. 34–54.

Thiery, J.P. and Sleeman, J.P. (2006) 'Complex networks orchestrate epithelial–mesenchymal transitions', *Nature Reviews Molecular Cell Biology*, 7(2), pp. 131–142.

Thomas, A.J. and Erickson, C.A. (2008) 'The making of a melanocyte: the specification of melanoblasts from the neural crest', *Pigment Cell & Melanoma Research*, 21(6), pp. 598–610.

Thomas, A.J. and Erickson, C.A. (2009) 'FOXD3 regulates the lineage switch between neural crest-derived glial cells and pigment cells by repressing MITF through a non-canonical mechanism.', *Development*, 136(11), pp. 1849–58.

Tinevez, J.-Y., Perry, N., Schindelin, J., Hoopes, G.M., Reynolds, G.D., Laplantine, E., Bednarek, S.Y., Shorte, S.L. and Eliceiri, K.W. (2017) 'TrackMate: An open and extensible platform for single-particle tracking', *Methods*, 115, pp. 80–90.

Tobin, D.J. and Paus, R. (2001) 'Graying: gerontobiology of the hair follicle pigmentary unit.', *Experimental Gerontology*, 36(1), pp. 29–54.

Todaro, G.J. and Green, H. (1963) 'Quantitative studies of the growth of mouse embryo cells in culture and their development into established lines', *The Journal of Cell Biology*, 17, pp. 219–313.

Tosney, K.W. (2004) 'Long-distance cue from emerging dermis stimulates neural crest melanoblast migration', *Developmental Dynamics*, 229(1), pp. 99–108.

Turcu, G., Nedelcu, R.I., Ion, D.A., Brînzea, A., Cioplea, M.D., Jilaveanu, L.B. and Zurac, S.A. (2016) 'CEACAM1: Expression and Role in Melanocyte Transformation', *Disease Markers*, 2016, pp. 1–8.

van Beuningen, S.F.B., Will, L., Harterink, M., Chazeau, A., van Battum, E.Y., Frias, C.P., Franker, M.A.M., Katrukha, E.A., Stucchi, R., Vocking, K., Antunes, A.T., Slenders, L., Doulkeridou, S., Sillevis Smitt, P., Altelaar, A.F.M., Post, J.A., Akhmanova, A., Pasterkamp, R.J., Kapitein, L.C., de Graaff, E. and Hoogenraad, C.C. (2015) 'TRIM46 Controls Neuronal Polarity and Axon

Specification by Driving the Formation of Parallel Microtubule Arrays.', *Neuron*, 88(6), pp. 1208–26.

Vandamme, N. and Berx, G. (2014) 'Melanoma cells revive an embryonic transcriptional network to dictate phenotypic heterogeneity', *Frontiers in Oncology*, 4, p. 352.

Van de Putte, T., Maruhashi, M., Francis, A., Nelles, L., Kondoh, H., Huylebroeck, D. and Higashi, Y. (2003) 'Mice Lacking Zfhx1b, the Gene That Codes for Smad-Interacting Protein-1, Reveal a Role for Multiple Neural Crest Cell Defects in the Etiology of Hirschsprung Disease–Mental Retardation Syndrome', *The American Journal of Human Genetics*, 72(2), pp. 465–470.

Vassar, R. and Fuchs, E. (1991) 'Transgenic mice provide new insights into the role of TGF-alpha during epidermal development and differentiation.', *Genes & Development*, 5(5), pp. 714–27.

van der Veen, C., Handjiski, B., Paus, R., Müller-Röver, S., Maurer, M., Eichmüller, S., Ling, G., Hofmann, U., Foitzik, K. and Mecklenburg, L. (1999) 'A Comprehensive Guide for the Recognition and Classification of Distinct Stages of Hair Follicle Morphogenesis', *Journal of Investigative Dermatology*, 113(4), pp. 523–532.

Van Exan, R.J. and Hardy, M.H. (1984) 'The differentiation of the dermis in the laboratory mouse', *American Journal of Anatomy*, 169(2), pp. 149–164.

Videira, I.F., Moura, D.F. and Magina, S. (2013) 'Mechanisms regulating melanogenesis', *Anais Brasileiros de Dermatologia*, 88(1), pp. 76–83.

Vosseller, K., Stella, G., Yee, N.S. and Besmer, P. (1997) 'c-kit receptor signaling through its phosphatidylinositide-3'-kinase-binding site and protein kinase C: role in mast cell enhancement of degranulation, adhesion, and membrane ruffling.', *Molecular biology of the cell*, 8(5), pp. 909–22.

Voytyuk, O., Lennartsson, J., Mogi, A., Caruana, G., Courtneidge, S., Ashman, L.K. and Rönnstrand, L. (2003) 'Src family kinases are involved in the differential signaling from two splice forms of c-Kit.', *The Journal of Biological Chemistry*, 278(11), pp. 9159–66.

Wagner, M.J., Stacey, M.M., Liu, B.A. and Pawson, T. (2013) 'Molecular mechanisms of SH2- and PTB-domain-containing proteins in receptor tyrosine kinase signaling.', *Cold Spring Harbor Perspectives in Biology*, 5(12), p. a008987.

Wakamatsu, N., Yamada, Y., Yamada, K., Ono, T., Nomura, N., Taniguchi, H., Kitoh, H., Mutoh, N., Yamanaka, T., Mushiake, K., Kato, K., Sonta, S. and Nagaya, M. (2001) 'Mutations in SIP1, encoding Smad interacting protein-1, cause a form of Hirschsprung disease.', *Nature Genetics*, 27(4), pp. 369–370.

Wang, B., Xiao, Z., Ko, H.L. and Ren, E.-C. (2010) 'The p53 response element and transcriptional repression', *Cell Cycle*, 9(5), pp. 870–879.

Wang, F., Yamauchi, M., Muramatsu, M., Osawa, T., Tsuchida, R. and Shibuya, M. (2011) 'RACK1 Regulates VEGF/Flt1-mediated Cell Migration via Activation of a PI3K/Akt Pathway', *Journal of Biological Chemistry*, 286(11), pp. 9097–9106.

Wang, W.-L., Healy, M.E., Sattler, M., Verma, S., Lin, J., Maulik, G., Stiles, C.D., Griffin, J.D., Johnson, B.E. and Salgia, R. (2000) 'Growth inhibition and modulation of kinase pathways of small cell lung cancer cell lines by the novel tyrosine kinase inhibitor STI 571', *Oncogene*, 19(31), pp. 3521–3528.

Wang, Y., Liu, J., Ying, X., Lin, P.C. and Zhou, B.P. (2016) 'Twist-mediated Epithelial-mesenchymal Transition Promotes Breast Tumor Cell Invasion via Inhibition of Hippo Pathway', *Scientific Reports*, 6(1), p. 24606.

Wang, Z.-Q., Si, L., Tang, Q., Lin, D., Fu, Z., Zhang, J., Cui, B., Zhu, Y., Kong, X., Deng, M., Xia, Y., Xu, H., Le, W., Hu, L. and Kong, X. (2009) 'Gain-of-function mutation of KIT ligand on melanin synthesis causes familial progressive hyperpigmentation.', *American Journal of Human Genetics*, 84(5), pp. 672–7.

Wäster, P., Eriksson, I., Vainikka, L., Rosdahl, I. and Öllinger, K. (2016) 'Extracellular vesicles are transferred from melanocytes to keratinocytes after UVA irradiation', *Scientific Reports*, 6(1), p. 27890.

Watt, F.M. and Fujiwara, H. (2011) 'Cell-extracellular matrix interactions in normal and diseased skin.', *Cold Spring Harbor Perspectives in Biology*, 3(4), p. a005124.

Wehrle-Haller, B. and Imhof, B.A. (2001) 'Stem Cell Factor Presentation to c-Kit. Identification of a basolateral targeting domain', *Journal of Biological Chemistry*, 276(16), pp. 12667–12674.

Wehrle-Haller, B. and Weston, J.A. (1995) 'Soluble and cell-bound forms of steel factor activity play distinct roles in melanocyte precursor dispersal and survival on the lateral neural crest migration pathway', *Development*, 121(3), pp. 731–742.

Wels, C., Joshi, S., Koefinger, P., Bergler, H. and Schaider, H. (2011) 'Transcriptional

activation of ZEB1 by Slug leads to cooperative regulation of the epithelial-mesenchymal transition-like phenotype in melanoma.', *The Journal of Investigative Dermatology*, 131(9), pp. 1877–85.

Weston, J.A. (1963) 'A radioautographic analysis of the migration and localization of trunk neural crest cells in the chick', *Developmental Biology*, 6(3), pp. 279–310.

Weston, J.A., Yoshida, H., Robinson, V., Nishikawa, S., T. Fraser, S. and Nishikawa, S. (2004) 'Neural crest and the origin of ectomesenchyme: Neural fold heterogeneity suggests an alternative hypothesis', *Developmental Dynamics*, 229(1), pp. 118–130.

Wheelock, M.J., Shintani, Y., Maeda, M., Fukumoto, Y. and Johnson, K.R. (2008) 'Cadherin switching.', *Journal of Cell Science*, 121(Pt 6), pp. 727–35.

Whitmarsh, A.J. (2007) 'Regulation of gene transcription by mitogen-activated protein kinase signaling pathways', *Biochimica et Biophysica Acta - Molecular Cell Research*, 1773(8), pp. 1285–1298.

Wille, J.J. and Kydonieus, A. (2003) 'Palmitoleic acid isomer (C16:1delta6) in human skin sebum is effective against gram-positive bacteria.', *Skin Pharmacology and Applied Skin Physiology*, 16(3), pp. 176–87.

Willmore-Payne, C., Holden, J.A., Tripp, S. and Layfield, L.J. (2005) 'Human malignant melanoma: detection of BRAF- and c-kit–activating mutations by high-resolution amplicon melting analysis', *Human Pathology*, 36(5), pp. 486–493.

Wooley, G.W. (1941) '"Misty" a New Coat Color Dilution in the Mouse, Mus musculus.', *The American Naturalist*, 75(760), pp. 507–508.

Xiao, M.-F., Xu, D., Craig, M.T., Pelkey, K.A., Chien, C.-C., Shi, Y., Zhang, J., Resnick, S., Pletnikova, O., Salmon, D., Brewer, J., Edland, S., Wegiel, J., Tycko, B., Savonenko, A., Reeves, R.H., Troncoso, J.C., McBain, C.J., Galasko, D. and Worley, P.F. (2017) 'NPTX2 and cognitive dysfunction in Alzheimer's Disease.', *eLife*, 6

Yamaguchi, H. and Condeelis, J. (2007) 'Regulation of the actin cytoskeleton in cancer cell migration and invasion', *Biochimica et Biophysica Acta - Molecular Cell Research*, 1773(5), pp. 642–652.

Yamauchi, A., Hadjur, C., Takahashi, T., Suzuki, I., Hirose, K. and Mahe, Y.F. (2013) 'Human skin melanocyte migration towards stromal cell-derived factor-1α demonstrated by optical real-time cell mobility assay: modulation of their chemotactic ability by α-melanocyte-stimulating hormone', *Experimental Dermatology*, 22(10), pp. 664–667.

Yang, F., Sun, L., Li, Q., Han, X., Lei, L., Zhang, H. and Shang, Y. (2012) 'SET8 promotes epithelial-mesenchymal transition and confers TWIST dual transcriptional activities', *The EMBO Journal*, 31(1), pp. 110–123.

Yang, J., Mani, S.A., Donaher, J.L., Ramaswamy, S., Itzykson, R.A., Come, C., Savagner, P., Gitelman, I., Richardson, A. and Weinberg, R.A. (2004) 'Twist, a Master Regulator of Morphogenesis, Plays an Essential Role in Tumor Metastasis', *Cell*, 117(7), pp. 927–939.

Yang, J. and Weinberg, R.A. (2008) 'Epithelial-Mesenchymal Transition: At the Crossroads of Development and Tumor Metastasis', *Developmental Cell*, 14(6), pp. 818–829.

Yang, M.-H., Hsu, D.S.-S., Wang, H.-W., Wang, H.-J., Lan, H.-Y., Yang, W.-H., Huang, C.-H., Kao, S.-Y., Tzeng, C.-H., Tai, S.-K., Chang, S.-Y., Lee, O.K.-S. and Wu, K.-J. (2010) 'Bmi1 is essential in Twist1-induced epithelial–mesenchymal transition', *Nature Cell Biology*, 12(10), pp. 982–992.

Yang, R., Jiang, M., Kumar, S.M., Xu, T., Wang, F., Xiang, L. and Xu, X. (2011) 'Generation of Melanocytes from Induced Pluripotent Stem Cells', *Journal of Investigative Dermatology*, 131(12), pp. 2458–2466.

Yoo, J.C., Lim, T. yeon, Park, J.S., Hah, Y.-S., Park, N., Hong, S.-G., Park, J.-Y. and Yoon, T.-J. (2013) 'SYT14L, especially its C2 domain, is involved in regulating melanocyte differentiation', *Journal of Dermatological Science*, 72(3), pp. 246–251.

Yoshida, H., Kunisada, T., Kusakabe, M., Nishikawa, S.I., Nishikawa, S.I., Bartlett, P.F. and Murphy, M. (1996) 'Distinct stages of melanocyte differentiation revealed by anlaysis of nonuniform pigmentation patterns.', *Development*, 122(4), pp. 1207–14.

Yue, B. (2014) 'Biology of the extracellular matrix: an overview.', *Journal of Glaucoma*, 23(8 Suppl 1), pp. S20-3.

Yue, F., Cheng, Y., Breschi, A., Vierstra, J., Wu, W., Ryba, T., Sandstrom, R., Ma, Z., Davis, C., Pope, B.D., Shen, Y., Pervouchine, D.D., Djebali, S., Thurman, R.E., Kaul, R., Rynes, E., Kirilusha, A., Marinov, G.K., Williams, B.A., Trout, D., Amrhein, H., Fisher-Aylor, K., Antoshechkin, I., DeSalvo, G., See, L.-H., Fastuca, M., Drenkow, J., Zaleski, C., Dobin, A., Prieto, P.,

Lagarde, J., Bussotti, G., Tanzer, A., Denas, O., Li, K., Bender, M.A., Zhang, M., Byron, R., Groudine, M.T., McCleary, D., Pham, L., Ye, Z., Kuan, S., Edsall, L., Wu, Y.-C., Rasmussen, M.D., Bansal, M.S., Kellis, M., Keller, C.A., Morrissey, C.S., Mishra, T., Jain, D., Dogan, N., Harris, R.S., Cayting, P., Kawli, T., Boyle, A.P., Euskirchen, G., Kundaje, A., Lin, S., Lin, Y., Jansen, C., Malladi, V.S., Cline, M.S., Erickson, D.T., Kirkup, V.M., Learned, K., Sloan, C.A., Rosenbloom, K.R., Lacerda de Sousa, B., Beal, K., Pignatelli, M., Flicek, P., Lian, J., Kahveci, T., Lee, D., James Kent, W., Ramalho Santos, M., Herrero, J., Notredame, C., Johnson, A., Vong, S., Lee, K., Bates, D., Neri, F., Diegel, M., Canfield, T., Sabo, P.J., Wilken, M.S., Reh, T.A., Giste, E., Shafer, A., Kutyavin, T., Haugen, E., Dunn, D., Reynolds, A.P., Neph, S., Humbert, R., Scott Hansen, R., De Bruijn, M., Selleri, L., Rudensky, A., Josefowicz, S., Samstein, R., Eichler, E.E., Orkin, S.H., Levasseur, D., Papayannopoulou, T., Chang, K.-H., Skoultchi, A., Gosh, S., Disteche, C., Treuting, P., Wang, Y., Weiss, M.J., Blobel, G.A., Cao, X., Zhong, S., Wang, T., Good, P.J., Lowdon, R.F., Adams, L.B., Zhou, X.-Q., Pazin, M.J., Feingold, E.A., Wold, B., Taylor, J., Mortazavi, A., Weissman, S.M., Stamatoyannopoulos, J.A., Snyder, M.P., Guigo, R., Gingeras, T.R., Gilbert, D.M., Hardison, R.C., Beer, M.A., Ren, B. and Mouse ENCODE Consortium (2014) 'A comparative encyclopedia of DNA elements in the mouse genome', *Nature*, 515(7527), pp. 355–364.

Yurchenco, P.D. and Ruben, G.C. (1988) 'Type IV collagen lateral associations in the EHS tumor matrix. Comparison with amniotic and in vitro networks.', *The American Journal of Pathology*, 132(2), pp. 278–91.

Zaidi, M.R., Day, C.-P. and Merlino, G. (2008) 'From UVs to Metastases: Modeling Melanoma Initiation and Progression in the Mouse', *Journal of Investigative Dermatology*, 128(10), pp. 2381–2391.

Zeron-Medina, J., Wang, X., Repapi, E., Campbell, M.R., Su, D., Castro-Giner, F., Davies, B., Peterse, E.F.P., Sacilotto, N., Walker, G.J., Terzian, T., Tomlinson, I.P., Box, N.F., Meinshausen, N., De Val, S., Bell, D.A. and Bond, G.L. (2013) 'A polymorphic p53 response element in KIT ligand influences cancer risk and has undergone natural selection.', *Cell*, 155(2), pp. 410–22.

Zhang, J. and Ma, L. (2012) 'MicroRNA control of epithelial–mesenchymal transition and metastasis', *Cancer and Metastasis Reviews*, 31(3–4), pp. 653–662.

Zhang, Z.H., Jhaveri, D.J., Marshall, V.M., Bauer, D.C., Edson, J., Narayanan, R.K., Robinson, G.J., Lundberg, A.E., Bartlett, P.F., Wray, N.R. and Zhao, Q.-Y. (2014) 'A Comparative Study of Techniques for Differential Expression Analysis on RNA-Seq Data', *PLoS ONE*, 9(8), p. e103207.

Zsebo, K.M., Williams, D.A., Geissler, E.N., Broudy, V.C., Martin, F.H., Atkins, H.L., Hsu, R.-Y., Birkett, N.C., Okino, K.H., Murdock, D.C., Jacobsen, F.W., Langley, K.E., Smith, K.A., Takeish, T., Cattanach, B.M., Galli, S.J. and Suggs, S. V. (1990) 'Stem cell factor is encoded at the SI locus of the mouse and is the ligand for the c-kit tyrosine kinase receptor', *Cell*, 63(1), pp. 213–224.

Appendices

Appendix A. Rt-PCR gels showing expression of key keratinocyte developmental markers. Note that the best bands have been taken from different experiments and reconstructed.

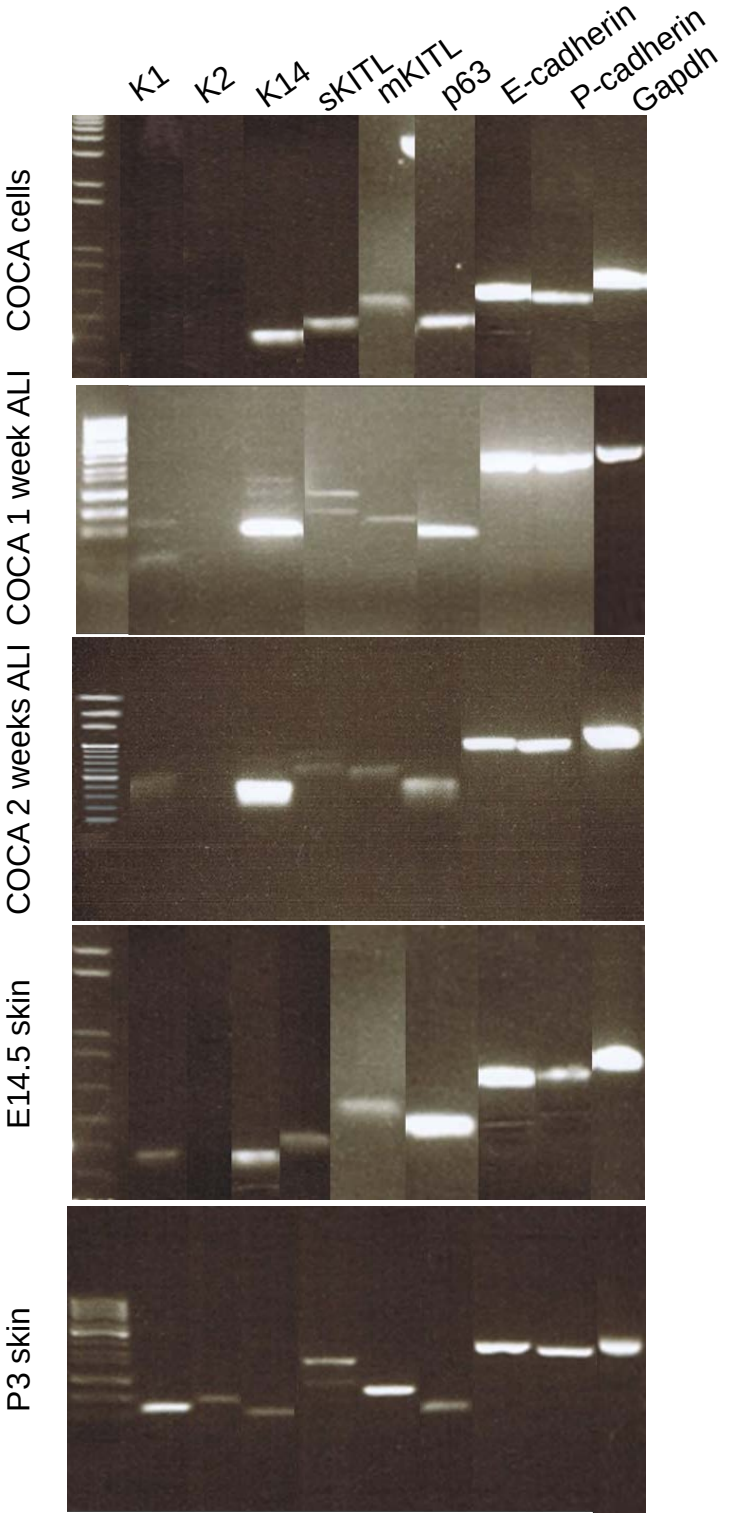

Appendix B. Plasmid maps of KIT and s/mKITL constructs. Maps show unique and common features, and some unique restriction sites.

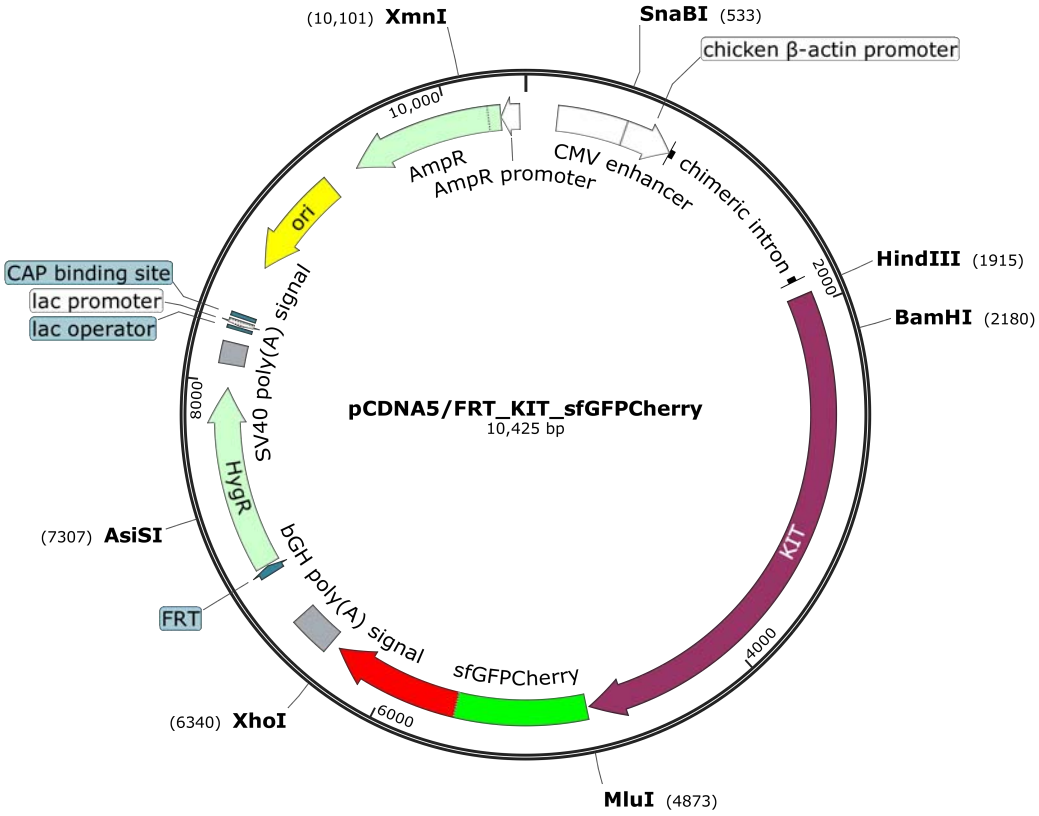

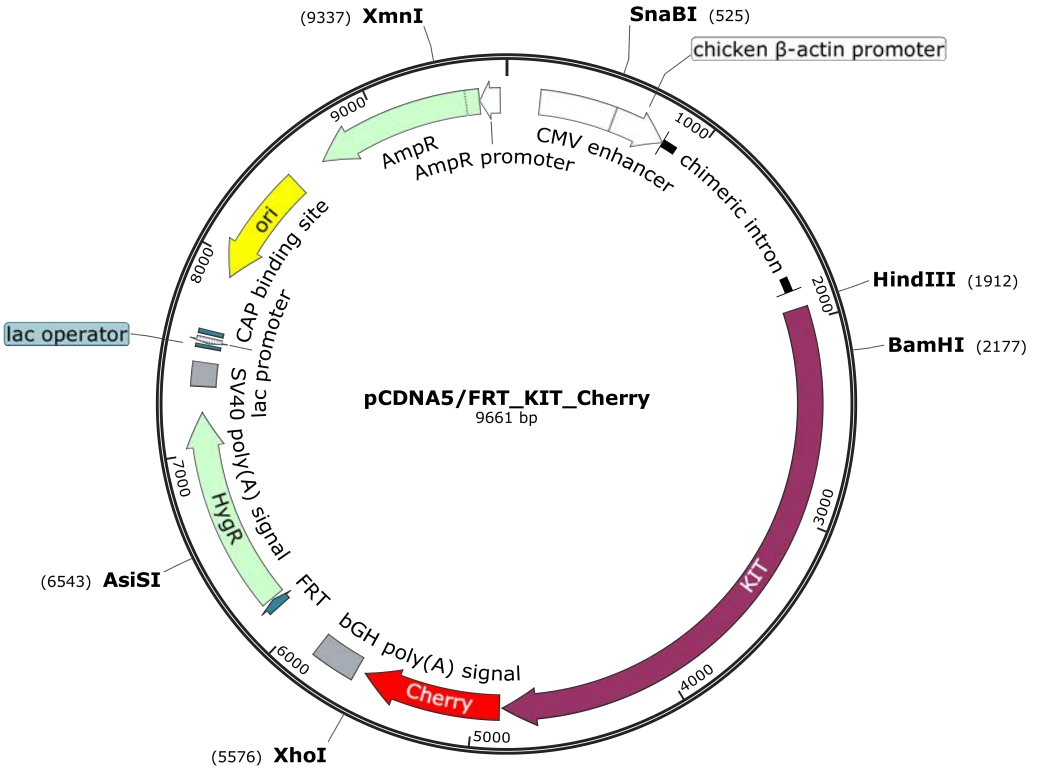

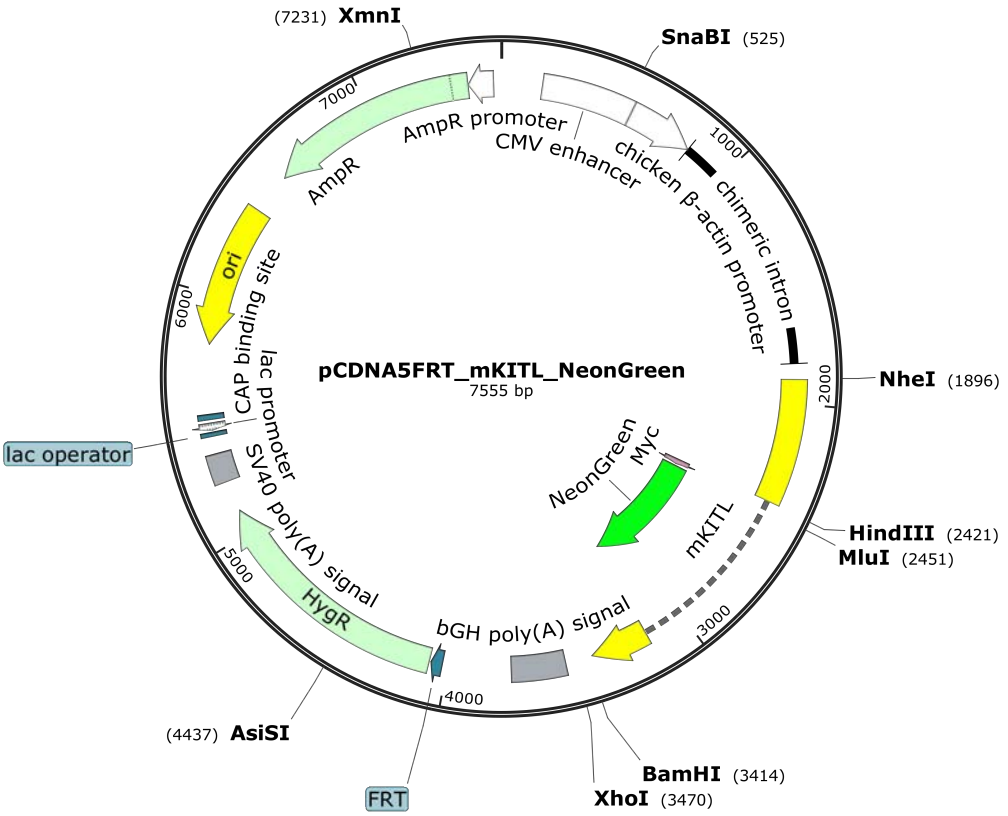
(7231) XmnI
SnaBI (525)
AmpR promoter
CMV enhancer
chicken β-actin promoter
chimeric intron
AmpR
ori
CAP binding site
lac promoter
lac operator
SV40 poly(A) signal
pCDNA5FRT_mKITL_NeonGreen
7555 bp
NheI (1896)
NeonGreen
Myc
mKITL
HindIII (2421)
MluI (2451)
HygR
bGH poly(A) signal
(4437) AsiSI
FRT
XhoI (3470)
BamHI (3414)

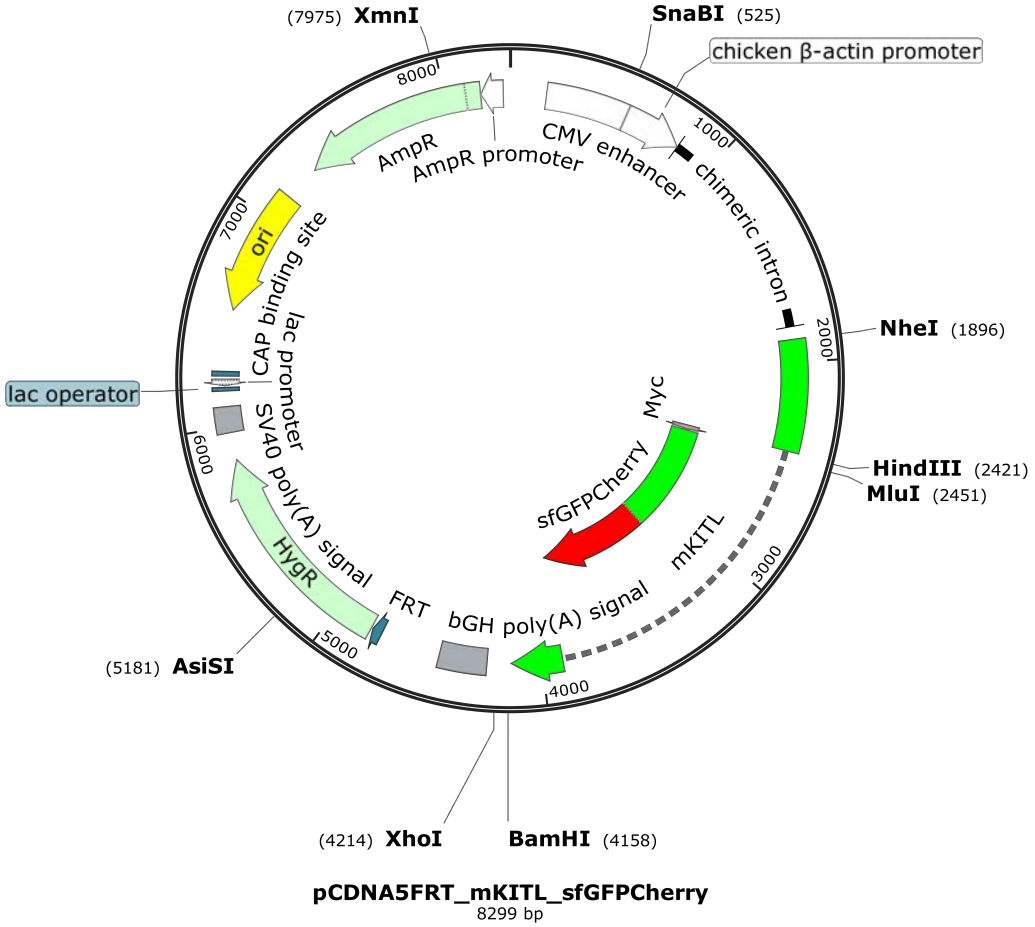
(7975) XmnI
SnaBI (525)
chicken β-actin promoter
AmpR
AmpR promoter
CMV enhancer
chimeric intron
ori
CAP binding site
lac promoter
lac operator
SV40 poly(A) signal
NheI (1896)
Myc
sfGFPCherry
mKITL
HindIII (2421)
MluI (2451)
HygR
FRT
bGH poly(A) signal
(5181) AsiSI
(4214) XhoI
BamHI (4158)
pCDNA5FRT_mKITL_sfGFPCherry
8299 bp

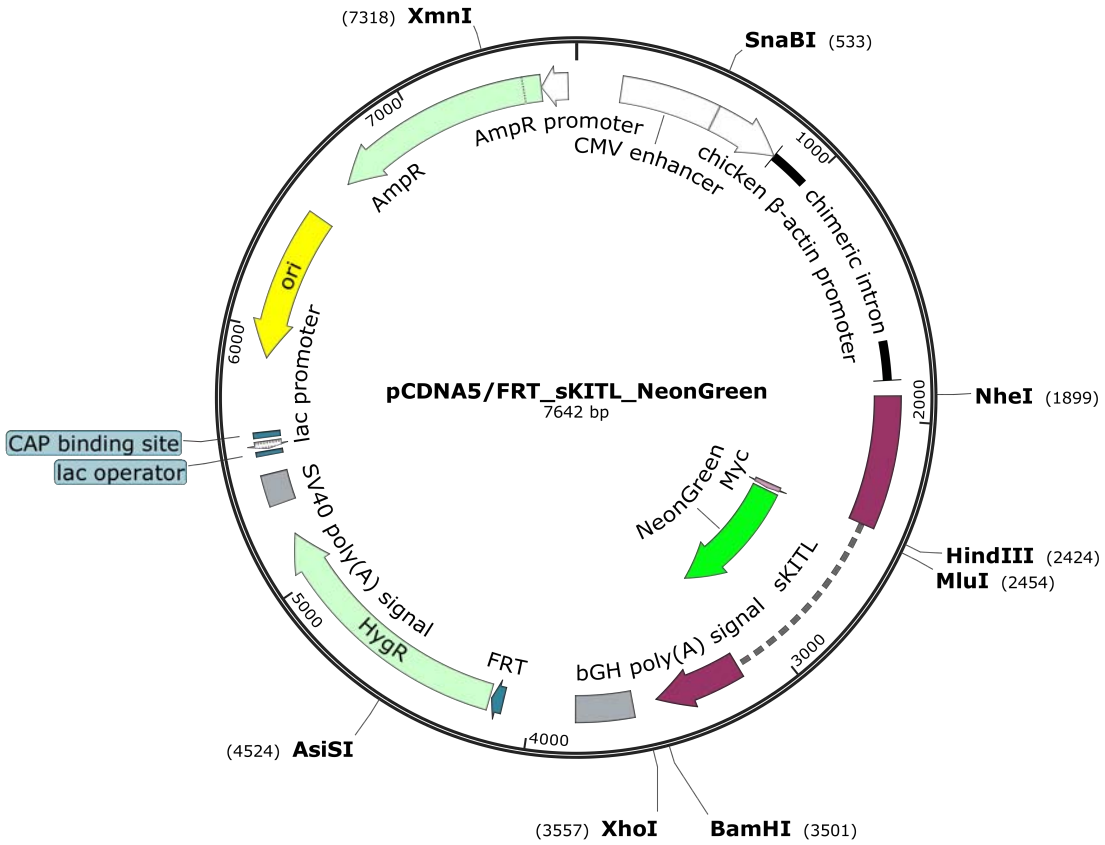
(7318) XmnI
SnaBI (533)
AmpR promoter
CMV enhancer
chicken β-actin promoter
chimeric intron
AmpR
ori
lac promoter
pCDNA5/FRT_sKITL_NeonGreen
7642 bp
NheI (1899)
CAP binding site
lac operator
NeonGreen
Myc
sKITL
HindIII (2424)
MluI (2454)
SV40 poly(A) signal
HygR
FRT
bGH poly(A) signal
(4524) AsiSI
(3557) XhoI
BamHI (3501)

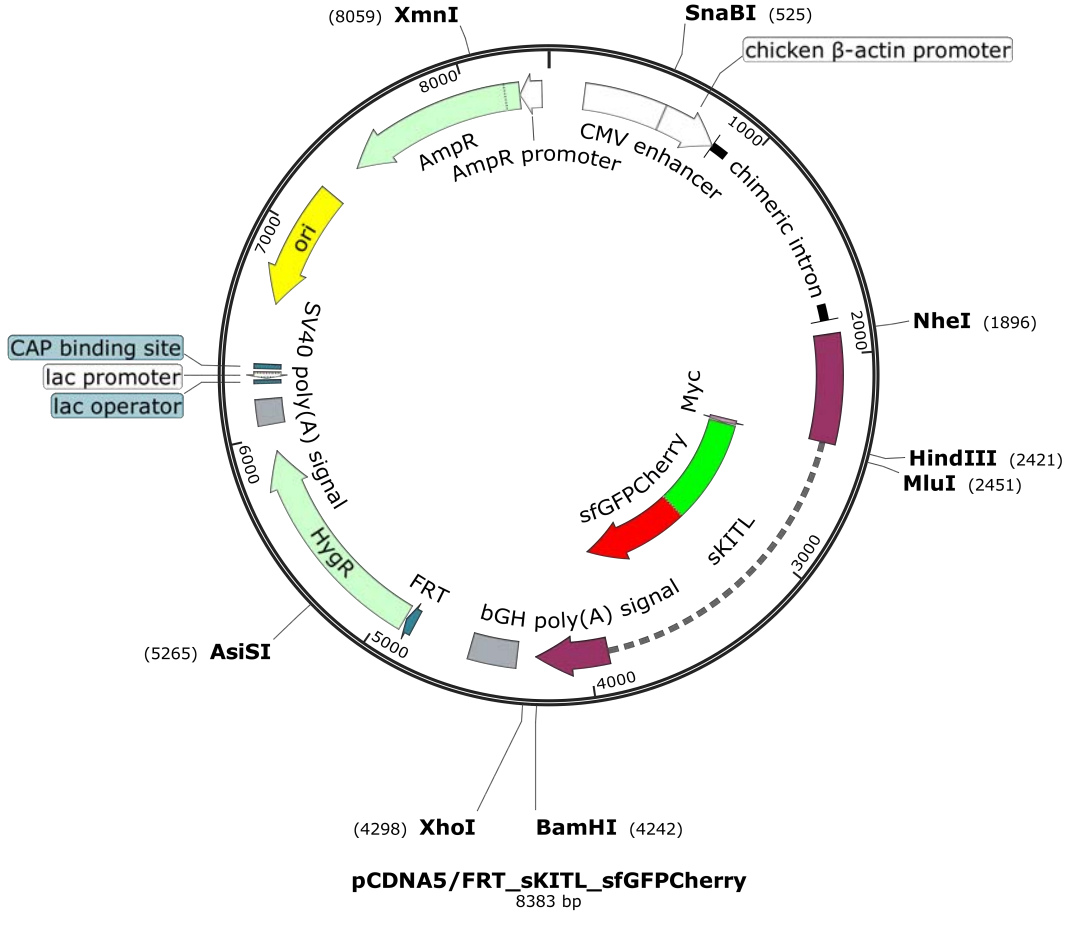
(8059) XmnI
SnaBI (525)
chicken β-actin promoter
AmpR
AmpR promoter
CMV enhancer
chimeric intron
ori
NheI (1896)
CAP binding site
lac promoter
lac operator
SV40 poly(A) signal
Myc
sfGFPCherry
HindIII (2421)
MluI (2451)
HygR
FRT
sKITL
bGH poly(A) signal
(5265) AsiSI
(4298) XhoI
BamHI (4242)
pCDNA5/FRT_sKITL_sfGFPCherry
8383 bp

Appendix C. Investigating the cadherin switch in HDs by IF. HDs were immunostained for the presence of E-cadherin and N-cadherin but results were inconclusive. Scale bars represent 100µm.